

Thermal and calorimetric evaluations of some bio-inspired fire-resistant coatings for ligno-cellulosic materials

Ms Ananya Thomas

A thesis submitted in fulfilment of the requirement for the degree of Doctor of Philosophy



Institute of Sustainable Industries and Liveable Cities (ISILC),

Victoria University, Melbourne

May 2020

Abstract

Through the current project, we have investigated the passive fire protection efficiency of some bio-inspired substrates, which included: β -cyclodextrin, dextran, potato starch, agar agar, tamarind, chitosan, rice bran and fish gelatin. In an attempt to enhance the passive fire protection attributes of these substrates, we prepared formulations of these with both inorganic and organic compounds, the latter included some phosphorus-containing compounds with the phosphorus atom in different chemical environments and oxidation states. Here we have also explored both the *reactive* and *additive* strategies. The degrees of functionalization were primarily gauged from inductively-coupled plasma/optical emission spectroscopy (ICP-OES), ^{31}P solid-state Nuclear Magnetic Resonance Spectroscopy (NMR). We also chose several thermal and calorimetric techniques for evaluating the efficacies of such formulations, such as: thermo-gravimetric analysis (TGA), pyrolysis combustion flow calorimetry (PCFC), a proprietary ignition propensity test and cone calorimetry. In addition, with a view to deciphering the elements of condensed phase mechanism, we carried out an estimation of the extents of phosphorus retention in the char residues (using ICP-OES) and chemical nature of the char residues (*via* solid-state NMR and Raman spectroscopies) that were obtained through the cone calorimetric runs. The unmodified counterparts were also subjected to the same set of analyses with a view to serving as controls. We also endeavoured to analyse the gaseous volatile fragments emanating from some of the additives using, either by employing gas chromatography/mass spectrometry (GC/MS), or pyrolysis-GC/MS, technique.

Phosphorus analyses, primarily, through ICP-OES on the recovered samples showed different degrees of incorporation. Such observations were verified through solid-state ^{31}P NMR spectroscopy. The thermograms of the modified substrates were noticeably different from the unmodified counterparts, both in terms of the general profiles and the amounts of char residues produced. Such observations correlated well with the relevant parameters obtained through the PCFC runs. Furthermore, we have carried out a detailed kinetic analyses of the thermograms of the unmodified substrates, obtained at different heating rates, using the Flynn Wall Ozawa (FWO) method, and through a proprietary software developed by our research group (SB method). We have also endeavoured to seek correlations, if any, among the various empirical parameters that were collated through the different test methods.

Overall, the modified systems containing phosphorus were found to be less combustible than the parent substrates, and thus can be considered as promising base matrices for environmentally-benign fire resistant coatings. With a view to understanding the overall

flammability profiles, optionally, in some of the formulations, initially we screened them through an ignitability propensity test that was developed in our laboratories. This was followed by cone calorimetric measurements on Radiata Pine plaques, particularly, coated with potato starch, chitosan, chitin, rice bran and fish gelatin. The results from the cone tests indicated that formulations based on fish gelatin endowed with the best fire protection property, followed by chitosan, whereas potato starch and rice bran seem to be ineffective as fire proofing agents.

When I am at my best, I am my father's daughter

-Unknown-

I dedicate this humble effort to my sweet and loving dad. You are always my hero.

Acknowledgement

I am forever thankful to my principal supervisor, Dr Paul Joseph, for all the guidance, support and encouragement he has given me from day one, without whom this thesis would not have been possible. I am also grateful to my associate supervisor, Professor Khalid Moinuddin, for his help and support throughout my PhD programme. Thanks are also due to Professor Stephen Bigger for allowing me to use the software to interpret the thermogravimetric data, and to Professor Andrew Smallridge for recording solution-state NMR spectra. I also greatly acknowledge the technical support from various people at Victoria University: Lyndon Mcindoe, Philip Dunn, Stephen Downing, Stacey Lloyd, Nishantha Illangantilaka, Mary Marshall and Larruceo Bautista.

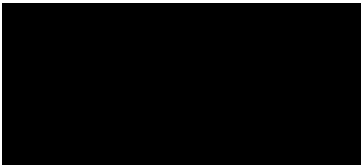
I also register my deep sense of gratitude to Nathan White and Joe Abraham, CSIRO, Clayton, for allowing me to use their cone calorimeter; Drs Luke O'Dell and Haijin Zhu for recording the solid-state NMR spectra; Joseph Pelle, Monash University, for giving me access to their analytical suite; Dr Svetlana Tretsiakova-McNally and Alosly Baby, Ulster University, UK, for help with 'bomb' calorimetric tests; and Dr Doris Pospiech and Christina Harnisch, Leibniz-Institut für Polymerforschung, Dresden, Germany, for conducting pyrolysis-GC/MS measurements.

I am greatly indebted to Victoria University for the provision of a Centenary Research Fellowship for my doctoral studies.

A very special word of thanks to my husband, Ajin Isac, who has been with me through all the tough times and for always keeping things going. Thanks are also due to my two year old son, Ian Sunny Isac, for being so patient despite my absence. Your *sunny smile* always brightens my day.

Student Declaration:

I, Anaya Thomas, declare that the PhD thesis entitled, *Thermal and calorimetric evaluations of some bio-inspired fire resistant coatings for ligno-cellulosic materials*, is no more than 100,000 words in length including quotes and exclusive of tables, figures, appendices, bibliography, references and footnotes. This thesis contains no material that has been submitted previously, in whole or in part, for the award of any other academic degree or diploma. Except where otherwise indicated, this thesis is my own work.

A solid black rectangular box used to redact the student's signature.

Signature

Date: 5 May 2020

Research outputs produced during the candidature:

I. Peer-reviewed papers

1. Thomas, A., Moinuddin, K., Bigger, S. B. & Joseph, P. A comparative study of deducing the Arrhenius parameters from thermograms obtained through a single and multiple heating rates (manuscript in preparation).
2. Tretsiakova-McNally, S., Douarin, A., Joseph, P. & Thomas, A. Enhancing Fire Performance of Wood substrates by Surface Coatings Based on Starch Colloids. *Polymers* (submitted).
3. Thomas, A., Moinuddin, K., Zhu, H., & Joseph, P. Passive fire protection of wood using some bio-derived fire retardants. *Fire Safety Journal*: <https://doi.org/10.1016/j.firesaf.2020.103074>.
4. Thomas, A., Joseph, P., Moinuddin, K., Zhu, H. & Tretsiakova-McNally, S. (2020). Thermal and Calorimetric Evaluations of Some Chemically Modified Carbohydrate-Based Substrates with Phosphorus-Containing Groups. *Polymers*, 12(3), 588.
5. Jones, M., Bhat, T., Kandare, E., Thomas, A., Joseph, P., Dekiwadia, C. & Wang, C. H. (2018). Thermal degradation and fire properties of fungal mycelium and mycelium-biomass composite materials. *Scientific Reports*, 8(1), 1-10.

II. Conference publications

1. Tretsiakova-McNally, S., Thomas, A., Joseph, P., Moinuddin, K. & Zhu, H. (2020, August). Formulation and characterisation of some bio-inspired substrates for passively fire protecting timber elements. *American Chemical Society National Meeting*, San Francisco, USA (under review).
2. Thomas, A., Joseph, P., Moinuddin, K. & Zhu, H. (2020, August). Analyses of the condensed and gaseous phases of passively fire protected Radiata pine samples using spectroscopic, chromatographic and hyphenated techniques. *American Chemical Society National Meeting*, San Francisco, USA (under review).

3. Tretsiakova-McNally, S., Le Douarin, A., Joseph, P., Ukleja, S., & Thomas, A. (2019, June). Passive Fire Protection of Wood Substrates using Starch-based Formulations. In *European Meeting on Fire Retardant Polymeric Materials*.
4. Thomas, A., Joseph, P., & Moinuddin, K. (2018, July). Thermal performance analysis of chemically modified carbohydrate based materials. *Proceedings of the 11th Asian-Australian Conference on Composite Materials*.

List of abbreviations:

With a view to simplifying the main text, the following abbreviations are used:

| | |
|-------------|--|
| 1. A-factor | Arrhenius factor |
| 2. AP | Diammoniumhydrogen phosphate |
| 3. AS/NZ | Australia/New Zealand (ref. standards) |
| 4. ASTM | American Society for Testing Materials |
| 5. ATR | Attenuated Total Reflectance |
| 6. CFD | Computational Fluid Dynamics |
| 7. D-band | Amorphous band |
| 8. DCM | Dichloromethane |
| 9. DEBP | Diethylbenzylphosphonate |
| 10. DECP | Diethylchlorophosphate |
| 11. DEPi | Diethylphosphite |
| 12. DEPP | Diethylpropylphosphonate |
| 13. DOPO | 9,10-Dihydro-9-oxa-10-phosphaphenenthrene-10-oxide |
| 14. DPT | Differential pressure transducer |
| 15. E_a | Activation energy |
| 16. EDXRD | Energy dispersive x-ray diffraction |
| 17. EPR | Electron paramagnetic resonance |
| 18. FR | Fire retardant |
| 19. FT-IR | Fourier-transform infrared spectrometry |
| 20. FWO | Flynn Wall Ozawa |
| 21. G band | Graphitic band |
| 22. GC | Gas chromatography |
| 23. HRC | Heat release capacity |
| 24. ICP-OES | Inductively coupled plasma optical emission spectrometry |
| 25. ISILC | Institute of Sustainable Industries and Liveable Cities |
| 26. ISO | International Organization for Standardization |
| 27. MAP | Monoammonium phosphate |
| 28. MS | Mass spectrometry |
| 29. MSD | Mass selective detector |
| 30. NBS | National Bureau of Standards |
| 31. NIST | National Institute of Standards Technology |

| | |
|----------|---------------------------------------|
| 32. NMR | Nuclear Magnetic Resonance |
| 33. PCFC | Pyrolysis combustion flow calorimetry |
| 34. pHRR | Peak heat release rate |
| 35. PVA | Polyvinylalcohol |
| 36. SB | Stephen Bigger's software |
| 37. TEA | Triethylamine |
| 38. TEPa | Triethylphosphate |
| 39. TEPi | Triethylphosphite |
| 40. TGA | Thermogravimetric analyses |
| 41. THF | Tetrahydrofuran |
| 42. THR | Total heat release |
| 43. TPP | Triphenylphosphine |
| 44. TPPO | Triphenylphosphineoxide |
| 45. WUI | Wildland Urban Interface |

Contents

| | |
|---|----|
| Chapter 1: Introduction and literature review | |
| 1.1 Background | 1 |
| 1.2 Ligno-cellulosic materials: degradation and combustion behaviour..... | 2 |
| 1.3 Combustion hazards of ligno-cellulosic materials in the context of bushfires | 6 |
| 1.4 Common methods to enhance the fire resistance of ligno-cellulosic materials | 8 |
| 1.5 The main aim of the project: | 13 |
| 1.6 Individual objectives: | 14 |
| Chapter 2: Materials and methods | |
| 2.1 Materials..... | 16 |
| 2. 2 Methods..... | 22 |
| 2.2.1 Synthetic procedures..... | 22 |
| 2.2.1.1 Phosphorylation reactions on carbohydrate based materials | 22 |
| 2.2.1.2 Syntheses of the derivative of chitosan through functionalization with 9,10-Dihydro-9-oxa-10-phosphaphenenthrene-10-oxide (DOPO)..... | 23 |
| 2.2.1.3 Synthesis of diethylbenzylphosphonate: <i>Michaelis-Arbuzov</i> reaction..... | 23 |
| 2.2.2 Formulation and coating for cone calorimetry | 24 |
| 2.2.3 Characterization techniques..... | 24 |
| 2.2.3.1 Solution-state NMR | 25 |
| 2.2.3.2 Inductively-coupled plasma optical emission spectroscopy (ICP-OES)..... | 25 |
| 2.2.3.3 Fourier-transform infrared spectroscopy (FT-IR)..... | 27 |
| 2.2.3.4 Thermogravimetric analysis (TGA):..... | 27 |
| 2.2.3.5 Pyrolysis combustion flow calorimetry (PCFC)..... | 28 |
| 2.2.3.6 Bomb calorimetry | 28 |
| 2.2.3.7 Gas chromatography/mass spectrometry (GC/MS)..... | 29 |
| 2.2.3.8 Pyrolysis-GC/MS | 29 |
| 2.2.3.9 Solid-state NMR | 29 |
| 2.2.3.10 Raman spectroscopy | 30 |
| 2.2.4 Flammability tests..... | 30 |
| 2.2.4.1 Dip-test through an in-house test rig..... | 30 |
| 2.2.4.2 Cone calorimetry..... | 31 |
| 2.2.5 Deduction of Arrhenius parameters from thermograms..... | 36 |
| 2.2.4.1 Flynn-Wall-Ozawa (FWO) method | 36 |

| | |
|---|-----|
| 2.2.4.2 SB method..... | 37 |
| Chapter 3: Results and discussion..... | |
| 3.1 Choice of materials..... | 44 |
| 3.1.1 Base substrates..... | 44 |
| 3.1.2 Phosphorylation reaction of carbohydrate-based materials..... | 45 |
| 3.1.2.1 Calculation of mol fraction of DECP functionalized units in modified oligosaccharides..... | 49 |
| 3.1.3 Syntheses of the derivative of chitosan through functionalization with 9,10-Dihydro-9-oxa-10-phosphaphenenthrene-10-oxide (DOPO)..... | 51 |
| 3.1.3.1 Calculation of mol fraction of DOPO functionalized units in modified chitosan..... | 53 |
| 3.1.4 Synthesis of diethylbenzylphosphonate: Michaelis-Arbuzov reaction..... | 54 |
| 3.1.5 Formulation and coating for cone calorimetry..... | 56 |
| 3.2 Characterization..... | 58 |
| 3.2.1 Thermogravimetric Analysis (TGA)..... | 58 |
| 3.2.1.1 Detailed kinetic analysis (FWO and SB methods)..... | 67 |
| 3.2.2 Pyrolysis combustion flow calorimetry (PCFC)..... | 78 |
| 3.3 Correlation between TGA and PCFC..... | 86 |
| 3.4 Flammability tests..... | 99 |
| 3.4.1 Dip test..... | 99 |
| 3.4.2 Cone tests..... | 102 |
| 3.5 Condensed-phase analysis..... | 116 |
| 3.5.1 Inductively-coupled plasma.optical emission spectroscopy (ICP-OES)..... | 116 |
| 3.5.2 Solid-state NMR spectra..... | 119 |
| 3.5.3. Raman spectroscopy..... | 125 |
| 3.6 Vapour-phase analyses of the additives (i.e. hyphenated techniques)..... | 127 |
| 3.6.1 Gas chromatography-mass spectrometry (GC/MS)..... | 128 |
| 3.6.2 Pyrolysis-gas chromatography/mass spectrometry..... | 132 |
| Chapter 4: Conclusions and suggestions for future work..... | |
| 4.1 Main conclusions..... | 142 |
| 4.2 Significant contributions arising from the present work..... | 144 |
| 4.3 Some suggestions for future work..... | 145 |
| References..... | |

Legends to figures:

Chapter 1

| | |
|--|---|
| <i>Figure 1. 1 Degradation pathway of cellulose, through a radical mechanism, resulting in the production of laevoglucosan</i> | 5 |
| <i>Figure 1. 2 Combustion cycle of a polymeric solid fuel</i> | 6 |
| <i>Figure 1. 3 Strategies to interrupt the combustion cycle</i> | 9 |

Chapter 2

| | |
|--|----|
| <i>Figure 2. 1 Chemical structure of β-cyclodextrin</i> | 17 |
| <i>Figure 2. 2 Chemical Structure of potato starch</i> | 17 |
| <i>Figure 2. 3 Chemical Structure of dextran</i> | 18 |
| <i>Figure 2. 4 Chemical structures of agarose (a) and agarpectin (b)</i> | 18 |
| <i>Figure 2. 5 Chemical structure (representative) of tamarind kernel powder</i> | 19 |
| <i>Figure 2. 6 Chemical structure of chitosan</i> | 19 |
| <i>Figure 2. 7 Chemical structure (representative) of fish gelatin</i> | 20 |
| <i>Figure 2. 8 Chemical structure of anti-oxidative phytochemicals present in rice bran</i> | 21 |
| <i>Figure 2. 9 Calibration curve of the Beer-Lambert law (generated by the inbuilt software of the instrument)</i> | 26 |
| <i>Figure 2. 10 A schematic sketch of the proprietary ignition propensity test</i> | 31 |
| <i>Figure 2. 11 A schematic diagram of cone calorimeter</i> | 33 |
| <i>Figure 2. 12 Plot showing values of $g(\alpha)$ vs. $p(x)$</i> | 42 |

Chapter 3

| | |
|--|----|
| <i>Figure 3. 1 A photograph showing Radiata pine plaques</i> | 44 |
| <i>Figure 3. 2 A schematic diagram of the phosphorylation reaction</i> | 46 |
| <i>Figure 3. 3 ^{31}P-NMR spectrum of β-cyclodextrin modified with phosphate groups</i> | 46 |
| <i>Figure 3. 4 ^{31}P-NMR spectrum of dextran modified with phosphate groups</i> | 47 |
| <i>Figure 3. 5 ^{31}P-NMR spectrum of potato starch modified with phosphate groups</i> | 47 |
| <i>Figure 3. 6 ^{31}P-NMR spectrum of agar agar modified with phosphate groups</i> | 48 |
| <i>Figure 3. 7 ^{31}P-NMR spectrum of tamarind modified with phosphate groups</i> | 48 |

| | |
|--|----|
| Figure 3. 8 Schematic diagram showing the chemical modification reaction of chitosan with DOPO | 52 |
| Figure 3. 9 ³¹ P-NMR spectrum of chitosan modified with DOPO groups | 52 |
| Figure 3. 10 FT/IR plots of modified and unmodified versions of chitosan | 53 |
| Figure 3. 11 ¹ H NMR spectrum of diethylbenzylphosphonate in CDCl ₃ | 55 |
| Figure 3. 12 ³¹ P-NMR spectrum of diethylbenzylphosphonate in CDCl ₃ | 55 |
| Figure 3. 13 Thermograms of modified and unmodified versions of β-cyclodextrin at 60°C min ⁻¹ | 61 |
| Figure 3. 14 Plot of the dm/dT vs. temperature (°C) for modified and unmodified versions of β-cyclodextrin | 61 |
| Figure 3. 15 Thermograms of modified and unmodified versions of dextran at 60°C min ⁻¹ ... | 62 |
| Figure 3. 16 Plot of the dm/dT vs. temperature (°C) for modified and unmodified versions of dextran | 62 |
| Figure 3. 17 Thermograms of modified and unmodified versions of potato starch at 60°C min ⁻¹ | 63 |
| Figure 3. 18 Plot of the dm/dT vs. temperature (°C) for modified and unmodified versions of potato starch | 63 |
| Figure 3. 19 Thermograms of modified and unmodified versions of tamarind at 60°C min ⁻¹ | 64 |
| Figure 3. 20 Plot of the dm/dT vs. temperature (°C) for modified and unmodified versions of tamarind..... | 64 |
| Figure 3. 21 Thermograms of modified and unmodified versions of agar agar at 60°C min ⁻¹ | 65 |
| Figure 3. 22 Plot of the dm/dT vs. temperature (°C) for modified and unmodified versions of agar agar | 65 |
| Figure 3. 23 Thermograms of modified and unmodified versions of chitosan at 60°C min ⁻¹ .. | 66 |
| Figure 3. 24 Plot of the dm/dT vs. temperature (°C) for modified and unmodified versions of chitosan | 66 |
| Figure 3. 25 A plot of log β vs. 1/T at various α values (given as the inset) for β-cyclodextrin | 68 |
| Figure 3. 26 A plot of log β vs. 1/T at various α values (given as the inset) for dextran | 69 |
| Figure 3. 27 A plot of log β vs. 1/T at various α values (given as the inset) for potato starch | 69 |
| Figure 3. 28 A plot of log β vs. 1/T at various α values (given as the inset) for tamarind | 70 |
| Figure 3. 29 A plot of log β vs. 1/T at various α values (given as the inset) for agar agar..... | 70 |
| Figure 3. 30 A plot of log β vs. 1/T at various α values (given as the inset) for chitosan | 71 |
| Figure 3. 31 An overlay of TGA at 10°C min ⁻¹ of all the six substrates | 76 |

| | |
|---|----|
| Figure 3. 32 A schematic diagram of the pyrolysis combustion flow calorimetry (PCFC) | 79 |
| Figure 3. 33 Plot of the heat release rate (HRR) (Wg ⁻¹) vs. temperature (°C) for modified and unmodified versions of β -cyclodextrin | 83 |
| Figure 3. 34 Plot of heat release rate (HRR) (Wg ⁻¹) vs. temperature (°C) for modified and unmodified versions of dextran | 83 |
| Figure 3. 35 Plot of heat release rates (HRR) (Wg ⁻¹) vs. temperature (°C) for modified and unmodified versions of potato starch. | 84 |
| Figure 3. 36 Plot of heat release rates (HRR) (Wg ⁻¹) vs. temperature (°C) for modified and unmodified versions of agar..... | 84 |
| Figure 3. 37 Plot of heat release rates (HRR) (Wg ⁻¹) vs. temperature (°C) for modified and unmodified versions of tamarind. | 85 |
| Figure 3. 38 Plot of heat release rates (HRR) (Wg ⁻¹) vs. temperature (°C) for modified and unmodified versions of chitosan..... | 85 |
| Figure 3. 39 Plots of the first derivative of the thermogram (60°C min ⁻¹) and HRR (from PCFC) for β -cyclodextrin | 87 |
| Figure 3. 40 Plots of the first derivative of the thermogram (60°C min ⁻¹) and HRR (from PCFC) for modified β -cyclodextrin | 87 |
| Figure 3. 41 Plots of the first derivative of the thermogram (60°C min ⁻¹) and HRR (from PCFC) for dextran..... | 88 |
| Figure 3. 42 Plots of the first derivative of the thermogram (60°C min ⁻¹) and HRR (from PCFC) for modified dextran..... | 88 |
| Figure 3. 43 Plots of the first derivative of the thermogram (60°C min ⁻¹) and HRR (from PCFC) for potato starch..... | 89 |
| Figure 3. 44 Plots of the first derivative of the thermogram (60°C min ⁻¹) and HRR (from PCFC) for modified potato starch..... | 89 |
| Figure 3. 45 Plots of the first derivative of the thermogram (60°C min ⁻¹) and HRR (from PCFC) for agar agar..... | 90 |
| Figure 3. 46 Plots of the first derivative of the thermogram (60°C min ⁻¹) and HRR (from PCFC) for modified agar agar..... | 90 |
| Figure 3. 47 Plots of the first derivative of the thermogram (60°C min ⁻¹) and HRR (from PCFC) for tamarind | 91 |
| Figure 3. 48 Plots of the first derivative of the thermogram (60°C min ⁻¹) and HRR (from PCFC) for modified tamarind | 91 |

| | |
|--|------------|
| <i>Figure 3. 49 Plots of the first derivative of the thermogram (60°C min⁻¹) and HRR (from PCFC) for chitosan</i> | <i>92</i> |
| <i>Figure 3. 50 Plots of the first derivative of the thermogram (60°C min⁻¹) and HRR (from PCFC) for modified chitosan</i> | <i>92</i> |
| <i>Figure 3. 51 Correlation of char residues (wt. %) from TGA experiments and PCFC runs of the substrates</i> | <i>93</i> |
| <i>Figure 3. 52 Correlation of char residues (wt. %) from TGA experiments and PCFC runs of the substrates vs. P wt. %.....</i> | <i>94</i> |
| <i>Figure 3. 53 Plot of heat release capacity (J g⁻¹K⁻¹) from PCFC experiments vs. P wt. %</i> | <i>95</i> |
| <i>Figure 3. 54 Plot of total heat release (kJ g⁻¹) from PCFC experiments vs. P wt. %.....</i> | <i>95</i> |
| <i>Figure 3. 55 Plot of peak heat release rate (W g⁻¹) from PCFC experiments vs. P wt. %</i> | <i>96</i> |
| <i>Figure 3. 56 Plot of calculated heats of combustion (kJ g⁻¹) vs. P wt. %.....</i> | <i>96</i> |
| <i>Figure 3. 57 A plot of activation energy of the base substrates vs. total heat release rates for unmodified substrates</i> | <i>97</i> |
| <i>Figure 3. 58 A plot of activation energy vs. apparent heats of combustion for unmodified substrates</i> | <i>98</i> |
| <i>Figure 3. 59 A plot of activation energy vs. heat release capacity for unmodified substrates</i> | <i>98</i> |
| <i>Figure 3. 60 A plot of activation energy vs. peak heat release rate for unmodified substrates</i> | <i>99</i> |
| <i>Figure 3. 61 An overlay of the HRR curves vs. time for uncoated and coated timber plaques from cone tests</i> | <i>104</i> |
| <i>Figure 3. 62 Thermograms of virgin and a physical mixture of fish gelatin containing sodium carbonate (SC) at 60°C min⁻¹.....</i> | <i>105</i> |
| <i>Figure 3. 63 Thermograms of virgin and a physical mixture of fish gelatin containing diammoniumhydrogenphosphate (AP) at 60°C min⁻¹</i> | <i>106</i> |
| <i>Figure 3. 64 Thermograms of virgin and a physical mixture of fish gelatin containing triphenylphosphine (TPP) at 60°C min⁻¹.....</i> | <i>106</i> |
| <i>Figure 3. 65 Thermograms of virgin and a physical mixture of fish gelatin containing triphenylphosphineoxide (TPPO) at 60°C min⁻¹.....</i> | <i>107</i> |
| <i>Figure 3. 66 Thermograms of virgin and a physical mixture of fish gelatin containing 9,10-dihydro-9-oxa-10-phosphahenanthrene-10-oxide (DOPO) at 60°C min⁻¹.....</i> | <i>107</i> |
| <i>Figure 3. 67 Thermograms of virgin and a physical mixture of fish gelatin containing diethylphosphite (DEPi) at 60°C min⁻¹</i> | <i>108</i> |

| | |
|--|-----|
| Figure 3. 68 Thermograms of virgin and a physical mixture of fish gelatin containing triethylphosphite (TEPi) at 60°C min ⁻¹ | 108 |
| Figure 3. 69 Thermograms of virgin and a physical mixture of fish gelatin containing triethylphosphite (TEPa) at 60°C min ⁻¹ | 109 |
| Figure 3. 70 Thermograms of virgin and a physical mixture of fish gelatin containing diethylpropylphosphonate (DEPP) at 60°C min ⁻¹ | 109 |
| Figure 3. 71 Thermograms of virgin and a physical mixture of fish gelatin containing diethylbenzylphosphonate (DEBP) at 60°C min ⁻¹ | 110 |
| Figure 3. 72 A plot of char residue (wt. %) from TGA and P-loading (wt. %)..... | 112 |
| Figure 3. 73 A plot of char residue (wt. %) from PCFC and P-loading (wt. %) | 112 |
| Figure 3. 74 A plot of char pHRR (W g ⁻¹) from PCFC and P-loading (wt. %)..... | 113 |
| Figure 3. 75 A plot of THR (kJ g ⁻¹) from PCFC and P-loading (wt. %) | 113 |
| Figure 3. 76 A plot of HRC (J g ⁻¹ K ⁻¹) from PCFC and P-loading (wt. %)..... | 114 |
| Figure 3. 77 A plot of h _c (kJ g ⁻¹) from PCFC and P-loading (wt. %)..... | 114 |
| Figure 3. 78 A plot of the char residue (wt. %) from PCFC and char residue (wt. %) from TGA | 115 |
| Figure 3. 79 Solid-state ³¹ P-NMR spectrum of char obtained from fish gelatin + TPP | 119 |
| Figure 3. 80 Solid-state ³¹ P-NMR spectrum of char obtained from fish gelatin + TPPO ... | 119 |
| Figure 3. 81 Solid-state ³¹ P-NMR spectrum of char obtained from fish gelatin + DOPO ... | 120 |
| Figure 3. 82 Solid-state ³¹ P-NMR spectrum of char obtained from fish gelatin + (NH ₄) ₂ HPO ₄ | 120 |
| Figure 3. 83 Solid-state ³¹ P-NMR spectrum of char obtained from fish gelatin + diethylphosphite (DEPi)..... | 121 |
| Figure 3. 84 Solid-state ³¹ P-NMR spectrum of char obtained from fish gelatin + triethylphosphite (TEPi)..... | 121 |
| Figure 3. 85 Solid-state ³¹ P-NMR spectrum of char obtained from fish gelatin + triethylphosphate (TEPa)..... | 122 |
| Figure 3. 86 Solid-state ³¹ P-NMR spectrum of char obtained from fish gelatin + diethylpropylphosphonate (DEPP) | 122 |
| Figure 3. 87 Solid-state ³¹ P-NMR spectrum of char obtained from fish gelatin + diethylbenzylphosphonate (DEBP) | 123 |
| Figure 3. 88 Raman spectrum of the char residue from unprotected wood (Radiata Pine).. | 126 |
| Figure 3. 89 Possible fragmentation pattern for DEPi | 129 |
| Figure 3. 90 Possible fragmentation pattern for TEPi | 130 |

| | |
|---|-----|
| <i>Figure 3. 91 Possible fragmentation pattern for TEPA</i> | 130 |
| <i>Figure 3. 92 Possible fragmentation pattern of DEBP</i> | 131 |
| <i>Figure 3. 93 Possible fragmentation pattern of DEBP</i> | 131 |
| <i>Figure 3. 94 TGA of diammoniumhydrogen phosphate in nitrogen under a heating rate of 10°C min⁻¹</i> | 132 |
| <i>Figure 3. 95 Scheme showing the first step in the decomposition of (NH₄)₂HPO₄</i> | 132 |
| <i>Figure 3. 96 TGA curve of TPP in nitrogen under a heating rate of 10°C min⁻¹</i> | 133 |
| <i>Figure 3. 97 First derivative of the TGA curve of TPP in nitrogen under a heating rate of 10°C min⁻¹</i> | 133 |
| <i>Figure 3. 98 GC and MS of TPP (pyrolysis temperature (288°C))</i> | 134 |
| <i>Figure 3. 99 TGA curve of TPPO in nitrogen under a heating rate of 10°C min⁻¹</i> | 134 |
| <i>Figure 3. 100 First derivative of the TGA curve of TPPO in nitrogen under a heating rate of 10°C min⁻¹</i> | 135 |
| <i>Figure 3. 101 GC and MS of TPPO (pyrolysis temperature: 340°C)</i> | 136 |
| <i>Figure 3. 102 TGA curve of TPPO in nitrogen under a heating rate of 10°C min⁻¹</i> | 136 |
| <i>Figure 3. 103 First derivative of the TGA curve of DOPO in nitrogen under a heating rate of 10°C min⁻¹</i> | 137 |
| <i>Figure 3. 104 GC and MS of DOPO (pyrolysis temperature (381°C))</i> | 137 |
| <i>Figure 3. 105 A schematic diagram of production of phosphorus-centred species in the gaseous phase in the case of solid organophosphorus additives</i> | 139 |
| <i>Figure 3. 106 A general schematic diagram of production of phosphorus acidic species, in the condensed phase through the elimination of ethene from the ester side arms of the liquid additive</i> | 140 |

Legends to tables:

Chapter 2

| | |
|--|-----------|
| <i>Table 2. 1 Details of chemical modification reactions</i> | <i>22</i> |
| <i>Table 2. 2 Details of the regarding the constitutions of the formulations for the passive fire protection coatings.....</i> | <i>24</i> |
| <i>Table 2. 3 Values of abscissa and ordinate for tamarind for the FWO method</i> | <i>37</i> |

Chapter 3

| | |
|---|------------|
| <i>Table 3. 1 Characterization data of the phosphorylated products</i> | <i>45</i> |
| <i>Table 3. 2 Details regarding the chemical environments of the P-containing organic additives</i> | <i>56</i> |
| <i>Table 3. 3 Details from TGA analyses</i> | <i>60</i> |
| <i>Table 3. 4 Activation energies of each substrates for different α values</i> | <i>71</i> |
| <i>Table 3. 5 Relevant parameters obtained using the FWO and SB methods</i> | <i>76</i> |
| <i>Table 3. 6 Details regarding various outputs from the SB method in the case of chitosan (as an example).....</i> | <i>77</i> |
| <i>Table 3. 7 PCFC data for modified and unmodified versions of base substrates</i> | <i>80</i> |
| <i>Table 3. 8 Heats of combustion values of various formulations.....</i> | <i>82</i> |
| <i>Table 3. 9 Time to ignition for test samples coated with various formulation (from the dip test)</i> | <i>101</i> |
| <i>Table 3. 10 Relevant parameters from cone measurements</i> | <i>103</i> |
| <i>Table 3. 11 Relevant parameters from PCFC tests of the coatings (fish gelatin as the base matrix).....</i> | <i>111</i> |
| <i>Table 3. 12 Phosphorus contents, determined through ICP/OES measurement, in coating formulations and the corresponding char residues</i> | <i>118</i> |
| <i>Table 3. 13 Chemical shift values (δ in ppm) of P nucleus in the additives and in the char residue.....</i> | <i>124</i> |
| <i>Table 3. 14 Details of Raman spectra of char residue</i> | <i>126</i> |
| <i>Table 3. 15 Retention times and fragmentation features of the various liquid additives</i> | <i>124</i> |
| <i>Table 3.16 Retention times and fragmentation features of various solid additives.....</i> | <i>135</i> |

CHAPTER 1: INTRODUCTION AND LITERATURE REVIEW

1.1 Background

Wildland fires, or bushfires, pose significant risks to life, economy and to the surrounding ecosystem. The Ash Wednesday fires (1983), Black Friday fires (1939), Gippsland fires and Black Sunday fires (1926) are some of the most destructive bushfires that took place in Australia. It is estimated that, owing to bushfires, approximately 6500 houses were destroyed between 1939 and 1997 in Australia alone (Justin Leonard & McArthur, 1999). Furthermore, the Black Saturday fires (2009), Black Christmas bushfires (2002), Canberra bushfires (2003) and Great Ocean Road bushfire (2015/2016) caused destruction of several hundreds of houses. The devastating effects of bush fires were also quite evident in the recent and unprecedented episodes that occurred in 2019/2020 summer. The 2019/2020 Australian bushfire season have destroyed more than 5900 buildings including 3048 homes (Benfield, 2020). Significant parts of these homes are made of wood-based materials, thus causing fire initiation from radiant heat, direct flame contact, or ember attacks. These findings are not only relevant to buildings in the Australian context, but are also recognised as critical factors of wildfire-related building destruction in other parts of the world including the United States and Canada. These unwanted events essentially indicate the need for extensive studies on the phenomenon of ignition and flame spread in fuel loads involving ligno-cellulosic materials, and the subsequent necessity to prevent them from causing large scale destruction to life and property. Furthermore, such studies will help to provide the sufficient input for fire safety engineers to predict fire behaviour of ligno-cellulosic materials and help to design strategies to mitigate the ensuing fire hazards involving them.

Fire being a very complex phenomenon have been the subject of many research, some of which include: analysing the fatalities associated with the occurrence of bushfires (Raphaelle Blanchi et al., 2014; Haynes, Handmer, McAneney, Tibbits, & Coates, 2010; McInnes et al., 2019); studying the impact of bushfires from an ecological perspective (Reid et al., 2016; Yates, Edwards, & Russell-Smith, 2009); evaluating the mechanism and ignitability of buildings during bushfires (Blanchi, Leonard, & Leicester, 2006; Leonard, Blanchi, & Bowditch, 2004; Justin Leonard & Bowditch, 2003; McArthur & Lutton, 1991); etc. However, only relatively very few studies have endeavoured to investigate the ignition of wood-based components, in detail, when used as external structural elements in Wildland Urban Interface (WUI) (Bakar, 2015; Hagen, Hereid, Delichatsios, Zhang, & Bakirtzis, 2009; Kozłowski & Władysław-Przybylak, 2008).

Bushfires are now being perceived as catastrophic events, which are beyond man's ability to control; hence, there is an urgent need to design mitigation strategies to help manage bushfires from causing damage to life/ property (Justin Leonard & Bowditch, 2003). It is highly important to reduce the propensity of ignition of timber-based materials, especially, when they form parts of structural elements outside buildings in the WUI. This could include fencing, decking, façade structures and wall linings, particularly in residential buildings. Most often, ignition and flaming combustion of such structural components stems from embers that are lofted around from a moving flame front associated with bush fires (Trucchia, Egorova, Butenko, Kaur, & Pagnini, 2019; Wadhvani, 2019; Wadhvani, Sutherland, & Moinuddin, 2019). Hence, it is prudent to devise means of passively protecting the vulnerable exposed structures of the timber elements. *Therefore, the current research topic was primarily formulated with a view to reducing the ignition propensity and flame spread of structural elements made of wood, through developing and testing of some bio-inspired passive protective coatings.*

1.2 Ligno-cellulosic materials: degradation and combustion behaviour

Responsibly harvested timber have been long identified as an effective means of reducing the over-dependence on fossil fuels (Freedman, Stinson, & Lacoul, 2009). Wood/ timber has been used as a construction material, globally, for thousands of years, primarily owing to their desirable properties like high strength to weight ratio, ease of availability, durability etc. Moreover, there is ample global supply for the foreseeable future, despite the worldwide trend towards deforestation. Recently, there has been also a renewed interest in the fabrication of products from timber, especially, for their use in high-rise buildings, which can be attributed to their environmentally benign nature and a near carbon neutrality. Also, modern timber is largely factory prepared and pre-fabricated which makes it easy to be brought to site for easy and fast assembly. This particularly makes timber construction more economical, cleaner, greener and smarter. Furthermore, the use of timber for construction can significantly reduce the environmental impact of construction over the other commonly used construction elements like steel and reinforced concrete (Buchanan & Levine, 1999; Freedman et al., 2009; Gustavsson & Sathre, 2006). In addition to the above benefits, being aesthetically pleasing, wood plays an integral part of building infrastructures in Australia, and provides as a main source of construction in homes/building infrastructures.

However, one important factor which limits the usage of timber as a building material, particularly in larger and high-rise buildings, are their combustible nature (Aseeva, Serkov, & Sivenkov, 2014). As fire safety is an important criterion of choice for determining the best building material to be used for construction, it is important to address this issue and design strategies to enhance their fire resistance. Furthermore, to design strategies and techniques, it is imperative to elaborately study their structure, properties, composition, and behaviour in real fire scenarios.

Wood is mainly composed of three components mainly: cellulose, hemicellulose and lignin. Among these three, the cellulose provides the mechanical and tensile strength of the matrix (Kishore & Mohandas, 1982; Mohan, Pittman Jr, & Steele, 2006). Cellulose is composed of long linear chains of *D*-glucose linked by β -1,4-glycosidic bonds, with a degree of polymerisation from 10,000 in some native wood species. Each of these chain units possess hydroxyl (-OH) groups at C₂, C₃ and C₆ positions, which has a strong tendency to form intra- and inter-molecular hydrogen bonds, that stiffen the chain and promotes a crystalline fibre structure and morphology. Furthermore, the cellulose imparts the tensile strength of the wood matrix, thereby enhancing the workability of the materials and their use in the construction industry. Generally, cellulose has a tendency to form crystals utilizing extensive intramolecular and intermolecular hydrogen bonding, thus making it completely insoluble in normal aqueous solutions.

Hemicellulose is the second major component of wood and are also known by the term, 'polyose'. Hemicellulose can be considered as a mixture of several components based on monosaccharides, such as, glucose, mannose, galactose, xylose, arabinose, and 4-*O*-methyl glucuronic acid and galacturonic acid residues. Generally, the degree of polymerisation in hemicellulose is relatively low than that of cellulose (for instance, the degree of polymerization of hemicellulose is typically around 50-300). It grows around the cellulosic fibres and are a group of non-structural, low molecular weight polysaccharides that are mostly heterogeneous in nature. It is to be noted here that hemicellulose primarily consists of heteropolysaccharide chains with short side-chains, whereas cellulose has mainly repeated units of glucose as the main structural feature.

The third major component of wood is lignin. It accounts for around 20-30 wt. % of wood, and primarily functions as a binding material that gives an overall rigidity to the wood. Primarily, lignin accounts for the compressive, shear strength of wood, and also significantly contributes

towards the rigid structure of wood (Babrauskas, 2002; Lowden & Hull, 2013; Rowell, 1984). Lignin has a cross-linked and three-dimensional structure, produced during their biosynthesis through radical dimerization and subsequent oligomerization of the constituent structural moieties.

Wood used in the construction/building industry can be broadly categorised into two: soft wood and hard wood. Generally, softwoods are those that originate from mostly coniferous trees (gymnosperms) and hardwoods are those that come from flowering plants (angiosperms). In softwood, the main cell is the tracheid, which constitutes almost 90% of their volume. In hardwoods, around 50% constitutes for fibre and fibre tracheids and are considerably shorter and thick walled than softwood tracheids (Lowden & Hull, 2013; Rowell, 1984). Furthermore, it may be noted that the arrangement of cells (tracheids, fibres etc.) in wood significantly contributes to their specific physical and chemical properties. The macroscopic characteristics of hardwood may be attributed to their varied distribution and variety of cells including the vessels (pores), parenchyma and fibres. The cellulose content is almost the same for both soft wood and hardwood; however, differences are found in the constituencies of lignin and hemicellulose. Lignin content in softwood accounts for around 25-35% and 18-25% in hardwoods. Variations are studied in the structure of lignin, wherein the former (softwood) are composed of guaiacyl units and the latter (hard wood) consists of syringyl and guaiacyl moieties. Owing to increased growth and vast availability, most softwoods are cheaper than hardwood (Lowden & Hull, 2013). Here again, distinctions in both structure and quality of hemicellulose have been identified in softwood and hardwood, where the main hemicellulose of softwood are galactoglucomannans and glucuronoarabinoxylan (10-18%). On the other hand, the hardwood hemicellulose is partly acetylated glucuronoxyylan (20-35%) and only a small quantity of glucomannan.

The thermal decomposition of wood in significantly low oxygen levels is termed as pyrolysis (Aseeva et al., 2014; Mohan et al., 2006; Poletto, Zattera, & Santana, 2012). When wood is exposed to high temperatures, the polymeric components of wood thermally decompose to laevoglucosan (1,6-anhydro- β -D-glucopyranose), char and also releases other volatile gases. Hemicellulose breakdown occurs during 180-350°C, followed by cellulose breakdown at 275-350°C and lignin breakdown at 250-500°C (Östman, Voss, Hughes, Jostein Hovde, & Grexa, 2001) (see Figure 1. 1).

The higher thermal stability of lignin may be attributed to their high molecular weight and their complex cross-linked structure. Depending on the operating conditions used, the process of pyrolysis may be subjectively classified as conventional and fast pyrolysis (Bridgwater, Meier, & Radlein, 1999; Mohan et al., 2006). Numerous studies have focussed on the pyrolysis of wood and their results indicate that although charred wood temperatures can be as high as 800°C, the main process of pyrolysis complete at around 500°C (Di Blasi, Signorelli, Di Russo, & Rea, 1999; Diertenberger & Hasburgh, 2016; Yang et al., 2006). Once the appropriate volatile-air fuel concentration has been reached, flaming combustion occurs due to the oxidation of the pyrolysed gases, whereas, further oxidation of the remaining char produces glowing or smouldering combustion (Babrauskas, 2002) (Figure 1. 2). Further studies have shown that above 500°C, volatile gas production are complete and the remaining char continues to smoulder and oxidise to form gases like carbon monoxide, carbon dioxide and water (Babrauskas, 2002; Diertenberger, 2002; White & Diertenberger, 2001).

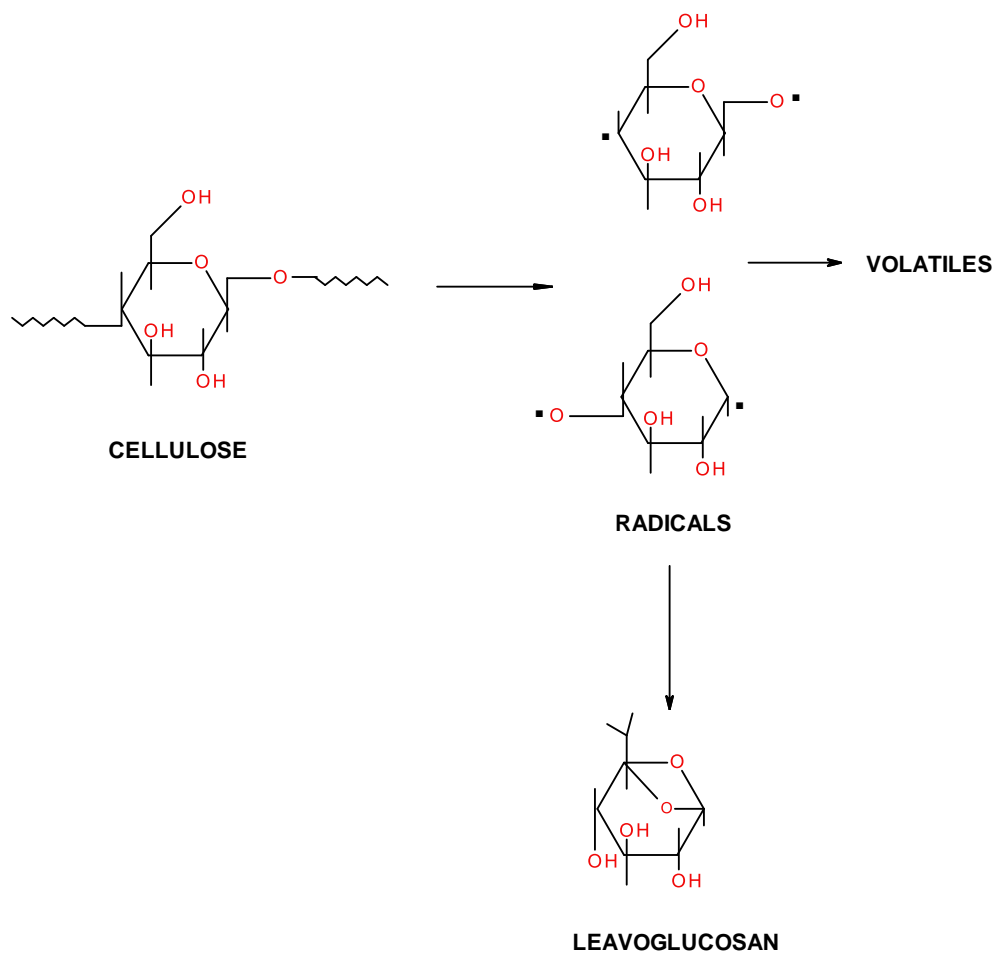


Figure 1. 1 Degradation pathway of cellulose, through a radical mechanism, resulting in the production of laevoglucosan

In order to understand the behaviour of wood in an event of fire, it is necessary to understand their process of decomposition. Generally, these processes are highly dependent on various parameters including temperatures, heating rate, gas composition etc. (Qu, Wu, Wu, Xie, & Xu, 2011; Spearpoint & Quintiere, 2001). Hence, data generated by conducting experiments on varying parameters can provide a deep insight on the fire behaviour of a material. According to a seminal report (Spearpoint & Quintiere, 2001), flammability of a material cannot be represented as a single value, but requires simultaneous consideration of a variety of parameters including ease of ignition, flame spread, heat release rates, peak heat release rate, heat release capacity, etc.

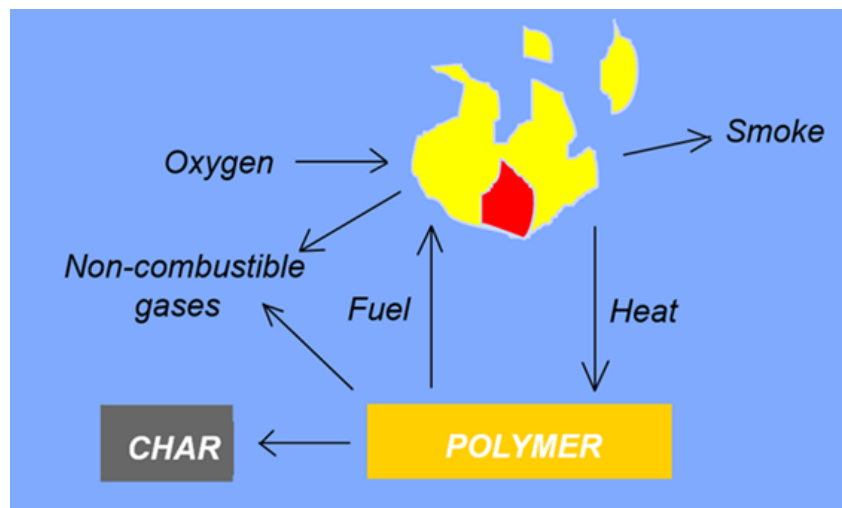


Figure 1. 2 Combustion cycle of a polymeric solid fuel (for example wood)

1.3 Combustion hazards of ligno-cellulosic materials in the context of bushfires

Post-fire studies in the Wildland Urban Interface has identified that ember attack are one of the most significant reasons for the ignition of structural elements (Abt, Kelly, & Kuypers, 1987; Barrow, 1944; Maranghides & Mell, 2009). This aspect is highly relevant in the context of the current project as we envisage that embers constitute the primary agent in initiating the ignition of timber-based construction elements when present outside residential buildings. The mechanistic aspect of ‘spot fires’ through ember attack remained an area largely unexplored, as it was difficult to replicate the process of wind driven ember attack on structures, until the

National Institute of Standards and Technology (NIST), USA, fabricated an ember generator, known as the 'Fire Dragon'. The NIST 'Fire Dragon' are capable of simulating wind driven embers (glowing or flaming), and can also generate repeatable ember showers similar to those emanating from burning conifers in real Wildland Urban Interfaces (Manzello & Suzuki, 2013). However, the CFD model of the NIST 'Fire Dragon' was found to show a non-uniform fluid velocity profile at the 'mouth' part of the model (Manzello, Cleary, Shields, & Yang, 2006; Manzello & Suzuki, 2013). As an extension to the NIST 'Fire Dragon', a similar firebrand generator prototype have been constructed at Institute of Sustainable Industries and Liveable Cities (ISILC), Victoria University, in recent years. This laboratory-scale firebrand generator is designed in such a way that it generates a uniform velocity profile, which equips it to be utilised for analysing the aerodynamics and scattering patterns of embers in a better way (Wadhvani, Sutherland, Ooi, Moinuddin, & Thorpe, 2017).

Several other studies have also focussed on determining the trajectories and burning rates of embers lofted by ground fire plumes. Burning rates of cylindrical and spherical shapes of various wood species were experimentally determined and further used to determine the maximum range of fire spread by using the assumption that embers fly at their terminal velocity of fall (Mahmud, 2016; Tarifa, Del Notario, & Moreno, 1965). This concept was further researched on and extended, and a model where lofting of embers by line thermals and fire plumes were postulated which also discussed the effect of wind and their impact on fire intensity (Albini, 1983). Furthermore, trajectories of spherical ember and metallic particles thrown at a given elevated height were studied (Tse & Fernandez-Pello, 1998). As an extension of this work, a model that was capable of addressing embers thrown from ground level or from an elevated height was developed (Anthenien, Stephen, & Fernandez-Pello, 2006). This numerical model can be used for predicting the trajectories that assist in numerically predicting the trajectories of embers that are in spherical, cylindrical or disk shaped. This model can be utilised in the present research project by using spherical, cylindrical and disk-shaped embers for the experiment.

Generally, there are two approaches for protecting infrastructures from fire attack, *viz.*, active fire protection and passive fire protection (Cozzani, Tugnoli, & Salzano, 2007). The former approach involves strategies that prevent from escalating the event (for e.g. water cooling systems like sprinklers). The latter approach involves a design/installation of a physical protection system to mitigate the effects of damage in a possible fire scenario (Correia, Branco, & Ferreira, 2010). In the context of protecting buildings from destructive fires, this approach

generally involves using paints/ coatings to improve the time to ignition, flame spread and total heat release rate (Lowden & Hull, 2013).

According to some researchers (Correia et al., 2010; Cozzani et al., 2007), active fire protection techniques are considered to be less reliable in terms of inhibiting a fire event to occur. On the other hand, recent studies have shown that passively coating building infrastructures greatly improved their fire reaction properties and have resulted in significant improvement on post-fire mechanical properties (Lau, Qiu, Zhou, & Chow, 2016; Sorathia, Beck, & Dapp, 1993). The primary aim of the passive protective agents is to delay the time to ignition and to effectively reduce the rate of heat release during the combustion process. The efficacy of these coatings can be determined by exposing them to different heat fluxes and studying their corresponding behaviours (Correia et al., 2010).

1.4 Common methods to enhance the fire resistance of ligno-cellulosic materials

Cellulose-based materials have been long identified to be materials having high risk of ignition and flame spread (Mindykowski, Fuentes, Consalvi & Porterie, 2011). Hence, several flame retardant additives have been developed to enhance their fire behaviours. One of the earliest fire retardants used on cellulosic materials involves the usage of alum solutions on wooden walls to make it fire resistant. In 1820, Gay-Lussac proposed a flame-retardant system based on ammonium phosphate combined with boric acid, alum solution and iron sulphate (LeVan, 1984). This is often referred to as one of the earliest phosphorous-based flame retardants reported in the literature. Generally, phosphorus-based compounds have shown to be one of the most efficient systems for fire proofing cellulosic materials (Gaan & Sun, 2007; Levchik & Weil, 2006; Liodakis, Fetsis, & Agiovlasis, 2009).

Many of the fire retardant compounds used today, require organic synthetic procedures that rely on fossil fuels and have been known to directly deteriorate our environment. Currently, there are several fire retardant chemicals used on wood, such as monoammonium phosphate (MAP), aluminium hydroxide, magnesium hydroxide, zinc borate, melamine, etc. However, several drawbacks have been observed associated with these compounds with the required loadings, such as, emission of toxic gases, and higher sensitivity to moisture, with the potential of increasing the moisture content of timber under humid conditions, etc. (Candan, Ayilimis, & Akbulut, 2011; Terzi, Kartal, White, Shinoda, & Imamura, 2011). Moreover, these compounds have been identified to be hazardous to human health (Batayneh, 2012).

Furthermore, many of the synthetic organic materials like halogenated fire retardant materials have been banned by national and international regulatory bodies in the last few decades. Taking into account these drawbacks addressed by the previous literature, the current research focused on developing safer alternatives to the currently used toxic fire retardant materials (Costes, Laoutid, Brohez, & Dubois, 2017; Daniel & Howell, 2017a, 2017b; Bob Howell, 2007; B. A. Howell, Oberdorfer, & Ostrander, 2018; Illy et al., 2015; Jones et al., 2018; Muhammad, Hussin, Man, Ghazali, & Kennedy, 2000; Sag et al., 2019).

Prior to discussing currently used bio-based fire retardant materials, it is important to understand the mechanisms of flame retardancy. This mainly occurs through two routes namely, condensed phase and vapour phase, or a combination of these routes. The former, mainly involves the formation of a char layer that acts as a barrier in the spread of the flame, by limiting the transfer of heat and oxygen to the material and eventually extinguishes the flame. The latter involves interrupting the radical gas phase of a fire, or in other words by disrupting the phase where the flammable gas are cooled, and thus their supply are reduced or suppressed (Joseph & Tretsiakova-Mcnally, 2011) (see Figure 1. 3). The mechanisms to enhance the flame retardancy of wood involves: varying the pathway of wood pyrolysis, isolating the surface layer, modifying/changing the thermal properties of wood and diluting pyrolysis gases. Most of the commercially available flame retardants attempt to modify their pyrolysis pathway and thereby enhance the char formation (Aseeva et al., 2014; Kozlowski & Wladyka-Przybylak, 2001).

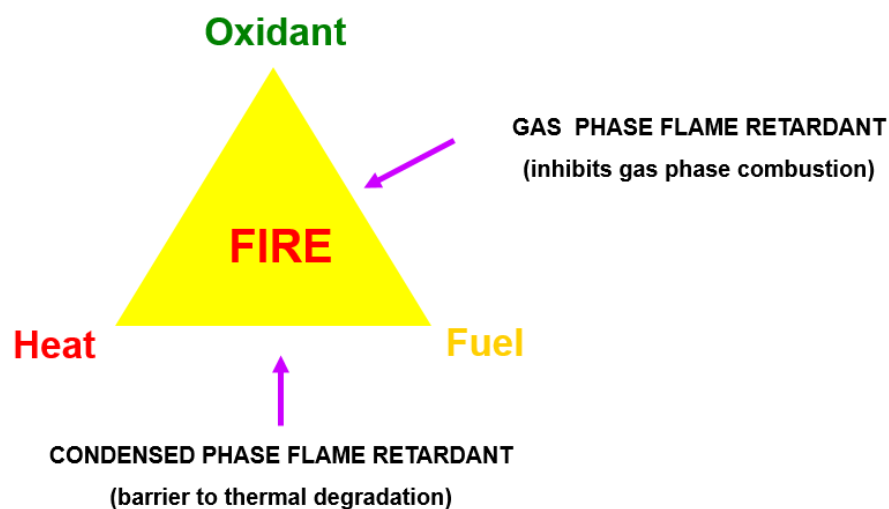


Figure 1. 3 Strategies to interrupt the combustion cycle

Charring properties of bio-based materials essentially improves their fire behaviours; however, their applicability is significantly reduced due to their general and overall higher combustible natures. For example, even though lignin provides excellent char yields at high temperatures, it significantly increases the ignitability; therefore, the material generates somewhat unreliable results in many standard prescription tests (Luda & Zanetti, 2019). In a study that analysed the burning behaviour of polypropylene that contained 20% lignin, the blend exhibited peak heat release rates that was three times lower than that of polypropylene. However, the time-to-ignition of the polypropylene-lignin complex had considerably decreased (Gallina et al., 1998). Nevertheless, polyhydric compounds are seen to be good charring agents in the presence of acid catalysts. Hence, carbohydrates have been recently identified to be worthy candidates for fire retardant formulations (Alongi, Pošković, Frache, & Trotta, 2010; Costes et al., 2017).

Starch is mainly used in intumescent flame-retardant systems as a carbon source (L. Wang, Sánchez-Soto, Abt, Maspoch, & Santana, 2016; X. Wang et al., 2010; Wu, Hu, Song, Lu, & Wang, 2009). Generally, intumescent systems require three components, which include an acid source, blowing agent and a carbonisation source. One of the most widely used intumescent system involves a combination of ammonium polyphosphate and pentaerythritol. Here, ammonium polyphosphate acts as an acid source (releases phosphoric acid) and as the blowing agent (releases ammonia), while pentaerythritol acts as the carbonisation agent. Studies have shown that a combination of starch and 1-5 wt. % of phosphorous and nitrogen containing compounds improves the fire behaviours of polylactic acid complexes mainly by decreasing their dripping behaviour (Fang et al., 2015). In another study, the researchers used a colloidal solution of potato starch and sea water on wood samples, which improved the overall flammability of the samples in terms of increased time to ignition and lower flame heights (Joseph, Bakirtzis, Richard, & Brulfert, 2017). Recently, wheat starch was chemically modified by a phosphate/urea system and used as an additive in wood fibres (Gebke et al., 2020). This study demonstrated that these systems have the potential to be used as alternatives to the commercially used flame retardants in the wood fibre industry. Their results from cone calorimetric runs and some smouldering tests indicated that a phosphate content of 3.5 wt. % gives the lowest levels of burning.

The oxidative modification of starch with copper and alkali salts gave excellent fire-retardant properties when applied to wood substrates as described in the literature (Sakharov, Sakharov, Lomakin, & Zaikov, 2014). Here, the observed fire-retardant behaviour are attributed, primarily, to the effect of oxidised starch having relatively high molecular weight that are

capable of forming a protective layer of char on the surface of the base matrix (wood). The char layer formed can act as an excellent heat-shielding barrier, thus impeding heat access to the wood surface and hence hindering the evolution of combustible gaseous products from the decomposition of wood. The fire-retardant efficiency of oxidized starch can be thought of emanating from their earlier thermal decomposition around 150 – 280 °C, resulting in the formation of the protective layer. This could also result in the reduction in the viscosity of starch, and associated intermolecular dehydration and decarboxylation reactions that enhance char production. The flammability of these samples were also tested using cone calorimetry, under an external heat flux of 35 kW m⁻², where the formation of an intumescent-type layer was also observed (Sakharov, Sakharov, Lomakin, & Zaikov, 2014).

Another related compound that has recently found application as a passive fire protecting agent is chitosan (Howell, Alomari, Dumitrescu, & Opperman, 2012). Chitosan is the deacetylated form of chitin, and are one of the few naturally occurring polymer which has an amino group pendent to their backbone. Over the recent years, chitosan has received much attention in flame retardant applications primarily owing to their carbohydrate structure containing hydroxyl groups, and can be used as char forming agents. Chitosan was chemically modified by a two-step chemical reaction and studied as a flame retardant in epoxy acrylate resin (Hu, Song, Pan, Hu, & Gong, 2012). In this reaction, phosphorous was grafted using phosphorous pentoxide in the first step, followed by glycidyl methacrylate groups in the second step. The modification provided an improvement in their char yield and enhanced their compatibility with epoxy acrylate resin. With increase in loading of this modified version of chitosan (glycidyl phosphorous chitosan), the fire behaviour of the material was improved. This modification in their thermal degradation mechanism enhanced the formation of char and further inhibited the release of combustible volatile products. In another study, an intumescent coating containing cationic chitosan and anionic ammonium phosphate was formed onto cotton fabric by a layer-by-layer assembly technique (Fang et al., 2015). This technique is a simple water-based technique to generate thin multilayer films, by alternatively assembling the deposition of positively and negatively charged nanoparticles on cellulosic substrates. Thermogravimetric analyses (TGA) of these substrates showed an increase in the amounts of char residue obtained at 700°C and a decrease in peak heat release rates and total heat release rates in pyrolysis combustion flow calorimetry (PCFC) tests than the uncoated substrates.

Oligosaccharides, such as β -cyclodextrin, has also attracted much interest as a fire retardant as they possess several hydroxyl groups and the charring process mainly involves opening of the

ring structure (Luda & Zanetti, 2019; Zhao, Xiao, Alonso, & Wang, 2017). It is followed by a loss of their glucosidic structures and hydroxyls, and build-up of carbonyl groups and aromatic structures similar to that of cellulose. Hence, they are tested as components of fire retardant formulations. Moreover, owing to their ability to form nano-sized structure and their ability to form inclusion complexes with other compounds are highly regarded. Alongi *et al.* illustrated the use of β -cyclodextrin as an intumescent flame retardant and as a nano-filler (Alongi *et al.*, 2010). This was prepared by crosslinking β -cyclodextrin units through carbonate linkages by mechanical grinding. These “nanosponges” trap low molecular weight phosphorous containing compounds, by acting as a synergistic flame retardant additive. These were then mechanically grinded with phosphorous containing compounds including triphenylphosphite, triethylphosphate, ammonium polyphosphate, dibasic ammonium phosphate and diethyl phosphoramidate, to make nanosponge phosphorous composites. Similarly, another study attempted to covalently modify β -cyclodextrin with phenylphosphonic dichloride (Feng, Su, & Zhu, 2011). This reaction involving a phosphorous containing compound would favour in generation of a phosphoric acid species upon combustion. This modified β -cyclodextrin compound was then used as a fire retardant additive in polylactic acid based composites. These were then analysed using TGA and clearly showed to be an effective flame retardant material.

Recently, a flame retardant film of agar agar, sodium alginate and boric acid were prepared through thermal solvent casting method (Hou, Xue, & Xia, 2018). This technique was repeated and prepared in the presence of varying concentrations of boric acid ranging from 2.5 to 15 wt. %. The flammability behaviour of the material were then tested using a vertical burning test which showed that increasing concentrations of boric acid exhibited enhanced fire behaviour of the material. Here, it is relevant to note that formulations with 10 and 15 wt. % of boric acid failed to undergo flaming combustion. However in other studies, agar agar did not give desirable results in flame retardancy in all circumstances, as expected. For example, in a study conducted by Wang *et al.*, aerogel composites based on xanthum gum and sodium montmorillonite clay were prepared using a freeze dry process (L. Wang, Schiraldi, & Sánchez-Soto, 2014). This study indicated that whilst the addition of agar to these composites enhanced the mechanical properties, their thermal stabilities were found to be inferior.

Fish gelatin was used to improve the compressive properties and flammability of polyvinyl alcohol (PVA) /montmorillonite aerogels, as reported in (Wang *et al.*, 2017). This may be attributed to the excellent compatibility and interfacial adhesion of PVA and gelatin. Cone calorimetric runs of these aerosols also showed significant decrease in the peak heat release

rates. Furthermore, the thermogravimetric analyses clearly showed that the incorporation of gelatin slowed down the decomposition of the PVA matrix, thereby improving their thermal stability. Another study used a vertical flammability test to rapidly screen flame retardant composition; a technique inspired from the UL-94 test (Deans, Li, Jefferson, & Schiraldi, 2018). In this test, wooden pieces (in the form of ‘tongue depressants’) were dipped in aqueous solutions of specific fire retardant solutions, and their respective flammability properties were analysed by performing a vertical burn test. The results showed that when tannic acid was used in combination with the required levels of fish gelatin, furnished optimum levels of fire proofing to the wood samples.

For the current project we have chosen a softwood variety of timber belonging to the Pine family (*Pinus radiata*) as the base substrate. Whilst the ease of ignition (especially when compared to the hardwood variety), and ensuing combustion hazards of softwood are well recognized, are often the material of choice for construction purpose, as they are less expensive, workable and almost readily available and can also be used on a broad range of applications (Boyd et al., 2007). Also, as softwood trees grow much faster than most hard wood tree varieties, it can be considered as a more renewable and sustainable resource. Moreover, in the Australian context, this variety is heavily used in construction and forms an integral part of structural elements, such as fencing, decking, façade, door frame, wall lining, etc. Hence we chose, Radiata Pine, a variety of softwood that is very commonly used in Australia for the purposes mentioned above. Through the current programme, we also endeavoured to develop bio-inspired fire-proofing agents by chemically incorporating phosphorus-containing moieties onto precursors obtained mainly from natural sources. The important feature of the research programme, therefore, was to develop bio-inspired compounds that can act as fire retardants (FR) with the aim of utilising them for protection/fabrication of soft wood-based construction materials.

1.5 The main aim of the project:

The overall aim of the research is to develop some bio-inspired fire-resistant protective coatings for construction elements based on timber with a view to reducing their ignition propensity and fire spread.

1.6 Individual objectives:

In order to achieve the overarching aim of the project the following individual objectives are identified:

1. To chemically modify some common carbohydrate-based substrates, such: β -cyclodextrin, dextran, agar agar, tamarind kernel powder, potato starch and chitosan, in a small scale (*ca.* 2 to 10 g)
2. To investigate the chemical nature and constitution of the modified substrates using spectroscopic techniques (FT-IR, solid-state NMR and ICP-OES)
3. To formulate mixtures of starch, rice bran, chitosan, fish gelatin with various inorganic and organic additives (these included: Na_2CO_3 (SC); $(\text{NH}_4)_2\text{HPO}_4$ (AP); triphenylphosphine (TPP); triphenylphosphineoxide (TPPO); 9,10-dihydro-9-oxa-10-phosphahenanthrene-10-oxide (DOPO); diethylphosphite (DEPi); triethylphosphite (TEPi); triethylphosphate (TEPa); diethylpropylphosphonate (DEPP) and diethylbenzylphosphonate (DEBP)
4. To analyze, in detail, the thermal degradation characteristics of the materials produced through 1 and 3 above by employing thermogravimetric analyses (TGA)
5. To gauge the ignition propensity and associated combustion parameters of the Radiata Pine and the chemical constituents of the formulations using an in-house test rig, PCFC and cone calorimetry
6. To characterize the morphology, elemental and chemical natures of the char residues using: Raman, solid-state NMR and Atomic Absorption (ICP-OES) spectroscopies
7. To analyze the gaseous phase-components from selected additives using hyphenated techniques (GC/MS and pyrolysis-GC/MS)
8. To develop analytical correlations among the various parameters obtained through experiments, such as TGA, PCFC and cone calorimetry, conducted on the base material and formulations
9. To deduce the apparent values of the activation energy of the base substrates, from thermograms obtained through the TGA measurements, using the Flynn-Wall-Ozawa method, and to test the validity of the corresponding results computed through the use an in-house software

CHAPTER 2: MATERIALS AND METHODS

2.1 Materials

The following carbohydrate-based materials were selected for the current study, and were obtained from Aldrich Chemical Company, except tamarind kernel powder that was sourced locally:

1. β -cyclodextrin
2. Dextran
3. Potato starch
4. Agar agar
5. Tamarind kernel powder
6. Chitosan
7. Rice bran
8. Fish gelatin

The reagents, solvents and other chemicals used for the preparative procedures were also primarily purchased from Aldrich Chemical Company, and included:

1. Diethylchlorophosphate (DECP)
2. Triethylamine (TEA)
3. Dichloromethane (DCM)
4. Nitric acid (HNO_3)
5. Sodium carbonate (Na_2CO_3) (SC)
6. Potassium carbonate (K_2CO_3)
7. Carbon tetrachloride (CCl_4)
8. Tetrahydrofuran (THF)
9. Diammonium hydrogen phosphate ($(\text{NH}_4)_2\text{HPO}_4$) (AP)
10. 9,10-dihydro-9-oxa-10-phosphahenanthrene-10-oxide (DOPO)
11. Triphenylphosphine (TPP)
12. Triphenylphosphineoxide (TPPO)
13. Diethylphosphite (DEPi)
14. Triethylphosphite (TEPi)
15. Triethylphosphate (TEPa)
16. Diethylpropylphosphonate (DEPP)

All the substrates, reagents and solvents were used as received, unless specified.

The chemical structures of the base materials are given below (Thomas, Joseph, Moinuddin, Zhu, & Tretsiakova-McNally, 2020):

I. β -cyclodextrin

β -cyclodextrins are seven membered sugar molecules with a cage-type structure that are produced from starch by enzymatic conversion (a representative structure is given below).

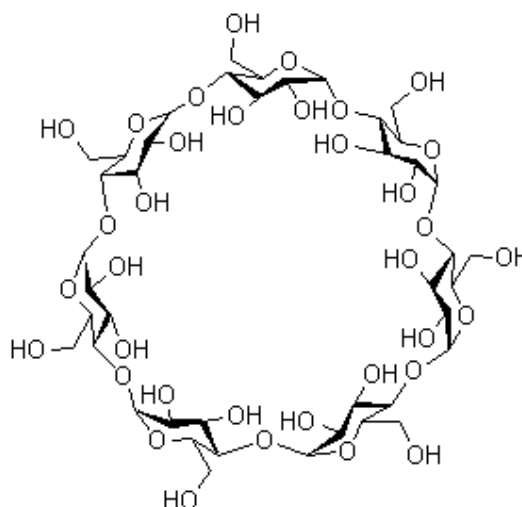


Figure 2. 1 Chemical structure of β -cyclodextrin

II. Potato starch

This is a polysaccharide that consists of large number of glucose units joined by α -glycosidic linkages, as shown below.

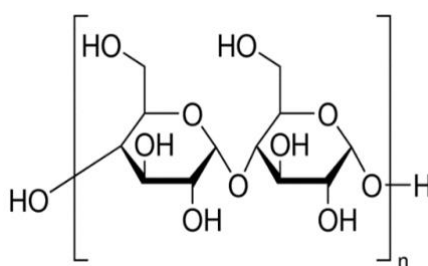


Figure 2. 2 Chemical Structure of potato starch

III. Dextran

Dextran can be considered as a derivative of starch, essentially, differing in the number and nature of the constituent molecular chains (i.e. chains are relatively shorter with a higher degree of branching).

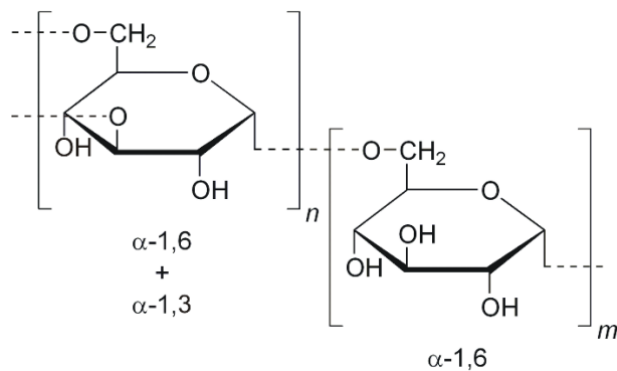


Figure 2. 3 Chemical structure of dextran

IV. Agar agar

Agar consists of a mixture of two types of polysaccharides- a linear polysaccharide agarose, and a heterogeneous mixture of smaller molecules called agarose and agarpectin.

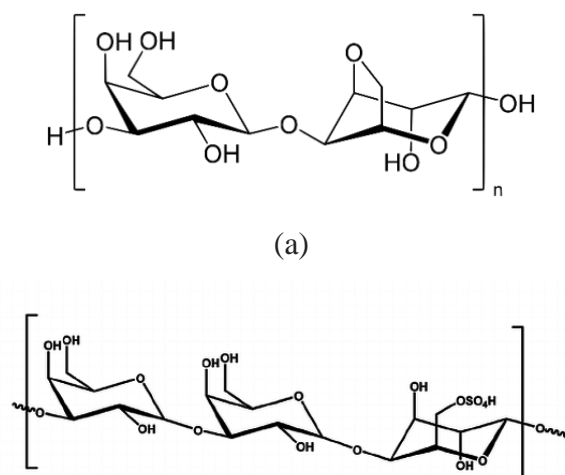


Figure 2. 4 Chemical structures of agarose (a) and agarpectin (b)

V. Tamarind kernel powder

Tamarind kernel powder primarily consists of a polysaccharide with an average molecular weight of *ca.* 52,000 and has a monomer constitution of mainly three sugars: glucose, galactose, and xylose, and generally in a molar ratio of 3:1:2.

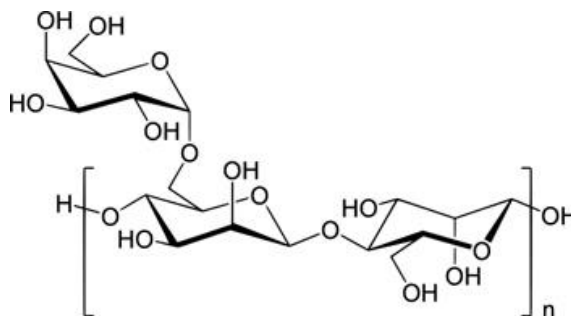


Figure 2. 5 Chemical structure (representative) of tamarind kernel powder

VI. Chitosan

Chitosan is generally obtained from the deacetylation of chitin, and are basically a glucose polymer containing amino pendant groups.

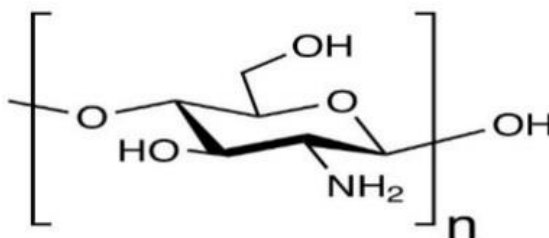


Figure 2. 6 Chemical structure of chitosan

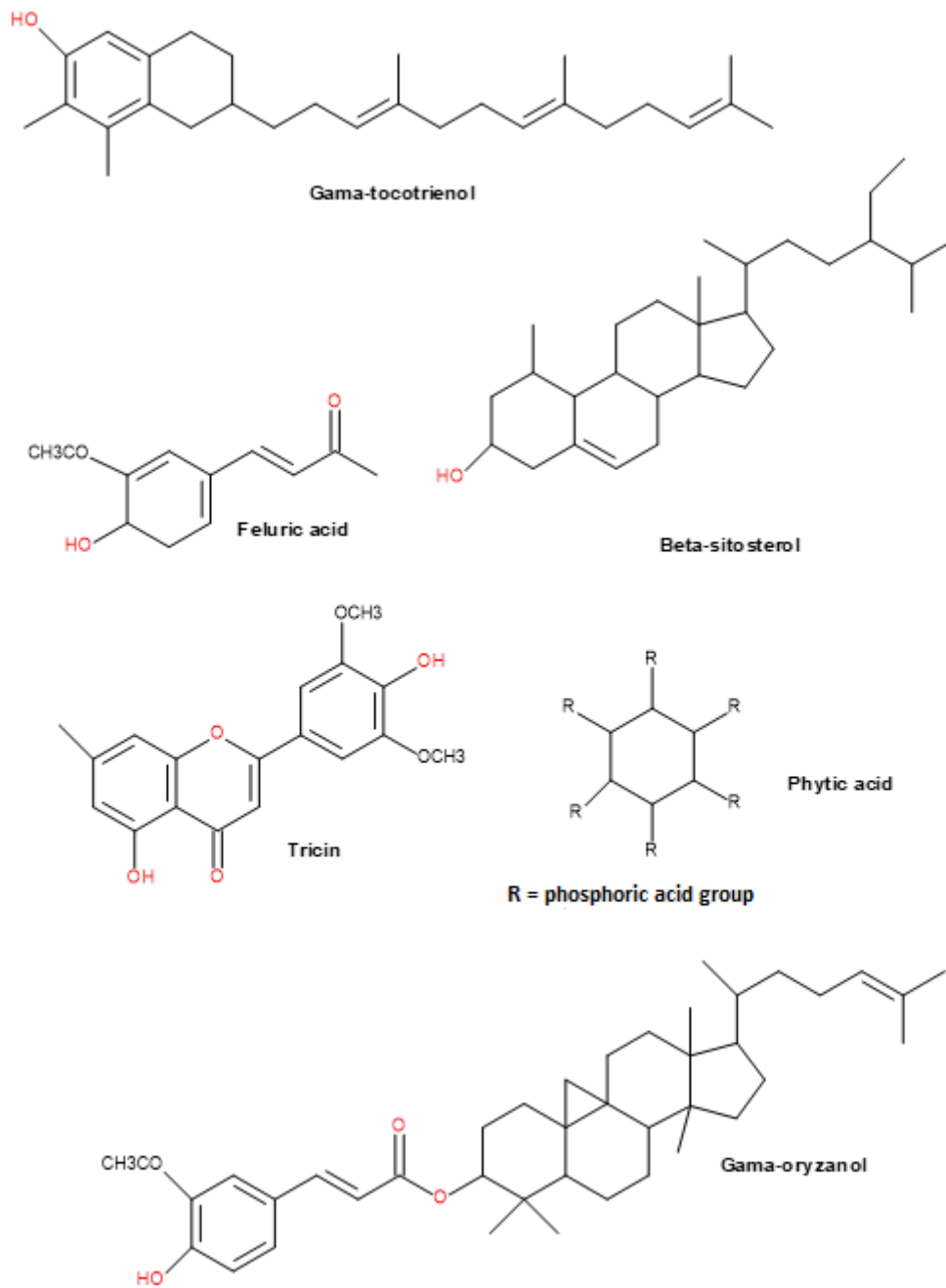


Figure 2. 8 Chemical structure of anti-oxidative phytochemicals present in rice bran

2. 2 Methods

2.2.1 Synthetic procedures

2.2.1.1 Phosphorylation reaction of carbohydrate based materials

A typical procedure on a ca. 2-3 g scale are as follows (Thomas, Joseph, Moinuddin, Zhu, & Tretsiakova-McNally, 2020):

Approximately 2.5 g of each material (β -cyclodextrin, or dextran, or potato starch, or agar agar, or tamarind kernel powder, as the case may be) were taken in a 250 cm³ conical flask, and about 40 cm³ of dry dichloromethane (DCM), containing triethylamine (TEA) (ca. 5 cm³, 0.036 mols), were added to each of them. To this mixture, 2.63 cm³ (0.018 mols) of dry diethylchlorophosphate (DECP) were introduced, and the contents were stirred at room temperature for about 24 hours. After the required reaction period, the contents of the conical flask were filtered through a qualitative filter paper in a Buckner funnel. The solid residue that was collected onto the filter paper was thoroughly washed with deionized water (ca. with 50 cm³ of deionized water \times 6 times). The product thus obtained was dried in a hot air oven (ca. 70°C) for at least 72 hours (see table below for details).

Table2. 1 Details of chemical modification reactions

| Sl. No. | Substrate | Sample weight (g) | DECP (g) | Recovered yield (wt. %) | P loading (wt. %) |
|---------|-----------------------|-------------------|----------|-------------------------|-------------------|
| 1 | β -cyclodextrin | 2.5 | 2.63 | 50 | 1.70 |
| 2 | Dextran | 2.4 | 2.63 | 79 | 1.00 |
| 3 | Potato starch | 2.3 | 2.63 | 55 | 3.20 |
| 4 | Agar agar | 2.7 | 2.63 | 67 | 5.55 |
| 5 | Tamarind | 2.8 | 2.63 | 68 | 6.68 |

2.2.1.2 Syntheses of the derivative of chitosan through functionalization with 9,10-Dihydro-9-oxa-10-phosphaphenanthrene-10-oxide (DOPO) (BA Howell et al., 2012)

Carbon tetrachloride (CCl₄) was first purified by passing through a column of basic activated alumina, and was then dried by keeping over molecular sieves (4 Å). About 6 g (0.028 mols) of DOPO were dissolved in mixture of CCl₄/THF (200 cm³; 2:1 by volume) by stirring at room temperature. To this *ca.* 4 g (0.02 mols based on the molar mass of the repeating unit) of chitosan were added, and stirred at room temperature for around 30 minutes. Subsequently, a solution of TEA (5 cm³, 0.036 mols) and CCl₄ (20 cm³) was added dropwise over a period of 30 minutes. The resulting mixture was then stirred overnight at room temperature, and the contents were made to reflux for another 2 hours. The resulting solids were collected by filtration at reduced pressure, and suspended in 200 cm³ of methanol, and stirred for 30 minutes and filtered. This process was repeated twice, and then with DCM, before the final recovery and drying of the product (*ca.* at 50°C for 24 hours). Yield = 2.5 g (recovered yield 25 wt. % based on the total mass of the reactants: i.e. chitosan and DOPO)

2.2.1.3 Synthesis of diethylbenzylphosphonate: *Michaelis-Arbuzov* reaction

The required amount of benzyl bromide (23.8 cm³, 0.2 mols) and triethyl phosphite (34.3 cm³, 0.2 mols) were refluxed at 90°C for 8 hours, followed by heating at 140°C for another two hours. The reaction mixture was subsequently rotatory evaporated at an elevated temperature (*ca.* 90°C) until the unspent reactants are removed from the product.

Yield = 45.5 g (1.9 mols- i.e. near quantitative yield)

¹H NMR (600 MHz, CDCl₃): δ = 7.27 (m, 5H, Ar), 3.98 (m, 4H, -P-O-CH₂-CH₃), 3.14 (d, 2H, -CH₂-Ar), 1.21 (t, 6H, -P-O-CH₂-CH₃)

³¹P NMR (243 MHz, CDCl₃): δ = 26.41

GC/MS: Retention time = 8.00 minutes; [M][±]-137 = 91 (benzylic radical: corresponding to the most abundant species)

2.2.2 Formulation and coating for cone calorimetry

Coating formulations of the base substrates (starch, chitosan, rice bran and fish gelatin, as the case may be) were obtained by mixing *ca.* 10 g of the above mentioned substrate in 100 cm³ of warm water (*ca.* 60°C). To this mixture, the required amount of the additive was added and stirred further to furnish a consistent dispersion (see in Table 2. 2 below). It should be also noted here that the masses of the various additives were normalized in terms of the number of mols used, i.e. 0.016 mols.

Table 2. 2 Details of the regarding the constitutions of the formulations for the passive fire protection coatings

| Sl. No. | Formulations | Additive (g) | P (wt. %) |
|---------|---|--------------|-----------|
| 1 | Substrate | --- | 0.00 |
| 2 | Substrate + Na ₂ CO ₃ | 1.70 | 0.00 |
| 3 | Substrate + K ₂ CO ₃ | 2.21 | 0.00 |
| 4 | Substrate + AP | 2.12 | 4.10 |
| 5 | Substrate + TPP | 4.20 | 3.48 |
| 6 | Substrate +TPPO | 4.46 | 3.43 |
| 7 | Substrate + DOPO | 3.46 | 3.68 |
| 8 | Substrate + DEPi | 2.20 | 4.05 |
| 9 | Substrate + TEPi | 2.66 | 3.97 |
| 10 | Substrate + TEPa | 2.91 | 3.62 |
| 11 | Substrate + DEPP | 2.88 | 3.85 |
| 12 | Substrate + DEBP | 3.65 | 3.63 |

2.2.3 Characterization techniques

The primary aim of the characterization methods were to elucidate the structural features, extents of incorporation of phosphorus-containing groups, and also to gauge the thermal and calorimetric properties of the modified materials. The unmodified counterparts were also

subjected to the same set of analyses to serve as controls for the purpose of comparison (Thomas, Joseph, Moinuddin, Zhu, & Tretsiakova-McNally, 2020). The instrumentation characteristics, basic working principles, and the associated results are given in the following sections.

2.2.3.1 Solution-state NMR

Generally for each run, *ca.* 30 wt.% solution of the analyte in the deuterated solvent was used (CDCl_3), and the spectra were collected at ambient-temperature probe conditions by employing a Bruker NMR instrument at 600 MHz for ^1H NMR and 242 MHz for ^{31}P NMR. The raw spectra were then processed using a proprietary software (Bruker TopSpin 4.0.8), and the residual solvent signals were used to calibrate the spectrum. In the case of ^{31}P , orthophosphoric acid was used as the external calibrant.

2.2.3.2 Inductively-coupled plasma optical emission spectroscopy (ICP-OES)

This is a widely used spectroscopic technique, based on atomic absorption, and are commonly used to identify and quantify the composition of elements by employing a plasma. Generally, in an ICP-OES machine, the plasma causes the atoms/ions to get excited. As a result, the electrons jump from a lower energy level to a higher level. When these electrons relax and reach their initial ‘ground state’, the energy is dissipated in the form of photons. These photons generally possess wavelengths that are characteristic of their respective elements. The constituent elements are generally quantified by comparing the intensities of the characteristic emission lines.

Calibration curve:

The Beer-Lamberts law governing the absorption of molecular species in dilute homogeneous media forms the basis for the calibration curve. According to the Beer-Lambert’s law, there exists a linear relationship between absorbance and concentration of an absorbing species, and can be stated in the form of the following equation:

$$A = \epsilon \times b \times c \quad (1)$$

where A is the measured absorbance;

ϵ is the molar extinction coefficient;

b is the path length;

c is the concentration of the absorbing species

Sample preparation:

The samples (polymeric, or char residues, as the case may be) were first accurately weighed (ca.10-15 mg) in triplicate, and were digested by boiling with 5 cm³ of Analytical Grade con. HNO₃ in 50 cm³ beakers. Upon digestion of the contents (i.e. chemically modified versions of β -cyclodextrin, dextran, potato starch, agar agar, tamarind, chitosan, or the char residues from the cone runs, as the case may be), the resulting solution were quantitatively transferred into a 25 cm³ volumetric flask, and made the solution to the mark with deionized water. In case of incomplete digestion, as inferred from the presence of residues, the contents were first filtered using a filter before making up to the required volume. The prepared solutions were transferred to 15 cm³ tubes before introducing into ICP-OES instrument (Shimadzu ICPE-9000). For, each of the samples the measurements were repeated three times, so as to attain a more accurate value of the phosphorous content in each of the samples (Thomas, Joseph, Moinuddin, Zhu, & Tretsiakova-McNally, 2020).

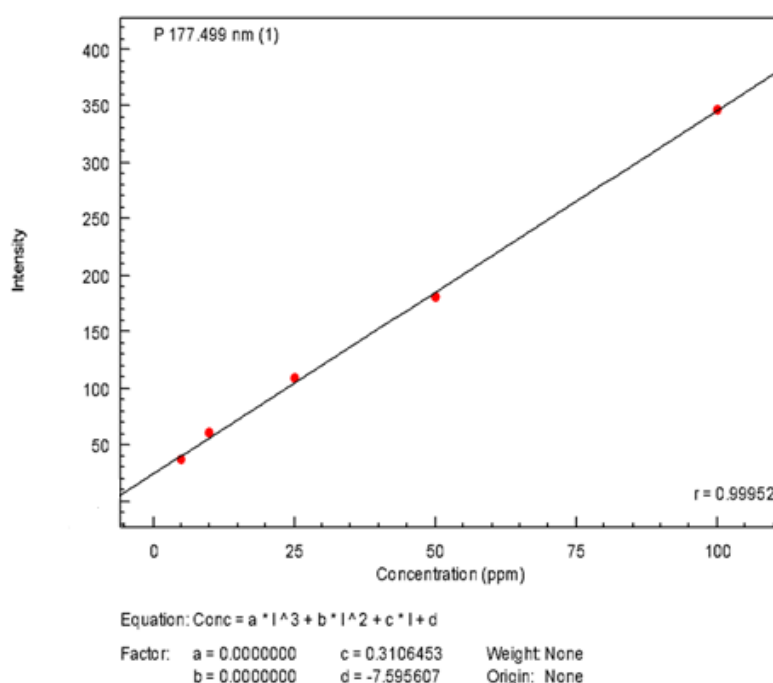


Figure 2. 9 Calibration curve of the Beer-Lambert law (generated by the inbuilt software of the instrument)

The figure shown above depicts the calibration curve of the Beer-Lambert relation which was subsequently used to quantitatively measure the amounts of phosphorus incorporation of the modified substrates, as well as the phosphorus retention in the char residues.

2.2.3.3 Fourier-transform infrared spectroscopy (FT-IR)

This technique is used to obtain the infrared absorption spectrum of a material. It simultaneously collects high spectral resolution data over a wide range of frequencies, often quoted as wave numbers (cm^{-1}). When infrared radiation of a particular bandwidth (generally 600 to 4000 cm^{-1}) are passed through the sample (taken as neat; i.e. in the attenuated total reflectance mode: ATR), some radiation are readily absorbed by the sample (depending on the characteristic functionalities present in the materials) and the remaining are transmitted through it. The resulting arrangement of wavelength vs. absorbance signals is the spectrum that represents a ‘molecular fingerprint’ of the specific sample (as different chemical structures produce different spectral fingerprints).

Prior to FT-IR analyses, the sample holder was wiped with acetone to make sure that the instrument does not pick a spectrum of an impurity present in the holder. Then a background ‘spectrum’ are recorded, followed by the spectrum of the sample (used as neat). All recordings were carried out on a Perkin-Elmer 1600 Series spectrometer with a resolution of 2 cm^{-1} and were averaged over 60 scans.

2.2.3.4 Thermogravimetric analysis (TGA):

This is, generally, a widely used method for analysing the thermal and thermo-oxidative degradation properties of materials, where the mass loss is monitored as a function of time, or temperature. It provides decomposition data of a specific material and can be subsequently used to effectively study their degradation kinetics and char formation characteristics. In the present study TGA runs were performed on samples (*ca.* 5-10 mg, in the form of a powder) under an atmosphere of nitrogen, from 30-800°C using a Mettler-Toledo instrument. It is relevant to note here that after the initial phases of a typical enclosure fire, the fuel loads are broken down under unventilated conditions, and hence their degradative behaviours resemble thermograms obtained under an inert atmosphere (i.e. nitrogen in this case). The runs were also

repeated at five heating rates (5, 10, 20, 30 and 60°C min⁻¹). The reproducibility at each heating rates were also periodically checked by performing duplicate/triplicate runs. The primary aim of the TGA analyses was to obtain the Arrhenius parameters (*A* and *E_a*).

2.2.3.5 Pyrolysis combustion flow calorimetry (PCFC)

This is a small-scale experimental technique used for evaluating the general flammability behaviours of materials. PCFC works on the principle of *oxygen consumption calorimetry* (Lyon & Walters, 2004). It is also known as micro-scale combustion calorimetry, in which a very small sample size (*ca.* 25-40 mg) provides a wide range of combustion/ flammability-related data (Joseph & Tretsiakova-McNally, 2012; Tretsiakova-McNally & Joseph, 2015; Thomas, Joseph, Moinuddin, Zhu, & Tretsiakova-McNally, 2020). PCFC separately reproduces the solid state and gas phase processes of flaming combustion in a non-flaming test by controlled pyrolysis of the sample. This process is carried out in an inert gas stream of nitrogen, or in a mixture of oxygen and nitrogen, with high temperatures to facilitate oxidation of the volatile products of pyrolysis. The heat release capacity values (J g⁻¹ K⁻¹) obtained are a material property that is a good indicator of the flammability of the material.

The other useful parameters that were obtained through PCFC include: heat release rates (HRRs), peak heat release rate (pHRR), total heat released (THR), mass of the residue left, effective heats of combustion (*h_c*) and the heat release capacity (HRC). In the present study, we employed a FAA Micro Calorimeter to obtain the thermograms. The samples were pyrolyzed in an inert atmosphere with nitrogen at a temperature range of (30-800°C). The mass of the samples were adjusted based on their respective oxygen consumption values (*ca.* 7-13%).

2.2.3.6 Bomb calorimetry

Caloric value of the Radiata Pine shavings was determined by using an IKA C 200 bomb calorimeter. The measurements were conducted on pelletized samples weighing about 1 g and in triplicate. The test samples were placed into the sample crucible, and the bomb was filled with oxygen up to 3 MPa of pressure, and subsequently the sample was ignited using an electric spark. The final calorific values were displayed by the instrument by employing a proprietary

software. The instrument was calibrated using analytical reagent grade benzoic acid (Joseph, Tretsiakova-McNally, & McKenna, 2012)

2.2.3.7 Gas chromatography/mass spectrometry (GC/MS)

For the GC/MS runs, a GCMS-QP2010 instrument with a capillary column with specifications as follows: ZB-5MS; length: 30 m; thickness: 0.5 μm ; diameter: 0.25 mm. The column oven temperature was set at 45°C and the injection temperature was set at 250°C. The carrier gas pressure was maintained at 86.6 kPa, with a column flow rate of 1.5 $\text{cm}^3 \text{min}^{-1}$ where the total flow was set at 154.4 $\text{cm}^3 \text{min}^{-1}$. The GC was coupled to the mass spectrometer which employed electron impact ionization. The associated operating parameters of the MS are as follows: ion source temperature: 250°C, interface temperature: 300°C; solvent cut time: 3 minutes; GC program time: 12.2 minutes).

2.2.3.8 Pyrolysis-GC/MS

Pyrolysis-GC/MS was performed with the pyrolysator Pyroprobe 5000 (CDS Analytical, Inc., Oxford, PA, USA) with platinum filament coupled with gas chromatograph GC7890A (Agilent Technologies, Santa Clara, CA, USA) with GC column HP-5MS (non-polar, length: 30 m; inner diameter: 250 μm ; layer thickness: 0.25 μm), (Agilent Technologies, Santa Clara, CA, USA). The carrier gas was helium with a gas flow rate of 1 $\text{cm}^3 \text{min}^{-1}$. The GC was equipped with the mass-selective detector MSD 5975C inert XL EI/CI (Agilent Technologies, Santa Clara, CA, USA) with a mass scan range between 15-550 m/z and EI at 70 eV. The samples were pyrolyzed at the temperatures of maximum mass losses found in TGA. The inlet temperature of the GC was variable, the oven temperature program fixed (2 minutes at 50°C; heating with 12 K min^{-1} to 280°C).

2.2.3.9 Solid-state NMR

The solid-state NMR (^{31}P with CP/MAS mode) spectra of the char residues was obtained by employing a 500 MHz Bruker Avance III spectrometer machine at ambient probe conditions. A 4 mm H/F-X double resonance probe was used to record ^{13}C and ^{31}P NMR spectra, typically

at 10 kHz, or optionally 8 kHz rotor speed, and the signals were calibrated against phosphoric acid as the external calibrant. The raw data were then processed by using a proprietary software from the manufacturer (TopSpin 4.0.8).

2.2.3.10 Raman spectroscopy

Raman spectra were recorded with powdered samples of the char residues, placed in aluminium pans, using a Perkin Elmer- Raman Micro 200 (Microscope with an optical lens of magnification fivefold). Typically, the spectra were scanned between a Raman shift range of 2000 to 150 cm^{-1} , with an exposure time of 8 seconds and number accumulations were set at 12 with a resolution of 4 cm^{-1} . The laser power used varied between 20 to 100 %, as required, to obtain spectra with an acceptable level of signal/noise ratio. A proprietary software associated with the instrument was used to compute the ratios of the graphitic, *G*, band (centred around 1580 cm^{-1}) and the amorphous, *D*, band (centred around 1350 cm^{-1})

2.2.4 Flammability tests

2.2.4.1 Dip-test through an in-house test rig

The ignition propensity of slender segments of Radiata Pine, coated with the formulation of choice, were gauged by employing an in-house method that are reminiscent of UL-94 test (Thomas, Moinuddin, Zhu & Joseph, 2020). In this test, a sample segment, measuring 100 mm \times 10 mm \times 2 mm, were coated with the formulation at one end, by dipping in the formulation for 30 minutes and allowed to dry for another 30 minutes, so as to cover a length of 30 mm. It was then clamped vertically so that the coated part formed the free end. Subsequently, a flame from a butane torch (*ca.* 1.5 cm in length) was applied for the required period so as a flaming combustion was sustained (see in Figure 2. 10). The time ignition for each material was measured several times, and averaged over at least four congruent values. The main impetus behind this kind of a test was to establish their utility as a quick laboratory-based screening test. Hence, we only chose to conduct dip test for a representative sample of formulations.

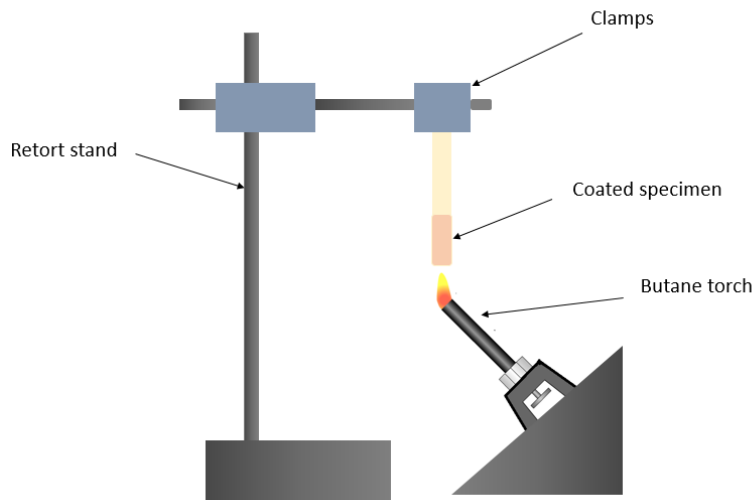


Figure 2. 10 A schematic sketch of the proprietary ignition propensity test

2.2.4.2 Cone calorimetry

The principle behind cone calorimetry was originally conceived and working methodology/instrumentation was developed in the early 1980's at the National Institute of Standards and Technology (NIST) in USA. The instrument measures a number of important parameters related to flaming combustion under an ambient atmosphere, including: time to ignition, heat release rates, total heat released, mass loss rates, effective heats of combustion, rate of smoke evolution, CO/CO₂, etc.

The underpinning principle behind the calculation of the heat release in a fire is based on accurately measuring the oxygen needed for flaming combustion of a fuel (i.e. 'oxygen combustion calorimetry'). This parameter, usually measured in kW m⁻², are considered to represent the intensity of a fire, and are also assumed to contribute to the fire growth of the fuel load. The underlying principle of oxygen consumption calorimetry is based on a previous work carried out by Thornton in 1917 (Thornton, 1917). This work reported that when common organic solid fuels underwent flaming combustion was found to release, for each gram of oxygen consumed, is more or less the same amount of heat energy, *ca.* 13.1 kJ (Huggett, 1980; Janssens & Parker, 1992). Huggett extended this work to a variety of solid fuels, and confirmed this observation (Janssens & Parker, 1992). Furthermore, it was also established that this value was not significantly affected by incomplete combustion. Therefore, it is to be concluded that

the heat released for most organic materials could be calculated from the consumption of oxygen to within an accuracy of $\pm 5\%$.

The instrument records very accurately the consumption of oxygen and simultaneously measures the mass loss rate of a solid fuel, and from the net mass loss and total heat energy release, the effective heat of combustion of the material can be determined. Furthermore, several other relevant parameters can be obtained from cone tests, such as: time-to-ignition, peak heat release rate, CO and CO₂ yields, smoke production, etc. It can also furnish information regarding the extent of combustion, and the combustion toxicity of the effluents.

Instrumentation

A diagram of a typical cone calorimeter is given in Figure 2. 11, and it comprises of:

- A conical-shaped electrical radiant heater, which are thought to simulate the grey body radiation from the soot in a typical room fire
- An ignition source
- A load cell
- Flow measuring instrumentation
- Paramagnetic oxygen analyzer
- CO/CO₂ analyzer
- Laser photometer for smoke measurements
- An on-line computer for data collection and analysis

Initially a suitable value for the external heat flux is selected, and subsequently the sample is exposed to this using a set of electrically-heated coil in the form of a truncated cone. Generally, the sample with a dimension of 100 mm x 100 mm and of specified thickness (20 mm in the present case) is exposed to the pre-determined irradiance from the conical-shaped heater. The imposed heat energy results in thermal degradation of the test material to varying extents, the latter depend on the chemical nature of the sample. The low-molecular weight volatiles emanating from the sample then mixes with ambient air, and this can often result in combustible mixtures. At this point, a spark ignitor is engaged with a view to initiating flaming combustion of the volatiles. The time required between the imposition of the external heat flux

to that of the appearance of a visible plume (for 10 seconds, or above) are measured as the time-to-ignition.

The effluent fluids are split into two, where the first stream is tested for CO and CO₂, whereas the second one is dried by passing through soda lime and silica gel before accurate measurements of the oxygen content by a sensitive analyzer. The data collection and recording are carried out intermittently by a proprietary software, which also calculates the heat release rates depending on the amounts of oxygen consumed at each point.

The cone calorimeter software uses a comma separated variable file, which enables the data to be handled using packages such as Microsoft Excel.

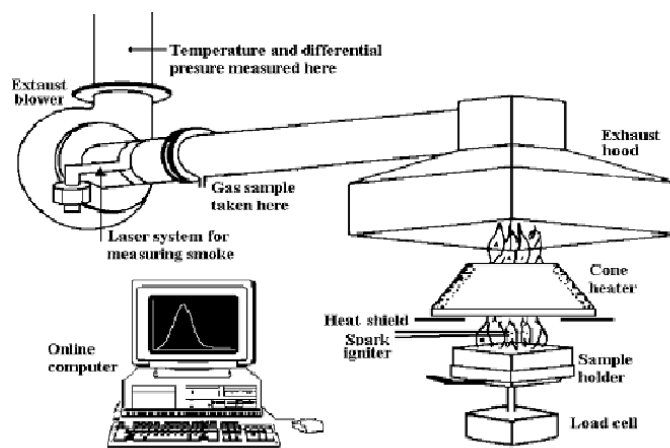


Figure 2. 11 A schematic diagram of cone calorimeter

Calibration

The cone calorimeter must be carefully calibrated prior to running a set of experiments. The general procedure are outlined below:

The drierite are first renewed if deemed necessary. The computer is then switched on and the 'conecalc' software is loaded. Ensuring that the main exhaust fan is turned off, the differential pressure transducer (DPT) and methane are zeroed.

The main extractor fan is then turned on and any water that has collected in the refrigerated trap is drained before the water supply is turned on. The cold trap, pump, load cell and ignition

source of the cone calorimeter are also turned on. The cone calorimeter fan is then turned on and adjusted so that the mass flow rate in the duct is measuring 30 g s⁻¹. This corresponds to a volume flow at the orifice plate of approximately 24 l s⁻¹.

- Oxygen analyzer

The oxygen flow is reduced to zero using the flow meter valve. Nitrogen is then passed through the sampling line at a flow rate of 200 cm³ s⁻¹. When the oxygen reading has stabilized, the oxygen analyzer is set to zero and the computer is also zeroed. The nitrogen source is then turned off and ambient air is allowed to pass through the cone calorimeter. When the oxygen reading has stabilized, the span is adjusted so the oxygen analyzer reads 20.95%. When this is achieved, the span on the computer programme is then selected followed by accept.

- CO, CO₂ analyzer

Ensuring that the cone calorimeter pump is switched off, the analyzer is automatically zeroed by pressing the calibration button on the analyzers control panel. Zero is then selected on the computer. The CO/CO₂ calibration gas is then turned on and the flow rate adjusted to 1.6 L min⁻¹. When the reading has stabilized, the calibration option is selected on the control panel and the CO component is selected. When the analyzer reads “calibration OK”, the span option is selected on the computer and the actual concentration (stored in the computer) is given. The calibration process is then repeated for the CO₂ component and accept is selected on the computer.

- Laser photometer

An opaque card is inserted into the laser side of the photometer and zero is selected on the computer. The opaque card is then removed and the shutter is closed. The photometer is then calibrated by inserting first the 0.8 and then the 0.3 interference filters in the beam between the duct and the detector, and selecting calibrate on the computer software. If the optical densities measured by the photometer are comparable with the optical densities of the filters, accept is selected on the computer. Soot yield can be calculated using this data.

- C factor calibration.

The methane burner is inserted into the holder and high purity methane gas (99.9%) is passed through the burner. The mass flow controller valve is adjusted so that the output from the methane flame is 5 kW. Positioning the spark arm above the burner ignites the methane, and

calibrate heat release is then selected on the computer. The computer automatically collects the data and calculates the value of C. After two minutes, enter is selected on the computer and an average value of C is given. If this value lies in the range of 0.040- 0.046, accept is selected on the computer and the calibration is complete. The methane cylinder is then turned off and the flame allowed to die which removes methane from the line.

- Sample preparation

The sample (100 mm × 100 mm) is accurately weighed and the thickness measured. The sample is then wrapped in aluminum foil with a thickness of 0.040 mm, shiny side towards the surface. The upper surface of the specimen is left uncovered. A layer of cotton blanket having a total thickness of 13-20 mm is placed in the sample holder. The foil-wrapped specimen is then placed on top of the ceramic fibre blanket and a horizontal holder edge frame is then placed over the sample holder. This results in 88 cm² of the sample surface being exposed to the radiant cone heater.

- Performing an experiment

On the computer, select run and type in all of the necessary details including file name, thickness, exposed area, orientation, etc.

Ensuring that the shutter isolating the sample from the heater is closed, place the sample holder (and specimen) onto the load cell and check that the mass recorded is comparable to the mass of the sample. The ignition arm should be positioned over the centre of the sample surface. Before running a test, it is essential to adjust the height of the sample surface to a position of 25 cm away from the bottom of the conical heater. Ideally, this should be done when the heater is cold. On the computer, select “perform pre-run calibrations” and wait until the machine is ready for a test.

When the machine is ready (as indicated by a graph showing heat release rate against time on the monitor), the shutter is opened exposing the sample to the radiant heat and button 1 on the handset is pressed simultaneously. This activates the start of the test. The sparking ignition source is then quickly positioned over the centre of the sample. When ignition occurs, button 2 on the handset is pressed, and the time to sustained ignition is automatically recorded. Button 3 on the handset can be used to record the time of any observations such as melting, spitting, swelling and char formation, etc.

When flaming ceases, Stop on the handset is then pressed. Keeping the heater shutter open, data should be collected for a further two minutes. At the end of the test, select F on the computer to finish collecting data. The ‘conecalc’ software will then process the data.

In this study, wood samples (Radiata Pine) measuring 100 mm × 100 mm × 20 mm were pre-conditioned in a chamber, kept at 25 ± 1°C and relative humidity of 50 ± 5 %, for at least a week prior to the measurements. The different formulations were uniformly applied onto the top surface of the wood samples (*ca.* 0.5 mm in thickness), and were left to dry in a fume cupboard overnight. The cone tests were conducted in triplicate in conformance with ISO 5660 (AS/NZ 3837), where piloted ignition at an external heat flux of 35 kWm⁻² was effected. As usual, the bottom part and sides of the sample were covered with aluminium foil, and was placed on *cotronic* material as the insulating layer.

2.2.5 Deduction of Arrhenius parameters from thermograms

2.2.5.1 Flynn-Wall-Ozawa (FWO) method

For the purpose of computing the energy of activation (E_a) for the degradation of all the six base materials, we have utilized the Flynn-Wall-Ozawa (FWO) method (Flynn & Wall, 1966; Ozawa, 1992). For this, initially, the TGA runs were carried out at five heating rates (i.e. 5, 10, 20, 30 and 60°C min⁻¹) in nitrogen, from 30 to 800°C. The data points thus obtained were transferred into an Excel file, and subsequently the degree of conversion (α values) were calculated using the following formula (see also in Table 2.3, as example: potato starch):

$$\alpha = (m_i - m_t) / (m_i - m_f) \quad (2)$$

After this, plots were constructed using the logarithm of the heating rates (i.e. $\log \beta$) as the ordinate and reciprocal of the temperature corresponding to α value as the abscissa. As expected, the plots were linear, typically, having an R^2 value of *ca.* 0.93 for tamarind (see in Table 2.3 below)

Table 2. 3 Values of abscissa and ordinate for tamarind for the FWO method (at $\alpha = 0.2$)

| Sl. No. | $\log \beta$ | Temp (°C) | Temp (T) (K) | 1/T |
|---------|--------------|-----------|--------------|------------|
| 1 | 0.6989 | 279 | 552 | 0.00181079 |
| 2 | 1.0000 | 287 | 560 | 0.00178704 |
| 3 | 1.3010 | 285 | 558 | 0.00179163 |
| 4 | 1.4771 | 309 | 582 | 0.00171812 |
| 5 | 1.7782 | 322 | 595 | 0.00167868 |

2.2.5.2 SB method (based on the algorithm/software developed by Professor Stephen Bigger, Victoria University, Melbourne, Australia) (Bigger, Cran, & Bohn, 2015; Bigger, Cran, & Tawakkal, 2015)

Basically in this approach, one of the non-isothermal thermogram is chosen. Here in all cases we chose the thermogram obtained at relatively low heating rate of 10°C min⁻¹ as this is expected to capture most of the underlying steps in the thermal degradative pathway of the unmodified substrate in question (β -cyclodextrin, or dextran, or potato starch, or agar agar, or tamarind kernel powder). As the first step the data points of the thermogram was transferred into an Excel file for subsequent manipulations, which primary involved identifying the main step of degradation, and then the following procedure is adopted (here potato starch is taken as an example).

1. m_i and m_f are first identified from the TGA Plot. The average values of the regions where the mass does not change significantly are chosen.
2. Next, the corresponding degrees of conversion, α , are calculated using $\alpha = (m_i - m_t) / (m_i - m_f)$. The range of α values chosen should be as large as possible but should also avoid those values of α that are close to 0 and 1 (ideally, 0.1 to 0.9), where the uncertainties are too high.
3. The values of T and mass of the range of α values selected are copied into a new excel workbook and the file is saved in Tab Delimited Text (.txt) format.
4. This file is then opened in the SB software using the *Read File* button and the desired input file (e.g. $m-T/^\circ C$) and the required heating rate is set correctly (10°C). When the data is successfully loaded a message appears in their status field with the name of the input file in the File field.
5. The values of m_i and m_f calculated in 1 are to be entered in the appropriate fields

- Click the Calc Step 1 button to perform the initial calculations.

Instructions: $b/^\circ\text{C min}^{-1}$ 10, $T_o/^\circ\text{C}$ 286.6, $T_f/^\circ\text{C}$ 319.5, m_o/mg 5.6152, m_f/mg 1.1655

Status: Calc Step 1 Complete

File: sb_tam_0.20.5.txt

Calc Step 2: $(da/dT)_{max}$, a_{max}

| # | t/min | T/oC | m/mg | alpha |
|----|----------|---------|---------|----------|
| 1 | 0 | 286.585 | 4.6865 | 0.208711 |
| 2 | 0.017587 | 286.755 | 4.68343 | 0.209401 |
| 3 | 0.035174 | 286.926 | 4.68028 | 0.210109 |
| 4 | 0.052761 | 287.104 | 4.67715 | 0.210812 |
| 5 | 0.070349 | 287.276 | 4.674 | 0.21152 |
| 6 | 0.087936 | 287.451 | 4.67085 | 0.212228 |
| 7 | 0.105523 | 287.619 | 4.66766 | 0.212945 |
| 8 | 0.123111 | 287.797 | 4.66446 | 0.213654 |
| 9 | 0.140697 | 287.973 | 4.66125 | 0.214365 |
| 10 | 0.158284 | 288.141 | 4.65803 | 0.215109 |
| 11 | 0.175872 | 288.314 | 4.65474 | 0.215848 |
| 12 | 0.193459 | 288.498 | 4.65145 | 0.216588 |
| 13 | 0.211046 | 288.674 | 4.64815 | 0.217329 |
| 14 | 0.228633 | 288.842 | 4.64483 | 0.218075 |
| 15 | 0.24622 | 289.007 | 4.64144 | 0.218837 |
| 16 | 0.263807 | 289.186 | 4.63806 | 0.219597 |
| 17 | 0.281395 | 289.361 | 4.63468 | 0.220356 |
| 18 | 0.298982 | 289.524 | 4.6313 | 0.221116 |
| 19 | 0.316569 | 289.705 | 4.62784 | 0.221894 |
| 20 | 0.334156 | 289.879 | 4.62438 | 0.222671 |
| 21 | 0.351743 | 290.048 | 4.62092 | 0.223449 |
| 22 | 0.36933 | 290.219 | 4.61743 | 0.224233 |
| 23 | 0.386918 | 290.391 | 4.61394 | 0.225017 |
| 24 | 0.404505 | 290.565 | 4.61037 | 0.22582 |
| 25 | 0.422092 | 290.742 | 4.60681 | 0.22662 |

Calc Step 3: Chart & Info, half width/ $^\circ\text{C}$

Calc Step 4: D1 One-Dimensional Diffusion, Deriv Meth Data

Calc Step 5: E_a U/kj mol $^{-1}$, E_s set/kj mol $^{-1}$, dE_p /kj mol $^{-1}$, Abort, Int Meth Data

- Next, click the Calc Sep 2 button which will calculate the $(da/dT)_{max}$ and a_{max} values.

Instructions: $b/^\circ\text{C min}^{-1}$ 10, $T_o/^\circ\text{C}$ 286.6, $T_f/^\circ\text{C}$ 319.5, m_o/mg 5.6152, m_f/mg 1.1655

Status: Calc Step 2 Complete

File: sb_tam_0.20.5.txt

Calc Step 2: $(da/dT)_{max}$ 1.544e-002, a_{max} 0.443648

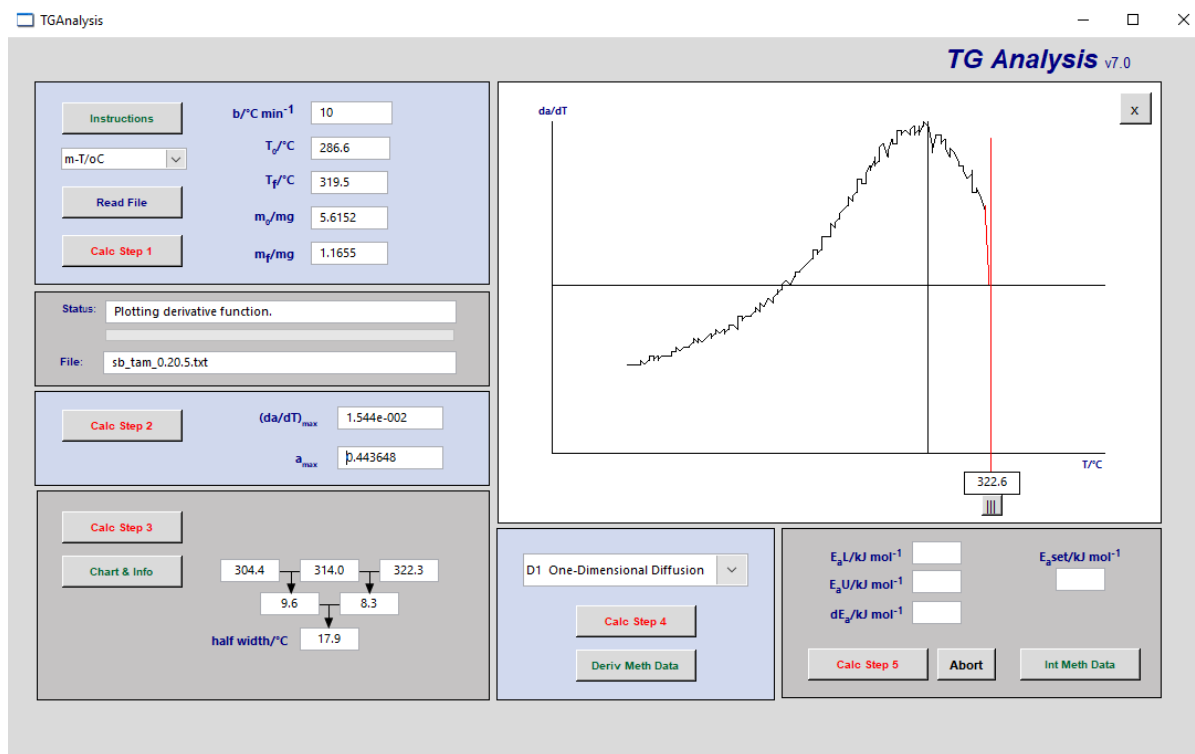
| # | t/min | T/oC | alpha | d(alpha)/dT |
|----|-------|--------|----------|-------------|
| 1 | 0.00 | 286.58 | 0.208711 | 0 |
| 2 | 0.02 | 286.76 | 0.209401 | 0.0041 |
| 3 | 0.04 | 286.93 | 0.210109 | 0.004043 |
| 4 | 0.05 | 287.10 | 0.210812 | 0.004031 |
| 5 | 0.07 | 287.28 | 0.21152 | 0.004081 |
| 6 | 0.09 | 287.45 | 0.212228 | 0.004155 |
| 7 | 0.11 | 287.62 | 0.212945 | 0.00415 |
| 8 | 0.12 | 287.80 | 0.213654 | 0.004068 |
| 9 | 0.14 | 287.97 | 0.214365 | 0.004201 |
| 10 | 0.16 | 288.14 | 0.215109 | 0.00429 |
| 11 | 0.18 | 288.31 | 0.215848 | 0.004143 |
| 12 | 0.19 | 288.50 | 0.216588 | 0.004114 |
| 13 | 0.21 | 288.67 | 0.217329 | 0.004323 |
| 14 | 0.23 | 288.84 | 0.218075 | 0.004529 |
| 15 | 0.25 | 289.01 | 0.218837 | 0.004424 |
| 16 | 0.26 | 289.19 | 0.219597 | 0.004291 |
| 17 | 0.28 | 289.36 | 0.220356 | 0.004494 |
| 18 | 0.30 | 289.52 | 0.221116 | 0.004458 |
| 19 | 0.32 | 289.71 | 0.221894 | 0.00438 |
| 20 | 0.33 | 289.88 | 0.222671 | 0.004547 |
| 21 | 0.35 | 290.05 | 0.223449 | 0.004594 |
| 22 | 0.37 | 290.22 | 0.224233 | 0.004571 |
| 23 | 0.39 | 290.39 | 0.225017 | 0.004587 |
| 24 | 0.40 | 290.57 | 0.22582 | 0.004567 |
| 25 | 0.42 | 290.74 | 0.22662 | 0.004565 |

Calc Step 3: Chart & Info, half width/ $^\circ\text{C}$

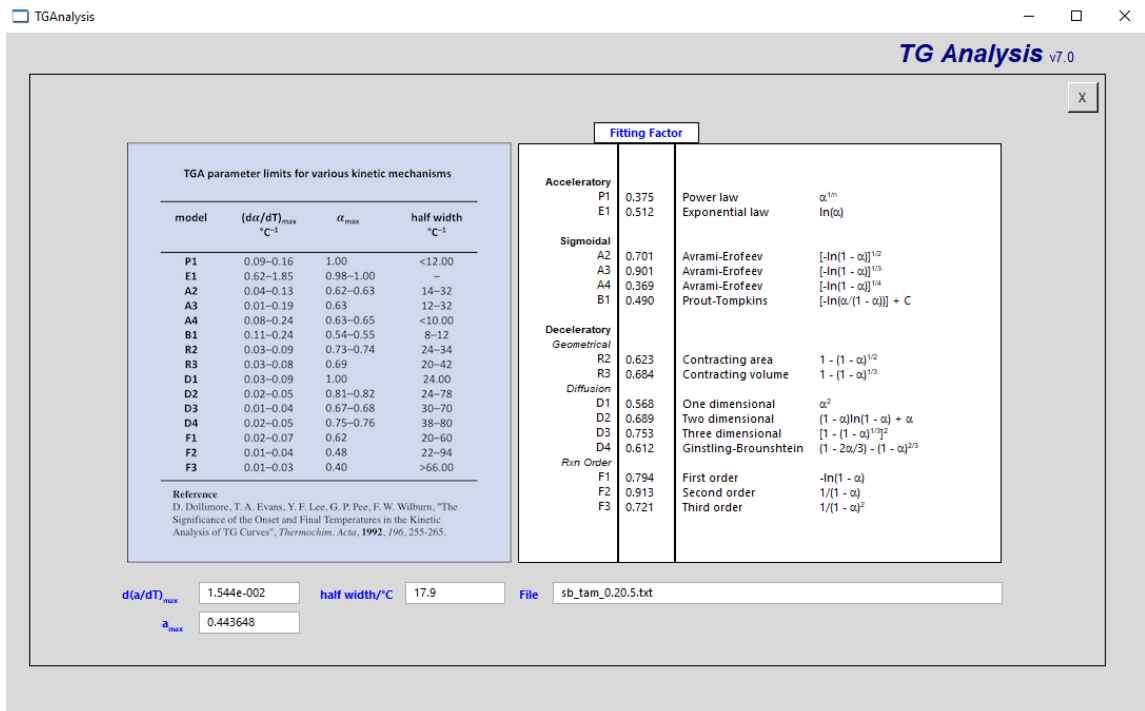
Calc Step 4: D1 One-Dimensional Diffusion, Deriv Meth Data

Calc Step 5: E_a U/kj mol $^{-1}$, E_s set/kj mol $^{-1}$, dE_p /kj mol $^{-1}$, Abort, Int Meth Data

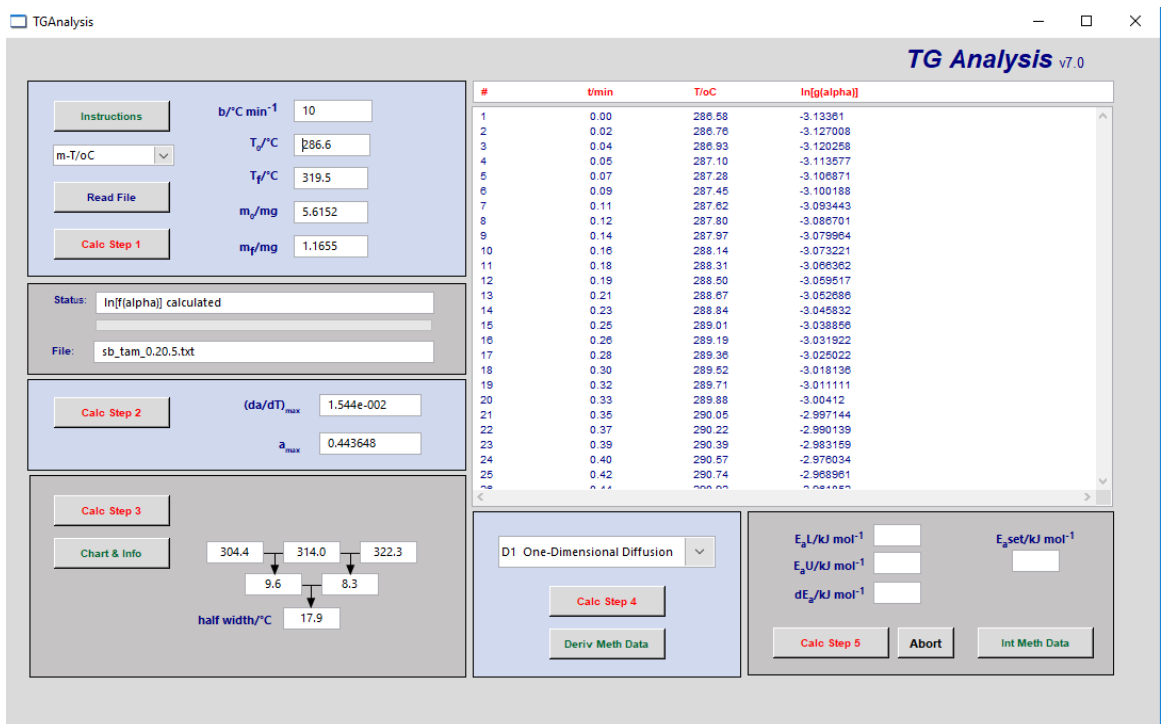
- Click Calc Step 3 button, which will produce the da/dT vs. $T/^\circ\text{C}$ along with a horizontal line (half-height line) whose vertical axis intercept is half of the maximum da/dT values. The cursor which appears can be moved along the temperature axis and the cursor handle is used to determine the lower and upper temperatures where the plot intersects the half height line.



- The Chart and Info button displays a listing of the kinetic models that can be used to fit the data along with a fitting parameter, ρ , for each model. This chart can be used to identify the most appropriate model for fitting the data.



10. Select the required model from the pull down menu and click Calc Step 4 which will produce a $\ln[g(\alpha)]$ that are needed to extract the activation energy and Arrhenius factor in the next step.



11. Start by scanning a wide range of E_a values with large incremental steps until a satisfactory convergence is reached. To determine the activation energy E_a , an iterative

numerical calculation is performed on the data, the convergence to the best fit is indicated by a minimum value of the averaged sum of the squares of the residuals.

| Ea/kJ mol ⁻¹ | A/min ⁻¹ | AvDevMean |
|-------------------------|---------------------|-----------|
| 140 | 2.872e+011 | 0.061626 |
| 141 | 3.315e+011 | 0.060607 |
| 142 | 4.111e+011 | 0.059671 |
| 143 | 5.100e+011 | 0.058826 |
| 144 | 6.325e+011 | 0.05806 |
| 145 | 7.845e+011 | 0.057307 |
| 146 | 9.730e+011 | 0.056759 |
| 147 | 1.207e+012 | 0.056231 |
| 148 | 1.490e+012 | 0.055787 |
| 149 | 1.850e+012 | 0.055416 |
| 150 | 2.301e+012 | 0.055113 |
| 151 | 2.853e+012 | 0.054866 |
| 152 | 3.638e+012 | 0.054729 |
| 153 | 4.386e+012 | 0.054644 |
| 154 | 5.438e+012 | 0.05463 |
| 155 | 6.743e+012 | 0.054683 |

12. Once the E_a value has been optimized, the corresponding Arrhenius A-factor can be obtained from the output window in this stage.

13. Enter the optimized E_a into the E_a field and click the Int Meth Data to obtain values of $g(\alpha)$ vs. $p(x)$.

14. This data will get automatically transferred to the clipboard and should be pasted in excel to produce a plot of $g(\alpha)$ vs. $p(x)$ (Figure 2. 12). This plot should be linear and ideally pass through the origin, upon extrapolation. This step is critical to confirm the appropriate fit of the kinetic model and the reliability of the E_a and A values obtained.

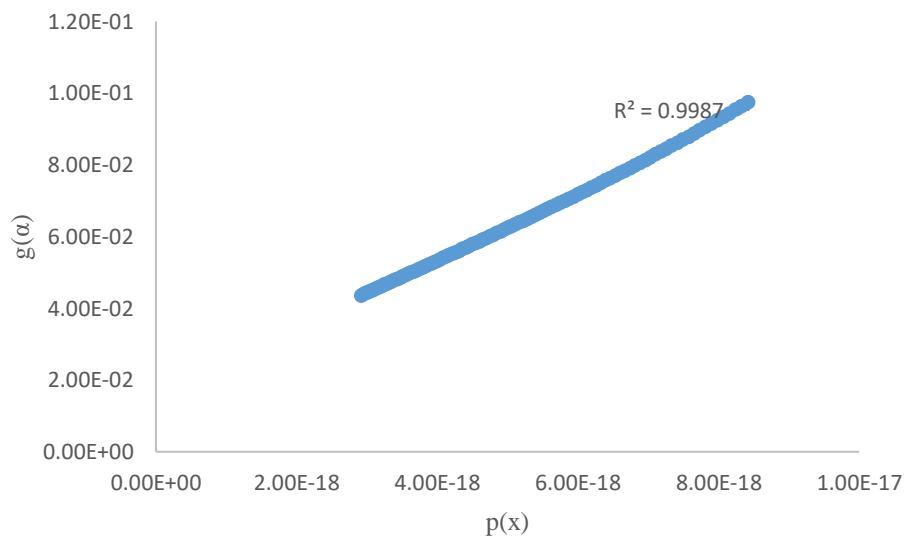


Figure 2. 12 Plot showing values of $g(\alpha)$ vs. $p(x)$

CHAPTER 3: RESULTS AND DISCUSSION

3.1 Choice of materials

3.1.1 Base substrates

Recently, starch has achieved an increased attention as a naturally occurring material that can be functionalised to further extend their applicability across various fields. The unique physiochemical properties and the large number of hydroxyl groups in starch molecules find potential to be modified and functionalised to meet specific requirements (A Blennow, Engelsen, Munck, & Møller, 2000; Andreas Blennow, Nielsen, Baunsgaard, Mikkelsen, & Engelsen, 2002; Demirgöz et al., 2000). Hence for the current study, we chose polysaccharide-based substrates, including: β -cyclodextrin, dextran, potato starch, tamarind, agar agar and chitosan, where all the substrates not only widely differed in terms of their molecular weights but also in terms of their chemical structures (see chapter 2; section 2.1; pages 17-21) for detailed structures of the different materials.

For the present project, we have chosen a softwood variety of timber belonging to the Pine (*Pinus radiata*, or commonly known as Radiata Pine) family as the base substrate (Figure 3. 1). whilst the ease of ignition (especially when compared to the hardwood variety), and ensuing combustion hazards of softwood are well recognized, it is often the material of choice for general construction purpose, as it is less expensive, workable and almost readily available, and thus can also be used on a broad range of applications (Ramage et al., 2017). As already mentioned, softwood trees grow much faster than most hard wood tree varieties, therefore, it can be considered as a more renewable and sustainable resource. Moreover, in the Australian context, this variety is heavily used in construction, were it forms an integral part of structural elements, such as fencing, decking, façade, door frame, wall lining, etc.



Figure 3. 1 A photograph showing Radiata pine plaques

As is seen from the above figure, the test samples had a pale yellowish tinge, and the average density was found to be 0.5 kg m⁻³. Bomb calorimetric runs (in triplicate) on shavings from the sample gave an average value of 17,940 J g⁻¹. The relevant parameters from the pyrolysis combustion flow calorimetric (PCFC) runs yielded the following values for the relevant parameters: pHRR = 126 W g⁻¹; THR = 11.0 kJ g⁻¹; HRC=130 Jg⁻¹ K⁻¹and $h_c = 13.8$ kJ g⁻¹.

3.1.2 Phosphorylation reactions on carbohydrate-based materials

Through this reaction, we aimed to carry out a simple single step condensation reaction of hydroxyls (-OH group) with diethylchlorophosphate (DECP), in the presence of a base, triethylamine (TEA) (see Figure 3. 2). Here, the base was expected to act as an acid scavenger, and the functionalisation by the phosphorus-bearing reagent to take place in the C₃ and/or C₆ positions (Andreas Blennow et al., 2002; Jianli et al., 2016; Muhammad et al., 2000). Table 3.1 summarises the quantities of the reagents involved, and the recovered yields of these reactions indicate an appreciable amount (*ca.* 50-80 wt. %). Furthermore, to gauge the incorporation of phosphorous during the reaction, both in terms of quality and quantity, we employed solid-state NMR and ICP-OES techniques (Thomas, Moinuddin, Zhu & Joseph, 2020) (see in Table 3. 1, and in Figures 3. 3 to 3. 7). The results from the analyses clearly showed noticeable extents of incorporation of phosphorous in all cases.

Table 3. 1 Characterization data of the phosphorylated products

| Sl. No. | Substrate | Sample mass (g) | Mass of recovered product (g) | Recovered yield (wt. %) | P loading *(wt. %) |
|---------|----------------|-----------------|-------------------------------|-------------------------|--------------------|
| 1 | β-cyclodextrin | 2.5 | 1.3 | 50 | 1.70 |
| 2 | Dextran | 2.4 | 1.9 | 79 | 1.00 |
| 3 | Potato starch | 2.3 | 1.3 | 55 | 3.20 |
| 4 | Agar agar | 2.7 | 1.8 | 67 | 5.55 |
| 5 | Tamarind | 2.8 | 1.9 | 68 | 6.68 |

*measured using ICP-OES (here the average values, over triplicate runs obtained as ppm, were subsequently converted into wt. %)

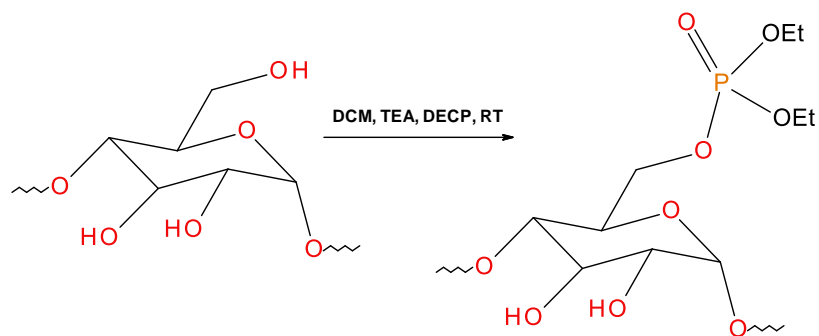


Figure 3. 2 A schematic diagram of the phosphorylation reaction

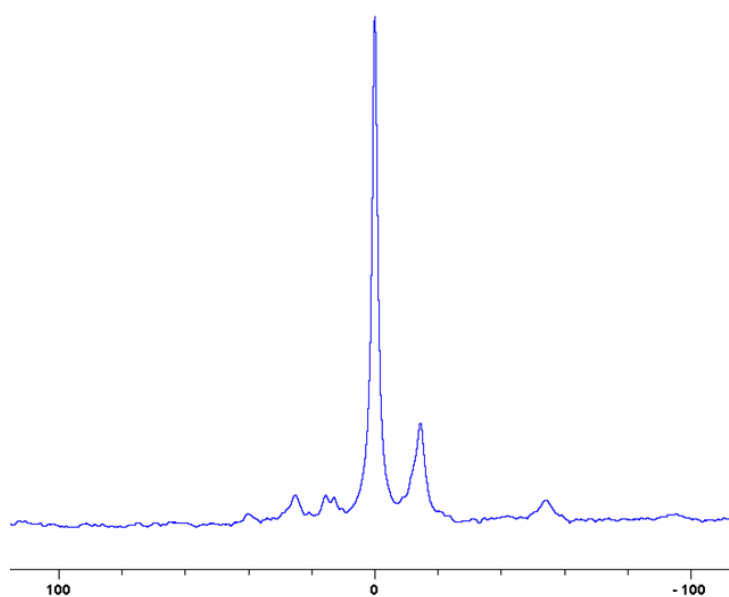


Figure 3. 3 ^{31}P -NMR spectrum of β -cyclodextrin modified with phosphate groups (the abscissa denotes the chemical shift values, δ , in ppm and the ordinate corresponds to the signal intensity in arbitrary units)

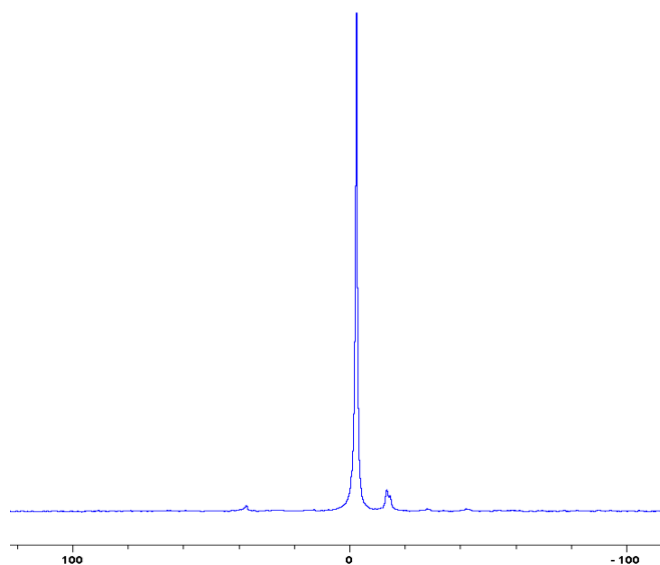


Figure 3. 4 ^{31}P -NMR spectrum of dextran modified with phosphate groups (the abscissa denotes the chemical shift values, δ , in ppm and the ordinate corresponds to the signal intensity in arbitrary units)

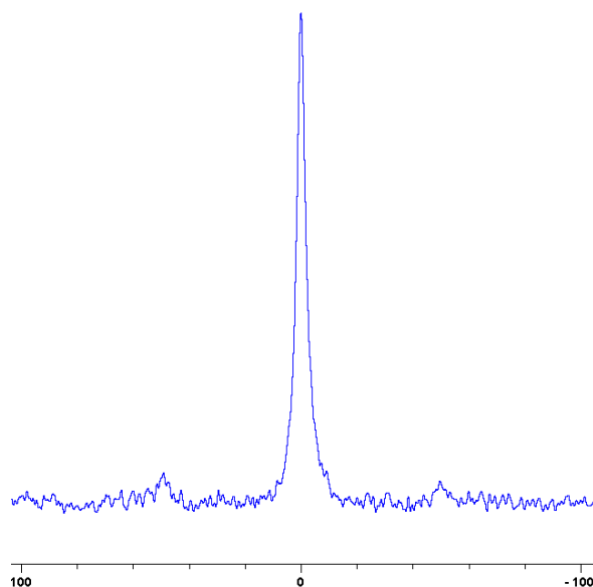


Figure 3. 5 ^{31}P -NMR spectrum of potato starch modified with phosphate groups (the abscissa denotes the chemical shift values, δ , in ppm and the ordinate corresponds to the signal intensity in arbitrary units)

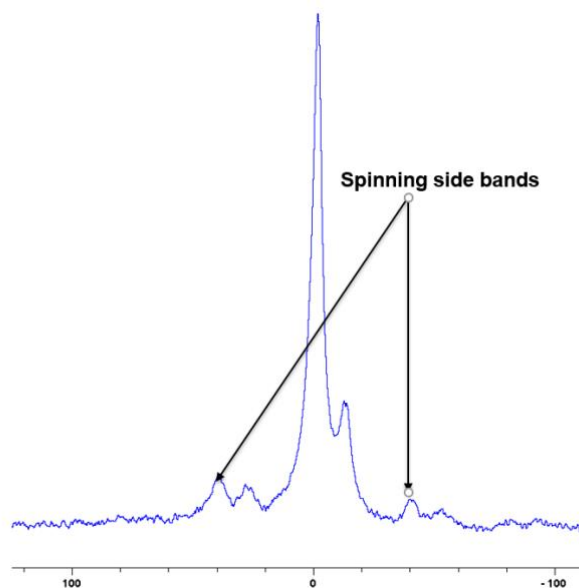


Figure 3. 6 ^{31}P -NMR spectrum of agar agar modified with phosphate groups (the abscissa denotes the chemical shift values, δ , in ppm and the ordinate corresponds to the signal intensity in arbitrary units)

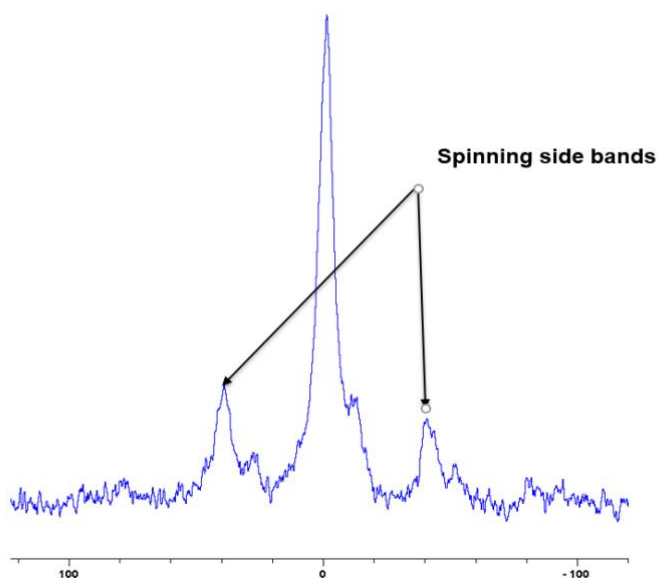


Figure 3. 7 ^{31}P -NMR spectrum of tamarind modified with phosphate groups (the abscissa denotes the chemical shift values, δ , in ppm and the ordinate corresponds to the signal intensity in arbitrary units)

The synthetic routes to phosphorylate the glucopyranose units of carbohydrate-based materials are well documented in the literature (Blennow et al., 2000; Andreas Blennow et al., 2002; Keglevich et al., 2015; Muhammad et al., 2000; Passauer, Liebner, & Fischer, 2009; Thomas, Joseph, Moinuddin, Zhu, & Tretsiakova-McNally, 2020). Keglevich *et al.* established that multiple phosphorylation reactions were possible with different propensities, and the amount of phosphorylation was found to occur predominantly in positions 6 and 3 (Keglevich et al., 2015). These observations were supported by Blennow *et al.* in their comprehensive review, where steric factors were also duly considered (Blennow et al., 2002). The evidence, primarily based on the ^{31}P spectrum, with regard to the exact position(s) and formation of multiple phosphorylated units was also reported (Passauer et al., 2009).

In the present case, it is to be assumed that phosphorylation occurred in positions 6 and 3. However, the relative predominance of substitution at a particular position in each case could not be gauged with certainty, given the rather broad ^{31}P signals obtained which are also exacerbated in some of the modified substrates (see for example, in the case of tamarind) owing to the presence of spinning side bands. It is also relevant to note here that a close shoulder peak with δ values that are less than zero (in the cases of tamarind and agar agar) can be attributed to dimeric phosphate groups formed from intra-chain dehydration reactions, whereas a distinct peak at δ around -18 ppm could indicate multiple phosphorylation within the same molecule (Ebdon et al., 2000). In general, relatively narrow peaks owing to phosphorylation can be attributed to un-associated phosphate functionalities (say, for example in the case of dextran), whereas broader peaks might result from inter-chain dehydration reactions.

3.1.2.1 Calculation of mol fraction of DECP functionalized units in modified oligosaccharides (i.e. the product from the reaction of DECP and β -cyclodextrin, dextran and potato starch)

a. β -cyclodextrin

Formula mass of glucose unit = 162

Formula mass of DECP = 172.55

Formula mass of DECP functionalised glucose unit = $(162 + 172.55) - 36.46 = 298.1$

Assuming the mol fraction of the unreacted glucose units as x , then the mol fractions of the modified glucose units would be $(1-x)$.

If the wt. % of P in the modified sample is 1.7, the following can be written:

$$31 (1-x) \times 100 / [162 x + 298.1 (1-x)] = 1.7$$

Solving for x , we obtain, $x = 0.78$; therefore, the mol fraction of the modified chitosan units is $(1-x) = (1-0.78) = 0.22$

b. Dextran

Formula mass of glucose unit = 162

Formula mass of DECP = 172.55

Formula mass of DECP functionalised glucose unit = $(162 + 172.55) - 36.46 = 298.1$

Assuming the mol fraction of the unreacted glucose units as x , then the mol fractions of the modified glucose units would be $(1-x)$.

If the wt. % of P in the modified sample is 1.0, we can write:

$$31 (1-x) \times 100 / [162 x + 298.1 (1-x)] = 1.0$$

Solving for x , we obtain, $x = 0.94$; therefore, the mol fraction of the modified chitosan units is $(1-x) = (1-0.94) = 0.06$

c. Potato starch

Formula mass of glucose unit = 162

Formula mass of DECP = 172.55

Formula mass of DECP functionalized glucose unit = $(162 + 172.55) - 36.46 = 298.1$

Assuming the mol fraction of the unreacted glucose units as x , then the mol fractions of the modified glucose units would be $(1-x)$.

If the wt. % of P in the modified sample is 3.2, we can write:

$$31 (1-x) \times 100 / [162 x + 298.1 (1-x)] = 3.2$$

Solving for x , we obtain, $x = 0.76$; therefore, the mol fraction of the modified chitosan units is $(1-x) = (1-0.76) = 0.24$

3.1.3 Syntheses of the derivative of chitosan through functionalization with 9,10-Dihydro-9-oxa-10-phosphaphenanthrene-10-oxide (DOPO)

The required modification reaction was carried out by following a literature precedent (Howell et al., 2012) where the phosphoramidate of the repeating unit in chitosan was obtained through the reaction of DOPO with its amino function (Figure 3. 8). The mass of the recovered product was 2.5 g, thus with an overall yield of about 25%. The chemical structure and constitution of the product was obtained through ICP-OES (2.4 wt. %), solid-state NMR (Figure 3. 9) and FT-IR (Figure 3. 10) spectroscopic techniques.

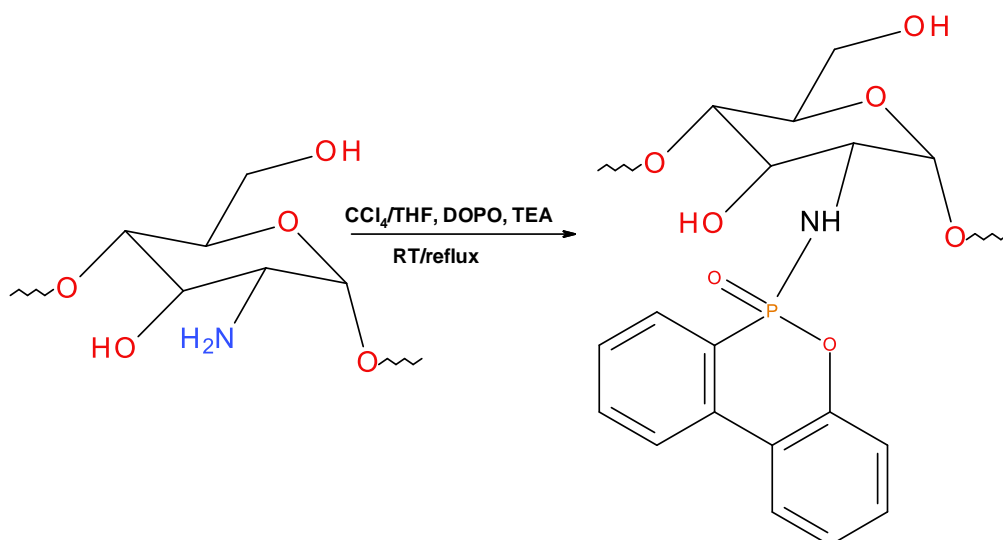


Figure 3. 8 Schematic diagram showing the chemical modification reaction of chitosan with DOPO

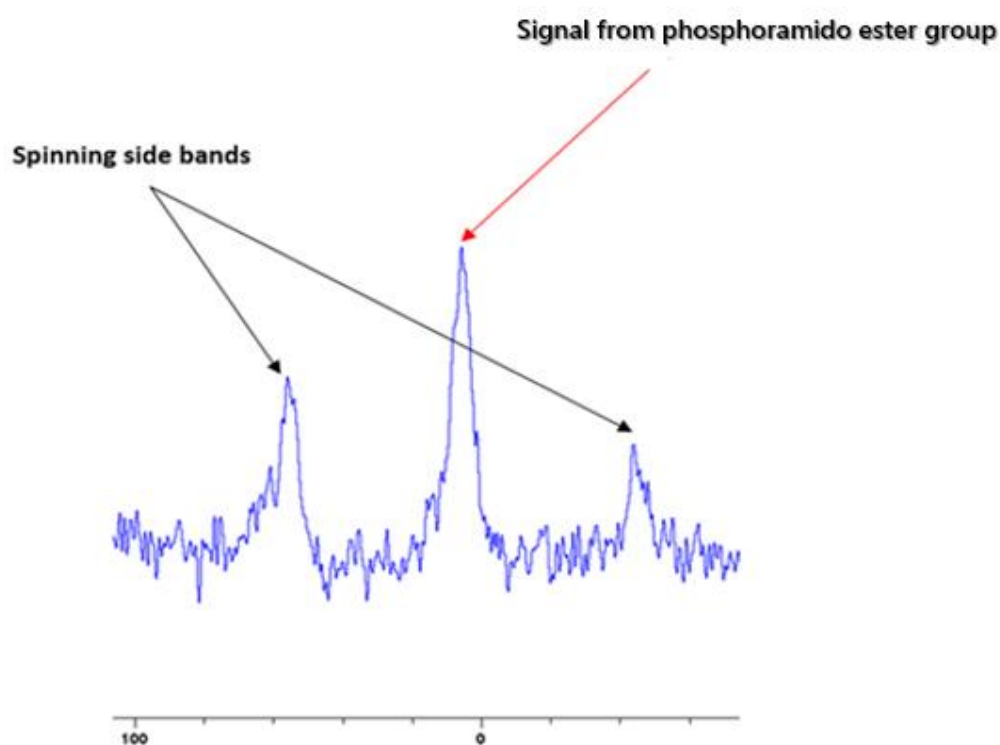


Figure 3. 9 ^{31}P -NMR spectrum of chitosan modified with DOPO groups (the abscissa denotes the chemical shift values, δ , in ppm and the ordinate corresponds to the signal intensity in arbitrary units)

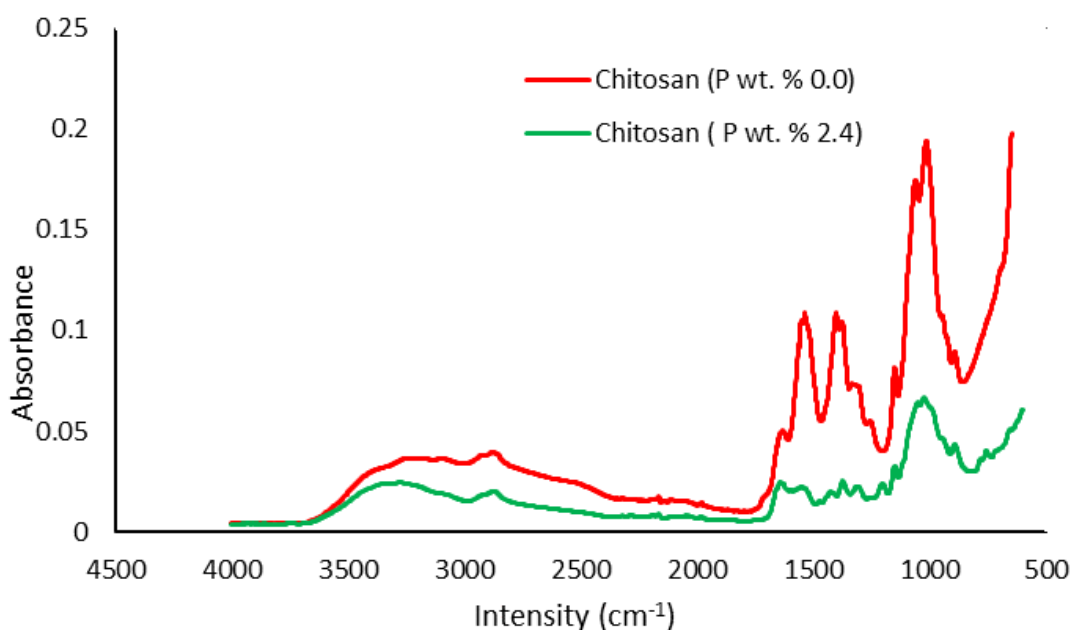


Figure 3. 10 FT-IR spectra of modified and unmodified versions of chitosan

The ^{31}P solid-state NMR gave unequivocal evidence for the incorporation of DOPO (signal at $\delta \sim 0$ ppm), and this inference was complemented through the characteristic features in the FT-IR spectrum of the product as compared to starting substrate (i.e. chitosan). The characteristic absorptions pertaining to the phosphate ester moieties (i.e. $-\text{P}=\text{O}$ and $-\text{P}-\text{O}-\text{C}-$ centred around 1300 to 1000 cm^{-1}) (Harwood, Moody, & Percy, 1999) were found to be present in the vibrational spectrum of the product. The extent of incorporation of the phosphorus was measured through ICP/OES (*ca.* 2.4 wt. %).

In this case also, the phosphorus loading, in wt. %, can be subsequently converted into the degree of functionalization for the chitosan monomeric unit (i.e. as in the cases of β -cyclodextrin, dextran and potato starch), as follows:

3.1.3.1 Calculation of mol fraction of DOPO functionalized units in modified chitosan (i.e. the product from the reaction of DOPO and chitosan)

Formula mass of chitosan unit = 161.2

Formula mass of DOPO = 216.2

Formula mass of DOPO functionalized chitosan unit = $(161.2 + 216.2) - 1 = 376.4$

Assuming the mol fraction of the unreacted chitosan units as x , then the mol fractions of the modified chitosan units would be $(1-x)$.

If the wt. % of P in the modified sample is 2.4, we can write:

$$31(1-x) \times 100 / [161.2x + 376.4(1-x)] = 2.4$$

Solving for x , we obtain, $x = 0.85$; therefore, the mole fraction of the modified chitosan units are $(1-x) = (1-0.85) = 0.15$

3.1.4 Synthesis of diethylbenzylphosphonate: Michaelis-Arbuzov reaction (Bhattacharya & Thyagarajan, 1981)

Given the relatively high reactivity of benzylic halides (benzyl bromide in this case) and, as expected, the thermally induced rearrangement of the intermediate, obtained by the reaction of benzyl bromide with triethylphosphite, readily proceeded to form the desired phosphonate with a good yield (Yield = 45.5 g; 0.19 mols). The purity of the product was also found to be high (> 98%) as was judged from their ^1H and ^{31}P spectra (Figures 3. 11 and 3. 12)

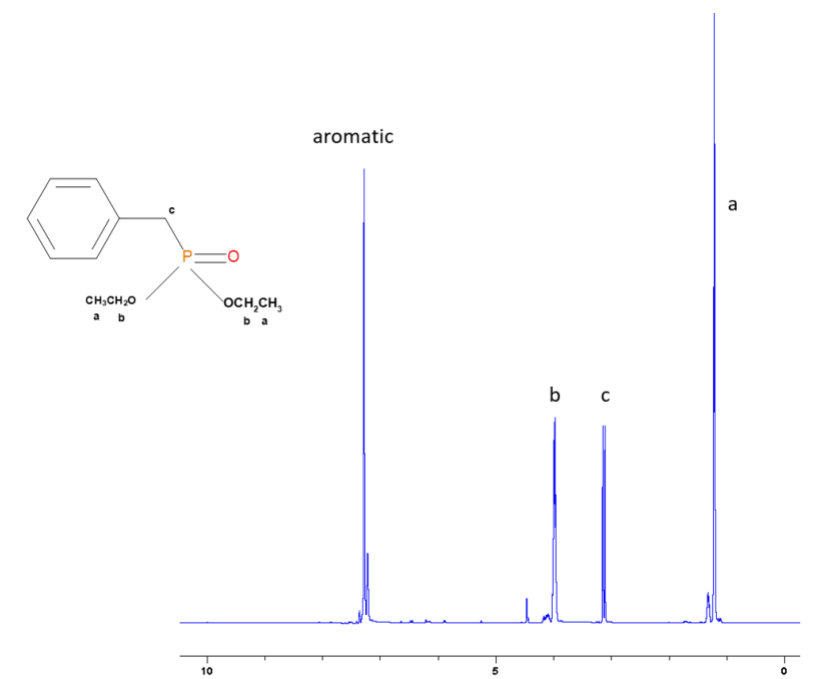


Figure 3. ^{11}H NMR spectrum of diethylbenzylphosphonate in CDCl_3 (the abscissa denotes the chemical shift values, δ , in ppm and the ordinate corresponds to the signal intensity in arbitrary units)

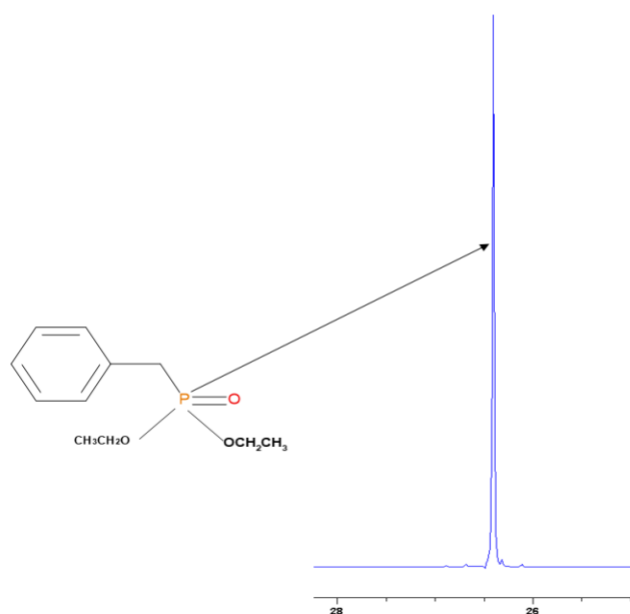
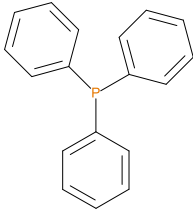
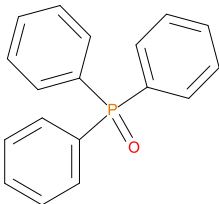
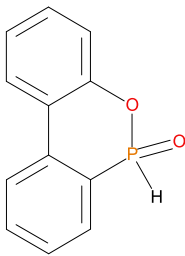
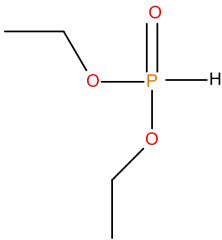


Figure 3. ^{31}P -NMR spectrum of diethylbenzylphosphonate in CDCl_3 (the abscissa denotes the chemical shift values, δ , in ppm and the ordinate corresponds to the signal intensity in arbitrary units)

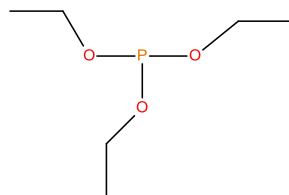
3.1.5 Formulation and coating for cone calorimetry

The chemical nature and oxidation states of the various P-containing additives that were utilized to make the formulations for coating (cone tests) are given in Table 3. 2.

Table 3. 2 Details regarding the chemical environments of the P-containing organic additives

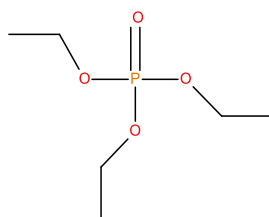
| Sl. No. | Sample | Chemical structure | Remark (class of compound/oxidation state of P atom) |
|---------|--|---|--|
| 1 | Triphenylphosphine (TPP) |  | Phosphine/III |
| 2 | Triphenylphosphine oxide (TPPO) |  | Phosphine oxide/V |
| 3 | 9,10-dihydro-9-oxa-10-phosphahenanthrene-10-oxide (DOPO) |  | Cyclic phosphine oxide/V |
| 4 | Diethylphosphite (DEPi) |  | Aliphatic, H-phosphite/III |

5 Triethylphosphite (TEPi)



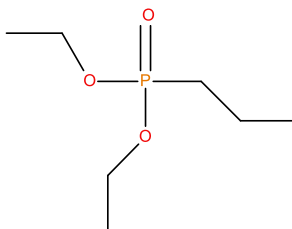
Aliphatic phosphite/III

6 Triethylphosphate (TEPa)



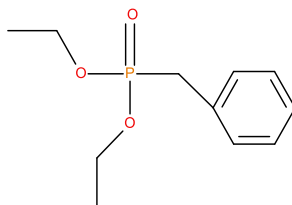
Aliphatic phosphate/V

7 Diethylpropylphosphonate (DEPP)



Aliphatic phosphonate/V

8 Diethylbenzylphosphonate (DEBP)



Benzylic phosphonate/V

As can be seen from Table 3.2, the additives chosen for the present study not only differ in terms of the chemical environments, but also in terms of the oxidation state, of the phosphorus atom (III, or V). They are also constituted of both solids and liquids, and differ in their melting, or boiling, temperatures. Here, the phosphine and phosphine oxides (i.e. TPP, and TPPO and DOPO) can be considered as stable versions of organo-phosphorus compounds with aromatic structural integrity, whereas the liquid ones (DEPi, TEPi, TEPa, DEPP and DEBP) are relatively easily volatile, and are also more amenable to thermal cracking. In this context, we have also endeavoured to identify the gaseous phase fragments emanating from these additives, under an electron impact (GC/MS), or upon thermolysis (i.e. pyrolysis-GC/MS) - the details are given in sections 3.6.1 and 3.6.2. Whilst some of the additives have been extensively used in the case of synthetic polymers (Ebdon et al., 2000; Salmeia & Gaan, 2015), to the best of our knowledge, they have not been explored as components for bio-sourced formulations for passively fire protecting ligno-cellulosic materials (Thomas et al., 2020).

3.2 Characterization

3.2.1 Thermogravimetric Analysis (TGA)

The thermograms of the modified versions of the substrates (β -cyclodextrin, dextran, potato starch, agar-agar, tamarind and chitosan) indicate obvious changes in the general profiles and induction temperatures, as compared with their unmodified counterparts (see in Table 3. 3 and Figures: 3. 13 to 3. 24). Dehydration and decomposition reactions are generally been considered as the main two processes associated with the degradation mechanisms of carbohydrate based substrates, the former occurring below 200°C and the latter between a range of temperatures (*ca.* 250 to 350°C). The volatilization of water molecules predominantly arise from adsorbed water (i.e. their moisture contents), and perhaps to lesser extents from dehydration (or ‘charring’ reactions that are analogues to those occurring in cases of mono, di, and oligosaccharide) (Greenwood, 1967; X. Liu et al., 2013). However, the second stage in the degradation can be attributed to the main chain bond cleavages producing combustible fragments including levoglucosan (see also in Figure 1.1; chapter 1; section 1.2; page 5)

As expected in all the cases of unmodified and modified materials, the test samples lose water (i.e. below *ca.* 200°C). It is also evident from the thermograms that the phosphorous modification facilitates noticeable improvement in their induction temperatures, which could

essentially mean that the modifications have made the substrates relatively more thermally stable. However, this trend is not seen in the case of temperature values at 50 wt. % mass loss. After the initial dehydration (at about *ca.* 70-130°C), the next step corresponds to the thermal decomposition of the unmodified substrates (i.e. main chain random bond cleavages occurring around 250°C). The temperature at 50 wt. % mass loss showed a minimum value in the case of phosphorous-modified substrates except for potato starch and chitosan. Furthermore, it is quite interesting to note that in all the cases, there are significant increase in the char yields in the modified substrates as compared to their unmodified counterparts (both in the case of char residues obtained at 400 and at 800°C). The char enhancements factor (in percentages) at 800°C also showed variations, whereas the normalized values to the P-loadings gave a maximum value of 48 in the case of dextran, and minimum value of 1.7 in the case of tamarind (Thomas, Joseph, Moinuddin, Zhu, & Tretsiakova-McNally, 2020).

Table 3. 3 Details from TGA analyses

| Sample | P (wt. %) | Induction Temp (°C) | Temp at 50 wt. % (°C) | Residue at 400°C (wt. %) | Final residue at 800°C (wt. %) | Increase in char residue (%) | Increase in char residue normalized to P-loading (%) |
|----------------|----------------------|--------------------------------|----------------------------------|---|---|---|---|
| β-cyclodextrin | 0.0 | 94.0 | 356 | 11.4 | 6.00 | | |
| β-cyclodextrin | 1.7 | 96.0 | 334 | 39.7 | 22.9 | 74 | 44 |
| Dextran | 0.0 | 85.0 | 340 | 15.2 | 9.80 | | |
| Dextran | 1.0 | 93.0 | 273 | 29.3 | 18.7 | 48 | 48 |
| Potato Starch | 0.0 | 93.0 | 335 | 18.3 | 11.9 | | |
| Potato Starch | 3.2 | 129 | 366 | 45.6 | 25.4 | 53 | 17 |
| Agar agar | 0.0 | 77.0 | 333 | 36.7 | 14.8 | | |
| Agar agar | 5.5 | 90.0 | 280 | 36.9 | 23.7 | 38 | 7.0 |
| Tamarind | 0.0 | 86.0 | 357 | 38.5 | 21.3 | | |
| Tamarind | 6.6 | 105 | 338 | 39.6 | 24.0 | 11 | 1.7 |
| Chitosan | 0.0 | 71.0 | 374 | 44.0 | 31.6 | | |
| Chitosan | 2.4 | 72.0 | 378 | 48.0 | 33.5 | 5.7 | 2.4 |

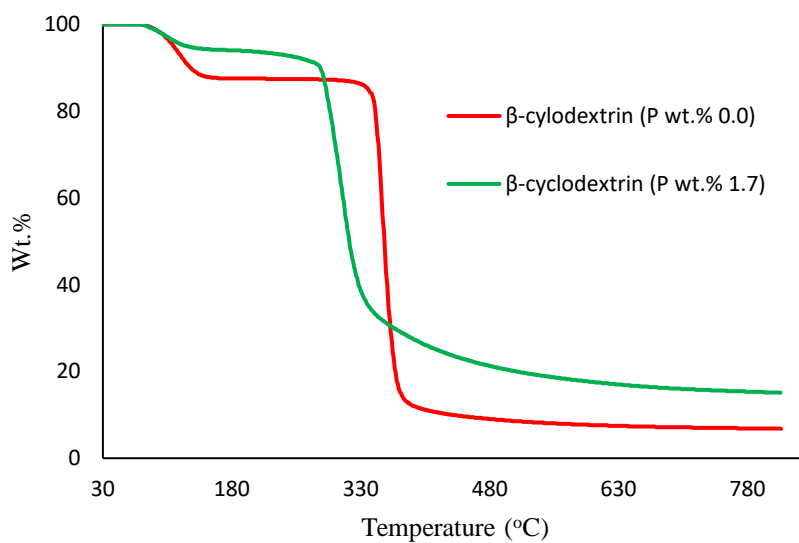


Figure 3. 13 Thermograms of modified and unmodified versions of β -cyclodextrin at 60 \circ C min⁻¹

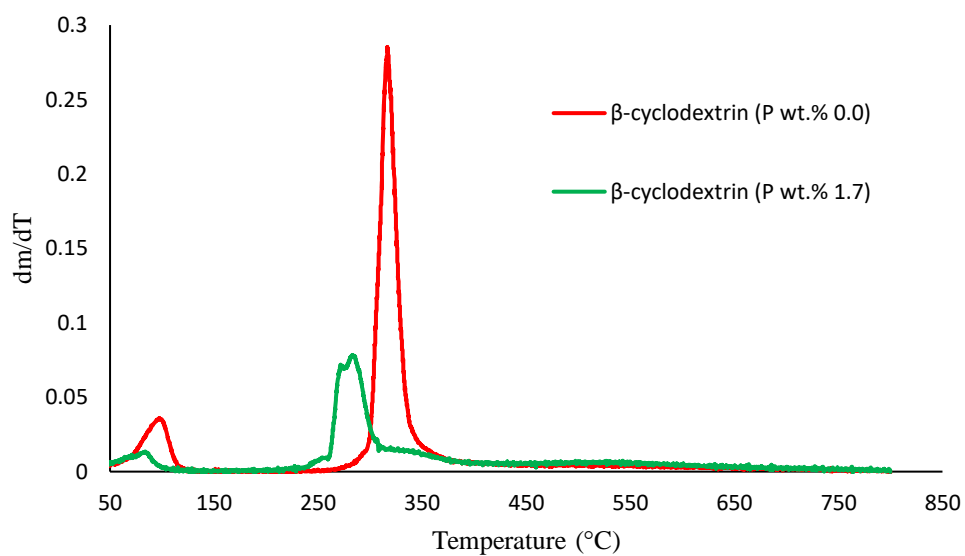


Figure 3. 14 Plot of the dm/dT vs. temperature (\circ C) for modified and unmodified versions of β -cyclodextrin

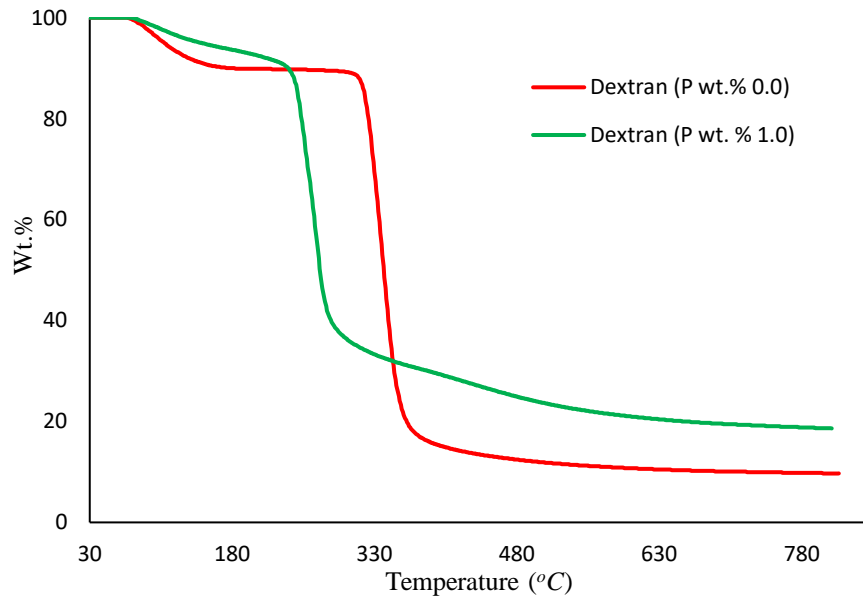


Figure 3. 15 Thermograms of modified and unmodified versions of dextran at 60°C min⁻¹

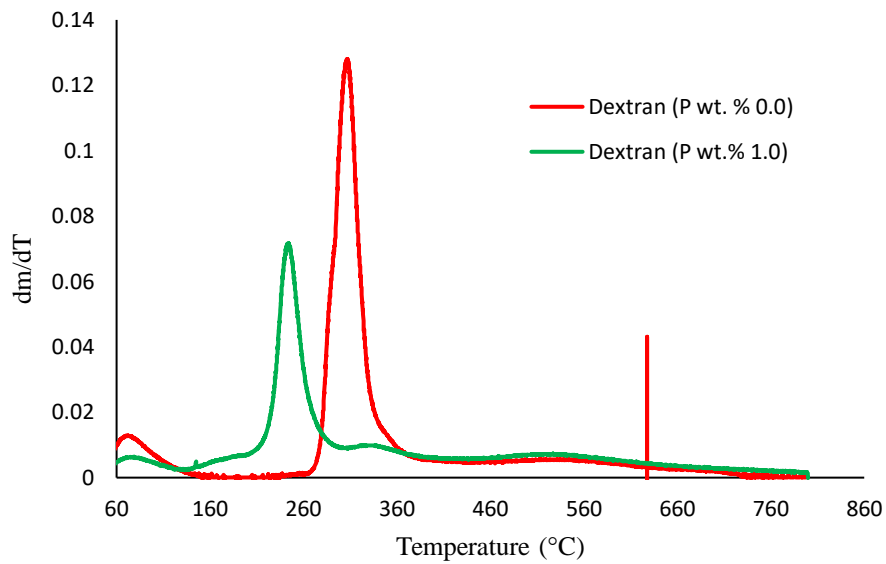


Figure 3. 16 Plot of the dm/dT vs. temperature (°C) for modified and unmodified versions of dextran

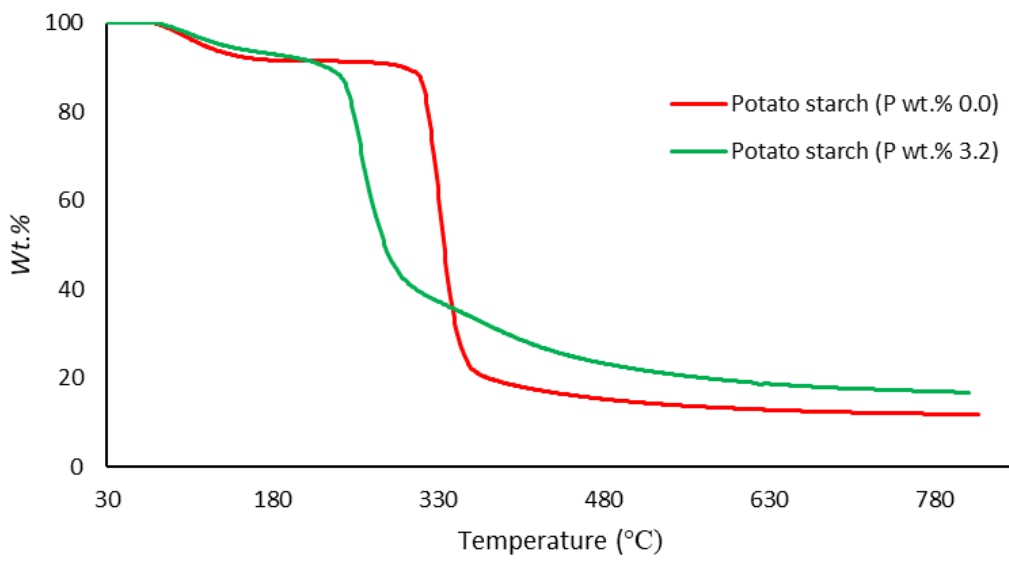


Figure 3. 17 Thermograms of modified and unmodified versions of potato starch at 60°Cmin⁻¹

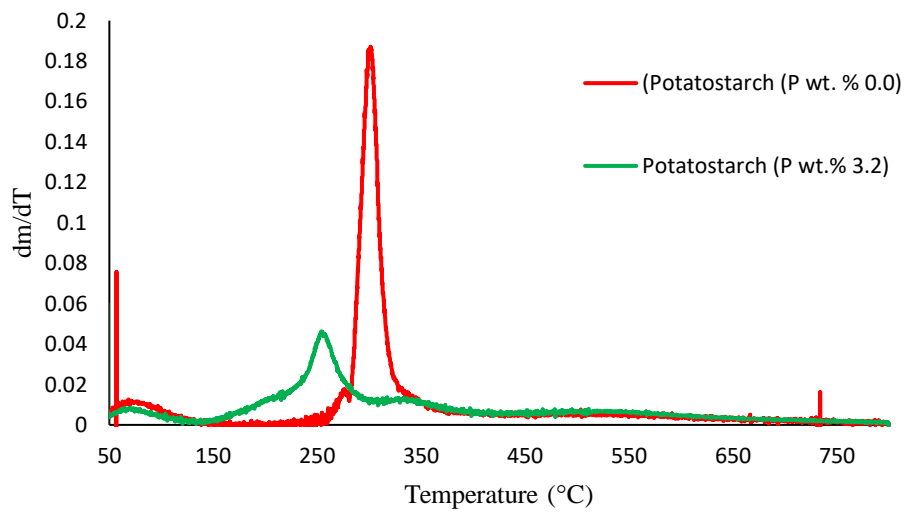


Figure 3. 18 Plot of the dm/dT vs. temperature (°C) for modified and unmodified versions of potato starch

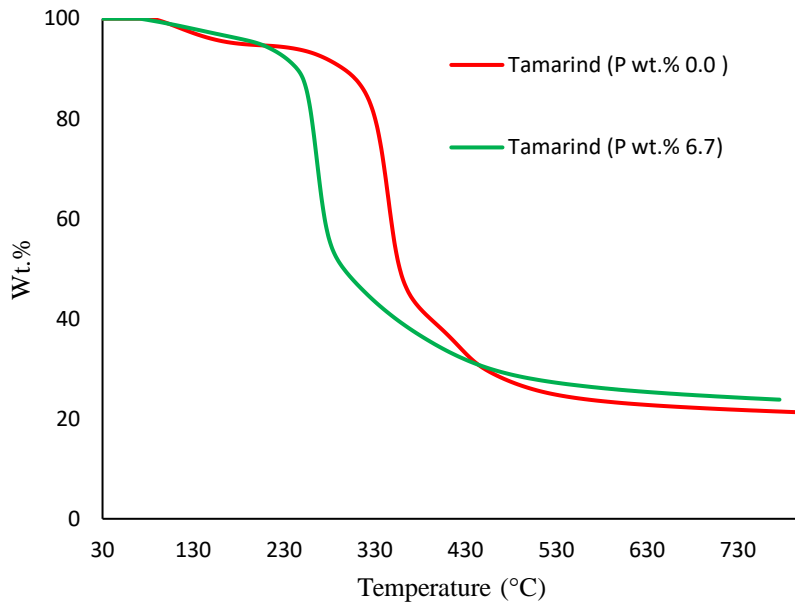


Figure 3. 19 Thermograms of modified and unmodified versions of tamarind at 60°C min⁻¹

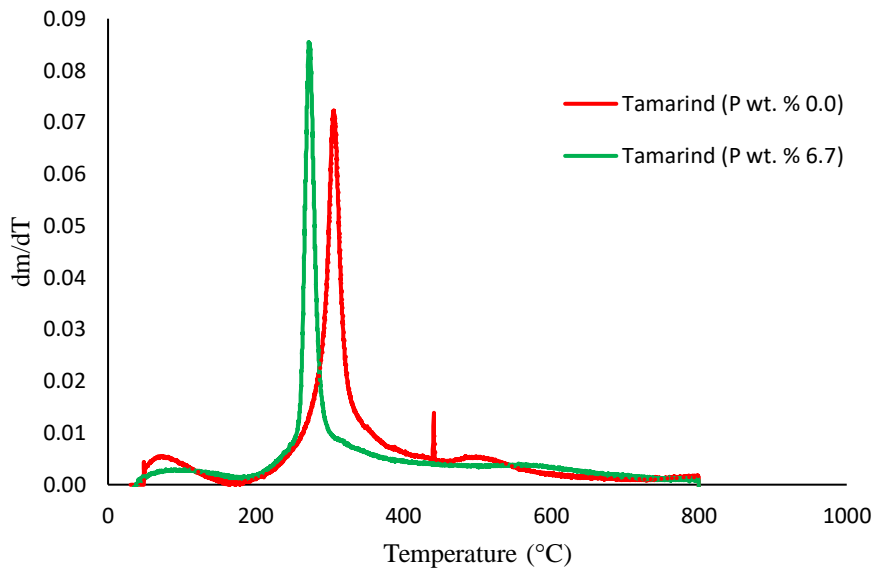


Figure 3. 20 Plot of the dm/dT vs. temperature (°C) for modified and unmodified versions of tamarind

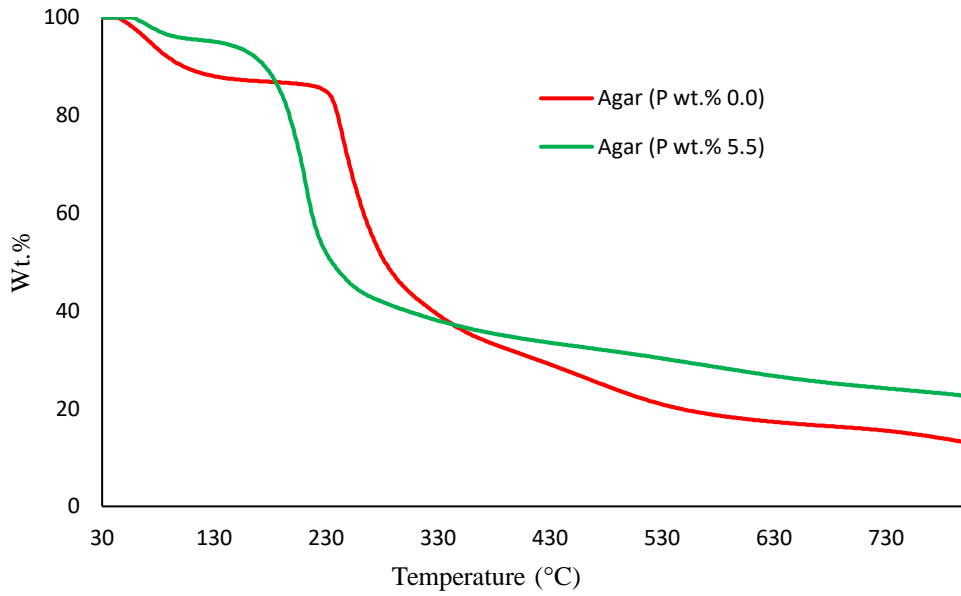


Figure 3. 21 Thermograms of modified and unmodified versions of agar agar at 60°C min⁻¹

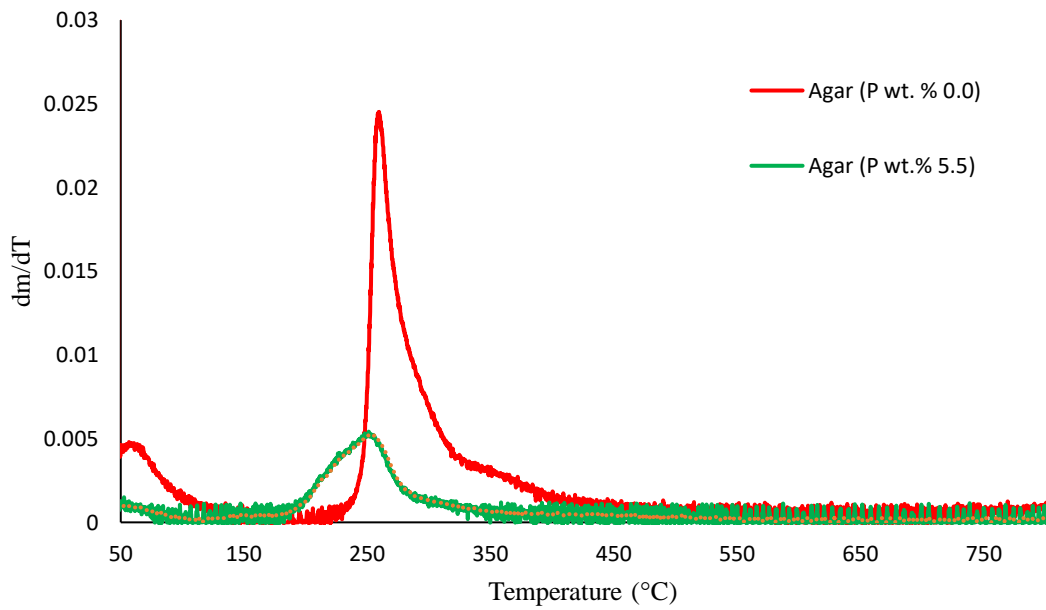


Figure 3. 22 Plot of the dm/dT vs. temperature (°C) for modified and unmodified versions of agar agar

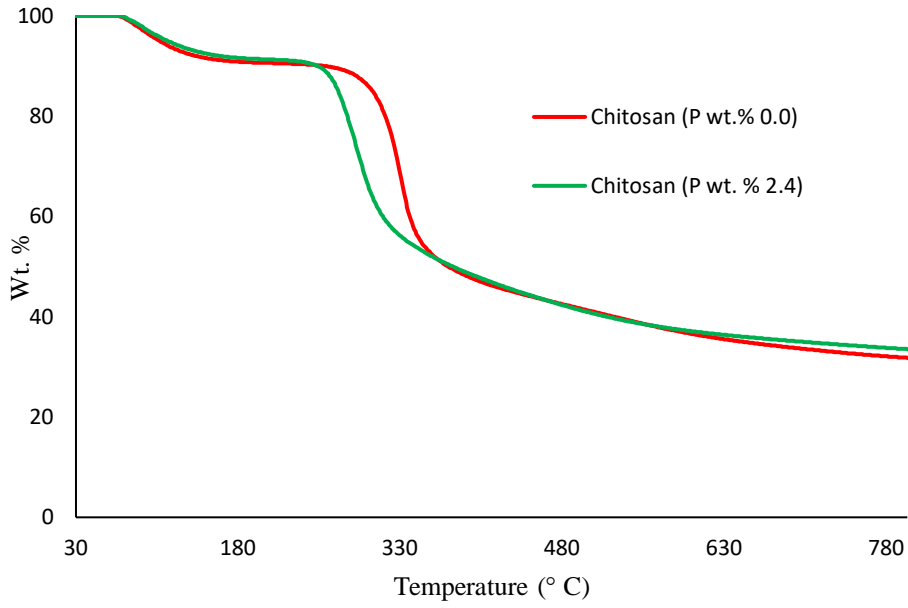


Figure 3. 23 Thermograms of modified and unmodified versions of chitosan at 60°C min⁻¹

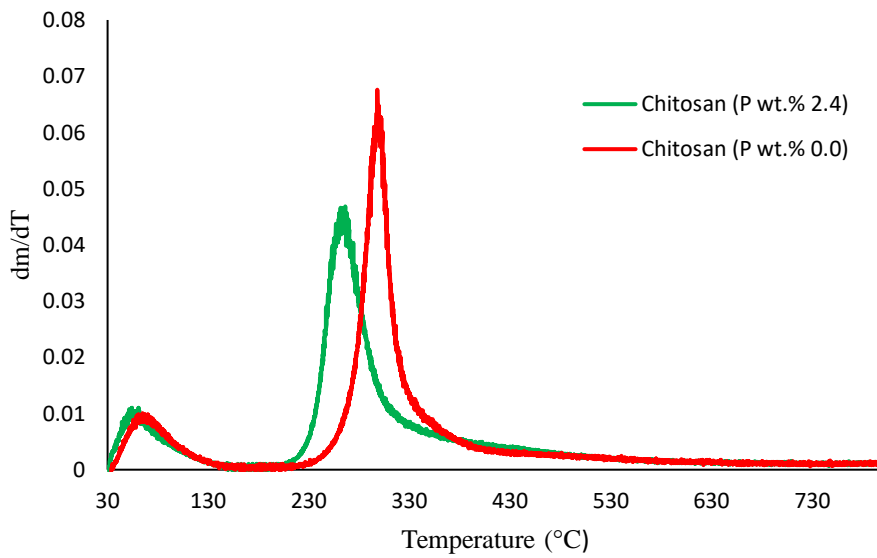


Figure 3. 24 Plot of the dm/dT vs. temperature (°C) for modified and unmodified versions of chitosan

3.2.1.1 Detailed kinetic analysis (FWO and SB methods)

Generally, the thermal and thermo-oxidative degradation of polymeric materials are complex processes involving consecutive and/or parallel steps. However, for the sake of simplicity, often the kinetic analysis of the data from a TGA thermogram is performed using a single step kinetic equation (Budrugeac, 2000). Furthermore, during the TGA runs, both isothermal and non-isothermal degradation regimes are adopted experimentally (Howell, 2002; Howell & Daniel, 2015; Yongjiang, Huaqing, Hongyan, Zhiping, & Chaohe, 2011). It is also quite evident here that the isothermal approach is thermodynamically more robust procedure than the latter one, where a single, or multiple heating rates are employed. In addition it is also assumed that, during the mathematical treatment of the data, the temporal integral (isothermal) is transformed to fit the multiple heating regime (non-isothermal), are not going to affect the reaction kinetics. However for complex multistep-process, the assumption may not be valid (Vyazovkin et al., 2011). Therefore, this inherently limits the application of the relevant parameters, especially, the values of E_a that are computed from non-isothermal methods. Whilst these values are still useful, particularly, to compare unmodified and modified polymeric systems, their validity in predicting the performance, or indeed life cycle predictions, of a particular material should be treated with caution.

The values obtained in the present work, through the use of non-isothermal heating regimes, both single and multiple rates, can be only at the best considered as ‘apparent’ values of E_a . Here, we chose a widely accepted model free method (Flynn-Wall-Ozawa method: different heating rates of 5, 10, 20, 30 and 60°C min⁻¹) (Flynn & Wall, 1966; Ozawa, 1992) and an in-house software developed by Professor Stephen Bigger (SB method) to study the kinetics of starch decomposition (Bigger, Cran, & Tawakkal, 2015) (by employing the data for a single heating rate of 10°C min⁻¹)

Flynn-Wall-Ozawa (FWO) method

For this analysis, the dynamic TGA analyses of the unmodified substrates (β -cyclodextrin, dextran, potato starch, agar agar, tamarind and chitosan) at various heating rates (10, 20, 30, 40 and 60°C min⁻¹) were carried out under an atmosphere of nitrogen. This method demonstrated that plotting log heating rate (β) against $1/T\alpha$ generally gave straight lines with a slope equal to $-0.4567(E_a/R)$. This is based on the following equation:

$$\log_{10} \beta = -2.315 + \log_{10} (AE_a/R) - \log_{10} g(\alpha) - 0.4567(E_a/RT\alpha) \quad (3)$$

The value of α (which are defined as the weight fraction of polymer reacted) at a particular temperature is calculated using the following equation:

$$\alpha = (m_i - m_t) / (m_i - m_f) \quad (4)$$

Where, m_i and m_f are the initial and final masses respectively, and m_t is the measured mass at a given temperature.

However in the case of carbohydrate substrates, it is worthy to note that the higher and lower values of α did not provide the expected linear relation as envisaged classically by Flynn-Wall-Ozawa method. For example, in the case of potato starch, the $\log\beta$ vs. $1/T$ plots only gave straight lines for α values, typically, between 0.2 and 0.6. Essentially, we followed the same methodology, in the case of the remaining substrates, which are given below.

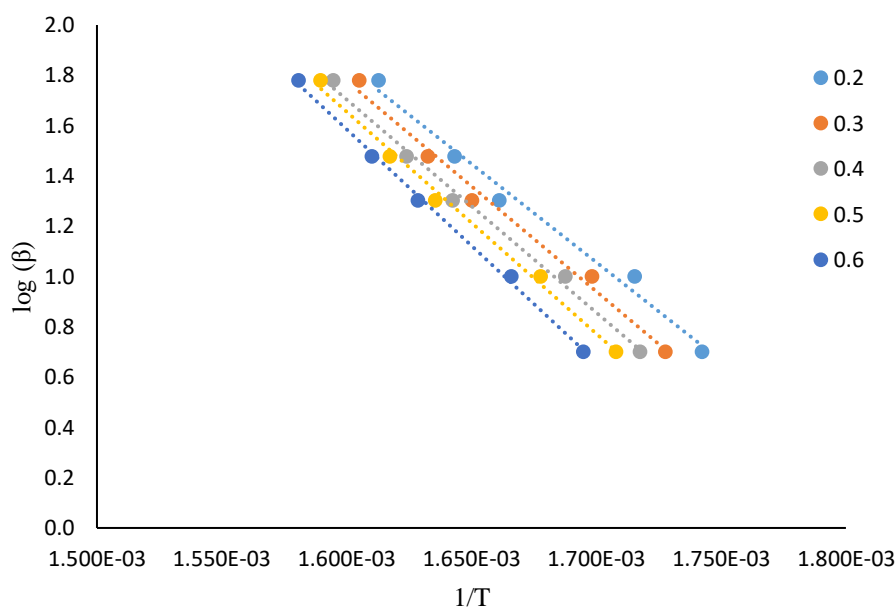


Figure 3. 25 A plot of $\log \beta$ vs. $1/T$ at various α values (given as the inset) for β -cyclodextrin

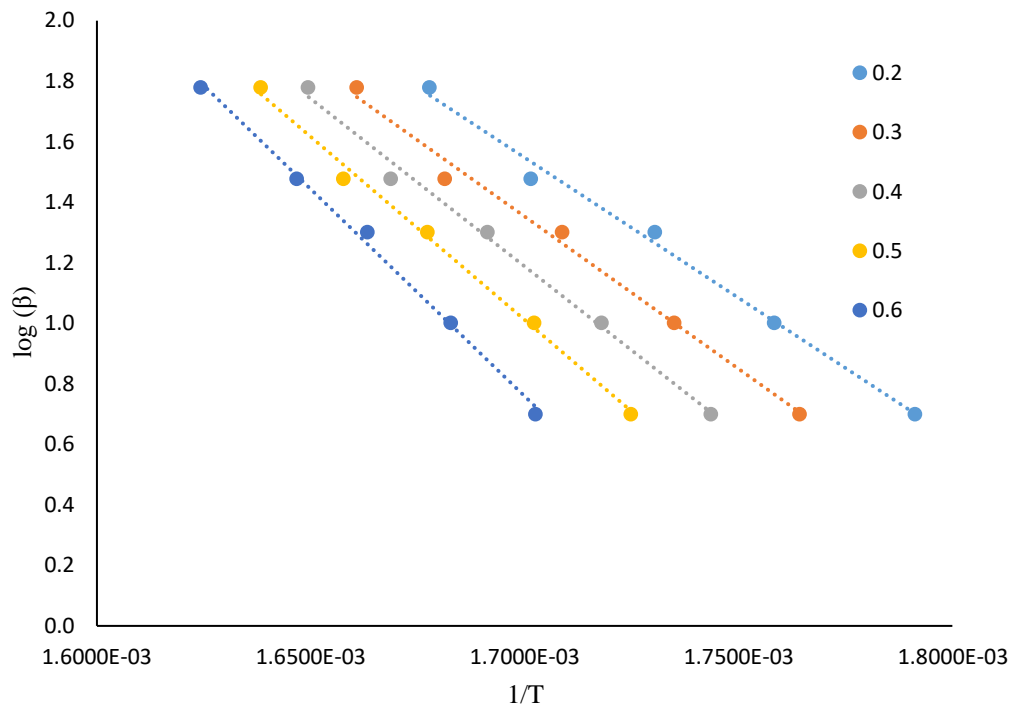


Figure 3. 26 A plot of $\log \beta$ vs. $1/T$ at various α values (given as the inset) for dextran

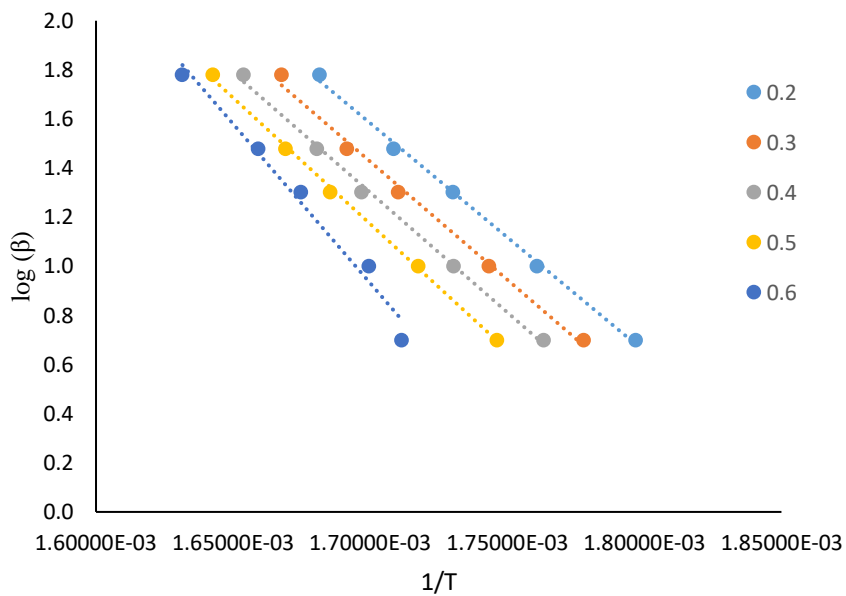


Figure 3. 27 A plot of $\log \beta$ vs. $1/T$ at various α values (given as the inset) for potato starch

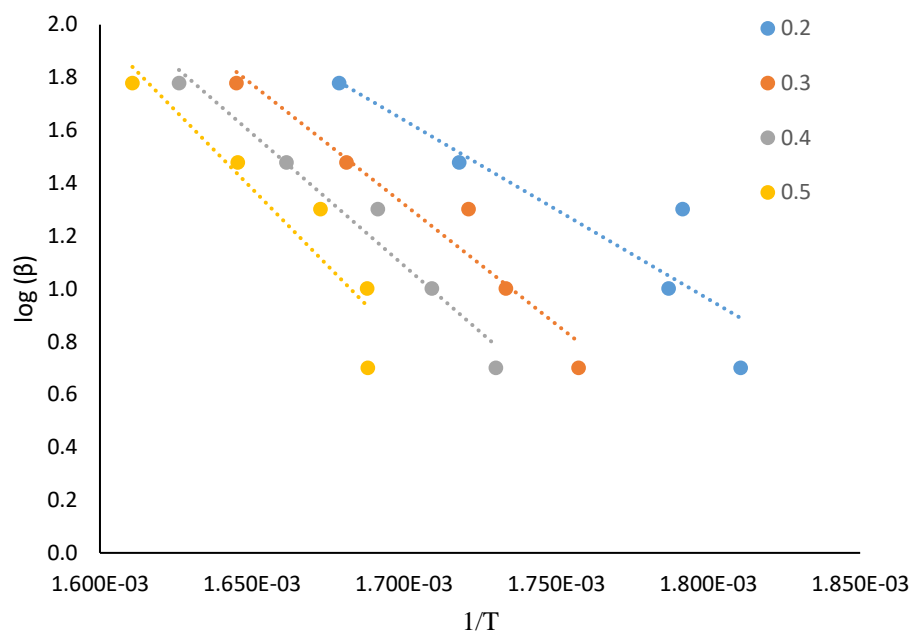


Figure 3. 28 A plot of $\log \beta$ vs. $1/T$ at various α values (given as the inset) for tamarind

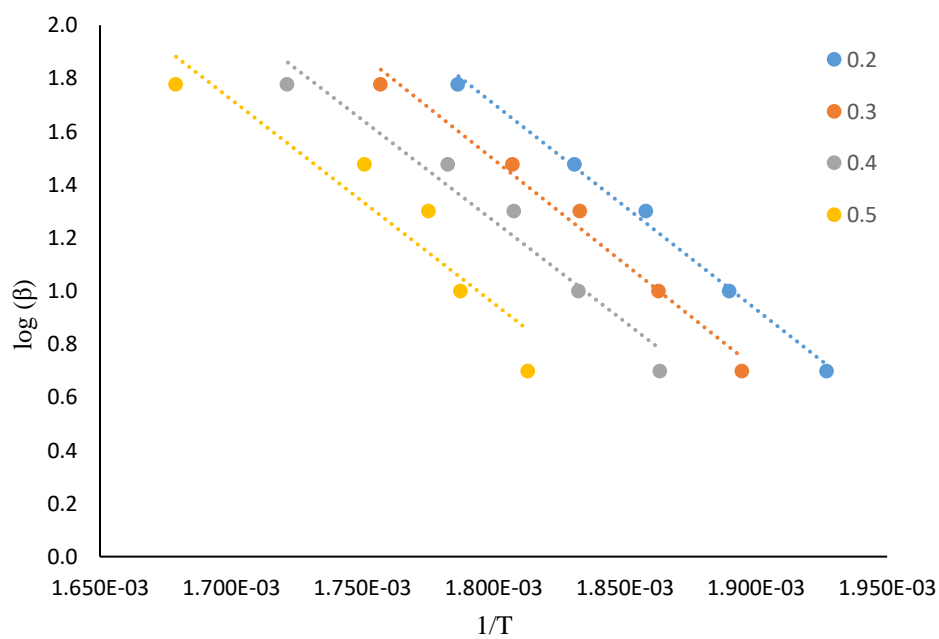


Figure 3. 29 A plot of $\log \beta$ vs. $1/T$ at various α values (given as the inset) for agar agar

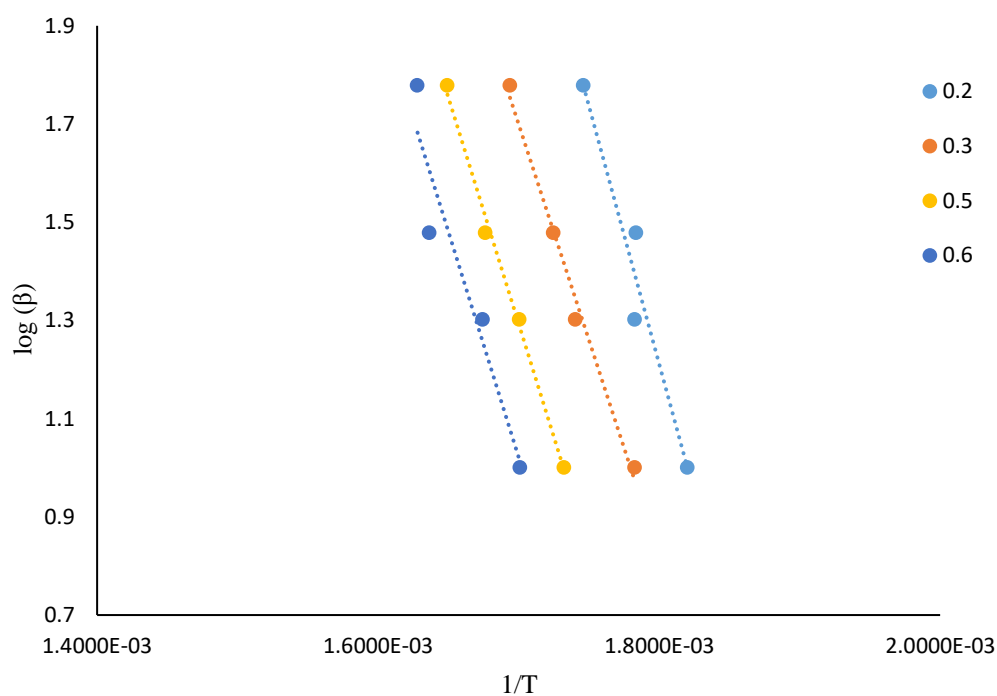


Figure 3. 30 A plot of $\log \beta$ vs. $1/T$ at various α values (given as the inset) for chitosan

The corresponding activation energies, in kJ mol^{-1} , for each of the α values are tabulated below (Table 3.4).

Table 3. 4 Activation energies of each substrates for different α values

| Sl. No. | α | Potato starch (kJ mol^{-1}) | β -cyclodextrin (kJ mol^{-1}) | Dextran (kJ mol^{-1}) | Agar agar (kJ mol^{-1}) | Tamarind (kJ mol^{-1}) | Chitosan (kJ mol^{-1}) |
|---------|----------|--|--|----------------------------------|------------------------------------|-----------------------------------|-----------------------------------|
| 1 | 0.2 | 169 | 143 | 169 | 141 | 123 | 191 |
| 2 | 0.3 | 175 | 152 | 183 | 143 | 165 | 160 |
| 3 | 0.4 | 178 | 154 | 202 | 138 | 182 | * |
| 4 | 0.5 | 187 | 161 | 220 | 140 | 213 | 168 |
| 5 | 0.6 | 236 | 169 | 249 | # | # | 167 |

*the linear plot obtained when $\alpha = 0.4$ turned out to be unreliable as revealed by the corresponding value of $E_a < 50$, which can be considered as incredibly low

no linear fit of the data were obtained for tamarind and agar agar (for $\alpha = 0.6$)

SB method (theoretical and computational approach):

The equation for the non-isothermal kinetic analysis of TGA data is generally derived from the standard kinetic expression for an isothermal experiment can be given as follows:

$$d\alpha/dt = k(T)f(\alpha) \quad (5)$$

where $f(\alpha)$ is a time-dependent function of α , the extent of reaction (see in eqn. 2 in case of FWO method), $k(T)$ is a temperature-dependent rate constant, T is the absolute temperature and t is time. The function $f(\alpha)$ can take on many different forms depending on the reaction kinetics of the system under investigation (Bigger, Cran, & Tawakkal, 2015).

In the case of non-isothermal kinetics, eqn. 3 can be conveniently changed from the time domain to the temperature domain as follows (Vyazovkin et al., 2011)

$$d\alpha/dt = (dT/dt) \times (d\alpha/dT) = \beta \times (d\alpha/dT) \quad (6)$$

where β is the heating rate, which is usually maintained as a constant.

Substituting eqn. 4 in eqn. 3 and integrating between the corresponding limits of $(0, T_0)$ and (α, T) where T_0 is the temperature at time $t = 0$ and T is the temperature at $t = t$ yields:

$$\int_0^\alpha d\alpha/f(\alpha) = (1/\beta) \int_{T_0}^T k(T)dT \quad (7)$$

Substituting the Arrhenius expression for $k(T)$ in eqn. 5 and defining $1/g(\alpha) = df(\alpha)/d\alpha$ yields:

$$g(\alpha) = (A/\beta) \int_{T_0}^T \exp(-E_a/RT)dT \quad (8)$$

where A is the Arrhenius A-factor, E_a is the apparent activation energy which is assumed to remain constant over the temperature range, and R is the ideal gas constant. The integral term in eqn. 6 is often referred to as the *Arrhenius integral*. Here, the valid assumption that $(A/\beta) \int_{T_0}^T \exp(-E_a/RT)dT \approx 0$ is usually made to simplify the Arrhenius integral so as to provide an analytical solution to eqn. 6 (Bigger, Cran, & Tawakkal, 2015). The resulting equation takes the following form:

$$g(\alpha) = (AE_a/R\beta) \int_x^\infty [\exp(-x)/x^2] dx \quad (9)$$

where $x = E_a/RT$ and can be written more simply as:

$$g(\alpha) = (AE_a/R\beta) \times p(x) \quad (10)$$

where the function $p(x)$ represents the integral $p(x) = \int_x^\infty [\exp(-x)/x^2] dx$.

Methods of data treatment

Vyazovkin *et al.* (Vyazovkin et al., 2011; Vyazovkin & Wight, 1998) suggested that equations of the form depicted by eqn. 6 and those equations derived from it such as eqns. 7 and 8 represent the foundation for the so-called *integral methods* of analysis. Clearly, the analyses of TGA results utilizing such equations that require solution to the Arrhenius integral are therefore deemed to be *integral methods* of analysis.

Conversely, the so-called *differential methods* of analysis avoid the historic difficulties that arise, for example, in solving Arrhenius integrals. This is achieved by combining eqns. 3 and 4 along with the expression for the Arrhenius equation without integrating the resulting equation:

$$d\alpha/dT = (A/\beta) \exp(-E_a/RT) \times f(\alpha) \quad (11)$$

Eqn. 10 is derived by taking the natural logarithms of both sides of eqn. 9:

$$\ln [(d\alpha/dT)/f(\alpha)] = \ln(A/\beta) - E_a/RT \quad (12)$$

An approach that utilizes the derivative $d\alpha/dT$ to process experimental data would thus be considered to be an example of a *differential* method of analysis.

In practice, the fact that all experimental data contain inherent noise can mean that one of the above methods of data analysis will produce more reliable values of the kinetic parameters than the other. It is claimed, for example, that integral methods are best suited for integral data such as TGA data because differentiating integral data tends to magnify the noise (Vyazovkin & Wight, 1998).

Another approach to the processing of TGA data in order to obtain kinetic parameters involves the so-called *iso-conversional* methods that have an advantage of not needing to have prior knowledge of the mathematical form of $f(\alpha)$. Such methods are based on the principle that at a constant degree of conversion the rate of a reaction is only a function of temperature (Flynn & Wall, 1966; Friedman, 1964; Ozawa, 1965).

Algorithms for non-isothermal TGA data analysis.

Algorithms and associated software suite were devised, in-house, to facilitate a convenient method of analyses for a wide range of non-isothermal TGA data. These computer-based algorithms are: (i) an algorithm for identifying suitable kinetic models for fitting the experimental data based on theoretical reference characteristics calculated by Dollimore *et al.* (Dollimore, Lerdkanchanaporn, & Alexander, 1997) for a given set of (T, α) input data and (ii) an iterative arithmetic algorithm that solves eqn. 8 without invoking assumptions, or approximations, in order to extract the two Arrhenius parameters. The overall approach delivers the so-called kinetic triplet (i.e. A , E_a and n) information and also enables one to assess whether the analysis has been appropriate in so far as the degradation occurred by a single mechanism over the temperature range.

Algorithm to identify kinetic model

This algorithm systematically calculates from the experimental (T, α) data, the values of three characteristic parameters $(d\alpha/dT)_{max}$, α_{max} and ΔT , where $(d\alpha/dT)_{max}$ is the maximum value of the derivative of α with respect to temperature, α_{max} is the value of α at which the maximum derivative value occurs, and ΔT is the half-height width of the $d\alpha/dT$ vs. T plot. The parameters are then compared with the corresponding ranges for these given in the reference data (Dollimore et al., 1997) for a number of different kinetic models, and a fit parameter, ρ , are calculated for each model.

Iterative numerical TGA analysis algorithm

Taking the natural logarithm of both sides of eqn. 8 and allowing for separate experimental measurements at different values of α_i as well as allowing for different values of the activation energy yields:

$$\delta_i(\alpha_i, E_{a,j}) = \ln[g(\alpha_i)] - \ln[p(\chi_i)] = AE_{a,j}/R\beta \quad (13)$$

Where $\delta_i(\alpha_i, E_{a,j})$ represents a single value of a difference function that exists for a given value of α_i and their corresponding χ_i value. The value of χ_i at a given value of $E_{a,j}$ is calculated from $\chi_i = E_{a,j}/RT_i$ where T_i is the temperature corresponding to the particular χ_i value (see for details in Chapter 2; Section 2.2.5.2; page 37-42).

Taken together, the two algorithms described herein provide a seemingly useful approach to obtaining plausible kinetic triplets for a given system under investigation provided complexities such as mechanistic changes are not encountered during the non-isothermal experiment (Bigger, Cran, & Bohn, 2015). It should be noted here that for the analyses using the SB method, we chose a moderate heating rate of 10°C min⁻¹ as it is assumed that at this heating rate, most of the representative degradation pathways of the unmodified substrates are essentially captured (see in Figure 3. 31 below).

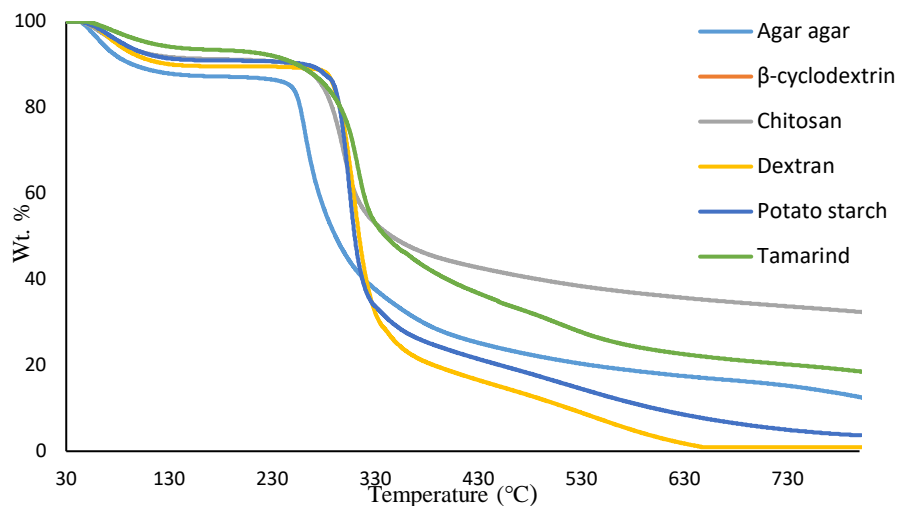


Figure 3. 31 An overlay of TGA at 10°C min⁻¹ of all the six substrates

Table 3. 5 Relevant parameters obtained using the FWO and SB methods

| Sl. No. | Substrate | E_a (FWO method) (kJ mol ⁻¹) | * E_a (SB method) (kJ mol ⁻¹) | A (s ⁻¹) | # R_2 | Kinetic model chosen |
|---------|-----------------------|--|---|------------------------|---------|----------------------------------|
| 1 | β -cyclodextrin | 156 | 118 | 7.74×10^9 | 0.997 | <i>Avrami-Erofeev</i> |
| 2 | Dextran | 205 | 160 | 6.93×10^{13} | 0.993 | <i>First order</i> |
| 3 | Potato starch | 189 | 188 | 1.03×10^{16} | 0.976 | <i>Contracting volume</i> |
| 4 | Agar agar | 141 | 140 | 4.78×10^{11} | 0.890 | <i>Two-Dimensional Diffusion</i> |
| 5 | Tamarind | 170 | 170 | 1.79×10^{13} | 0.990 | <i>Ginstling-Brounshtein</i> |
| 6 | Chitosan | 146 | 164 | 6.71×10^{13} | 0.995 | <i>One dimensional diffusion</i> |

* E_a values were chosen in conformance with their corresponding values obtained through Flynn-Wall-Ozawa method

#the R_2 value denotes the linear fit parameter constructed through $g(\alpha)$ vs. $p(x)$, where $p(x)$ is deduced from an appropriate integral form of the Arrhenius equation (Bigger, Cran, & Bohn, 2015).

Table 3. 6 Details regarding various outputs from the SB method in the case of chitosan (as an example)

| Sl. No. | Kinetic model | Equation | E_a (kJ mol ⁻¹) | A (s ⁻¹) | R_2 |
|---------|--------------------------|------------------------------------|-------------------------------|------------------------|--------|
| 1 | P1 Power Law | α/n | *--- | --- | --- |
| 2 | E1 Exponential law | $\ln(\alpha)$ | *--- | --- | --- |
| 3 | A2 Avrami-Erofeev Model | $[-\ln(1-\alpha)]^{1/2}$ | 43.0 | 1.029×10^3 | 0.9933 |
| 4 | A3 Avrami-Erofeev Model | $[-\ln(1-\alpha)]^{1/3}$ | 26.0 | 1.880×10^1 | 0.9931 |
| 5 | A4 Avrami-Erofeev Model | $[-\ln(1-\alpha)]^{1/4}$ | 18.0 | 2.631×10^0 | 0.9930 |
| 6 | B1 Prout-Tompkins | $[-\ln(\alpha/(1-\alpha))] + C$ | *--- | --- | --- |
| 7 | R1 Contracting area | $1-(1-\alpha)^{1/2}$ | 86.0 | 1.682×10^7 | 0.9944 |
| 8 | R3 Contracting volume | $1-(1-\alpha)^{1/3}$ | 89.0 | 6.174×10^6 | 0.9942 |
| 9 | D1 One dimensional | α^2 | 164 | 8.417×10^{13} | 0.9952 |
| 10 | D2 Two dimensional | $(1-\alpha)\ln(1-\alpha) + \alpha$ | 175 | 9.164×10^{14} | 0.9744 |
| 11 | D3 Three dimensional | $[1-(1-\alpha)^{1/3}]^2$ | 187 | 1.235×10^{16} | 0.9765 |
| 12 | D4 Ginstling-Brounshtein | $(1-2\alpha/3) - (1-\alpha)^{2/3}$ | 179 | 2.181×10^{15} | 0.9751 |
| 13 | F1 First order | $-\ln(1-\alpha)$ | 95.0 | 2.330×10^7 | 0.9880 |
| 14 | F2 Second order | $1/(1-\alpha)$ | 32.0 | 1.487×10^1 | 0.9050 |
| 15 | F3 Third order | $1/(1-\alpha)^2$ | 72.0 | 1.400×10^5 | 0.7580 |

*no values for E_a were given by the software;

#the software yielded a zero value as the fitting factor

Given that FWO method involves multiple heating rates, the values of E_a obtained could be considered as more reliable than the output from the proprietary software, where the data points accrued through a single heating rate are used as the preliminary input parameters (i.e. in the

case of SB method; see in Table 3. 5). Furthermore, the former method (i.e. FWO method) is an essentially model free option, whereas the latter (SB method) has the flexibility to choose from a host of possible models (about 14 in total). However, the choice of the preferred model in the current work is based, primarily, on the nearest value of E_a to that corresponds to the value calculated through the FWO method. Here it is also relevant to note that in doing so, the corresponding R_2 values were either 0.9, or above, indicating a strong correlation for the linear fit. In addition, the orders of the values for the Arrhenius factor were within what is normally expected for bond-cleavage processes; however, their absolute values may not bear any correlation with the actual physio-chemical processes that accompany such bond breaking reactions. In any case, the computed value and the correspondingly chosen values for E_a should be only considered as *apparent* values that are useful in some instances for the purpose of comparison amongst closely related substrates.

3.2.2 Pyrolysis combustion flow calorimetry (PCFC)

PCFC assesses the flammability properties of materials using only milligrams of the sample and thus can be used a tool for screening new materials. The seminal work behind this technique was carried out at the Federal Aviation Administration in USA in the late 1990's (Lyon & Walters, 2004). PCFC is assumed to reproduce and decipher the solid-state and gaseous-phase elements of flaming combustion, in a non-flaming test regime, through a rapid and controlled pyrolysis of the sample in an inert atmosphere (i.e. in nitrogen) followed by high-temperature oxidation (i.e. combustion) of the pyrolyzate components in the presence of oxygen. PCFC parameters have been found to correlate fairly well with the conventional flame tests like cone calorimetry, limiting oxygen index (LOI) and UL-94 test (Cogen, Lin, & Lyon, 2009; Lin, Cogen, & Lyon, 2007). This technique was also extensively used in the case of several commercially important thermoplastic materials (ASTM D7309) (Joseph & Tretsiakova-McNally, 2012; Morgan, Wilkie, & Nelson, 2012; Scharrel, Pawlowski, & Lyon, 2007; Sonnier, Otazaghine, Ferry, & Lopez-Cuesta, 2013; Tretsiakova-McNally & Joseph, 2015).

Essentially, PCFC works on the principle of accurately measuring the consumption of oxygen accompanying the combustion of the volatiles produced from the test sample. Hence the technique comes under the class of calorimetry called *oxygen consumption calorimetry*. This type of calorimetry is originally based on the experimental observation that the net heat of

combustion of typical organic molecules per mol of oxygen consumed is relatively a constant (i.e. $419 \pm 19 \text{ kJ mol}^{-1}$, or $13.1 \pm 0.6 \text{ kJ g}^{-1}$). This value was found to be largely unaffected by the chemical constitution of the material undergoing combustion. Huggett later confirmed that this result is valid for a range of combustible forest products, chemical compounds, and organic polymers, and eventually came to be known as the Huggett's principle (Huggett, 1980). Subsequently, this principle became the basis and preferred method for determining the heat released by various solid fuels undergoing flaming combustion, a classical example being the cone calorimeter (ISO: 5660; AS/NZS: 3837).

In a PCFC instrument (sometimes dubbed as a 'Micro Cone'), a linear heating programme is employed (typically 1°C s^{-1}) where milligrams of a test sample is degraded in nitrogen. Here, the production of volatiles and char residues (as the case may be) are assumed to mimic what happens to a material, prior to the onset of flaming combustion, in a real fire scenario. Subsequently, the volatiles are swept from the pyrolysis zone, by an inert stream of (nitrogen) to a second chamber (a tubular furnace) kept at flame temperatures (*ca.* 900°C), and a forced non-flaming combustion is effected through under an atmosphere of nitrogen/oxygen mixture (80/20 vol./vol. in the present case). The products of combustion (typically CO_2 , H_2O , and other oxides depending on the chemical composition of the solid fuel) are removed from the carrier gas stream, by employing suitable scrubbers, and the transient heat release rate is calculated from the measured flow rate and the oxygen concentration, after applying a correction factor for the dispersion of the flow. The instrument produces a plot of the heat release rate (HRR in W g^{-1}) vs. time.

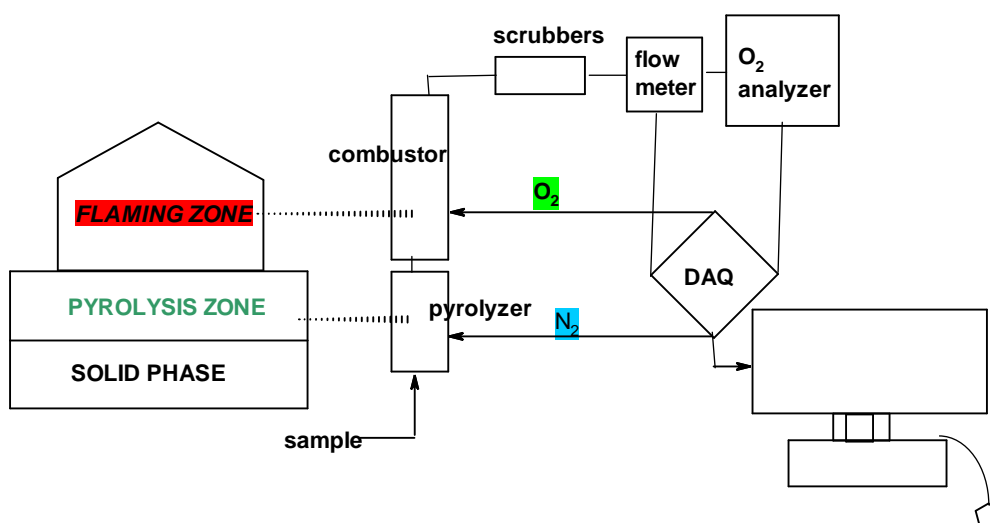


Figure 3. 32 A schematic diagram of the pyrolysis combustion flow calorimetry (PCFC)

The maximum value of the HRR (i.e. peak heat release rate: pHRR) normalized for the initial sample mass and heating rate will yield the heat release capacity ($\text{J g}^{-1} \text{K}^{-1}$). This parameter can be considered as an intrinsic property of the material, which will only depend on the chemical constitution of the materials, and their value can be considered as the flammability parameter for the material. The integration of the PCFC heat release rate curve over the time will yield the total heat released (THR), and the latter upon normalisation of the mass of the material that underwent combustion will lead to the effective heat of combustion of the material (see in Table 3. 8).

Table 3. 7 PCFC data for modified and unmodified versions of base substrates

| Sample | P (wt. %) | * T_{max} (TGA) (°C) | Temp to pHRR (°C) | pHRR (W g^{-1}) | THR (kJ g^{-1}) | Heat Release Capacity ($\text{J g}^{-1} \text{K}^{-1}$) | Char yield (wt. %) |
|-----------------------|--------------|------------------------------|----------------------------|-------------------------------|-------------------------------|--|-----------------------|
| β -cyclodextrin | 0.0 | 317 | 342 | 453 | 11.6 | 459 | 11.11 |
| β -cyclodextrin | 1.7 | 287 | 290 | 66.0 | 4.20 | 67.0 | 25.54 |
| Dextran | 0.0 | 309 | 319 | 289 | 10.4 | 288 | #--- |
| Dextran | 1.0 | 247 | 252 | 200 | 7.50 | 217 | 23.52 |
| Potato Starch | 0.0 | 303 | 310 | 363 | 10.4 | 368 | 12.50 |
| Potato Starch | 3.2 | 258 | 260 | 57.0 | 3.90 | 60.0 | 31.85 |
| Agar agar | 0.0 | 262 | 272 | 256 | 12.3 | 250 | 3.680 |
| Agar agar | 5.5 | 248 | 234 | 219 | 8.30 | 234 | 23.40 |
| Tamarind | 0.0 | 305 | 326 | 158 | 10.0 | 155 | 25.12 |
| Tamarind | 6.6 | 274 | 291 | 126 | 8.10 | 128 | 29.36 |
| Chitosan | 0.0 | 298 | 321 | 103 | 6.60 | 107 | #--- |
| Chitosan | 2.4 | 264 | 267 | 24.1 | 3.65 | 27.0 | 31.12 |

*here the value of T_{max} is taken from the corresponding TGA curve, where it the value of the temperature were maximum rate of degradation was observed when the first derivative was taken as the ordinate- see also in Figures 3. 13, 3. 15, 3. 17, 3. 19, 3. 21, 3. 23

#the value is not given here as the pyrolysis char residue could not be determined accurately (the residue was rather sticky and blown-up in nature, and hence it was not able to be retrieved fully after the run).

As can be seen from table 3. 7, and from the figures: 3. 33 to 3. 38, the modified substrates undergo combustion earlier as compared to the unmodified counterparts. Concomitantly, the values for the peak heat release rates (pHRR) and the total heat released (THR) are correspondingly lower in the case of phosphorus-modified systems. These values definitely demonstrate the combustion inhibitory effects of the modifying groups in the gaseous phase (i.e. occurring in the second stage of the PCFC run). In addition, the char yields obtained for the modified materials were also correspondingly higher. This attribute furnishes corroborative evidence for the combustion inhibitory effects, and also possibly reflecting the altered thermal cracking mechanism(s) operating in the solid-phase (i.e. in first stage of the PCFC test), resulting in lesser amounts of combustible volatiles emanating from the degrading test material. Here the phosphorylated units in the monomeric units of the substrates could catalyse further dehydration reactions, and/or result in the formation of dimeric/oligomeric polyphosphate functionalities (Thomas et al., 2020).

As expected, the temperature to pHHR also shows a lower values in the case of the modified versions as compared to the virgin materials. More importantly the heat release capacity values, which can be considered to be a more fundamental quantity under the experimental regime, also show noticeable decrease in the case of the modified substrates. It should be noted here that among the six substrates studied, the extents of the variations in the relevant parameters obtained from PCFC (i.e. Temp to pHHR, pHRR, THR, HRC) of the unmodified and phosphorus-modified substrates were also different. These variations need to be expected given that the phosphorus loading in each case differ and that the representative chemical nature of the chain/of the constituent monomeric unit of each substrate also vary widely.

The combustion inhibitory effects of the P-containing groups can be also expected to reflect in the values of the effective heats combustion of these materials. The apparent values of heats of combustion (h_c) of solid fuels can be calculated from the THR values normalized to the mass fractions of the material that underwent combustion, where the required denominator can be obtained from the initial mass of the material and amount of char residue obtained (Solórzano, Moinuddin, Tretsiakova-McNally & Joseph, 2019) (see in eqn. 14).

$$h_c = \frac{THR}{1-Y_p} \quad (14)$$

For example, in the case of β -cyclodextrin:

$$h_c = \frac{THR}{1 - Y_p} = \frac{11.6}{1 - 0.11} = 13.03 \text{ kJ g}^{-1}$$

The values thus obtained are given in Table 3. 8. The relatively lower values for the apparent heats of combustion, which in turn seemed to depend on the extent of phosphorus loading, can be attributed to the changes in the amounts and/or nature of the pyrolysis gases generated by the first stage in the experiment (Thomas, Joseph, Moinuddin, Zhu, & Tretsiakova-McNally, 2020).

Table 3. 8 Heats of combustion values of various formulations

| Sample | P (wt. %) | Pyrolysis residue (g g⁻¹) | <i>h_c</i> (kJ g⁻¹) |
|-----------------------|----------------------|---|---|
| β -cyclodextrin | 0.0 | 0.11 | 13.03 |
| β -cyclodextrin | 1.7 | 0.25 | 5.600 |
| Dextran | 0.0 | --- | *--- |
| Dextran | 1.0 | 0.27 | 6.980 |
| Potato Starch | 0.0 | 0.23 | 11.81 |
| Potato Starch | 3.2 | 0.31 | 5.650 |
| Agar agar | 0.0 | 0.04 | 12.76 |
| Agar agar | 5.5 | 0.23 | 10.78 |
| Tamarind | 0.0 | 0.25 | 13.30 |
| Tamarind | 6.6 | 0.27 | 11.36 |
| Chitosan | 0.0 | --- | *--- |
| Chitosan | 2.4 | 0.31 | 5.290 |

*the values are not given here as the pyrolysis char residue could not be determined accurately (the residue was rather sticky and blown-up in nature, and hence it was not able to be retrieved fully after the run)

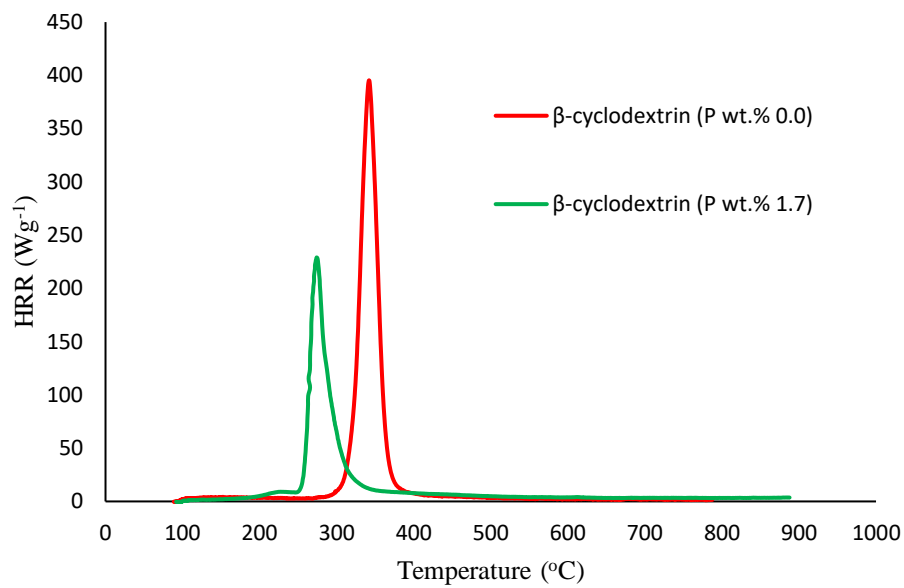


Figure 3. 33 Plot of the heat release rate (HRR) (Wg^{-1}) versus temperature ($^{\circ}C$) for modified and unmodified versions of β -cyclodextrin

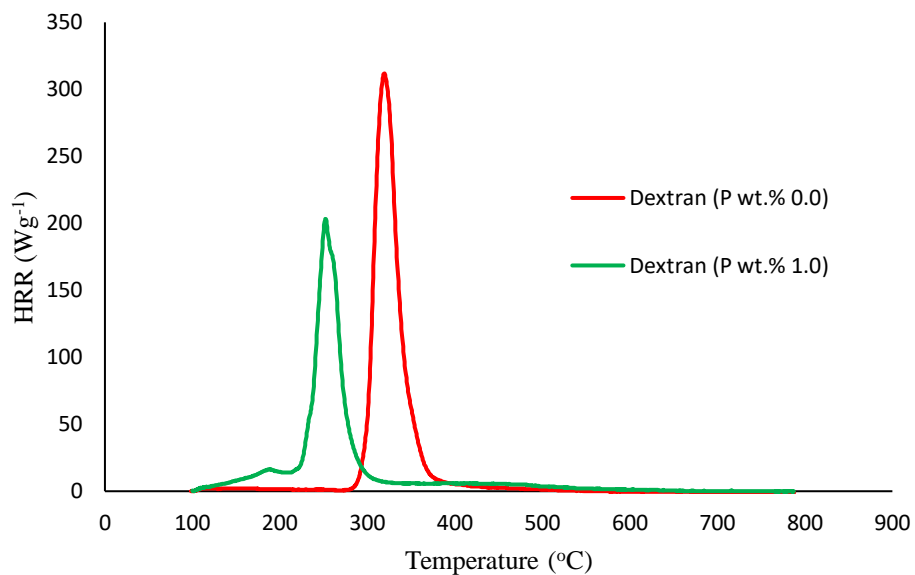


Figure 3. 34 Plot of heat release rate (HRR) (Wg^{-1}) versus temperature ($^{\circ}C$) for modified and unmodified versions of dextran

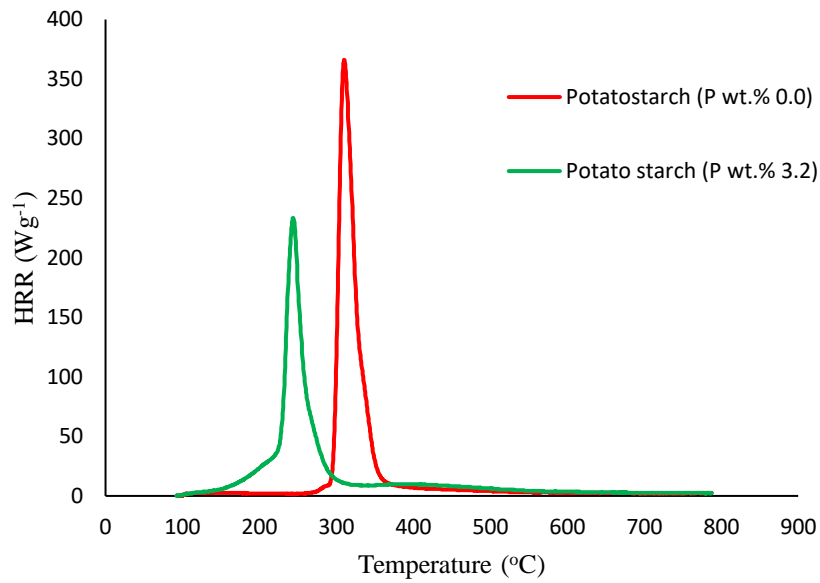


Figure 3. 35 Plot of heat release rates (HRR) (Wg-1) versus temperature (°C) for modified and unmodified versions of potato starch.

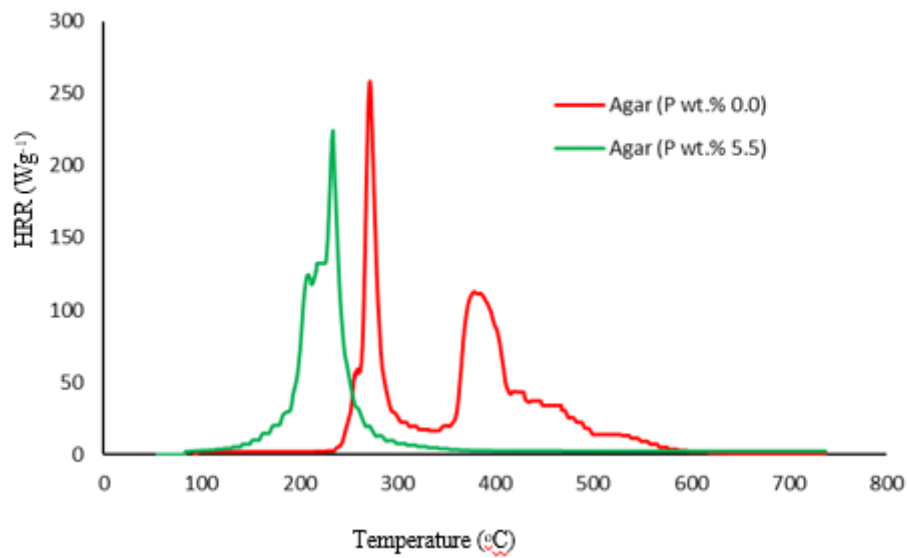


Figure 3. 36 Plot of heat release rates (HRR) (Wg-1) versus temperature (°C) for modified and unmodified versions of agar agar

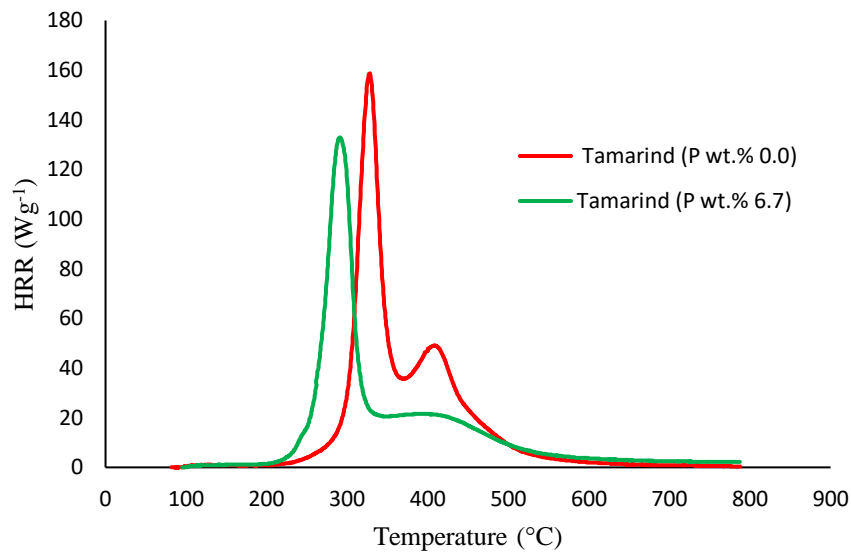


Figure 3. 37 Plot of heat release rates (HRR) (Wg^{-1}) versus temperature ($^{\circ}C$) for modified and unmodified versions of tamarind

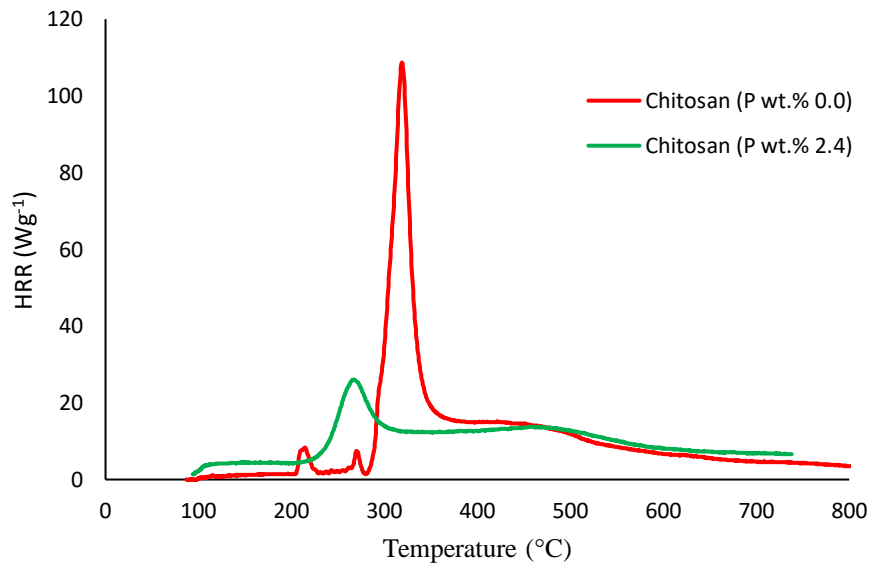


Figure 3. 38 Plot of heat release rates (HRR) (Wg^{-1}) versus temperature ($^{\circ}C$) for modified and unmodified versions of chitosan

3.3 Correlation between TGA and PCFC

With a view to deciphering correlations, if any, between TGA and PCFC runs, we have plotted the derivative of the mass loss from the TGA curve obtained under a heating rate of $60\text{ }^{\circ}\text{C min}^{-1}$ along with the corresponding HRR curve from the PCFC run, with temperature (in $^{\circ}\text{C}$) as the common abscissa (see in Figures: 3. 39 to 3. 50). Here it is to be noted that the heating rate in the TGA thermogram and the heating rate while obtaining the HRR curve are selected to have the same value (i.e. $60\text{ }^{\circ}\text{C min}^{-1}$ in TGA and $1\text{ }^{\circ}\text{C s}^{-1}$ in PCFC). However, owing to the inherent differences in the sensitivity/accuracy of the two types of instrumental techniques, there will be invariably some degree of deviance whilst aligning the mean values of the individual peaks. Whilst the first stage of a PCFC run can be considered to be almost similar to that happening in a TGA test, the PCFC instrument generates the curve during the combustion stage (i.e. the second stage in PCFC test) whereas the first derivative of the mass loss, as plotted from a TGA run, occur in a non-oxidative atmosphere (i.e. under nitrogen). Nonetheless, some useful trends were observed through this exercise.

For instance, the first minor peaks in all derivative curves from TGA can be attributed to the loss of water (through evolution of physically bound water, and presumably to a lesser extent by the dehydration of the monomeric units of base substrate) are absent in the HRR curve from the PCFC tests, as water can be assumed to be incombustible. However, the second main degradation step (owing to main chain cleavage, dehydration reactions, production of laevoglucose or their analogues, other smaller fragments, etc.) as shown by the TGA correspondingly reflected in the PCFC curves. Here it is also highly relevant to note that the T_{max} (i.e. the temperature at maximum degradation) from the TGA experiment and the temperature to $p\text{HRR}$ from the PCFC test are close together see in Table 3. 7). Therefore, the main chain degradation step in the TGA can be considered as the ‘fuel production’ stage whereby combustible volatiles are produced (similar to the process happening in the first stage in the PCFC run), and the volatiles thus produced undergo combustion reaction in the second stage in the PCFC test. The above trends seem to apparently deviant in the cases of substrates like, agar agar, tamarind and chitosan. Here prominent second peaks are observed in the HRR curves, whereas the corresponding peaks are either less prominent, or are completely absent, in the TGA thermograms. This could arise due to some sort of secondary oxidation of the volatiles already present in the gaseous phase in the PCFC test (thus not showing up as mass losses in corresponding region of the TGA thermogram). In the absence of the any

corroborative evidence as to the nature and/or oxidation pathway of such volatiles, the above explanation should be treated with caution.

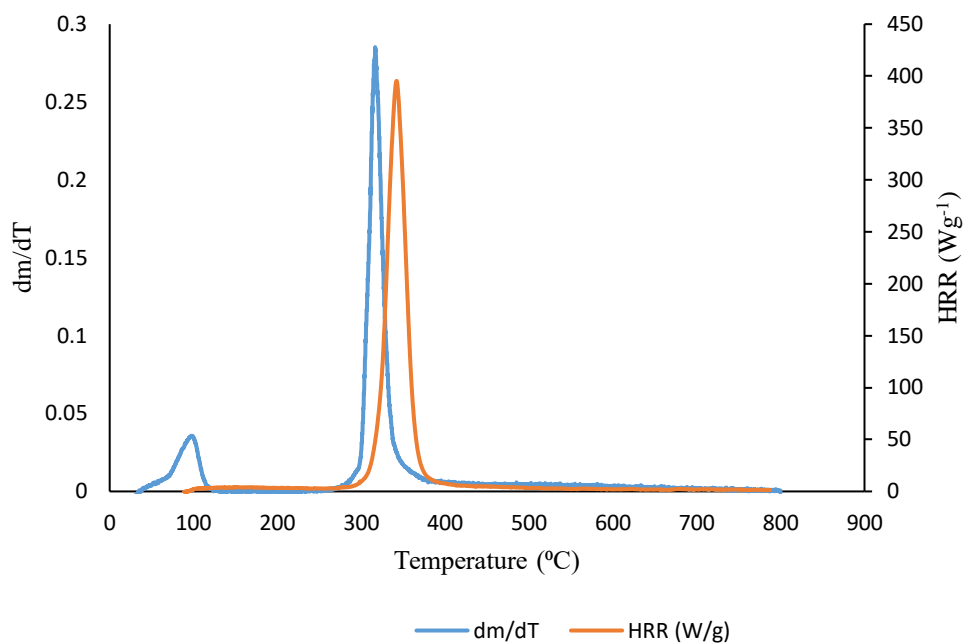


Figure 3. 39 Plots of the first derivative of the thermogram ($60^{\circ}\text{C min}^{-1}$) and HRR (from PCFC) for β -cyclodextrin

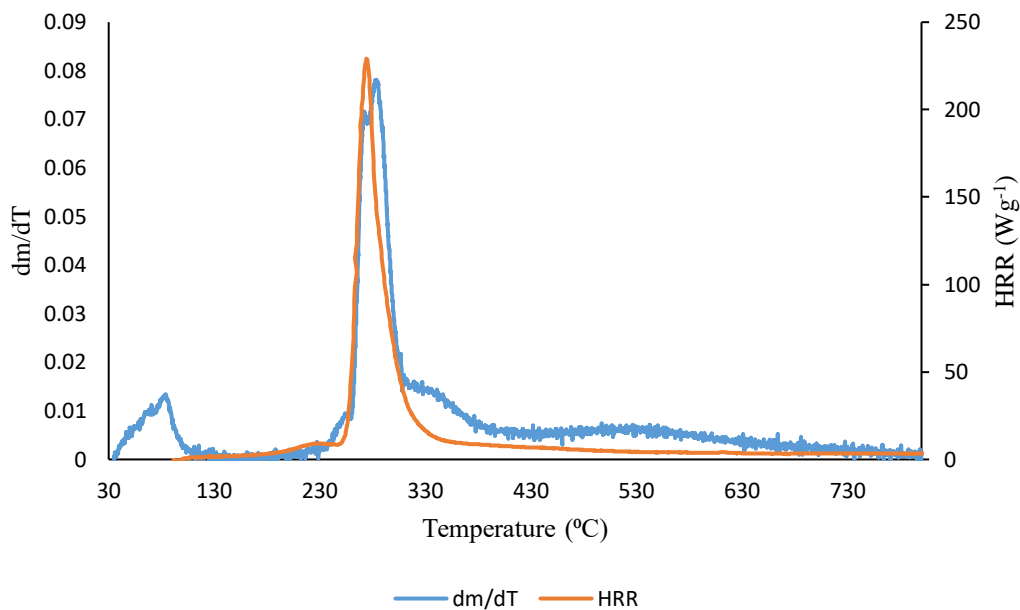


Figure 3. 40 Plots of the first derivative of the thermogram ($60^{\circ}\text{C min}^{-1}$) and HRR (from PCFC) for modified β -cyclodextrin

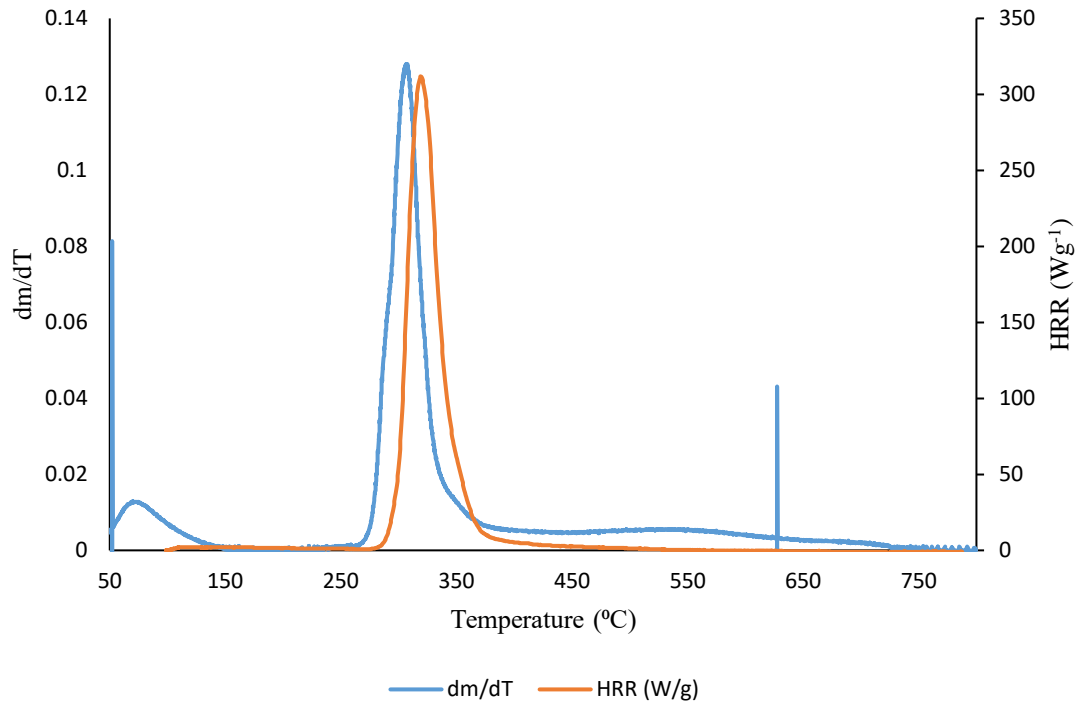


Figure 3.41 Plots of the first derivative of the thermogram ($60^{\circ}C\ min^{-1}$) and HRR (from PCFC) for dextran

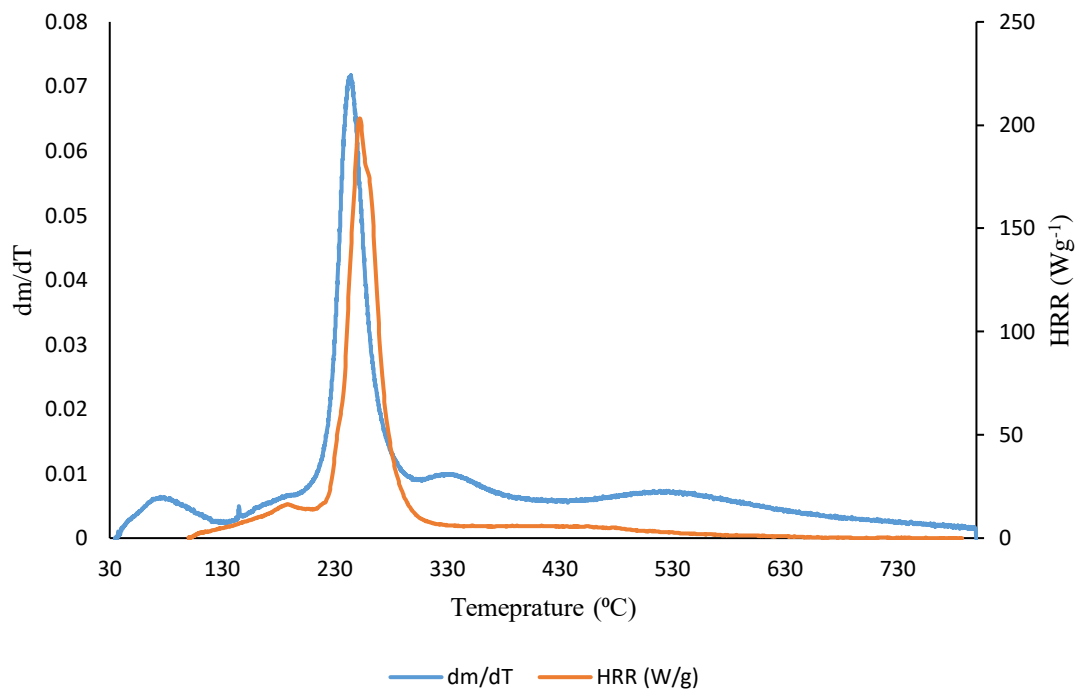


Figure 3.42 Plots of the first derivative of the thermogram ($60^{\circ}C\ min^{-1}$) and HRR (from PCFC) for modified dextran

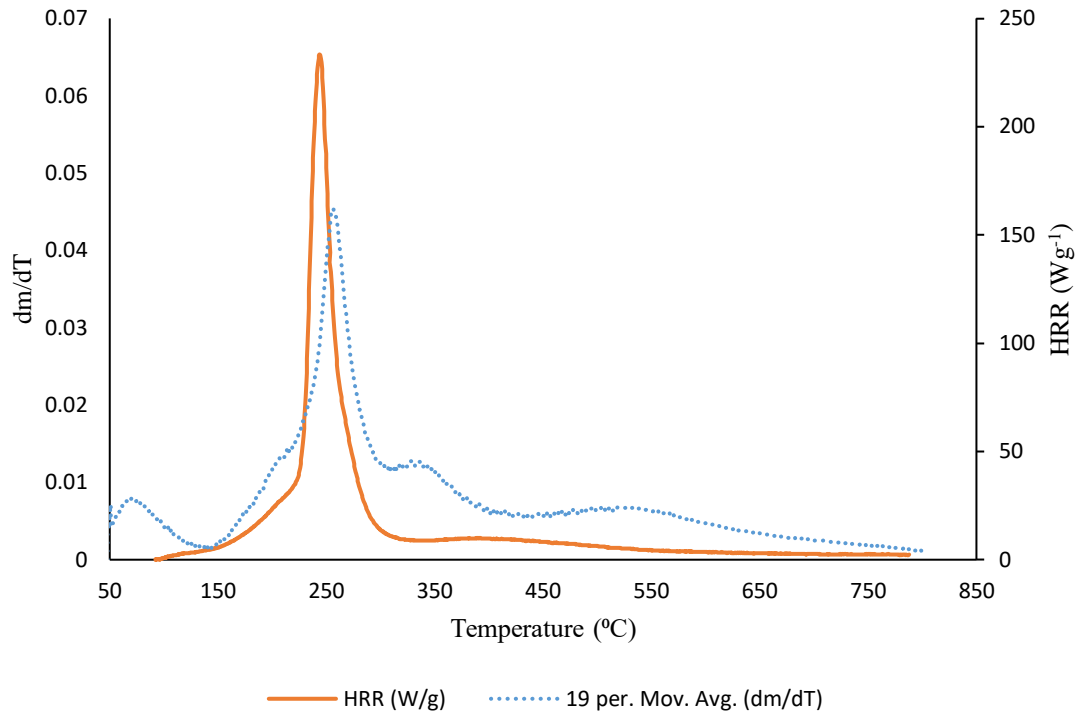


Figure 3.43 Plots of the first derivative of the thermogram (60°C min⁻¹) and HRR (from PCFC) for potato starch

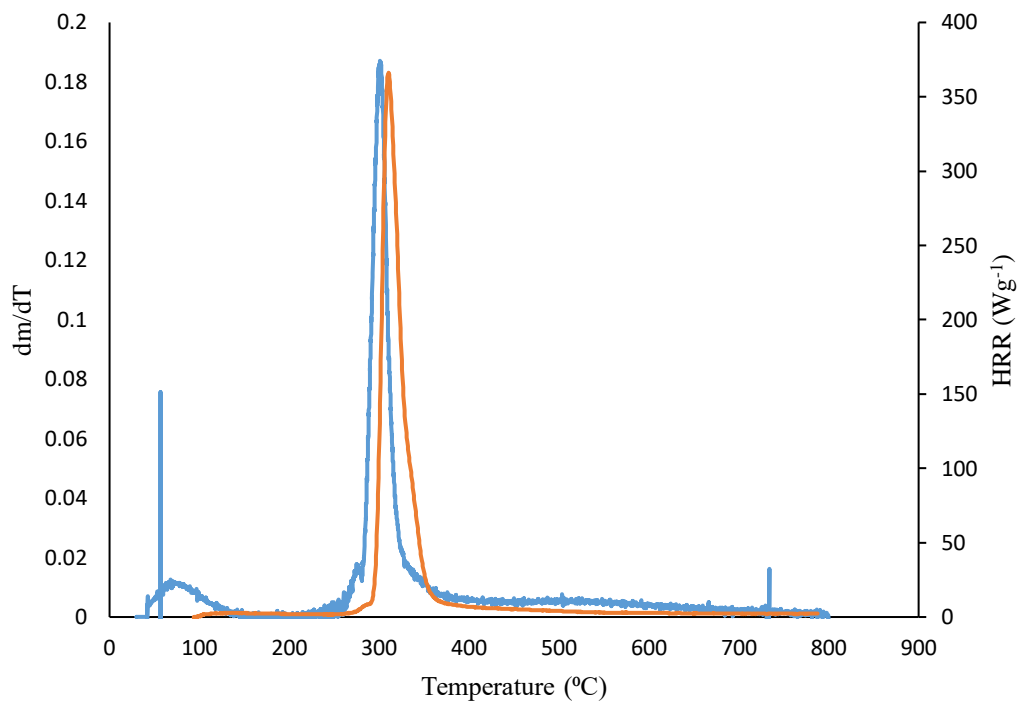


Figure 3.44 Plots of the first derivative of the thermogram (60°C min⁻¹) and HRR (from PCFC) for modified potato starch

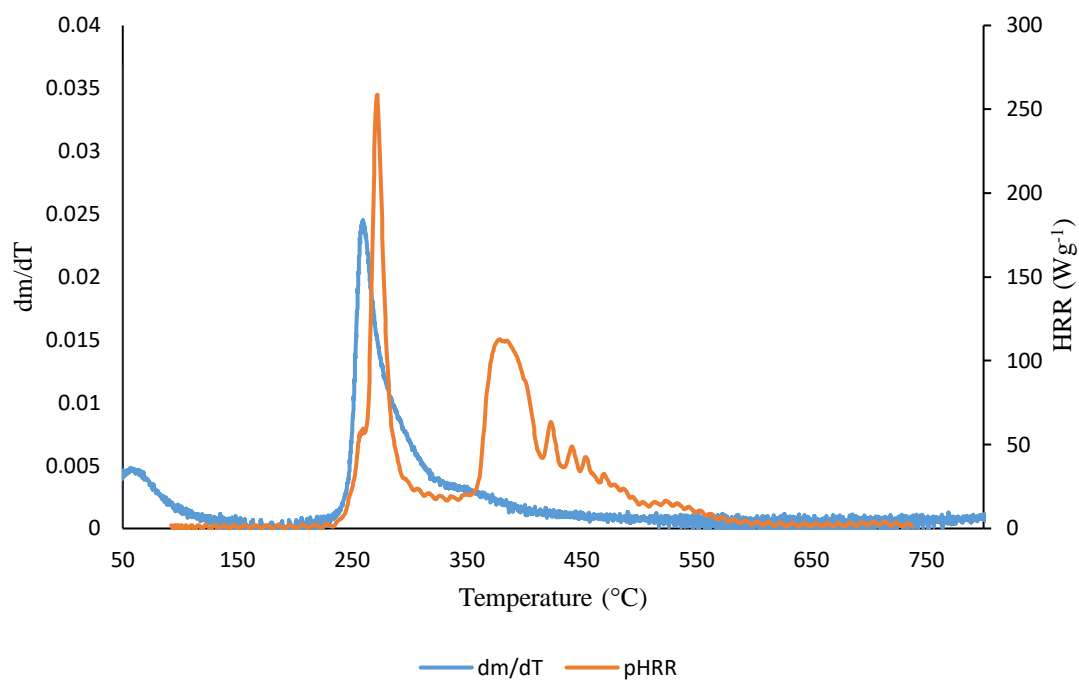


Figure 3.45 Plots of the first derivative of the thermogram (60°C min⁻¹) and HRR (from PCFC) for agar agar

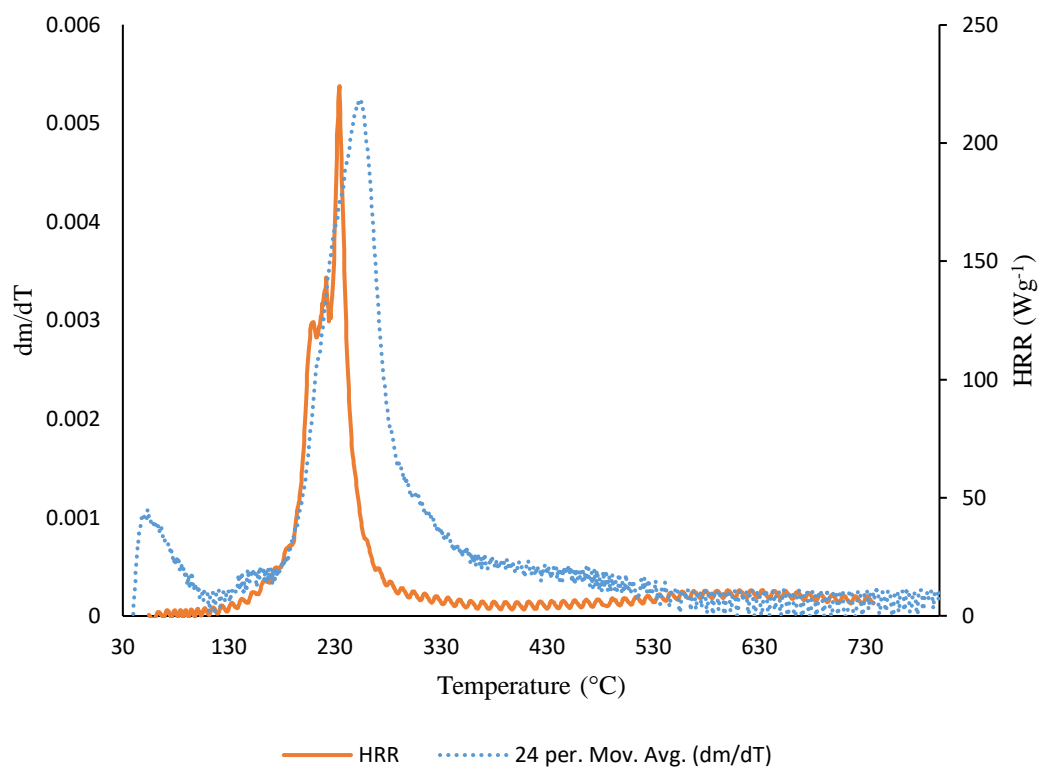


Figure 3.46 Plots of the first derivative of the thermogram (60°C min⁻¹) and HRR (from PCFC) for modified agar agar

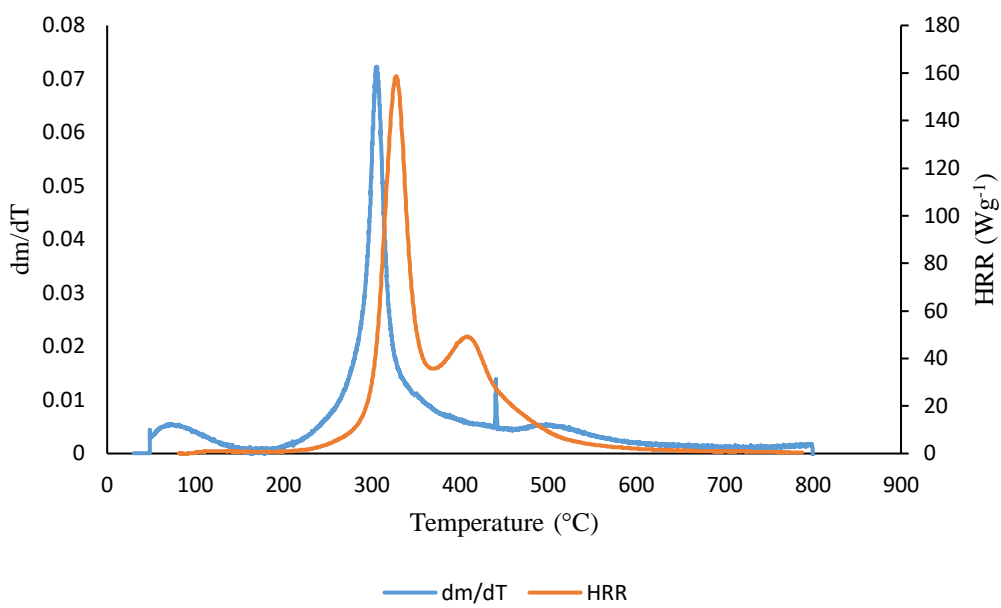


Figure 3. 47 Plots of the first derivative of the thermogram (60°C min⁻¹) and HRR (from PCFC) for tamarind

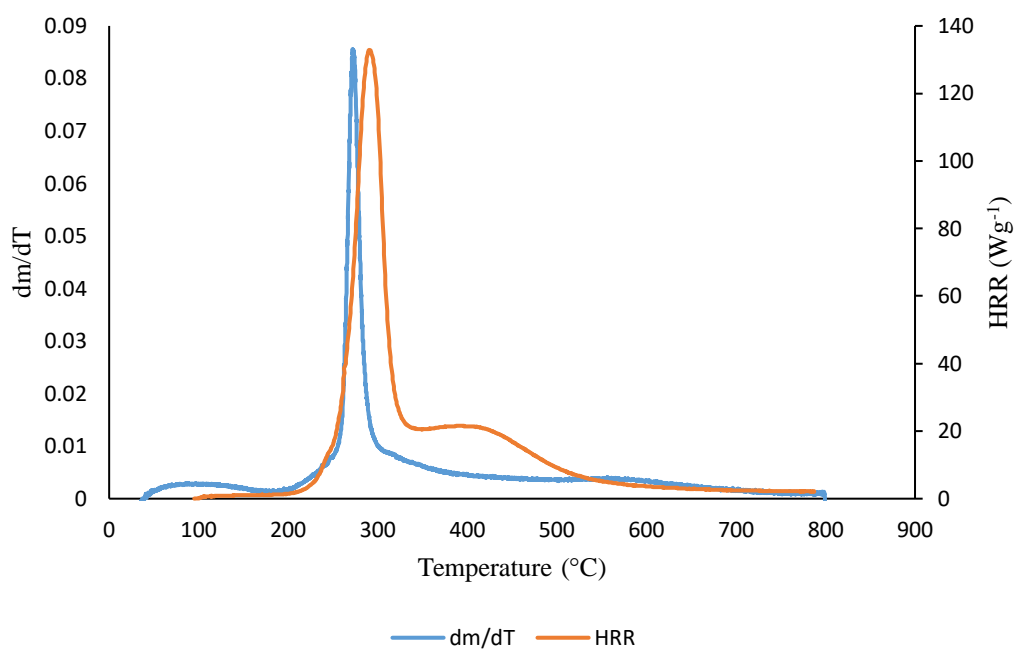


Figure 3. 48 Plots of the first derivative of the thermogram (60°C min⁻¹) and HRR (from PCFC) for modified tamarind

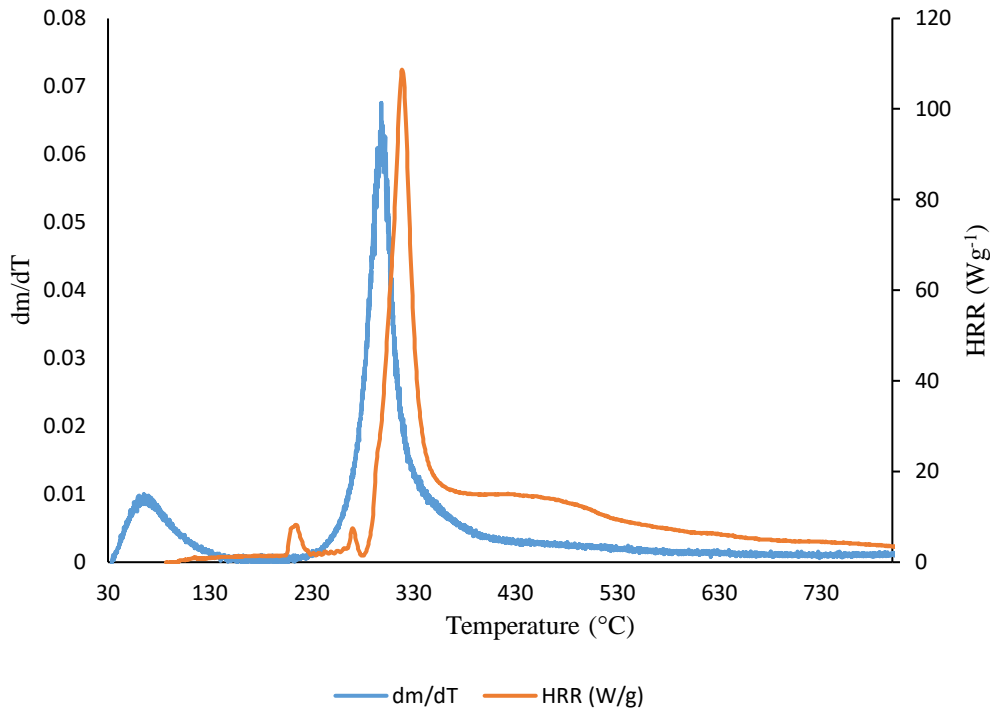


Figure 3.49 Plots of the first derivative of the thermogram (60°C min⁻¹) and HRR (from PCFC) for chitosan

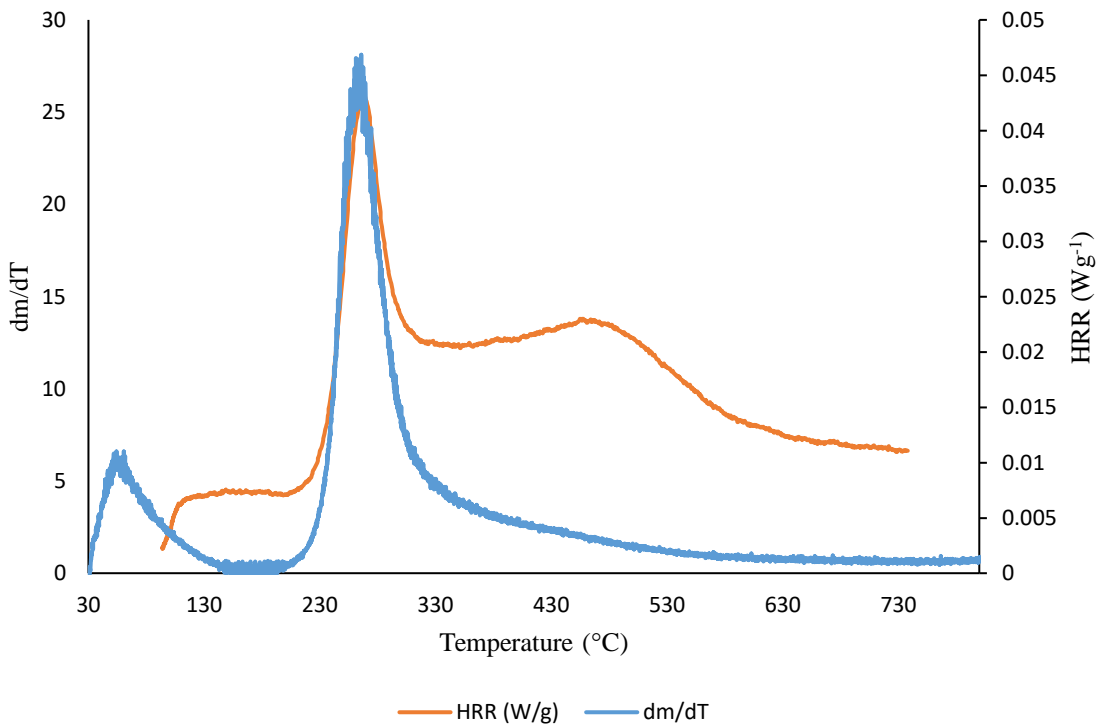


Figure 3.50 Plots of the first derivative of the thermogram (60°C min⁻¹) and HRR (from PCFC) for modified chitosan (a drift for the PCFC curve is observed here- possibly can be considered as an artefact from the machine's output)

We have also noticed some degree of correlation of the results from TGA and PCFC in terms of the amounts of char residues obtained for all the substrates (see Figure 3. 51), albeit the different underlying operating conditions for the techniques, i.e. a programmed heating in an inert atmosphere in the case of TGA (purely thermal degradation) against a forced combustion in the latter stage of a PCFC run. However as mentioned earlier, the degradative processes in a TGA experiment can be thought of as the fuel production stage (hence the amount of combustible volatiles) in the case of solid fuels. Therefore, this should be considered as the first stage in a PCFC experiment, where the material is pyrolysed in a nitrogen atmosphere. It can be also seen here that there exists a noticeable relationship between the combustion inhibitory effects of the phosphorus-containing groups and their loadings (see, for example in Figure 3. 52). As mentioned earlier, phosphorus modification of the base substrates can result in the altered degradative pathways thus changing the nature and composition of the pyrolysis gases. This is in agreement with literature precedents, especially, in the case of some commercially important thermoplastics, where acceptable levels of flame retardation are observed with phosphorus loadings (between 2.0 and 5.0 wt. %) achieved through a reactive strategy, whereas any higher loadings often resulting in diminished returns (Ebdon et al., 2000; Joseph & Tretsiakova-McNally, 2012; Price et al., 2007; Thomas, Joseph, Moinuddin, Zhu, & Tretsiakova-McNally, 2020).

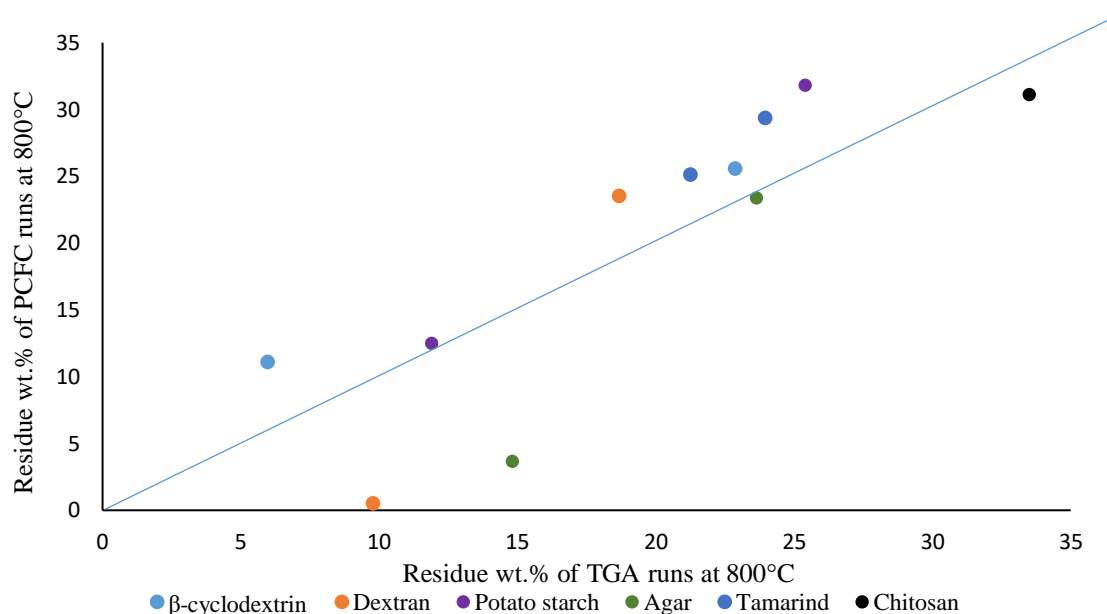


Figure 3. 51 Correlation of char residues (wt. %) from TGA experiments and PCFC runs of the substrates (an associated line is included in the figure to denote the general trend in the data points)

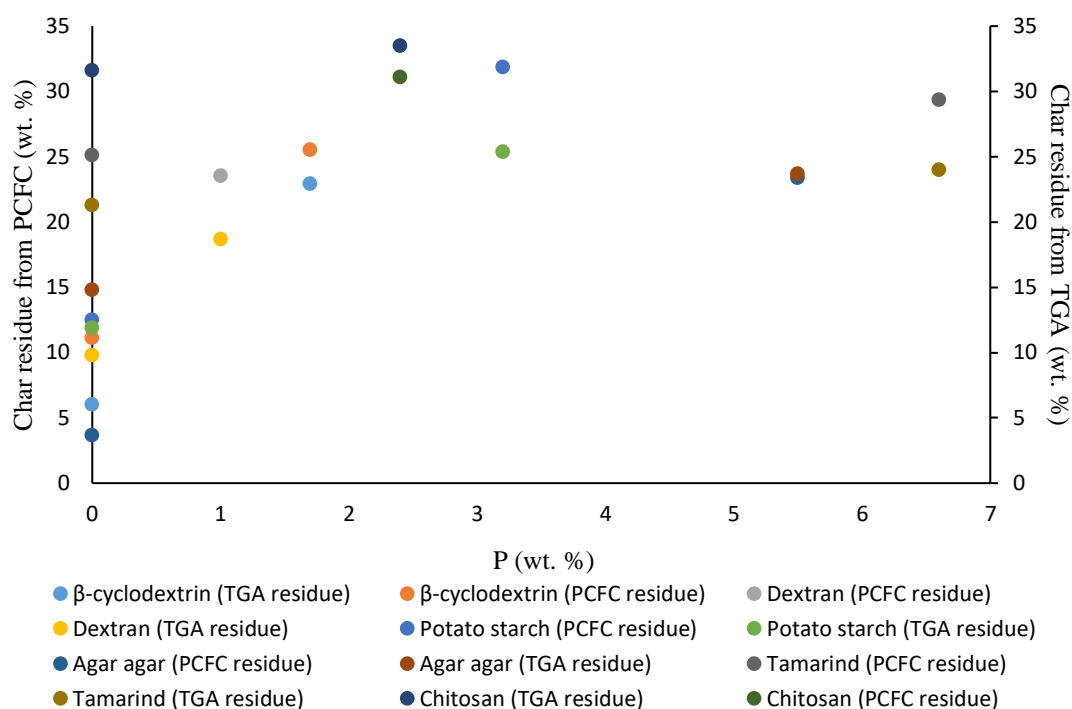


Figure 3. 52 A plot of char residues (wt. %) from TGA experiments and PCFC runs of the substrates vs. P wt. %

The influence of the covalently-bound P-bearing groups are also evident in the values of the relevant parameters obtained from the PCFC tests (see in Figures: 3. 53 to 3. 56). The values of HRC, THR, pHRR and EHC show a decrease as compared to the unmodified counter parts in the case of all the six base substrates under investigation. Here it should be noted that the extents of the fall in these values do not seem to be entirely dependent on the P-loadings but also appears to depend on the chemical nature of the substrate in question. For example, chitosan is found to have relatively the lowest values for the parameters under consideration, whereas tamarind in spite of relatively much higher P-loading gave the lowest return.

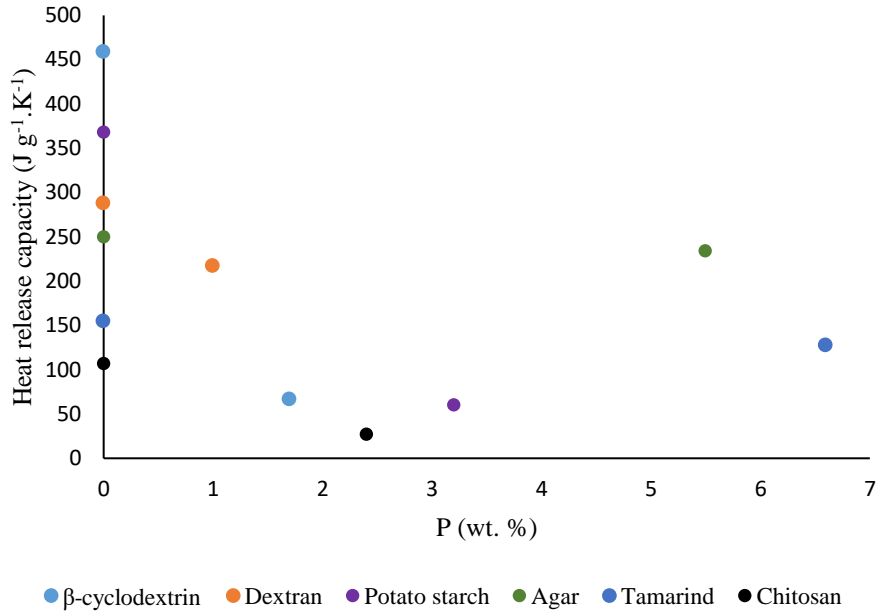


Figure 3. 53 Plot of heat release capacity (J g⁻¹.K⁻¹) from PCFC experiments vs. P wt. %

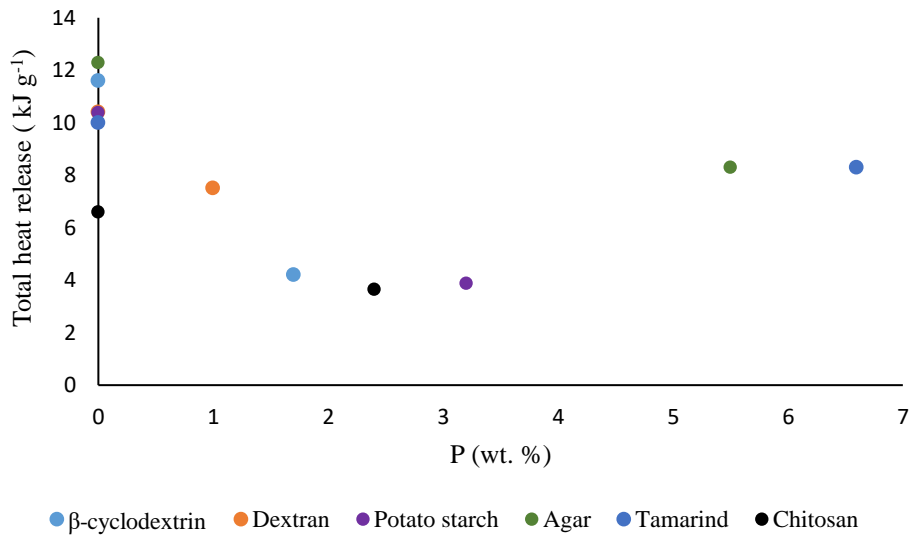


Figure 3. 54 Plot of total heat release (kJ g⁻¹) from PCFC experiments vs. P wt. %

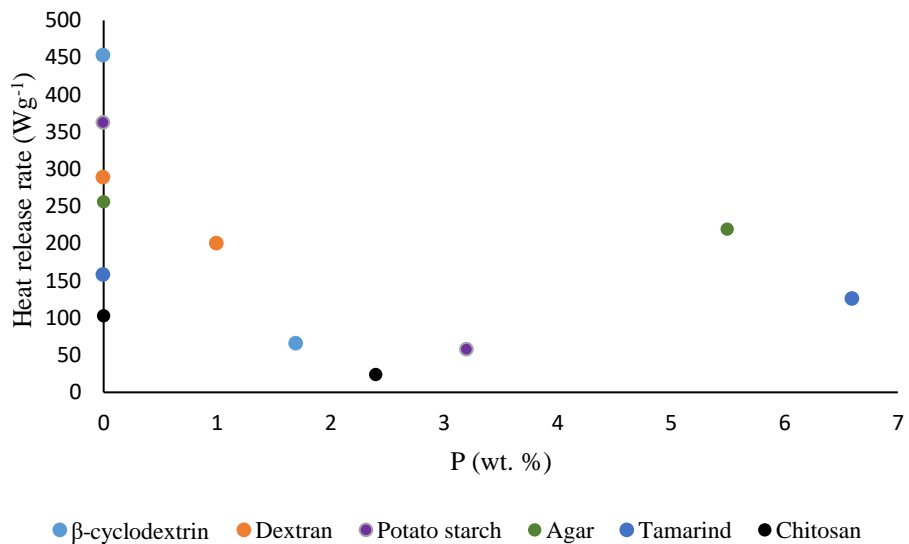


Figure 3. 55 Plot of peak heat release rate (W g⁻¹) from PCFC experiments vs. P wt. %

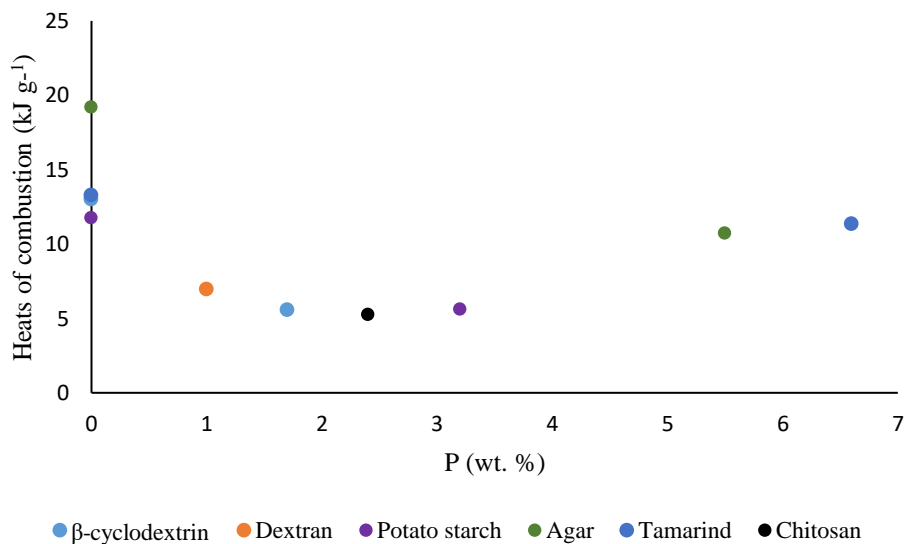


Figure 3. 56 Plot of calculated heats of combustion (kJ g⁻¹) vs. P wt. %

In figures 3. 57 and 3. 58 the values of HRC and h_c were plotted against E_a (obtained from the FWO method) for the unmodified substrates with a view to identifying any trends in the plotted data. As can be seen from these figures (Figures 3. 57 to 3. 60), the values of pHRR, THR, HRC and h_c noticeably varied amongst the unmodified substrates, and progressively decreased, as expected, with increase in the values of E_a . However, the trend especially in some cases (i.e. for pHRR and HRC) was not smooth, and chitosan showed particularly low values for pHRR and THR). Agar agar and tamarind showed similar variations for these parameters, whereas the remaining three substrates, namely, β -cyclodextrin, dextran and potato starch exhibited uniform gradation among the respective values with increases in values of E_a . As the calculated values of E_a , from FWO method, essentially reflect the energetic needs for bond cleavage reactions, and therefore higher values are expected to result in corresponding decreases in the values of some of the relevant combustion parameters such as, pHRR, THR and HRC. However, any deviations from a uniform gradation in the values could be attributed to the differences in the chemical nature and constitution among these substrates.

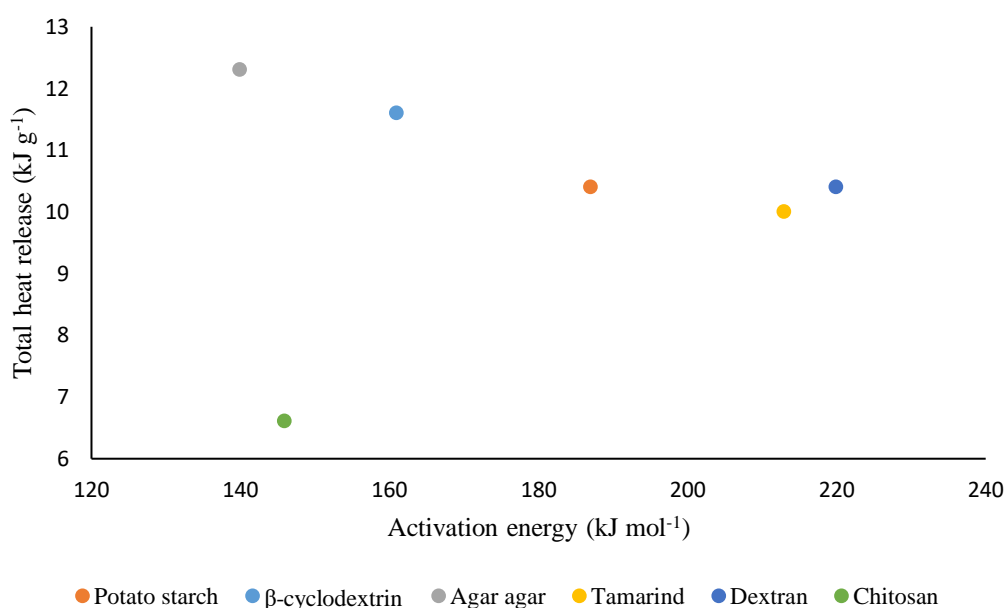


Figure 3. 57 A plot of activation energy of the base substrates vs. total heat release rates for unmodified substrates

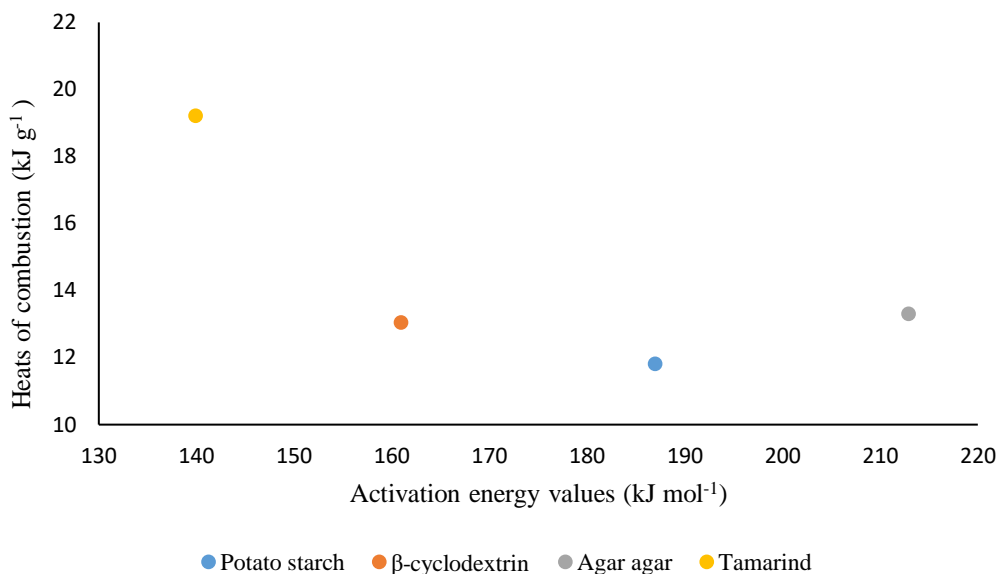


Figure 3. 58 A plot of activation energy *vs.* apparent heats of combustion for unmodified substrates

(Note: pyrolysis residue could not be measured accurately for chitosan and dextran as it expanded considerably and spilled over the pan upon the degradation/combustion- hence the corresponding values of h_c for these substrates could not be calculated)

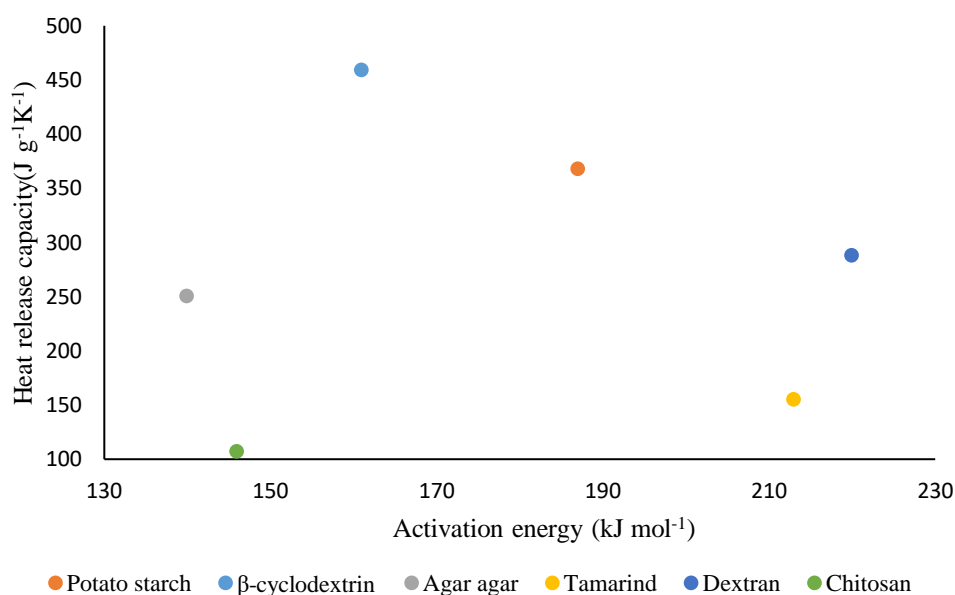


Figure 3. 59 A plot of activation energy *vs.* heat release capacity for unmodified substrates

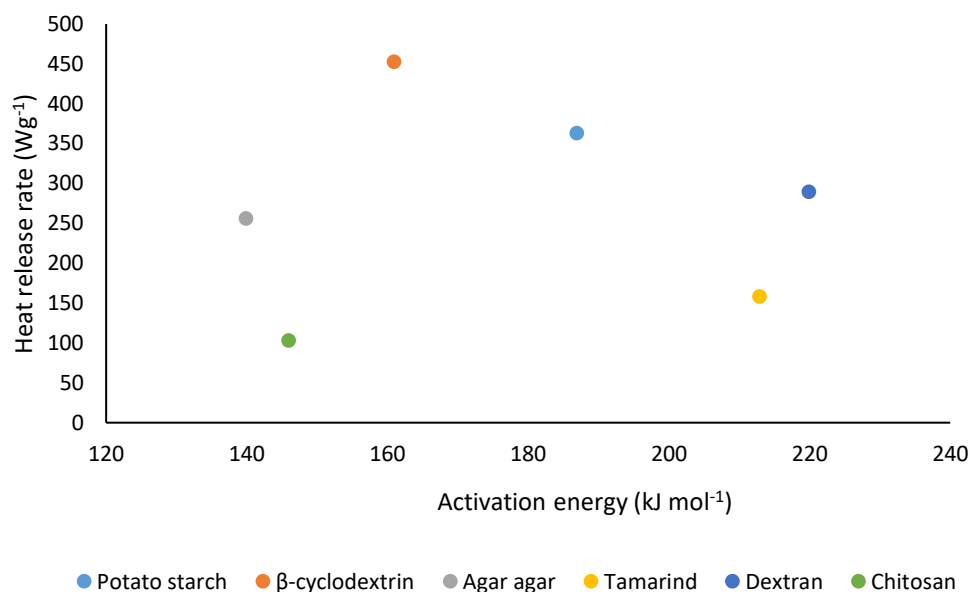


Figure 3. 60 A plot of activation energy vs. peak heat release rate for unmodified substrates

3.4 Flammability tests

3.4.1 Dip test- refer to the paper

As expected, the values of time to ignition (recorded in seconds), as measured manually through visual observations, remained rather scattered. Hence, we made 8-10 measurements in each case, and the averages of typically four congruent values are quoted in Table 3. 9. In this proprietary experiment, we also applied formulations of the base matrices containing both inorganic (Na_2CO_3 , K_2CO_3 and $(\text{NH}_4)_2\text{HPO}_4$) and organic additives (TPP and DOPO). It is relevant to note here that the time to ignition can only be considered as a low level indicator of the fire hazard of solid materials. However, the method can be considered as a simple laboratory-scale test, and it led to some generalizations as to the efficacies of the formulations before we proceeded to cone calorimetric measurements (Thomas, Moinuddin, Zhu & Joseph, 2020).

The thermal decomposition of the carbonate (i.e. K_2CO_3 in the present case) produced CO_2 , thus increasing the time to ignition in all of formulations incorporating them. On the other hand, the incorporation the phosphate seems to produce the opposite effect. This may be attributed to the production of combustible ammonia gas upon decomposition of $(\text{NH}_4)_2\text{HPO}_4$,

whereas the other product, H_3PO_4 , do not seem to exert any inhibitory effect, if at all, in the condensed phase. In the cases of formulations containing the phosphorus-containing organic additives, some degree of combustion inhibitory effect seems to be in operation, except perhaps in the case of fish gelatin. Here again, the corresponding results should be treated with some degree of caution.

Table 3. 9 Time to ignition for test samples coated with various formulation (from the dip test)

| Sl. No. | Sample | Time to ignition (s ± STDEV) |
|----------------|---|---|
| 1 | Uncoated sample | 32 ± 5 |
| 2 | Starch | 31 ± 3 |
| 3 | Starch + Na ₂ CO ₃ | 38 ± 6 |
| 4 | Starch + K ₂ CO ₃ | 47 ± 4 |
| 5 | Starch + (NH ₄) ₂ HPO ₄ | 26 ± 3 |
| 6 | Starch + DOPO | 35 ± 7 |
| 7 | Starch + TPP | 33 ± 6 |
| 9 | Chitosan | 36 ± 4 |
| 10 | Chitosan+Na ₂ CO ₃ | 39 ± 3 |
| 11 | Chitosan+ K ₂ CO ₃ | 67 ± 7 |
| 12 | Chitosan + (NH ₄) ₂ HPO ₄ | 27 ± 5 |
| 13 | Chitosan + DOPO | 34 ± 3 |
| 14 | Chitosan + TPP | 40 ± 3 |
| 15 | Fish gelatin | 27 ± 8 |
| 16 | Fish gelatin + Na ₂ CO ₃ | 38 ± 4 |
| 17 | Fish gelatin + K ₂ CO ₃ | 41 ± 8 |
| 18 | Fish gelatin + (NH ₄) ₂ HPO ₄ | 28 ± 3 |
| 19 | Fish gelatin + DOPO | 28 ± 3 |
| 20 | Fish gelatin + TPP | 23 ± 2 |
| 21 | Rice bran | 26 ± 3 |
| 22 | Rice bran + Na ₂ CO ₃ | 33 ± 5 |
| 23 | Rice bran + K ₂ CO ₃ | 49 ± 7 |
| 24 | Rice bran + (NH ₄) ₂ HPO ₄ | 26 ± 4 |
| 25 | Rice bran + DOPO | 34 ± 6 |
| 26 | Rice bran + TPP | 30 ± 7 |

3.4.2 Cone tests

Initially, we coated the formulations of the substrates (dispersions of starch, chitosan, fish gelatin and rice bran alone) onto the test wood plaques (see details of the procedure in chapter 2; section 2.2.4.2; page 31). The coated samples were allowed to cure overnight in a fume cupboard, and the uniformity and overall morphology of the coatings (*ca.* 0.5 mm in thickness) were inspected visually. It was found that the coatings through formulations, based on starch and chitosan, were rather diffused and patchy, and thus did not form a coherent layer. However, the coatings from formulations of fish gelatin and rice bran were comparatively of a better quality, and they uniformly covered the surfaces of the test specimens. Hence, we chose to restrict the ensuing investigations, in details, pertaining to the formulations based on fish gelatin and rice bran even though the relevant parameters from the initial cone measurements for chitosan seemed promising (especially the ignition propensity which was gauged in terms of the $T_{ig} = 98$ s; see in Table 3. 10). However, in the case of the starch coated samples, all the indicators from the cone measurements, under an external irradiance of 35 kW m⁻², pointed to their ineffectiveness in passively fire protecting the underlying wood material.

For formulations involving rice bran, it was found that the measured parameters, as compared with the unprotected wood, in fact showed the opposite trends than what are normally expected. This could be attributed to the ease of degradation of the constituents forming the rice bran (see in chapter 2; Figure 2.8; page 21) coupled to the production of combustible volatiles, like the coating based on starch. Notable exceptions were the reduction in the values of the THR (from 97 to 82 MJ m⁻²) and EHC (from 11.5 to 9.60 MJ kg⁻¹) as compared to the uncoated wood. However, the presence of P-containing additive in formulations with rice bran failed to produce the desired effects as revealed by the values of T_{ig} , pHHR. On the contrary, coatings based on fish gelatin proved to yield the better results in all cases, and the overall best values were found to occur in the case of fish gelatin incorporating DOPO (reduction in pHHR by about 54%; reduction in THR by 50% and h_c by 54%). The fire retardant effect of DOPO is established, and are well documented in the literature (Salmeia & Gaan, 2015). In addition, the enhanced effects brought in by DOPO could be attributed to phosphorus/nitrogen interactions. It should be also noted here that in the flaming mode, as encountered in cone tests, all the test specimens formed similar amounts of char residues (18- 23 wt. %).

Table 3. 10 Relevant parameters from cone measurements

| Sl. No. | Sample | T_{ig} (s) | pHRR (kW m ⁻²) | THR (MJ m ⁻²) | Char Residue (wt. %) | h_c (MJ kg ⁻¹) |
|---------|---|-----------------|-------------------------------|------------------------------|-------------------------|---------------------------------|
| 1 | Timber | 38 | 148 | 97.0 | 20 | 11.5 |
| 2 | Chitosan | 98 | 138 | 90.0 | 21 | 9.70 |
| 3 | Potato starch | 29 | 169 | 129 | 18 | 14.5 |
| 4 | Rice bran | 26 | 198 | 110 | 21 | 12.0 |
| 5 | Rice bran + Na ₂ CO ₃ | 23 | 186 | 82.0 | 20 | 9.60 |
| 6 | Rice bran + (NH ₄) ₂ HPO ₄ | 23 | 201 | 90.0 | 25 | 11.8 |
| 7 | Rice Bran + DOPO | 22 | 169 | 92.0 | 21 | 10.8 |
| 8 | Rice Bran + TPP | 15 | 201 | 111 | 19 | 12.5 |
| 9 | Fish gelatin | 46 | 139 | 93.0 | 22 | 10.1 |
| 10 | Fish gelatin + Na ₂ CO ₃ | 35 | 150 | 96.0 | 18 | 9.90 |
| 11 | Fish gelatin + (NH ₄) ₂ HPO ₄ | 35 | 114 | 86.0 | 19 | 9.30 |
| 12 | Fish gelatin + TPP | 53 | 149 | 91.0 | 20 | 10.3 |
| 13 | Fish gelatin + TPPO | 25 | 157 | 98.0 | * | * |
| 14 | Fish gelatin + DOPO | 29 | 68.0 | 50.0 | 23 | 5.30 |
| 15 | Fish gelatin + DEP | 32 | 186 | 129 | 20 | 13.0 |
| 16 | Fish gelatin + TEPI | 48 | 198 | 128 | 21 | 13.0 |
| 17 | Fish gelatin + TEPa | 41 | 161 | 130 | 21 | 13.9 |
| 18 | Fish gelatin + DEPP | 58 | 174 | 145 | 19 | 14.2 |
| 16 | Fish gelatin + DEBP | 48 | 200 | 126 | 20 | 13.93 |

*note here that the values obtained here were not reliable as they fell in the region of <1

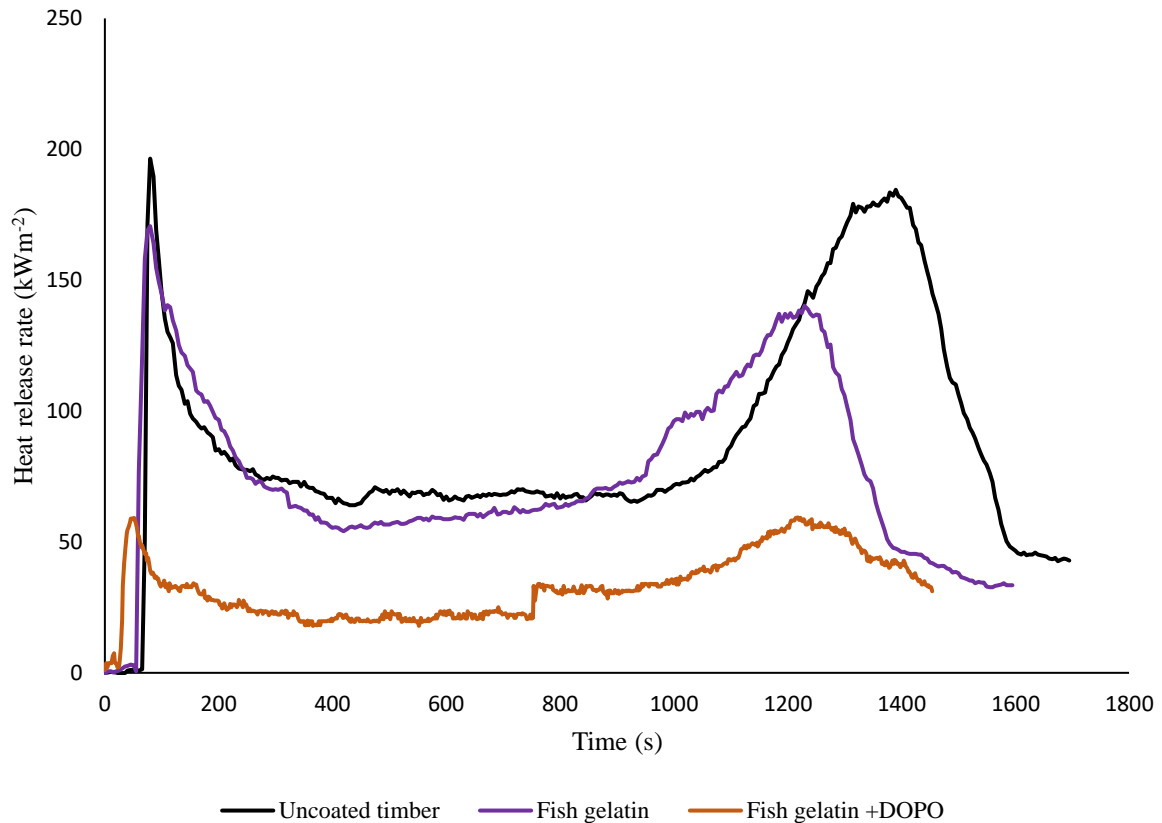


Figure 3. 61 An overlay of the HRR curves vs. time for uncoated and coated timber plaques from cone tests- as expected, the general profile of the HRR curves shows the typical characteristics of a thermally thick material (Drysdale, 2011)

In the case of the formulations of fish gelatin with P-containing liquid additives, some degree of antagonistic effects were observed, primarily judging by the values of pHRR, THR and h_c , as compared to uncoated and the samples coated with fish gelatin alone. Perhaps the only notable exception to this was the nominal enhancements in the time to ignition values. This effectively points to the fact that the P-containing liquid additives are capable of exerting some inhibitory effects, at least, in the very early stages of degradation of the base matrix, thus causing a slight decrease in the ignition propensity of the base matrix. In order to gain a deeper understanding of the degradation of the formulations involving fish gelatin, we performed TGA runs on all the formulations, and figures: 3. 62 to 3. 71. For the purpose of comparison each figure also has overlays of the virgin and the formulation. Generally, it can be seen that whilst overall profiles of the thermograms of the virgin material and each of the formulation differ to various extents, and are very profound in the cases of the formulation containing TPP, whereas the corresponding profiles are strikingly similar in the cases of formulations incorporating, DEPi and DEBP. In the case of the remaining formulations the degree of deviance of the

thermograms also vary to different extents. Such differences in the profiles of the thermograms can be attributed to the influence of a particular additive in bringing about the changes in the degradation profile of the base substrate (i.e. fish gelatin).

It is also interesting to note here that except in the case of the formulation containing AP, TPP and TEPI, all the mixtures have slightly lower temperatures for the induction of the initial degradation, however invariably results in either same or even lower char yields (the formulation containing TEPI was found to be the only exception). Take together it can be concluded that the liquid additives, whilst seem to exert some degree of inhibition for the base substrate to undergo ignition, are ineffective as fire retardants. The latter attribute could result from the inability of the gaseous fragments (see in section 3.6), emanating from these additives, in suppressing the gaseous phase combustion reactions and or the inadequacy of them to retard thermal degradation of the solid base matrix in spite of their retention in the char residues (see section 3.5).

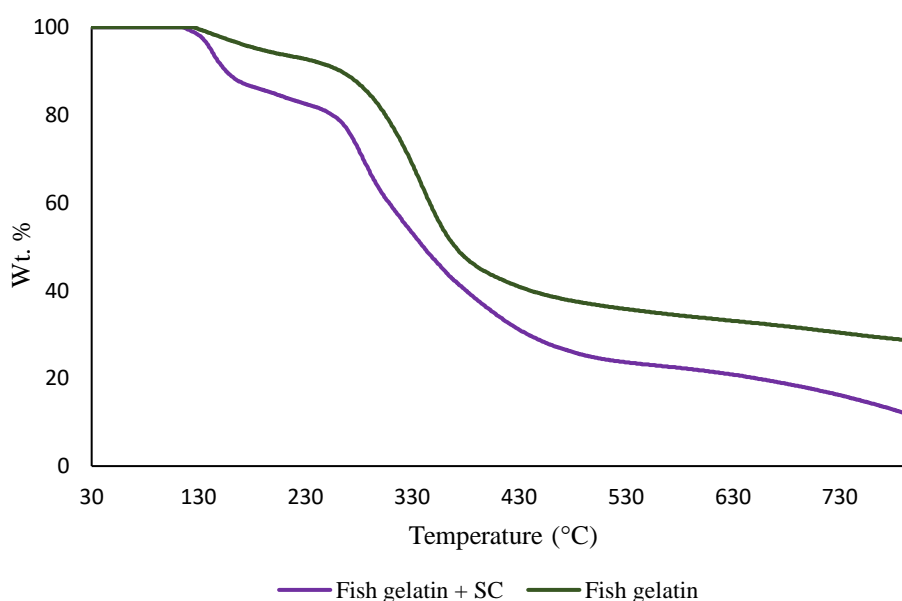


Figure 3. 62 Thermograms of virgin and a physical mixture of fish gelatin containing sodium carbonate (SC) at 60°C min⁻¹

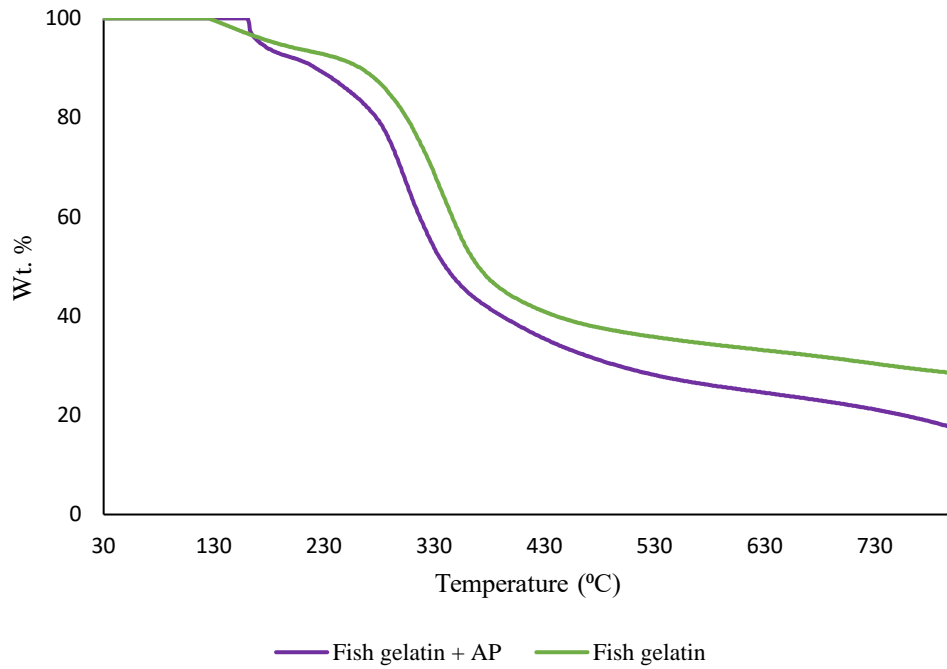


Figure 3. 63 Thermograms of virgin and a physical mixture of fish gelatin containing diammonium hydrogen phosphate (AP) at 60°C min⁻¹

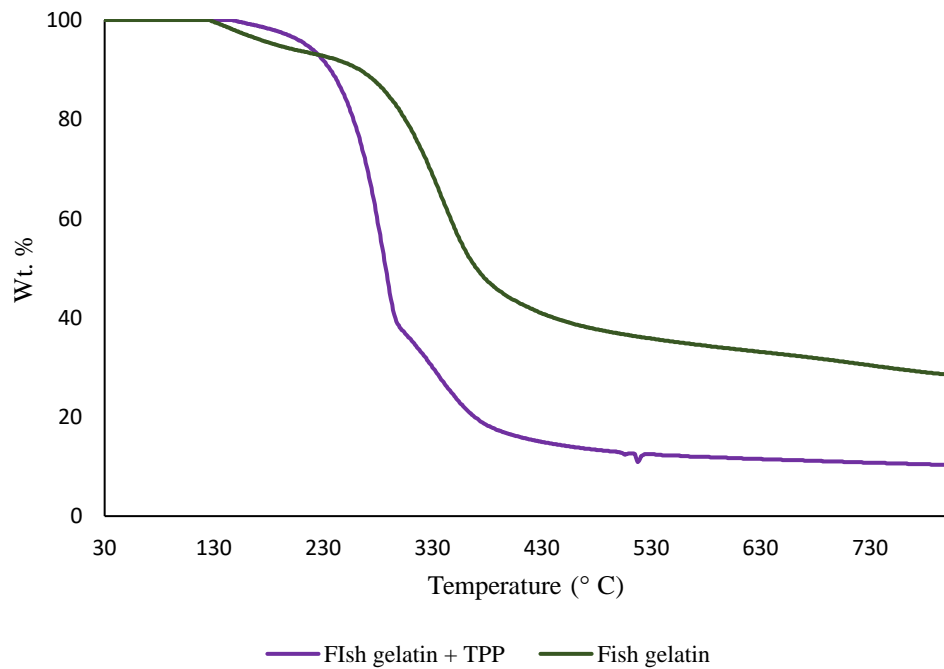


Figure 3. 64 Thermograms of virgin and a physical mixture of fish gelatin containing triphenylphosphine (TPP) at 60°C min⁻¹

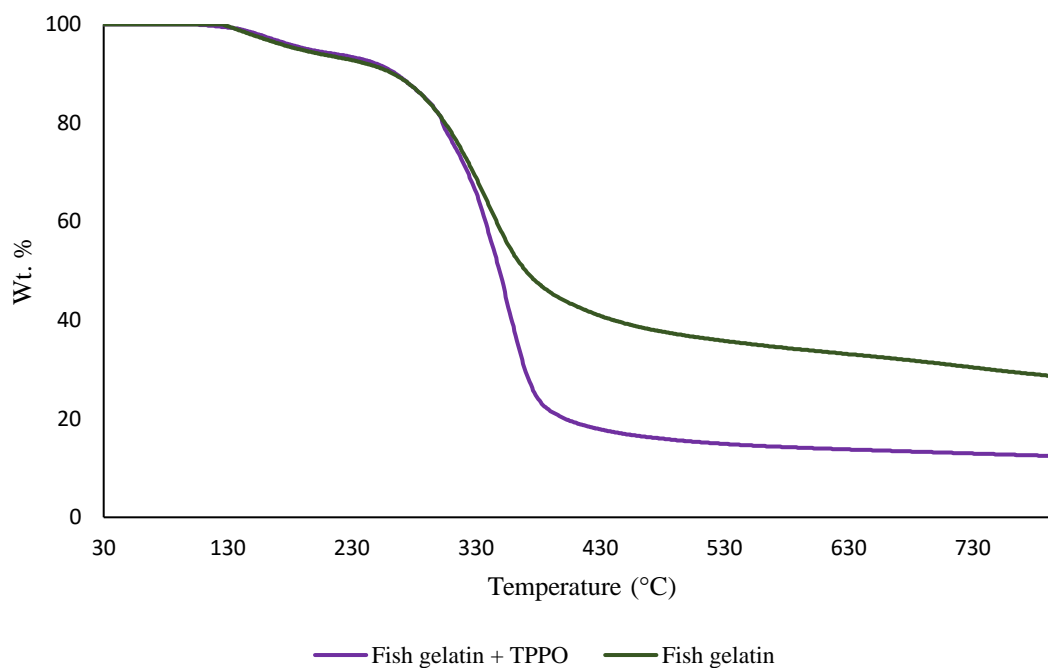


Figure 3. 65 Thermograms of virgin and a physical mixture of fish gelatin containing triphenylphosphineoxide (TPPO) at 60°C min⁻¹

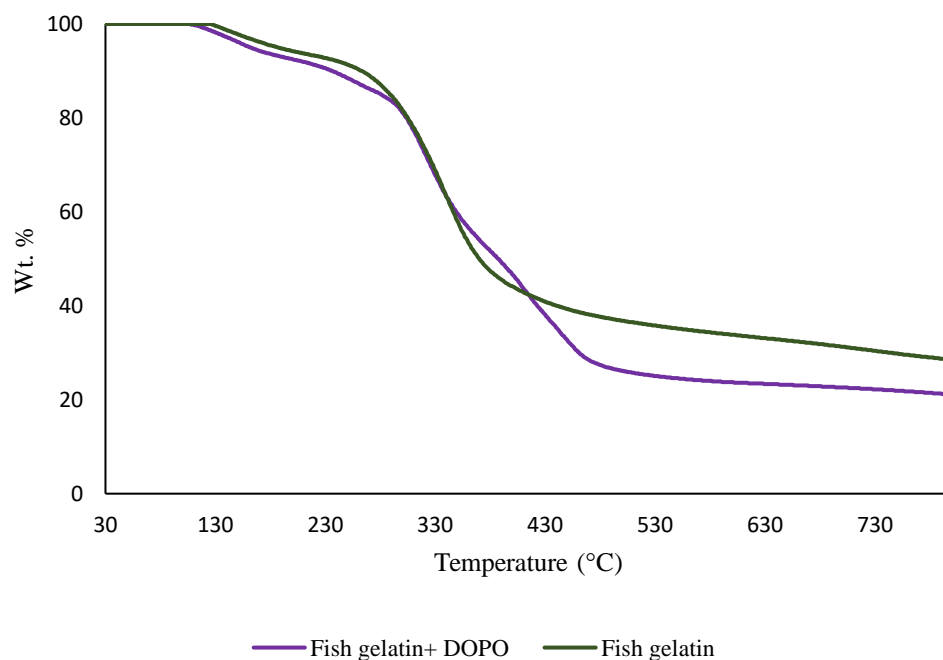


Figure 3. 66 Thermograms of virgin and a physical mixture of fish gelatin containing 9,10-dihydro-9-oxa-10-phosphaphenanthrene-10-oxide (DOPO) at 60°C min⁻¹

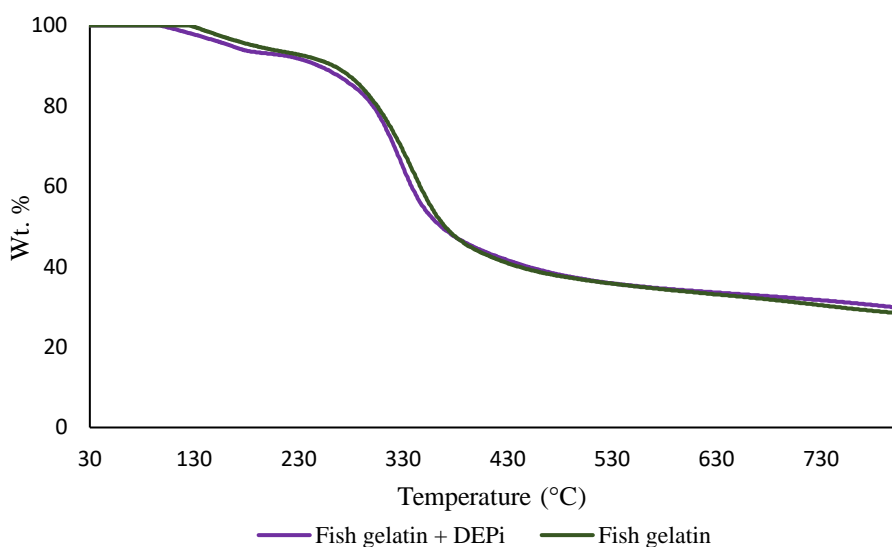


Figure 3. 67 Thermograms of virgin and a physical mixture of fish gelatin containing diethylphosphite (DEPi) at 60°C min⁻¹

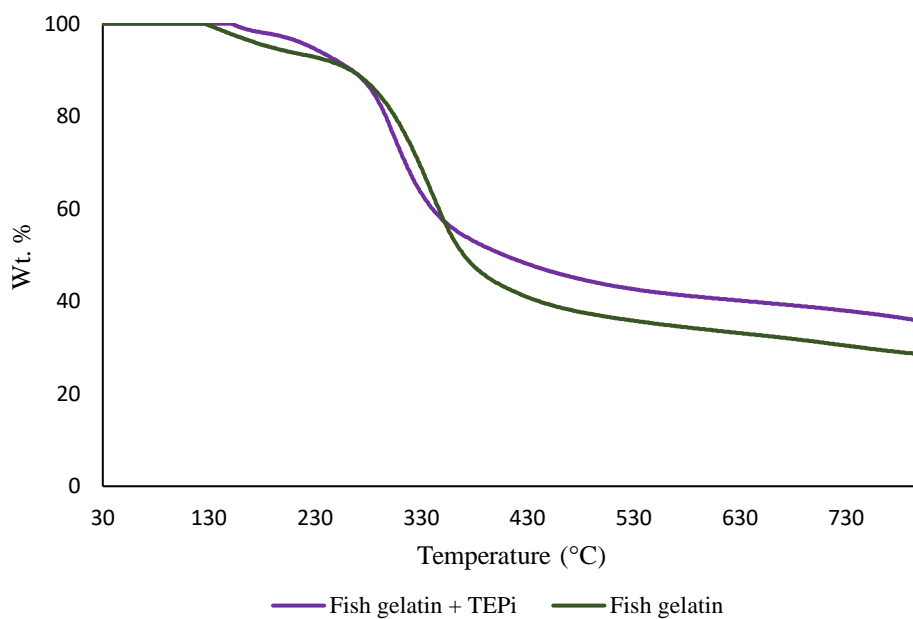


Figure 3. 68 Thermograms of virgin and a physical mixture of fish gelatin containing triethylphosphite (TEPi) at 60°C min⁻¹

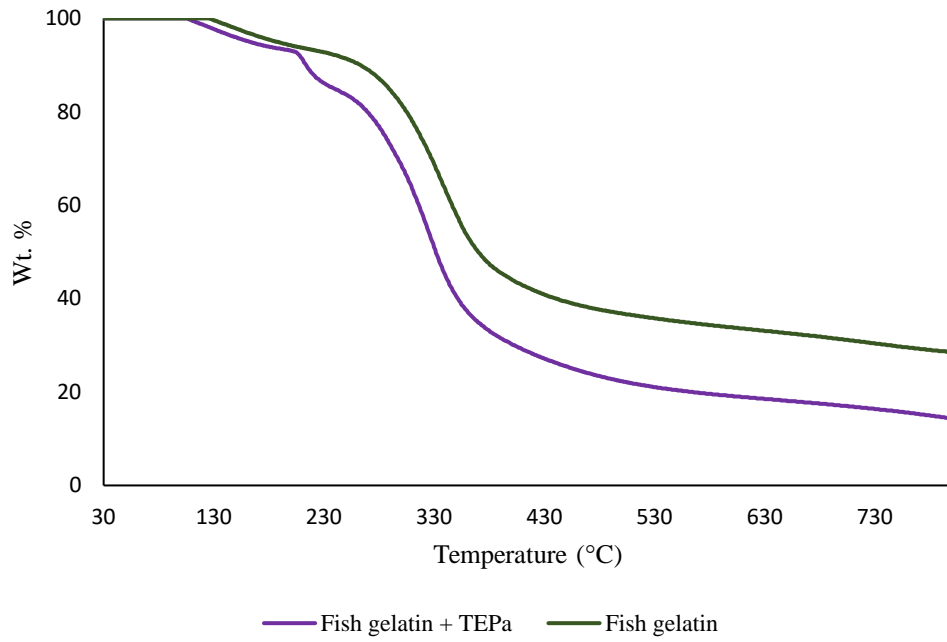


Figure 3. 69 Thermograms of virgin and a physical mixture of fish gelatin containing triethylphosphite (TEPa) at 60°C min⁻¹

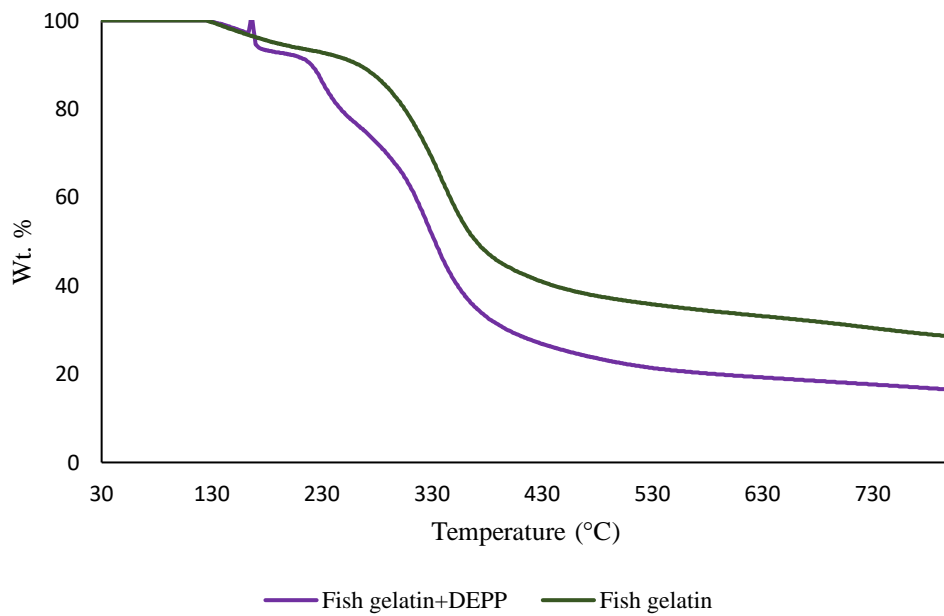


Figure 3. 70 Thermograms of virgin and a physical mixture of fish gelatin containing diethylpropylphosphonate (DEPP) at 60°C min⁻¹

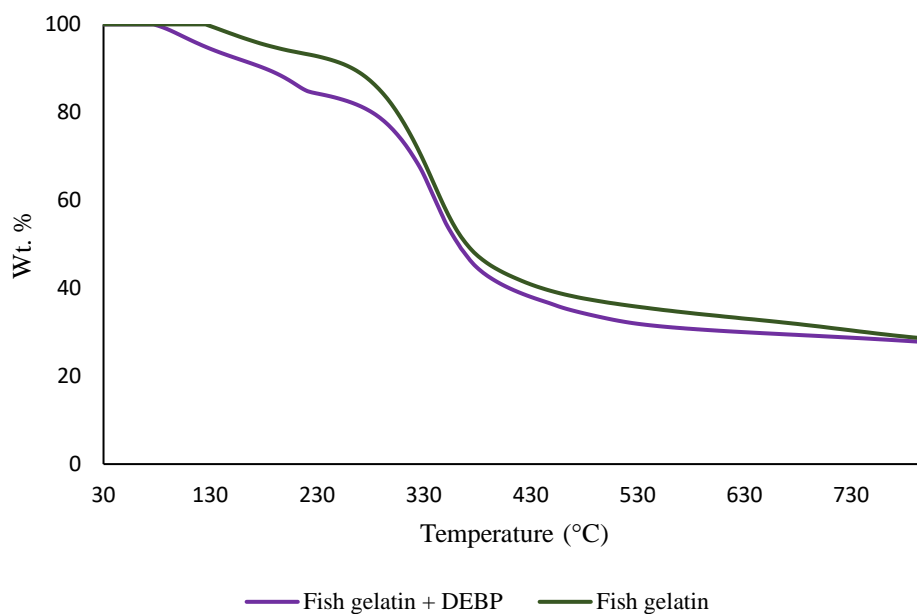


Figure 3. 71 Thermograms of virgin and a physical mixture of fish gelatin containing diethylbenzylphosphonate (DEBP) at 60^o C min⁻¹

With a view to gathering more detailed information regarding the thermal behaviours and combustion attributes of the formulations of fish gelatin containing various additives, we also endeavoured to do the PCFC tests on them. The results from these tests are summarized in table 3. 11 below.

Table 3. 11 Relevant parameters from PCFC tests of the coatings (fish gelatin as the base matrix)

| Sl. No. | Sample | P loading (wt. %) | Temp to pHRR (°C) | pHRR (W g ⁻¹) | THR (kJ g ⁻¹) | Heat Release Capacity (J g ⁻¹ K ⁻¹) | Char yield (wt. %) | h _c (kJg ⁻¹) |
|---------|---------------------|-------------------|-------------------|---------------------------|---------------------------|--|--------------------|-------------------------------------|
| 1 | Fish gelatin | 0.00 | 312 | 112 | 10.6 | 126 | 27.78 | 10.32 |
| 2 | Fish gelatin + SC | 0.00 | 279 | 98.0 | 10.6 | 103 | *--- | --- |
| 3 | Fish gelatin + AP | 4.10 | 289 | 78.0 | 5.20 | 289 | 24.10 | 4.960 |
| 4 | Fish gelatin + TPP | 3.48 | 304 | 414 | 26.6 | 423 | 10.31 | 25.50 |
| 5 | Fish gelatin + TPPO | 3.43 | 322 | 164 | 16.1 | 184 | 1.500 | 16.10 |
| 6 | Fish gelatin + DOPO | 3.68 | 419 | 128 | 24.4 | 138 | *--- | --- |
| 7 | Fish gelatin + DEPi | 4.05 | 272 | 71.0 | 10.6 | 85.0 | 32.20 | 10.28 |
| 8 | Fish gelatin + TEPi | 3.97 | 292 | 105 | 10.8 | 112 | 27.50 | 10.53 |
| 9 | Fish gelatin + TEPa | 3.62 | 306 | 156 | 10.2 | 168 | 29.79 | 9.900 |
| 10 | Fish gelatin + DEPP | 3.85 | 321 | 101 | 12.6 | 109 | 18.75 | 12.41 |
| 11 | Fish gelatin + DEBP | 3.63 | 328 | 91.0 | 8.90 | 90.0 | 23.89 | 8.660 |

*Pyrolysis residue could not be measured accurately as the sample expanded considerably and spilled over the pan upon the degradation/combustion

As can be seen from the above table, the values of the relevant empirical parameters (such as, pHRR, THR, HRC, char yields, h_c , etc.) are rather spread for the formulations containing different additives. Such deviations can be attributed to the inherent differences arising from: chemical nature of the additives; phosphorus loadings; degradation pathways of the individual additives; extents of interactions, if any between the additives and the base matrix; etc. The plots of some of the relevant parameters (pHRR, THR, HRC, char yields- from both TGA and PCFC and h_c) against P-loadings (wt. %), and finally the char yields from TGA and PCFC are given below (see in Figures 3. 72 to 3. 78).

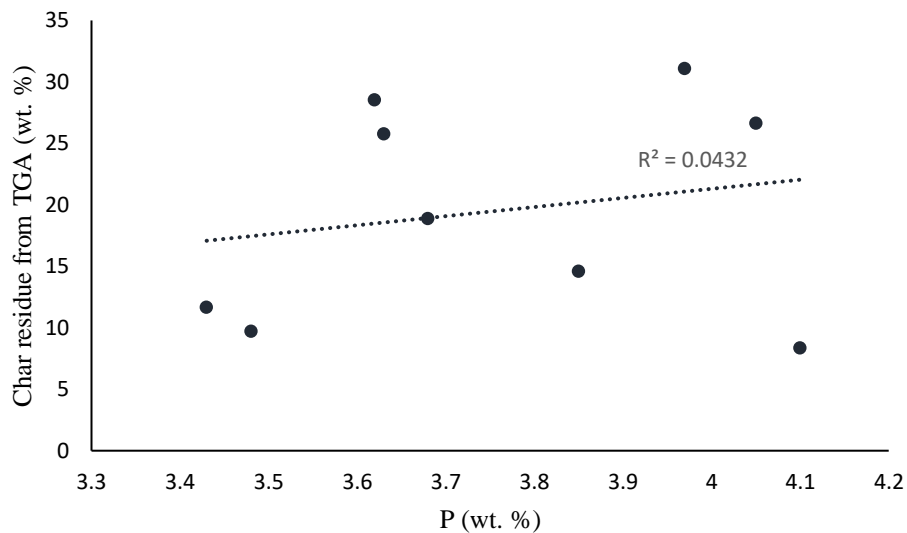


Figure 3. 72 A plot of char residue (wt. %) from TGA and P-loading (wt. %)

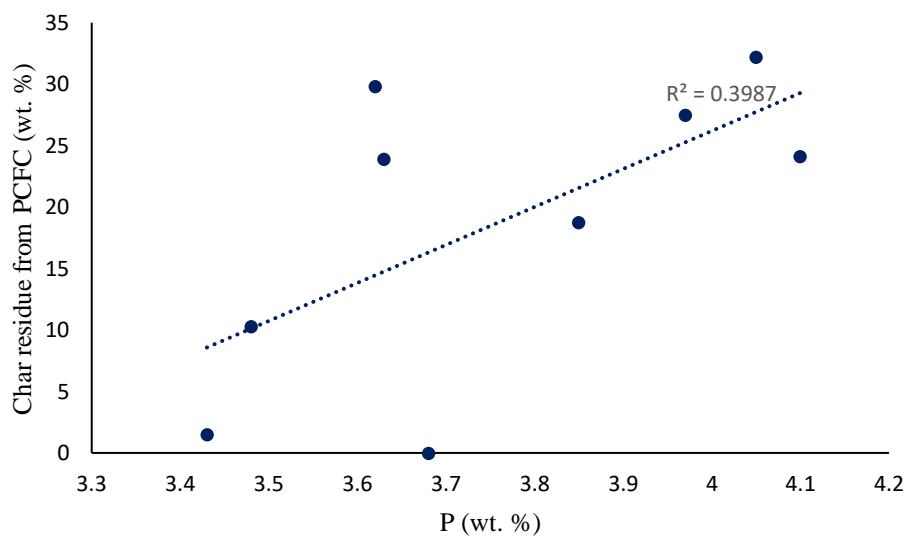


Figure 3. 73 A plot of char residue (wt. %) from PCFC and P-loading (wt. %)

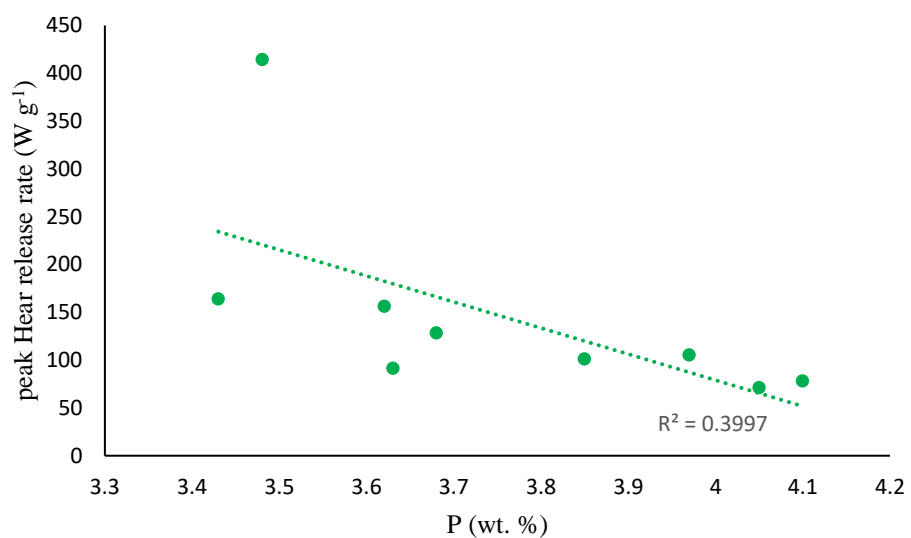


Figure 3. 74 A plot of char pHRR (W g⁻¹) from PCFC and P-loading (wt. %)

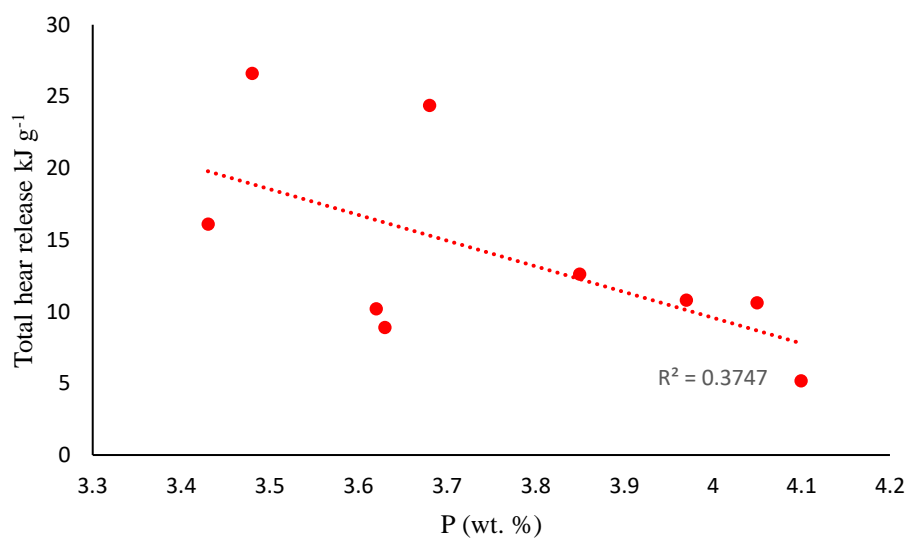


Figure 3. 75 A plot of THR (kJ g⁻¹) from PCFC and P-loading (wt. %)

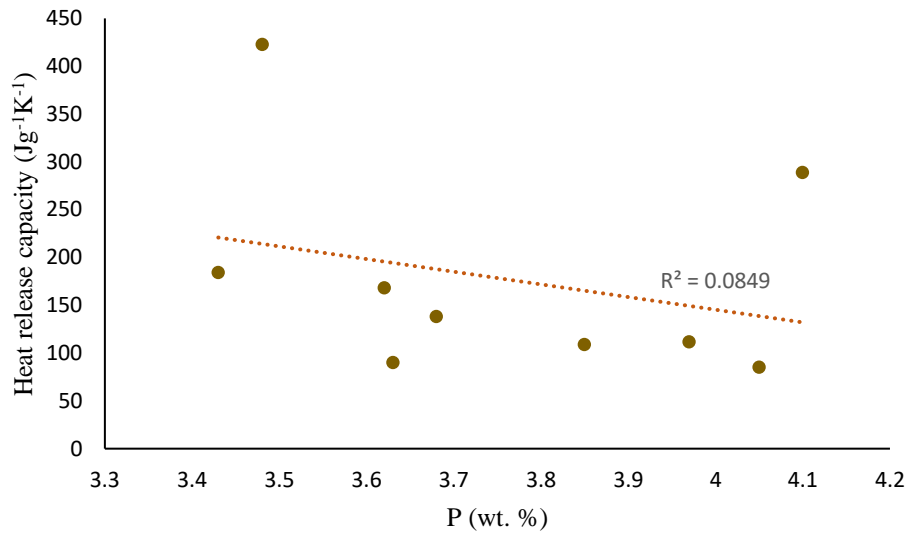


Figure 3. 76 A plot of HRC (J g⁻¹ K⁻¹) from PCFC and P-loading (wt. %)

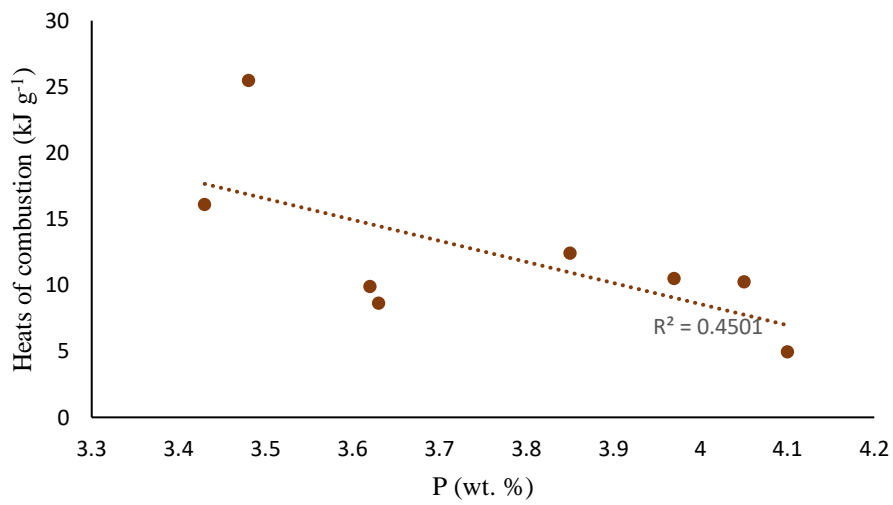


Figure 3. 77 A plot of h_c (kJ g⁻¹) from PCFC and P-loading (wt. %)

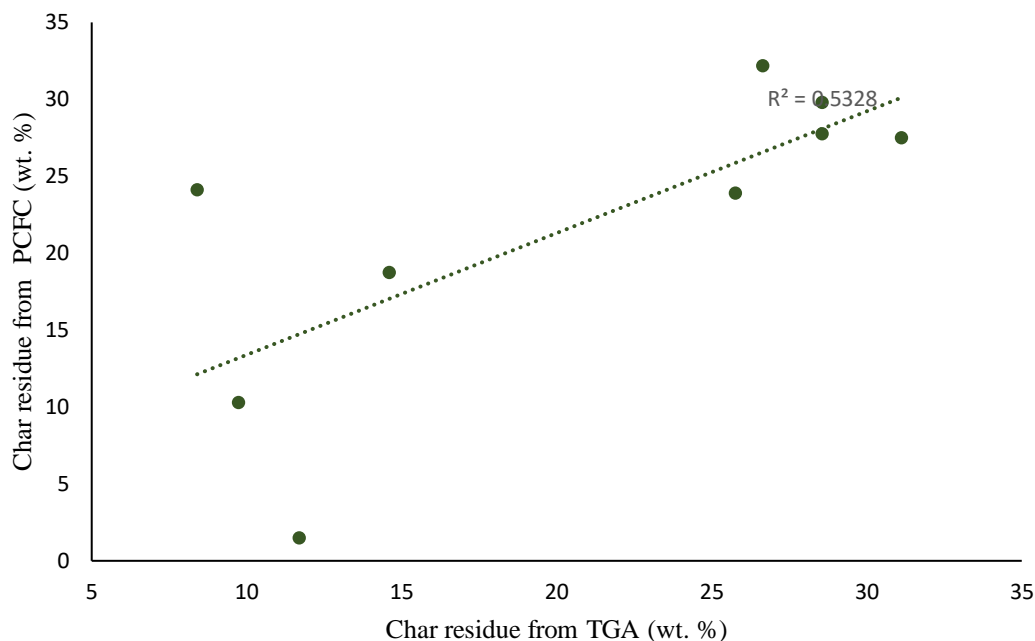


Figure 3. 78 A plot of the char residue (wt. %) from PCFC and char residue (wt. %) from TGA

As can be noticed from Figures 3. 72 to 3. 78, the phosphorus-containing additives do exert different degrees of condensed phase activities, and it is also apparent that the degrees of such effects generally increase with P-loadings. From the plots, some underlying trends can be identified, as follows (here the corresponding R^2 values for the linear trend lines may be taken as an indication of the degrees of correlation amongst the empirical parameters):

The plot of the char yield values from TGA experiments with corresponding P-loadings appear to be rather scattered without presenting any discernible pattern (Figure 3. 72). This could be attributed to the fact that during the temperature-programmed TGA run in nitrogen, the formulation only undergoes pyrolysis and any combustion inhibitory effect(s), if at all present, cannot be manifested.

On the contrary, the corresponding values of char residues obtained through PCFC runs can be considered to constitute an upward trend with increases in P-loadings, where forced combustion is effected in the second stage of the experiment (Figure 3. 73).

The first stage in a PCFC run can be considered to be very similar to that occurring during the TGA test, and hence the plot of the corresponding char residues shows (Figure 3. 78) some degree of correlation.

The pHRR *vs.* P (wt. %) also showed a noticeable trend except in the case of TPP, where a unexpectedly high value was recorded (Figure 3. 74).

As expected, the THR *vs.* P (wt. %) showed similar trend as in one above (since THR is obtained by integrating the area under the HRR curve, and therefore the values of pHRR are embedded in calculating the corresponding value of THR (Figure 3. 74). Here apart from the formulation containing TPP, DOPO also showed rather a high value for THR.

HRC values *vs.* P (wt. %) also showed a trend, more or less like in 4 and 5 above with the exception in the case of TPP and AP, the latter with a relatively larger P-loading (Figure 3. 75)

As expected, the trend in the variation of h_c *vs.* P (wt. %) followed more or less the same trend as in the plot of THR *vs.* P (wt. %) since effective heats of combustion values are obtained from the corresponding THR values after normalizing with the mass fraction that underwent degradation/combustion (Figure 3. 76)

3.5 Condensed-phase analysis

3.5.1 Inductively-coupled plasma optical emission spectroscopy (ICP-OES)

The phosphorus loadings of the formulations varied within a relatively narrow range that corresponded to a 0.016 molar loading of the additive in each case (i.e. 3.43 to 4.10 wt. %), whilst the extents of phosphorus retention in the char residues exhibited a wider range of values (i.e. 3.52 to 7.82 wt. %). Therefore, it can be inferred that the phosphorus-containing additives do exhibit varying degrees of condensed phase activity. However, the exact extents of this

effect cannot be directly gauged from the values of the initial phosphorus loading, or retention, owing to the fact that the char residue can be very inhomogeneous and the exact contributions of the underlying burnt/partially burnt wood towards the residue, therefore, cannot be determined with any certainty.

The initial P loading for the various formulations used for cone calorimetric tests can be calculated. Furthermore, from the char yields obtained through the cone runs and extent of phosphorus retention in the char residues, the wt. % of phosphorus escaped into the vapour phase can also be calculated, as shown below (see also in Table 3. 12).

$$\text{Wt. \% of P} = \frac{\frac{31}{\text{Fr. mass of additive}} \times \text{mass of additive} \times 100}{(\text{mass of fish gelatin} + \text{mass of additive})}$$

For example, fish gelatin when mixed with DOPO (Fr. mass = 216)

$$\text{Wt. \% of P} = \frac{\frac{31}{216} \times 3.46 \times 100}{(10 + 3.46)} = 3.68$$

$$P \text{ loading (theoretical max. in the char)} = \frac{P \text{ loading (initial)}}{\text{Char yield (from cone)}} \times 100$$

$$P \text{ loading (theoretical max. in the char)} = \frac{3.68}{20} \times 100 = 16$$

Table 3. 12 Phosphorus contents, determined through ICP/OES measurement, in coating formulations and the corresponding char residues

| Sl. No. | Sample | Wt.% P in the coating | Char yield (wt. %) from cone | Theoretical maximum of P loading in the char (wt. %) | P loading (ppm) | Wt.% P in the char | Wt. % of P in the gaseous phase |
|---------|---------------------|-----------------------|------------------------------|--|-----------------|--------------------|---------------------------------|
| 1 | Fish gelatin + AP | 4.10 | 21 | 19.52 | 36.6 | 7.82 | 59.93 |
| 2 | Fish gelatin + DOPO | 3.68 | 23 | 16.00 | 24.45 | 6.06 | 62.12 |
| 3 | Fish gelatin + TPP | 3.48 | 20 | 17.40 | 14.73 | 4.46 | 74.36 |
| 4 | Fish gelatin + TPPO | 3.43 | *--- | *--- | 11.23 | 3.50 | *--- |
| 5 | Fish gelatin + DEPi | 4.05 | 20 | 20.25 | 9.02 | 4.68 | 76.89 |
| 6 | Fish gelatin +TEPi | 3.97 | 21 | 18.90 | 3.84 | 2.83 | 85.02 |
| 7 | Fish gelatin +TEPa | 3.62 | 21 | 17.24 | 2.15 | 3.16 | 81.67 |
| 8 | Fish gelatin + DEPP | 3.85 | 19 | 20.26 | 4.63 | 2.04 | 89.93 |
| 9 | Fish gelatin + DEBP | 3.63 | 20 | 18.15 | 1.68 | 1.85 | 89.80 |

*could not be determined as the cone instrument erroneous values for the char yield

As expected, the liquid additives, owing to their volatility as compared to the solid ones, showed a relatively higher presence in the vapour phase. Furthermore, it can be seen that relatively substantial amounts of phosphorus-containing species from phosphine and the phosphine oxides were also presumably released into the vapour phase through fragments emanating from the thermal pyrolysis in the condensed phase (Gaan & Sun, 2007). The chemical environment of the phosphorus moieties retained in the condensed phase can be assessed from the ^{31}P solid-state NMR (section 3.5.2 below) and the fragmentation patterns of the additives can be deduced from GC/MS, or pyrolysis-GC/MS (sections 3.6.1 and 3.6.2, respectively).

3.5.2 Solid-state NMR spectra

In the following Figures 3. 79 to 3. 87 the ^{31}P signals obtained through solid state NMR measurements on powdered char residues collected from the cone experiments are given:

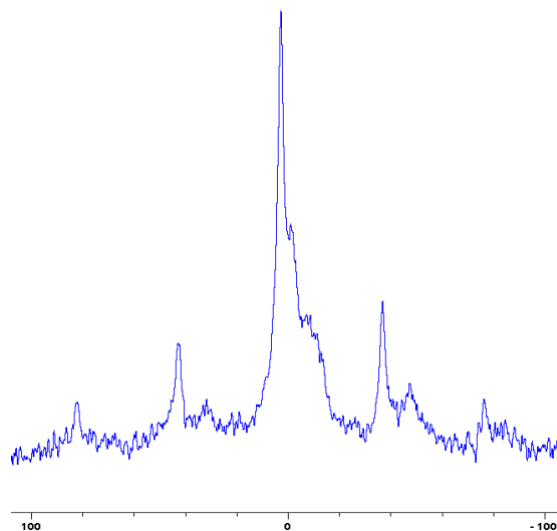


Figure 3. 79 Solid-state ^{31}P -NMR spectrum of char obtained from fish gelatin + TPP (the abscissa denotes the chemical shift values, δ , in ppm and the ordinate corresponds to the signal intensity in arbitrary units)

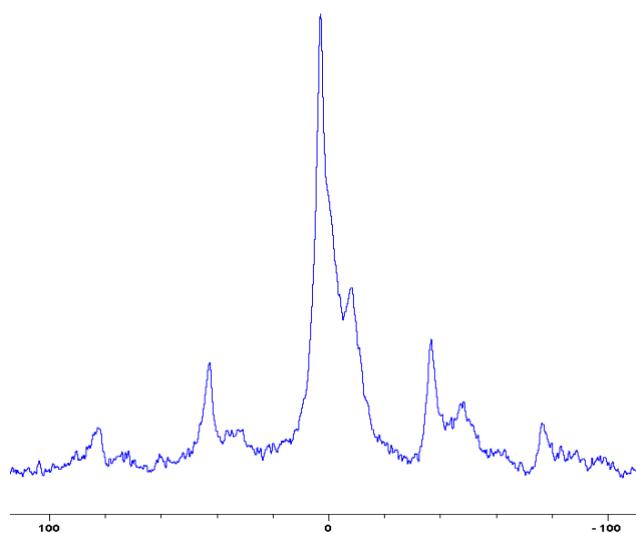


Figure 3. 80 Solid-state ^{31}P -NMR spectrum of char obtained from fish gelatin + TPPO (the abscissa denotes the chemical shift values, δ , in ppm and the ordinate corresponds to the signal intensity in arbitrary units)

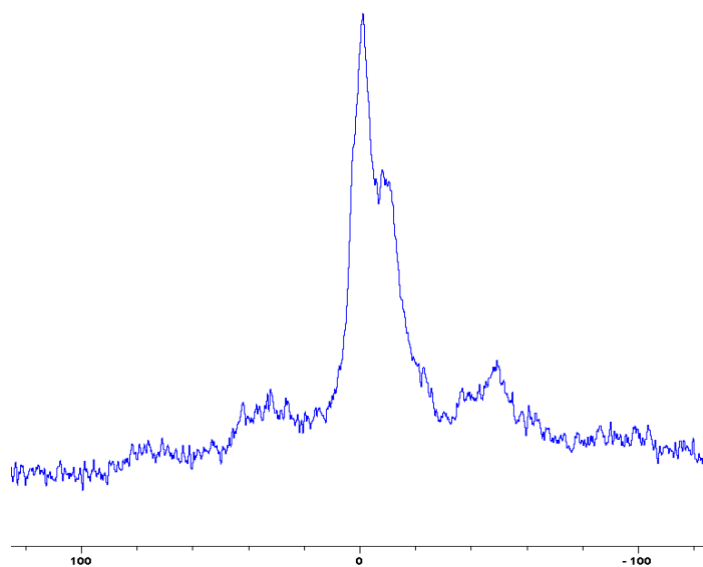


Figure 3. 81 Solid-state ^{31}P -NMR spectrum of char obtained from fish gelatin + DOPO (the abscissa denotes the chemical shift values, δ , in ppm and the ordinate corresponds to the signal intensity in arbitrary units)

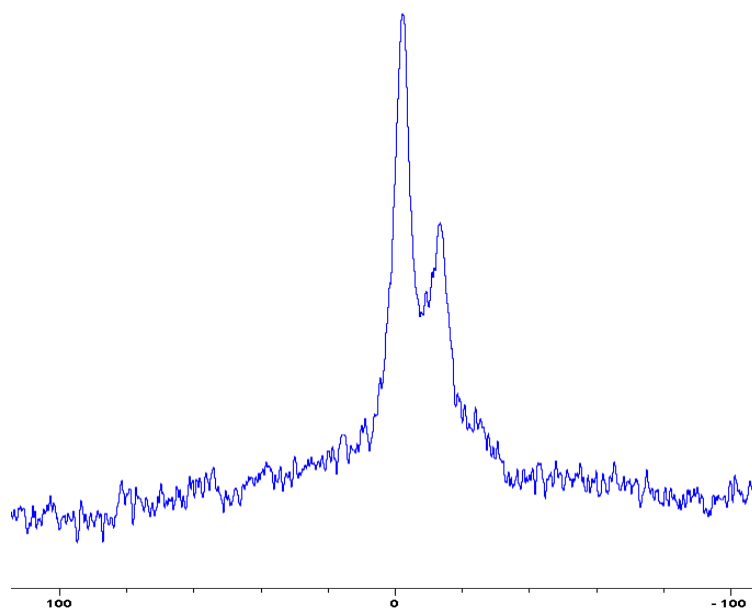


Figure 3. 82 Solid-state ^{31}P -NMR spectrum of char obtained from fish gelatin + $(\text{NH}_4)_2\text{HPO}_4$ (the abscissa denotes the chemical shift values, δ , in ppm and the ordinate corresponds to the signal intensity in arbitrary units)

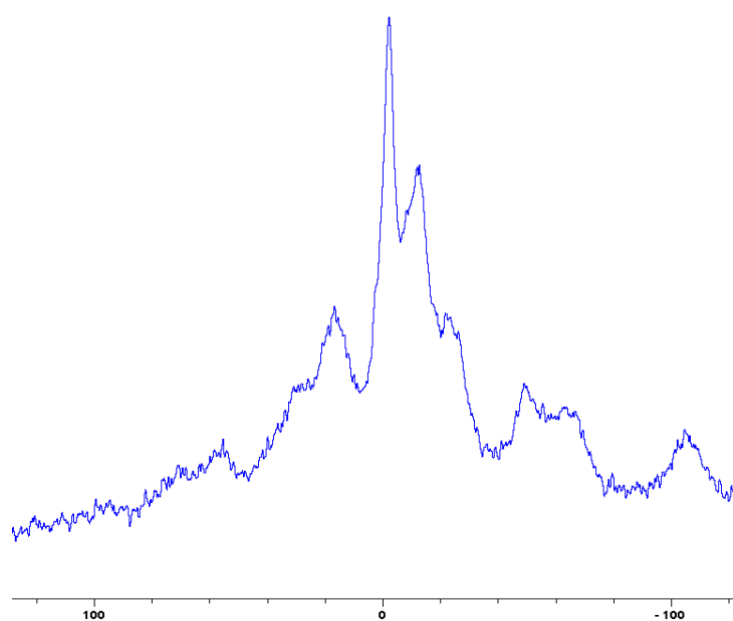


Figure 3. 83 Solid-state ^{31}P -NMR spectrum of char obtained from fish gelatin + diethylphosphite (DEPi) (the abscissa denotes the chemical shift values, δ , in ppm and the ordinate corresponds to the signal intensity in arbitrary units)

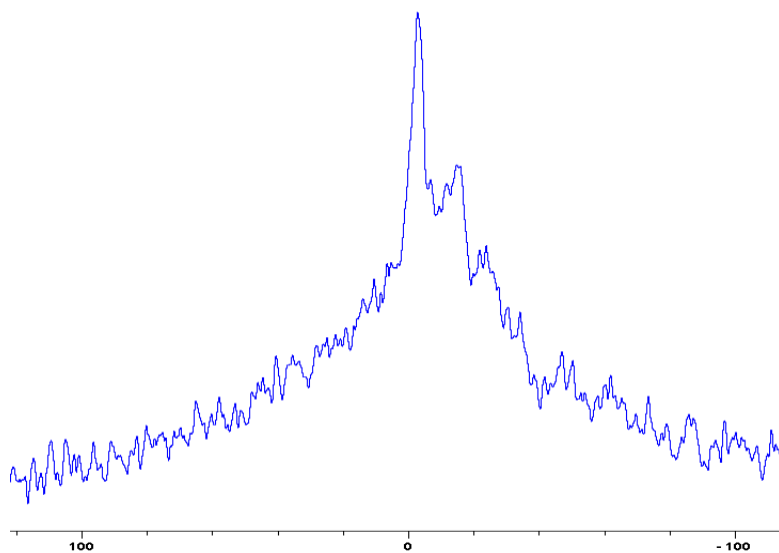


Figure 3. 84 Solid-state ^{31}P -NMR spectrum of char obtained from fish gelatin + triethylphosphite (TEPi) (the abscissa denotes the chemical shift values, δ , in ppm and the ordinate corresponds to the signal intensity in arbitrary units)

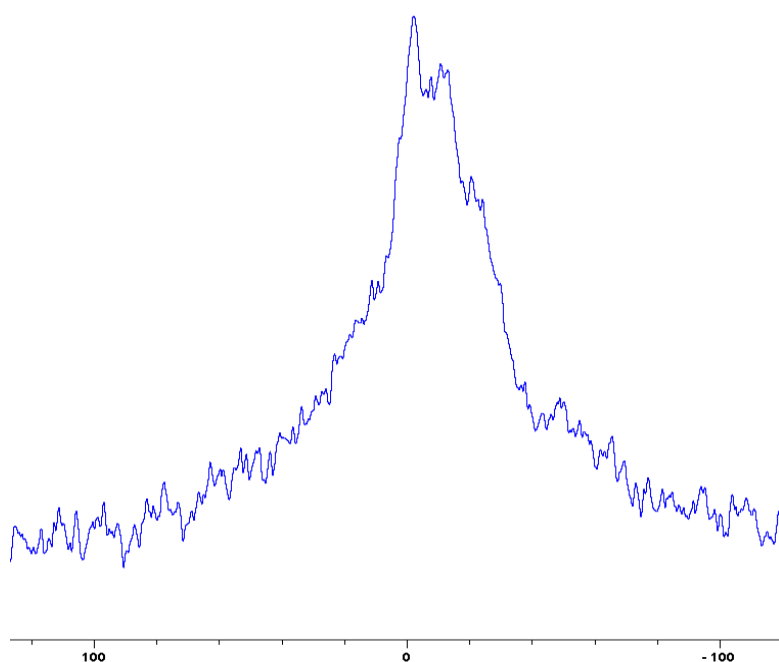


Figure 3. 85 Solid-state ^{31}P -NMR spectrum of char obtained from fish gelatin + triethylphosphate (TEPa) (the abscissa denotes the chemical shift values, δ , in ppm and the ordinate corresponds to the signal intensity in arbitrary units)

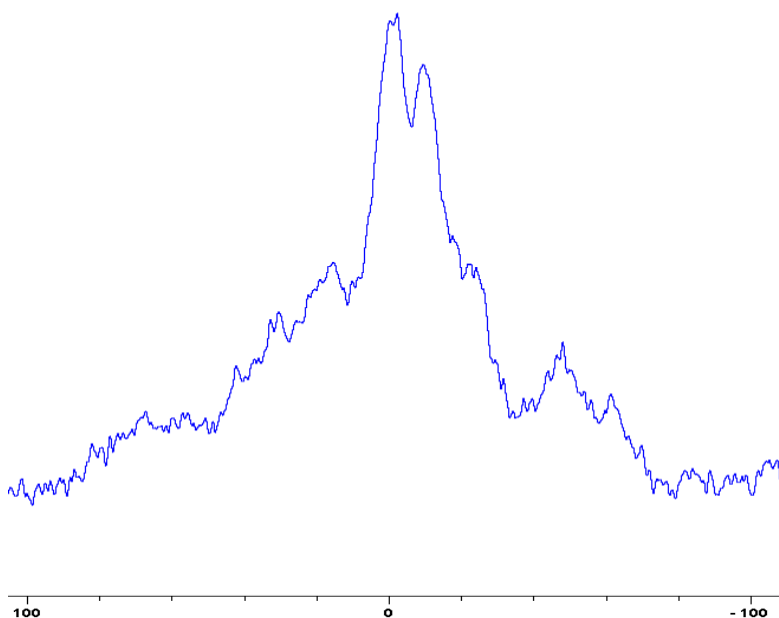


Figure 3. 86 Solid-state ^{31}P -NMR spectrum of char obtained from fish gelatin + diethylpropylphosphonate (DEPP) (the abscissa denotes the chemical shift values, δ , in ppm and the ordinate corresponds to the signal intensity in arbitrary units)

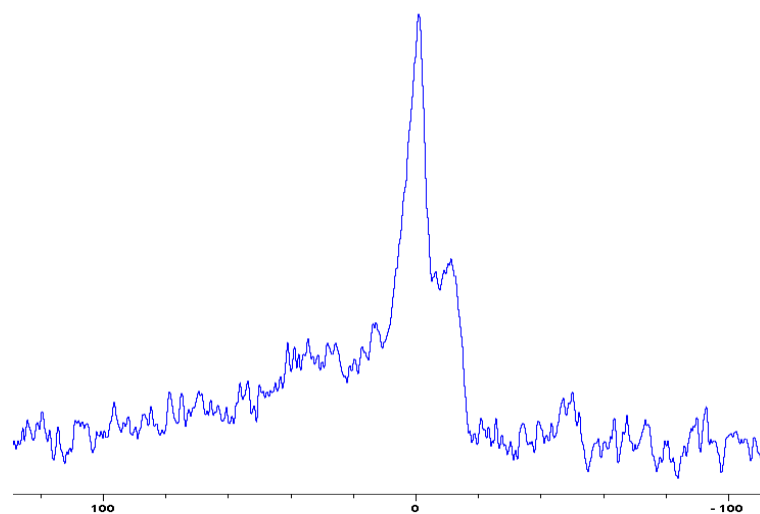


Figure 3. 87 Solid-state ^{31}P -NMR spectrum of char obtained from fish gelatin + diethylbenzylphosphonate (DEBP) (the abscissa denotes the chemical shift values, δ , in ppm and the ordinate corresponds to the signal intensity in arbitrary units)

Table 3. 13 Chemical shift values (δ in ppm) of P nucleus in the additives and in the char residue

| Sl. No. | Additive | δ value for ^{31}P of the additives *(solution-state) | δ value for ^{31}P of the char residue# |
|---------|----------|--|---|
| 1 | AP | 0.02 | -2.3 (-13.4) |
| 2 | TPP | -7.10 | 2.9 (-8.5) |
| 3 | TPPO | 27.6 | 2.9 (-8.5) |
| 4 | DOPO | 16.7 | -1.3 (-9.8) |
| 5 | DEPi | 7.30 | -2.3 (-13.1) |
| 6 | TEPi | 7.30 | -3.3 (-15.0) |
| 7 | TEPa | -1.00 | -2.6 (-10.8) |
| 8 | DEPP | 32.2 | -1.3 (-9.1) |
| 9 | DEBP | 26.4 | -1.0 (-10.8) |

*from ^{31}P solution-state NMR spectrum- here the protons were decoupled during the acquisition of ^{31}P NMR, and hence do not show ^1H - ^{31}P coupling patterns

#the major peak from solid-state NMR of the char residue, where the values in the parentheses represent the chemical shift (δ) of the ‘shoulder’ peak. It is relevant to note here that the ^{31}P solid state NMR of the char residues were acquired without broad band decoupling of residual protons that might be present in the char residues.

As expected, phosphorus acid species ($\delta \sim 0$ ppm), or oligomeric phosphate moieties ($\delta \sim -10$ ppm), are generated from the initial cracking/condensation reactions of AP, DEPi, TEPi, TEPa, DEPP and DEBP. However, cracking of TPP, TPPO and DOPO are bound to produce phenyl, or biphenyl species, and the phosphorus atom is likely to go into vapour phase either in the elemental form and/or as oxide species. Therefore, the signals in the latter cases can be attributed to unburnt phosphine (TPP), or phosphines oxide (TPPO, or DOPO), where the coupling patterns (scalar, including long-range) owing to ^1H - ^{31}P are also evident. The features

of such patterns in a solid state NMR spectrum (i.e. due to any unburnt additive) could be often complicated by the presence of rather prominent spinning side bands (see for example, in case of TPP, TPPO and DEHPi). By looking at the complementary information that was gathered through pyrolysis-GC/MS and GC/MS, we were able to formulate some plausible fragmentation pathways the case of the additives (see in section 3.6).

3.5.3. Raman spectroscopy

The structural features of char residues can be deduced from observing the relevant signal intensities in the Raman spectra (Joseph et al., 2012; T. Liu, Jing, Zhang, & Fang, 2018; Tawiah et al., 2019; Xu, Lei, Xu, Zhang, & Zhang, 2017). In the present study, we recorded the Raman spectra from representative char residues where the intensities of the graphitic (*G* band, associated with the vibrations of plane terminal glass carbons- unorganized carbon structure) and amorphous (*D* band, owing to an E_{2g} vibrational mode of graphitic sp^2 bonded carbon atoms- graphitic layered structure) were compared (see Figure 3. 88). Hence the ratios of the intensities of the bands (i.e. I_G/I_D), as measured through their respective areas, were different for all the test samples, and were indicative of the degree of graphitization of the carbonaceous residues obtained upon burning (Table 3. 14) . Generally, higher intensity of the *G* band with respect to the *D* band points to a more coherent char structure (Thomas, Moinuddin, Zhu & Joseph, 2020). The char residue from fish gelatin + TPPO was evidently richer in the graphitic region (ratio = 1.32) as compared to the residues of other formulations, and the corresponding value was the least in the case of fish gelatin + DEPP (ratio = 0.33). In the case of other systems, only fish gelatin + DEBP showed a higher value (ratio = 0.93), as compared with the unmodified substrate (0.73), whereas all other systems generally showed lower values.

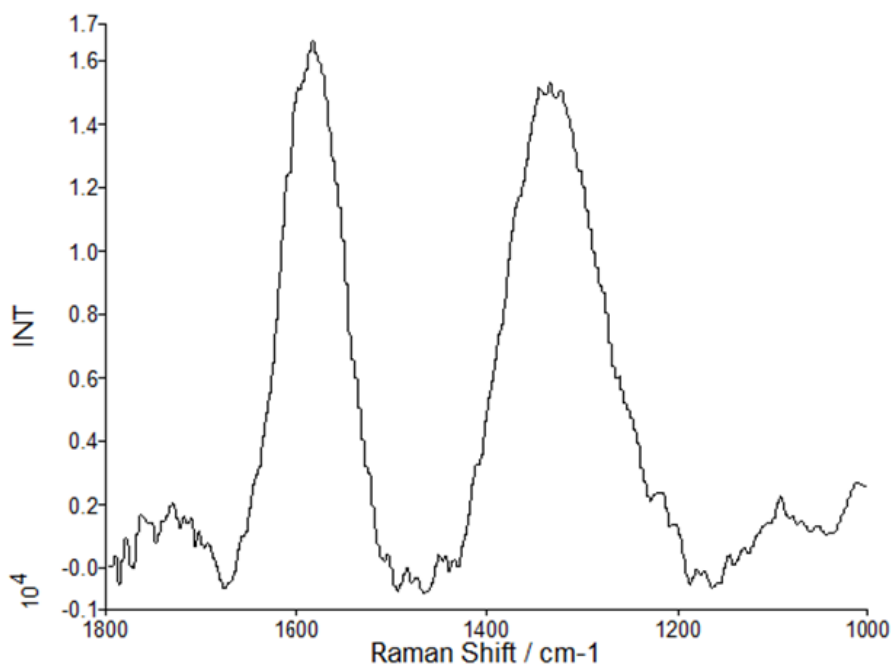


Figure 3. 88 Raman spectrum of the char residue from unprotected wood (Radiata Pine): the abscissa denotes the Raman shift values in (cm⁻¹) and the ordinate represents the signal intensity in arbitrary units

Table 3. 14 Details of Raman spectra of char residue

| Sl. No. | Char residue | Intensity of the G band (<i>I_G</i>) | Intensity of the D band (<i>I_D</i>) | Ratio (<i>I_G/I_D</i>) |
|---------|---------------------|--|--|--|
| 1 | Unprotected wood | 18030 | 24830 | 0.73 |
| 2 | Fish gelatin + AP | 21850 | 30360 | 0.72 |
| 3 | Fish gelatin + TPP | 476979 | 1099132 | 0.43 |
| 4 | Fish gelatin + TPPO | 450413 | 343278 | 1.32 |
| 5 | Fish gelatin + DOPO | 648452 | 1030772 | 0.63 |
| 6 | Fish gelatin + DEPi | 580753 | 1002797 | 0.58 |
| 7 | Fish gelatin + TEPi | 515705 | 954779 | 0.54 |
| 8 | Fish gelatin + TEPa | 570280 | 943631 | 0.60 |
| 9 | Fish gelatin + DEPP | 402813 | 1238529 | 0.33 |
| 10 | Fish gelatin + DEBP | 846410 | 913333 | 0.93 |

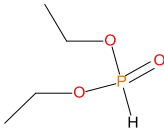
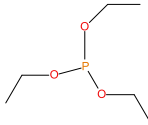
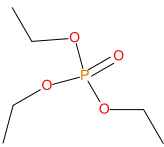
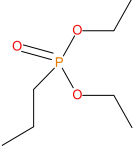
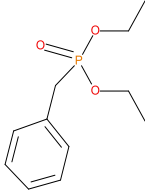
3.6 Vapour-phase analyses of the additives (i.e. hyphenated techniques)

With a view to obtaining more insight into the thermal cracking of the additives, we carried out some gaseous phase analyses of the volatiles emanating from them using ‘hyphenated’ techniques, such as GC-MS (for the liquid additives: DEPi, TEPi, TEPa, DEPP and DEBP), or pyrolysis-GC/MS (for solid additives: TPP, TPPO and DOPO). Here it should be noted that thermolysis of these additive under a flaming mode (i.e. under relatively higher heating rates and within lower time scales, and with varying degrees of oxygen ingress) cannot be directly compared to those occurring under a progressive heating according to a pre-determined temperature ramp, followed by an electron impact (as in a GC/MS), or under a thermally induced degradation at a pre-set temperature (in pyrolysis-GC/MS). Albeit, the basic assumption that regardless of the mode and rate of inducing bond cleavages in the additives, the weaker bonds are broken to result in relatively stable species can be considered as valid within reason.

The details of the liquid samples, retention times and major species recorded by the mass spectrometer are given in table below (Table 3. 15). In the case of the liquid samples that underwent fragmentation, the molecular ion peak was only shown up in the case of TEPa, where less conspicuous signals corresponding to $[M]_{\pm 1}$ were evident in the cases of DEPi and TEPa. In the case of the phosphonate additives, such as DEPP and DEBP, the molecular ions initially formed seem to have undergone rapid fragmentation resulting in stable species (with m/z values of 125 and 95 respectively).

3.6.1 Gas Chromatography-Mass Spectrometry (GC/MS)

Table 3.15 Retention times and fragmentation features of the various liquid additives

| Sl. No. | Sample (chemical name) | Chemical structures | Retention time (min) | Molar mass | [M] ⁺ | [M] ⁺ ±1 | [M] (100%) | Other predominant species/remarks |
|---------|------------------------|---|----------------------|------------|------------------|---------------------|------------|-----------------------------------|
| 1 | DEPi |  | 4.65 | 138 | ---- | 139 | 83 | 111 |
| 2 | TEPi |  | 3.91 | 166 | Yes | ---- | 65 | 139 |
| 3 | TEPa |  | 5.20 | 182 | ---- | 183.05 - | 99.00 | 127 |
| 4 | DEPP |  | 5.01 | 180 | ---- | ---- | 125 | 43 |
| 5 | DEBP |  | 8.01 | 228 | --- | ----- | 91 | 118 |

From the presence of the $[M]^+$, or $[M]^+ \pm 1$, and/or nature of $[M]^+$. (100%) and the major species, we could formulate the following fragmentation pathways in the case of the liquid additives, as follows:

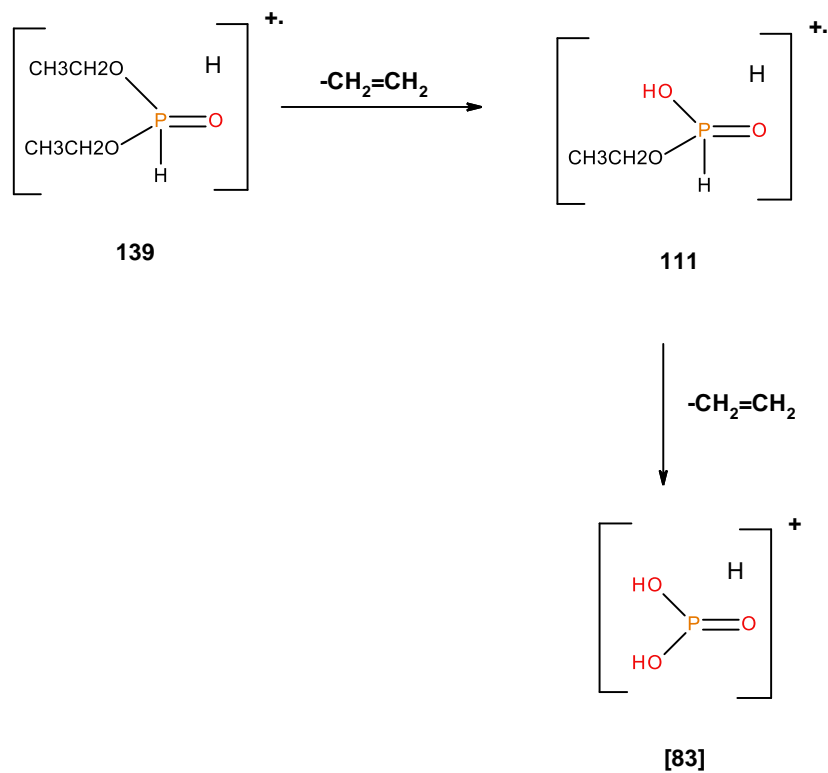


Figure 3. 89 Possible fragmentation pattern for DEPi

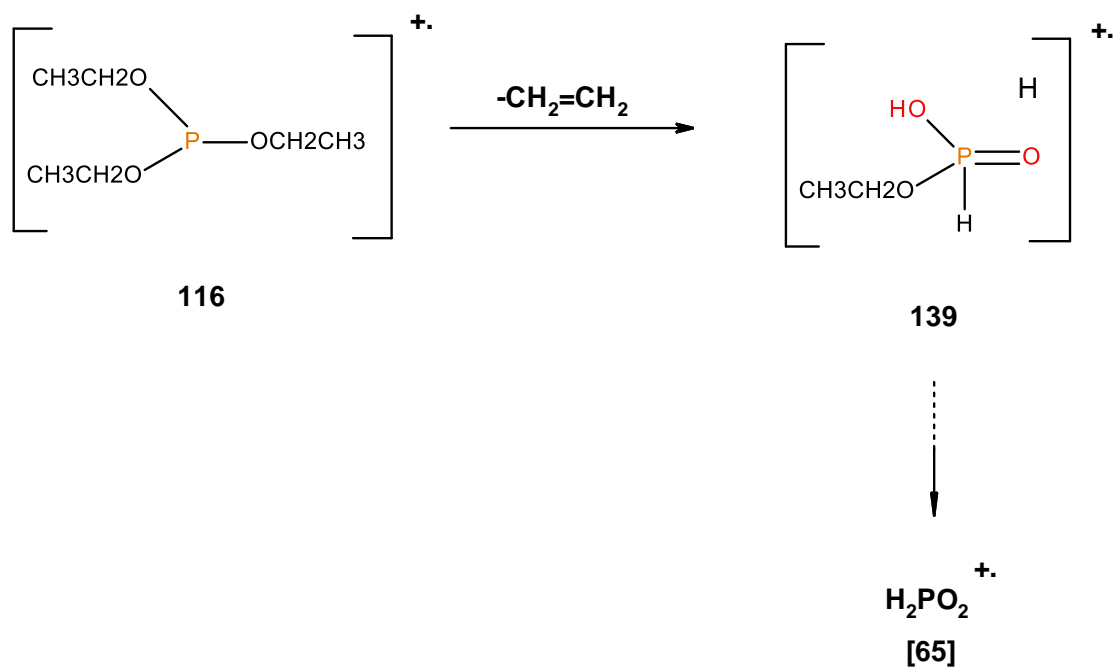


Figure 3. 90 Possible fragmentation pattern for TEPEi

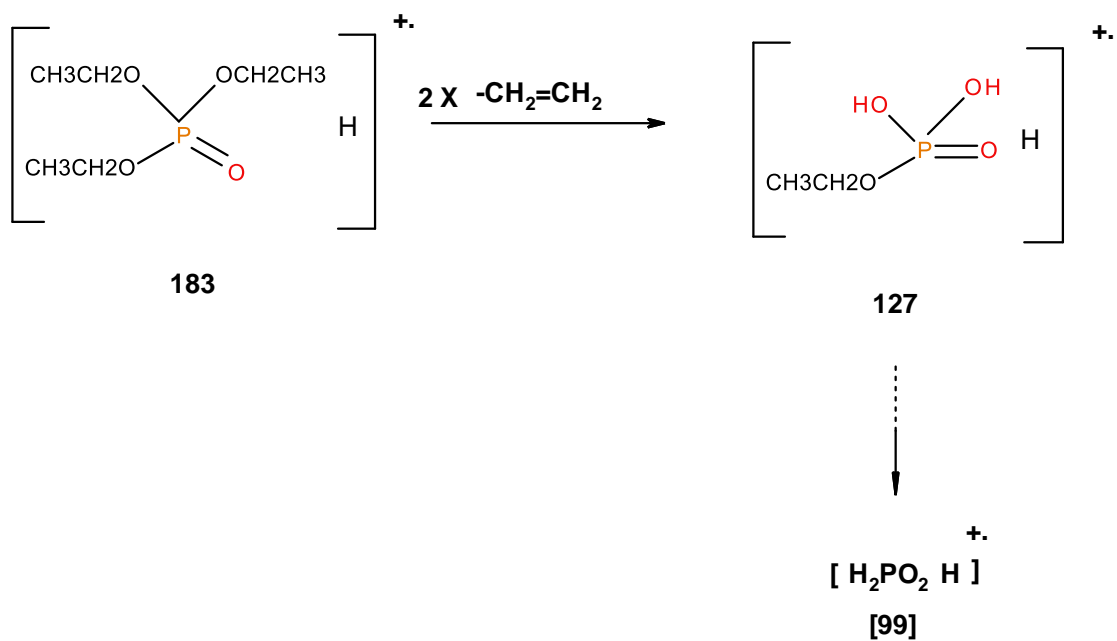


Figure 3. 91 Possible fragmentation pattern for TEPEa

3.6.2 Pyrolysis-gas chromatography/mass spectrometry (pyrolysis-GC/MS)

The temperatures for pyrolysis of the solid organophosphorus compounds were selected on the basis of the first derivatives of their thermogram (in nitrogen at heating rate of 10°C min⁻¹, and from 30 to 900°C). The inorganic solid additive, i.e. (NH₄)₂HPO₄, was not included in this study as it is assumed to undergo a two-step degradation yielding ammonia gas and phosphoric acid in the first step (*ca.* 70°C), followed by the degradation of the product, ammonium dihydrogen phosphate to produce oxides of phosphorus and nitrogen and ammonia (*ca.* 155°C), as shown below is the first step in the degradation.

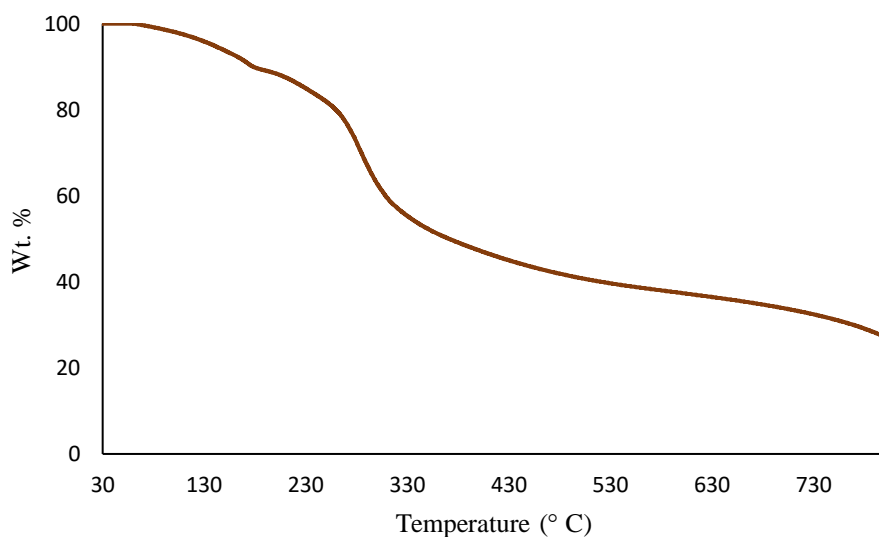


Figure 3. 94 TGA of diammonium hydrogen phosphate in nitrogen under a heating rate of 10°C min⁻¹

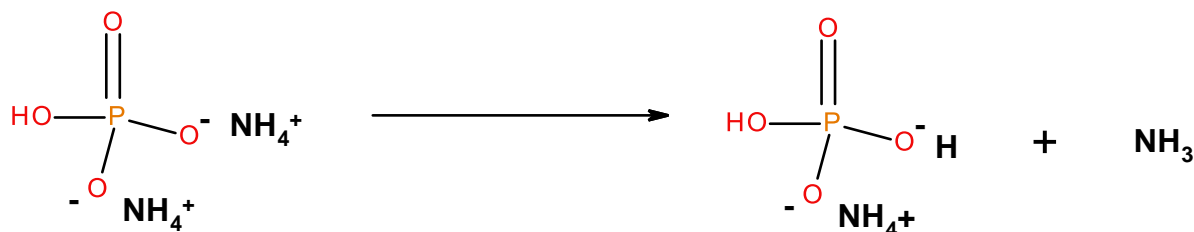


Figure 3. 95 Scheme showing the first step in the decomposition of (NH₄)₂HPO₄

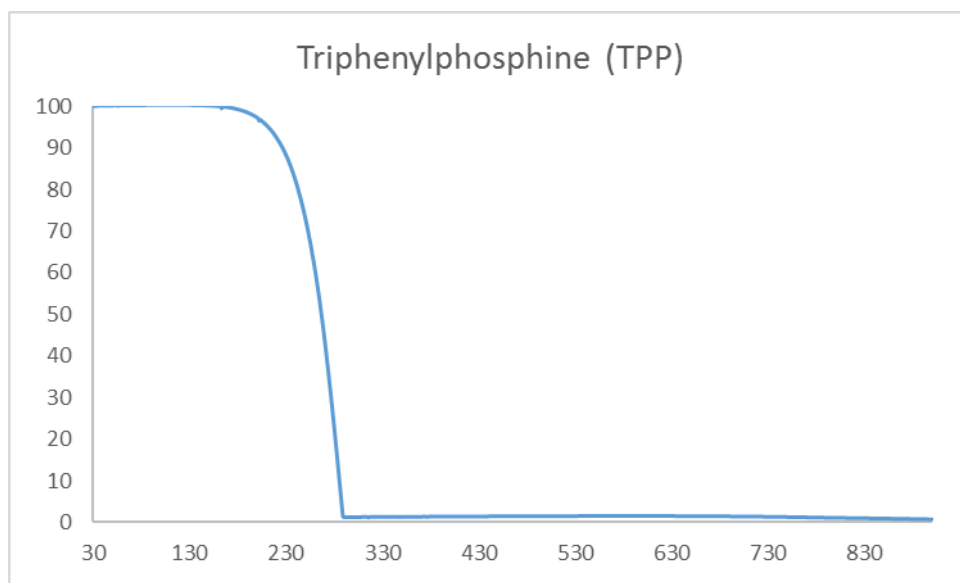


Figure 3. 96 TGA curve of TPP in nitrogen under a heating rate of 10°C min⁻¹

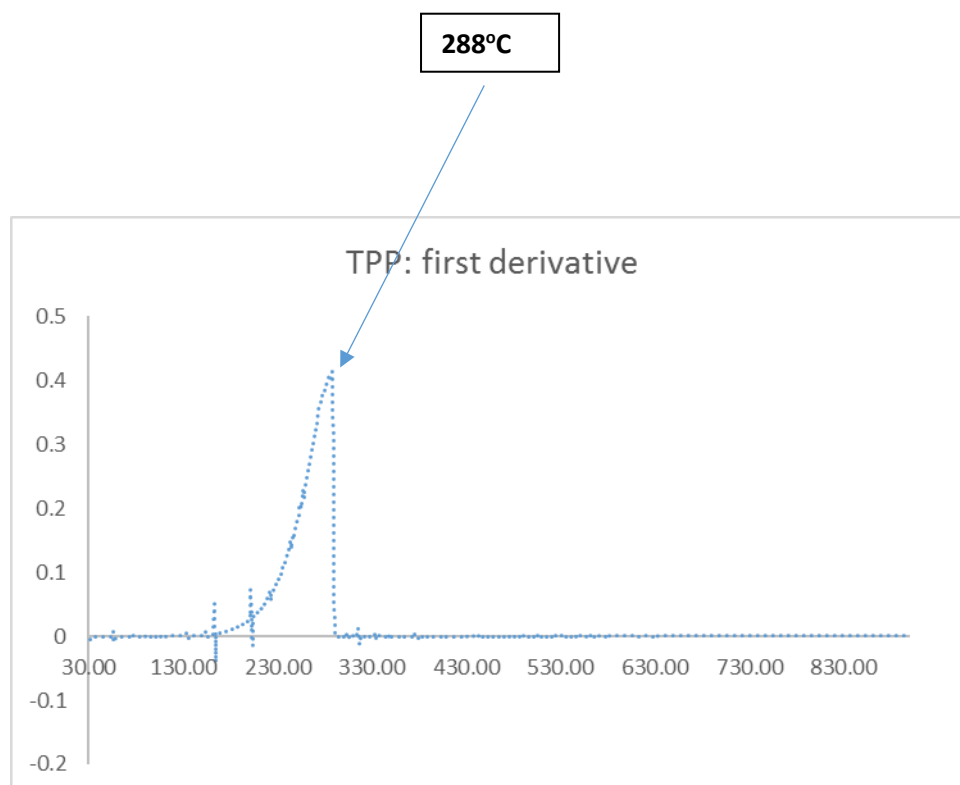


Figure 3. 97 First derivative of the TGA curve of TPP in nitrogen under a heating rate of 10°C min⁻¹

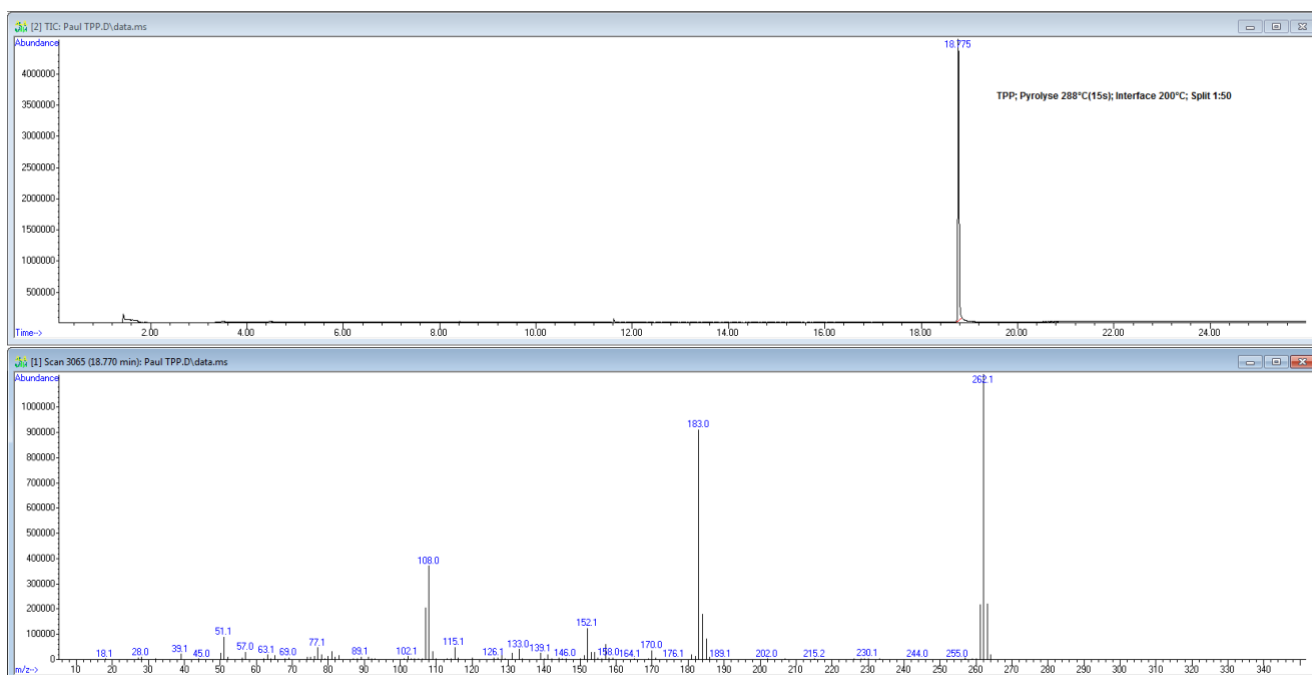


Figure 3. 98 GC and MS of TPP (pyrolysis temperature (288oC)

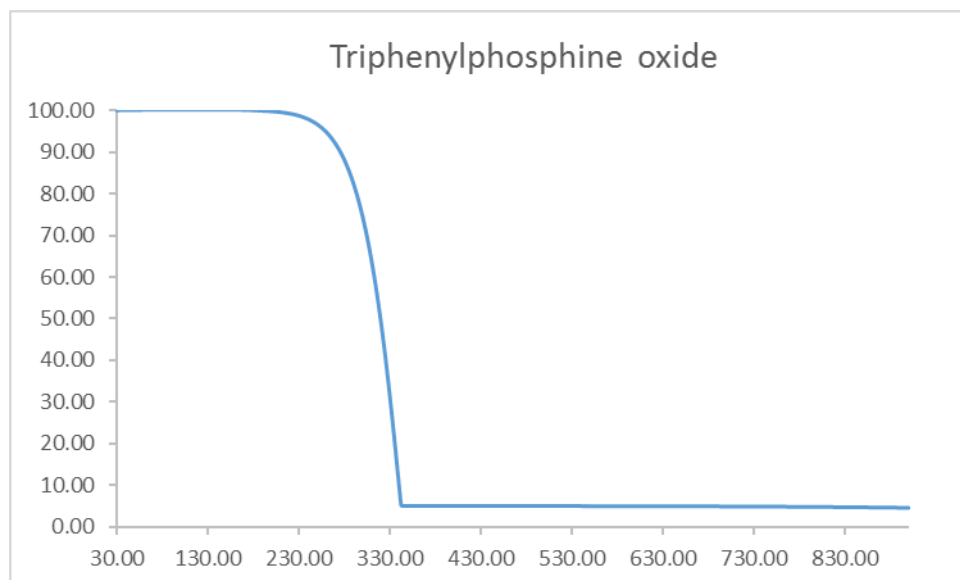


Figure 3. 99 TGA curve of TPPO in nitrogen under a heating rate of 10oC min-1

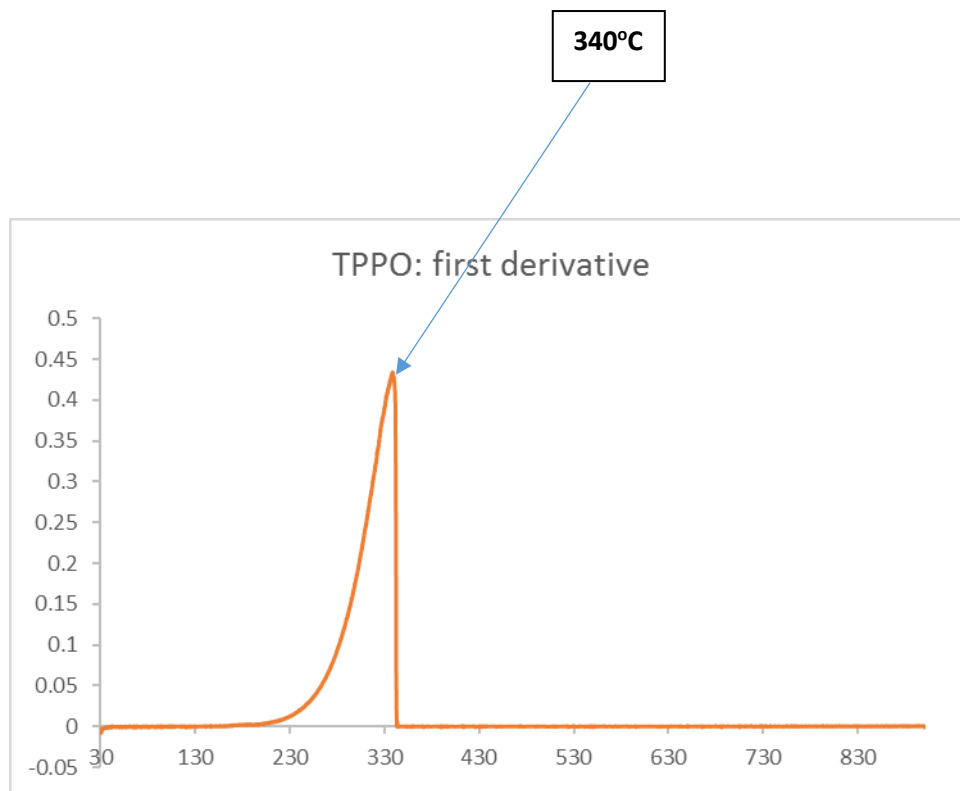
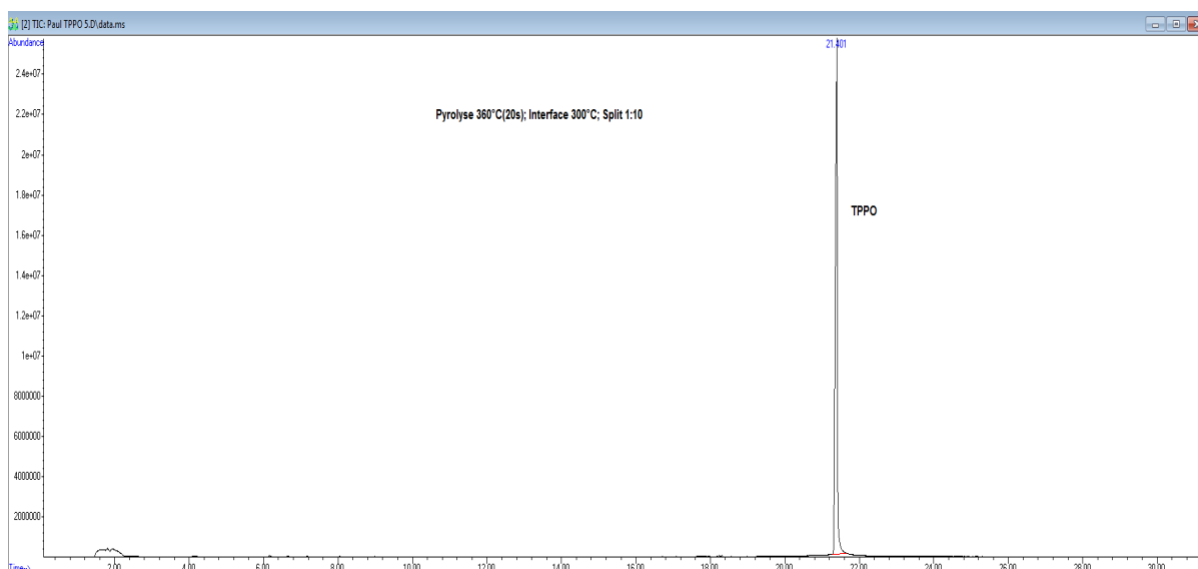


Figure 3. 100 First derivative of the TGA curve of TPPO in nitrogen under a heating rate of $10^{\circ}\text{C min}^{-1}$



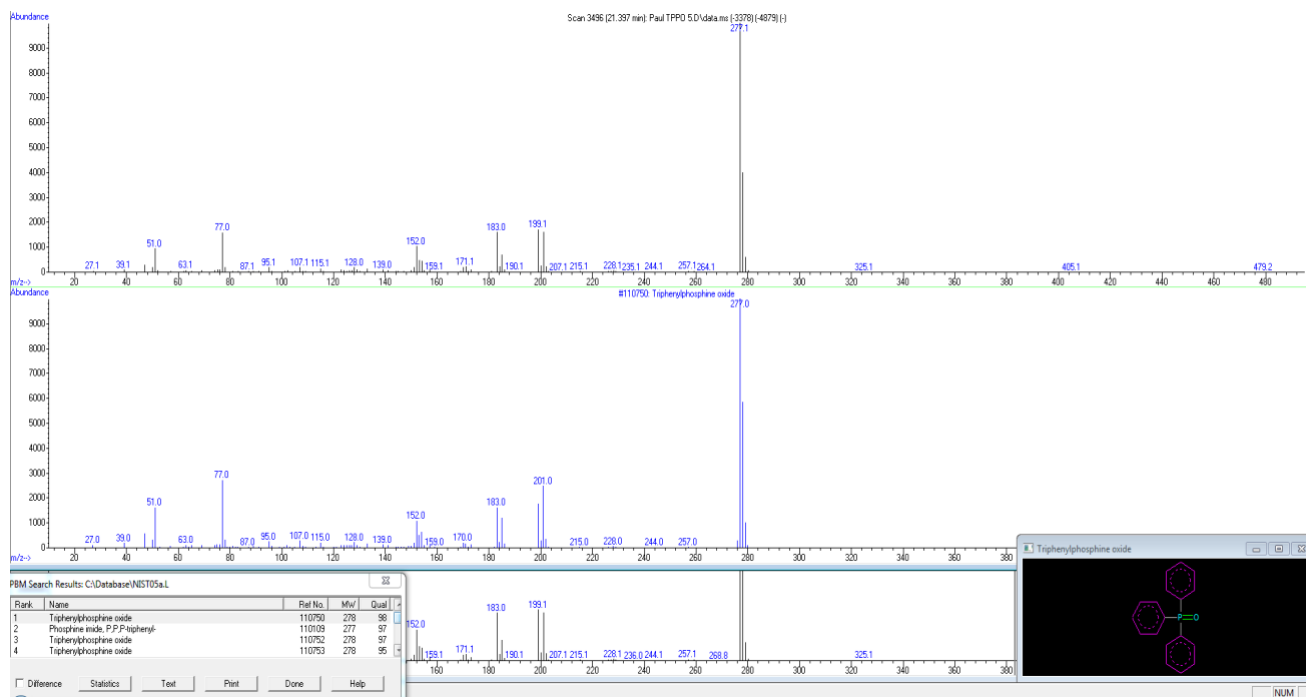


Figure 3. 101 GC and MS of TPPO (pyrolysis temperature: 340°C)

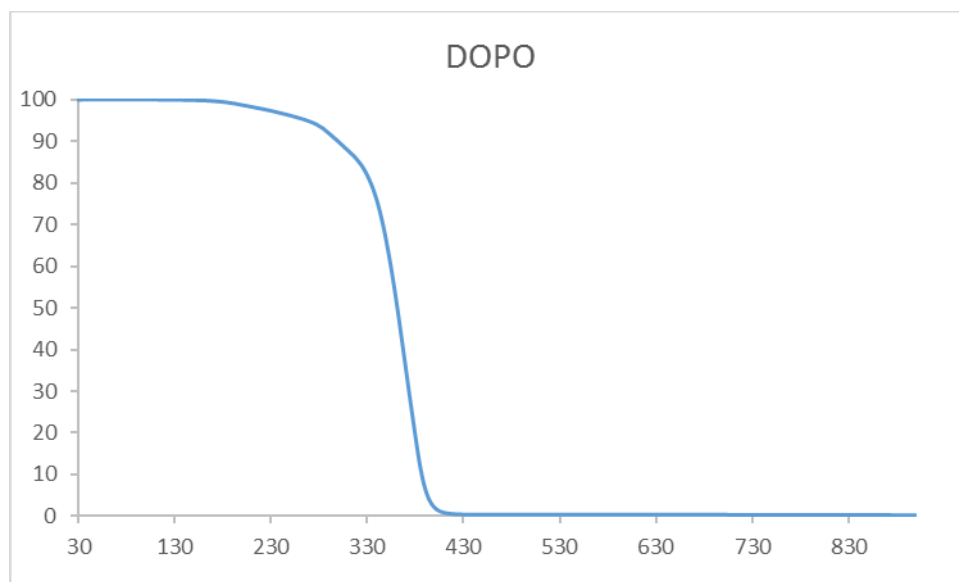


Figure 3. 102 TGA curve of TPPO in nitrogen under a heating rate of 10°C min⁻¹

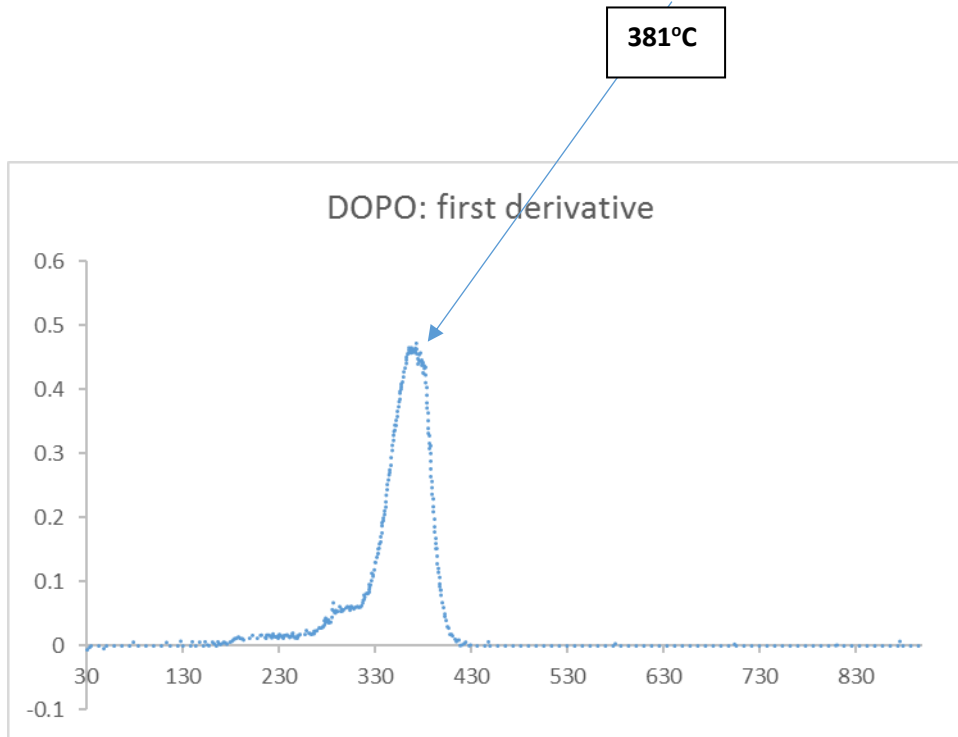


Figure 3. 103 First derivative of the TGA curve of DOPO in nitrogen under a heating rate of 10°C min⁻¹

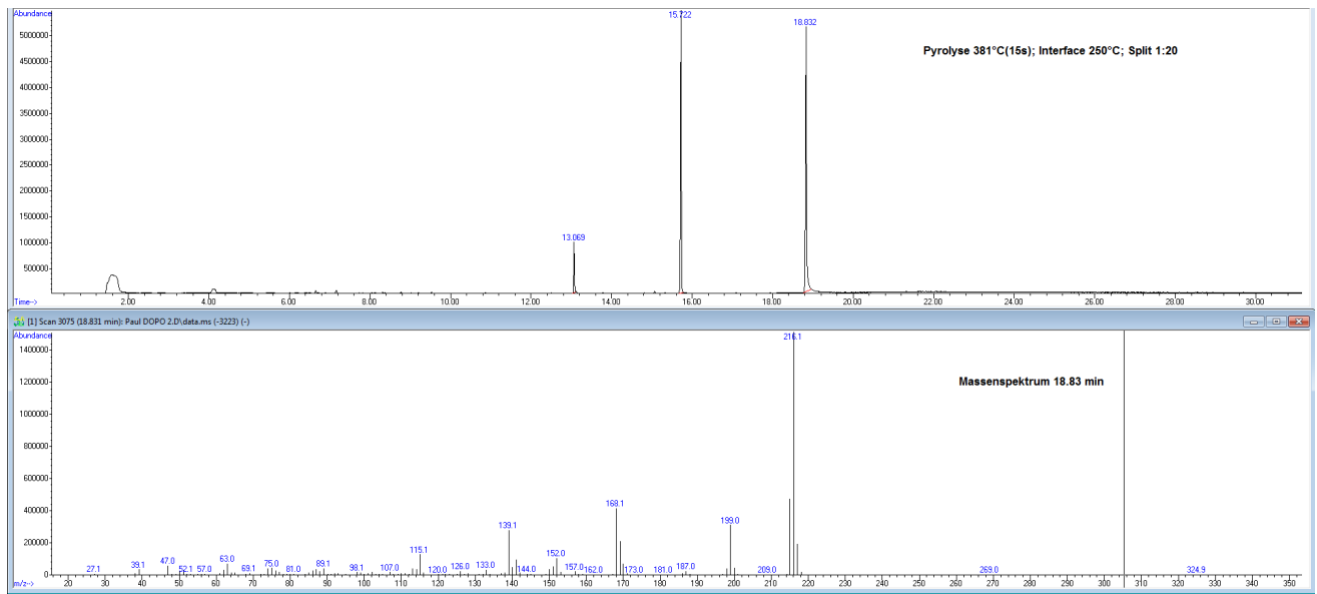
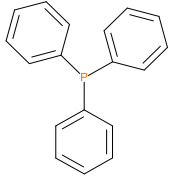
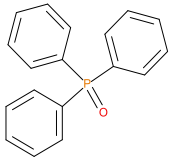
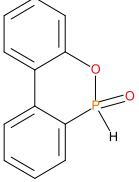


Figure 3. 104 GC and MS of DOPO (pyrolysis temperature (381°C))

It is very clear from the GC/MS of TPP and TPPO, the molecular ion initially produced showed typical fragmentation pattern of aromatic phosphine and phosphine oxide (above their normal melting points, but below the corresponding boiling points), as the case may be. However, in the case of DOPO, three distinct peaks were obtained in the chromatogram, and the corresponding mass spectra were indicative of DOPO (retention time = 18.83 minutes); degradation product of DOPO (retention time = 15.72 minutes, with fragments from DOPO with m/z values of: 152, 170, 199 and 200); *o*-hydroxybiphenyl (retention time = 13.07 minutes)- see for details in table 3. 16 below:

Table 3. 16 Retention times and fragmentation features of the various solid additives

| Sl. No. | Sample (chemical name) | Chemical structures | mp/bp (°C) | Pyrolysis temp. (°C) | Retention time (min) | Molar mass | [M] ⁺ _{±1} |
|---------|------------------------|---|--------------------------------|----------------------|------------------------------|------------|--------------------------------|
| 1 | TPP |  | 80/377 | 288 | 18.775 | 263 | 262 |
| 2 | TPPO |  | 154- 158/360 | 340 | 21.401 | 278 | 277 |
| 3 | DOPO |  | 116- 120/200 (at 1mm Hg) | 381 | 18.830 *15.72/ #13.070 | 216 | 216 |

*indicative of degradation product of DOPO

#indicate of *o*-hydroxybiphenyl

Judging primarily from the results of the pyrolysis-GS/MS studies of the solid organophosphorus additives (TPP, TPPO and DOPO), and the corresponding outcomes from

GC/MS for the liquid additives, we envisage the following degradation pathways of these compounds.

In the case of the solid additives such as TPP and TPPO, typically above their melting points but below their boiling temperatures, volatilization is first effected followed by the cleavage of the P-Ar bonds to form aromatics, either phenyl or biphenyl compounds, and resulting in the release of P, oxygenated phosphorous moieties in the gaseous phase- elemental phosphorus and/or oxides are found to be active in the vapour phase (Joseph & Tretsiakova-Mcnally, 2011). Here it should be noted that the presence of phosphorus (as gauged through ICP/OES: Table 3. 12) and the chemical environment of phosphorus bearing moieties in the condensed phase (see the respective ^{31}P NMR spectrum: in Figure 3. 79 to 3. 81) clearly indicate that the phosphine, or phosphine oxide as the case may be, are retained as such without undergoing thermal degradation.

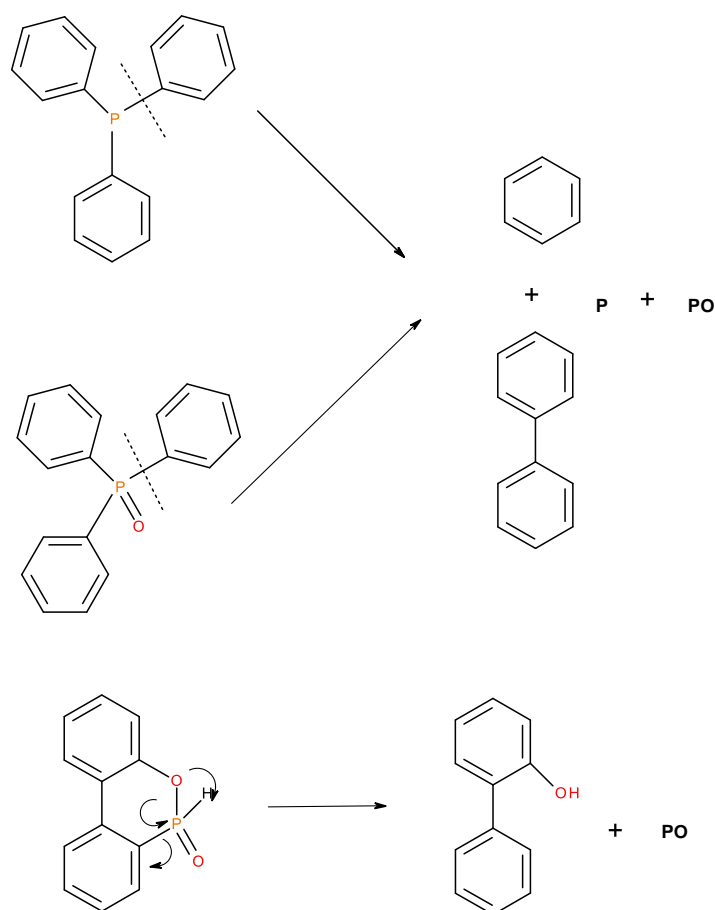


Figure 3. 105 A schematic diagram of production of phosphorus-centred species in the gaseous phase in the case of solid organophosphorus additives

In the case of the liquid additives, such as DEPi, TEPi, TEPa, DEPP and DEBP, it appears that the thermal cracking of the side phosphate, or phosphonate, group is favoured through a

preferred cyclic intermediate liberating ethene, and the latter can be considered as entropically favourable- see in Figure 3. 106 (Joseph & Tretsiakova-McNally, 2012; Tretsiakova-McNally & Joseph, 2015).

In the case of the liquid additives, especially, with the P-atom in the oxidation state of V, elimination can be considered as very feasible through the six membered ring intermediate, where as in the case of the phosphite (where the P-atom is in the oxidation state of III) it has to go through a five membered ring intermediate, or through a six membered analogue if prior oxidation of P(III) to P(V) is assumed. It is relevant to note here that there are unequivocal evidence for the presence of phosphorus acid species in the char residues from the corresponding ^{31}P solid-state NMR (signals centred at $\delta \sim 0.0$ ppm).

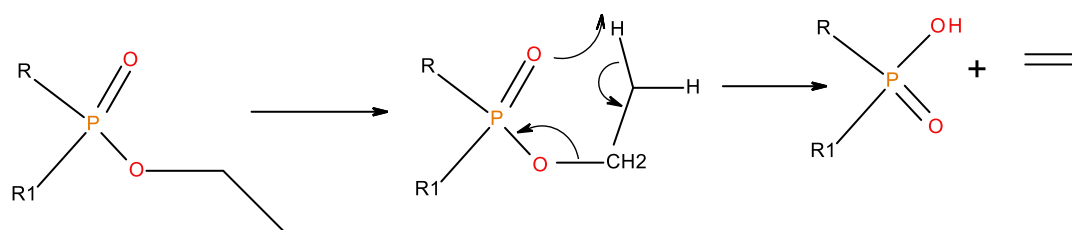


Figure 3. 106 A general schematic diagram of production of phosphorus acidic species, in the condensed phase through the elimination of ethene from the ester side arms of the liquid additive

CHAPTER 4: CONCLUSIONS AND SUGGESTIONS FOR FUTURE WORK

4.1 Main conclusions

The following main conclusions can be drawn from the current study:

1. Through the present work, we have successfully modified different carbohydrate based materials (β -cyclodextrin, dextran, potato starch, agar agar and tamarind) by covalently binding phosphate groups through the reaction of diethylchlorophosphate (DECP) with the appropriate base substrates in dispersions in dichloromethane (DCM), in the presence of trimethylamine (TEA).
2. Following a literature precedent, we have also chemically modified chitosan with 9,10-Dihydro-9-oxa-10-phosphaphenethrene-10-oxide (DOPO).
3. The extents and chemical natures of the phosphorus modified products, obtained through 1 and 2, were established through spectroscopic means (ICP-OES, solid-state NMR and FT-IR).
4. Diethylbenzylphosphonate, one of the phosphorus-containing additives, was also successfully synthesised by employing the well-known Michael-Arbuzov reaction, resulting in the desired product with an acceptable level of purity and in a near quantitative yield.
5. The results from the various thermal and calorimetric characterisation techniques (TGA and PCFC) indicated that the general profiles of the thermograms and the relevant combustion parameters from PCFC of phosphorous modified substrates, both by the *additive* and *reactive* routes were different from the unmodified control samples. Furthermore, in the case of the products obtained through the reactive route, there is clear evidence that the *covalently* bound phosphorus groups exerted noticeable levels of combustion inhibitory effects.
6. With a view to obtaining the Arrhenius parameters (primarily A and E_a) of the base substrates, we used the well-known Flynn-Wall-Ozawa (FWO method, which employed five heating rates) and an in-house proprietary (SB software that utilized only one heating rate). Given that FWO method is essentially based on a model free

approach that also makes use of multiple heating rate, it can be considered in the present context as superior to the SB method, where the input data are gathered essentially from a thermogram obtained at a heating rate of 10°C min⁻¹. Furthermore, the SB method furnishes different values of E_a depending on the model in question. In other words, for obtaining activation energies of carbohydrate based unmodified substrates, FWO method seems to work more effectively than SB method, and hence we chose the E_a values obtained through the FWO method for the correlation studies. However, when it comes to obtaining other kinetic parameters including A value, the SB method gives a straight forward A value, which would otherwise require tedious calculations (i.e. through FWO method). In summary, we found both methods useful; however, the values of E_a obtained in each case should only be considered at best as *apparent* values.

7. We were able to identify limited correlations, primarily between the TGA parameters and corresponding empirical quantities obtained from the PCFC tests.
8. In this study, we used an in-house test rig (dip test) reminiscent of the UL-94 technique, to use as a quick screening technique for understanding the efficacy of the various test formulations in reducing the ignition propensity of slender segments of Radiata Pine samples.
9. The cone calorimeter results showed that the formulations made from fish gelatin and DOPO gave the best results in regards of enhancing the flame retardancy of the timber (Radiata Pine) plaques. However, this attribute was not reflected in the corresponding TGA and PCFC analyses, and therefore no discernible correlations between the results from cone calorimeter, TGA and PCFC could be identified. Therefore, as expected, it can be concluded that generally the degradation of the base substrate(s) and the additive were substantially different in the TGA (pyrolytic decomposition at a pre-set heating rate), PCFC (programmed pyrolysis followed by forced non-flaming combustion) and cone (degradation under ambient conditions followed by flaming combustion) tests. Hence all the three test regimes are evidently different in terms of energetic requirements, rates of underlying physio-chemical processes and time scales.
10. We were also successful, to a limited extent, to decipher the degree, nature and relative predominance of the condensed- and vapour-phase activities of the different additives

through a combination of standard (Atomic Absorption, solid-state NMR and Raman spectroscopies), and optionally through ‘hyphenated’ (pyrolysis-GC/MS and GC/MS), techniques.

11. From the results obtained from the current project we firmly believe that some promising systems warrant further investigations (see in chapter 5: Suggestions for future work).

4.2 Significant contributions arising from the present work

1. We have carried out detailed investigations, and also demonstrated, the utility of several agricultural products/wastes materials as base matrices for bio-inspired FRs for ligno-cellulosic materials.
2. We have also established the solid-state NMR technique (^{31}P) as a reliable technique to unequivocally establish the modification of the base substrates with phosphorus-containing reagents.
3. Furthermore, we have identified ICP-OES as a reliable technique in finding corroborative evidence to the extents of phosphorylation reactions.
4. The kinetics of thermograms were elucidated through two dynamic methods, the standard FWO method and by employing an in-house software (SB method). Here, we also endeavoured to draw comparisons amongst the various kinetic parameters and brought about the limitations and validities of the two approaches.
5. We were also able to draw useful correlations, where applicable, among the relevant parameters from the TGA and PCFC experiments.
6. We have extensively used, with success, some standard and optionally ‘hyphenated techniques’ to analyse the mechanism(s) operating in the condensed and vapour phases of these novel formulations, obtained through both the *additive* and *reactive* approaches. Here, we were also able to suggest specific degradative pathways of the various solid and liquid additives.

7. The ‘dip test’ methodology that we devised through the current project can be extensively used as a quick laboratory scale test methodology for screening the efficacies of fire proofing formulations for different polymeric materials.

4.3 Some suggestions for future work

The present project opens up a number of worthwhile avenues of further study, which can be listed below:

1. The phosphorus-modification reactions of all the substrates needs to be scaled up to generate enough materials for the dip test and cone calorimetry.
2. This study only included the FWO method to calculate the activation energies of the base substrates. This can be further extended to determine the activation energies of the chemically modified substrates and physical admixtures. In conjunction, the SB software can be utilised to compare the differences in activation energies of the modified and unmodified substrates, and also to compute the values of the Arrhenius parameter (A).
3. The cone calorimetric studies has indicated that the formulation of fish gelatin containing DOPO imparted excellent fire proofing properties to the base matrix (Radiata Pine). These formulations can be further investigated in detail, using different loadings of DOPO, with a view to finding out the optimal level of incorporation of phosphorus.
4. Pyrolysis-GC/MS studies should be also extended to additives such as diammoniumhydrogen phosphate and the liquid additives.
5. The surface of the char residues from the cone calorimeter test runs can be further investigated in terms of assessing their surface morphology using a Scanning Electron Microscope (SEM), and the elemental composition and depth profile by using energy dispersive x-ray diffraction technique (EDXRD).

6. The nature of trapped P-centred radical can be identified with appropriate electron paramagnetic resonance spectroscopy (EPR).
7. It is highly desirable to investigate the weatherability attributes, including the propensity for microbial growth, of the coated surface of the test specimens.

REFERENCES

List of references:

- Abt, R., Kelly, D., & Kuypers, M. (1987). The Florida Palm Coast Fire: an analysis of fire incidence and residence characteristics. *Fire Technology*, 23(3), 230-252.
- Albini, F. A. (1983). *Potential spotting distance from wind-driven surface fires* (309). US Department of Agriculture, Forest Service, Intermountain Forest and Range Experiment Station.
- Alongi, J., Pošković, M., Frache, A., & Trotta, F. (2010). Novel flame retardants containing cyclodextrin nanosponges and phosphorus compounds to enhance EVA combustion properties. *Polymer Degradation and Stability*, 95(10), 2093-2100.
- Anthenien, R. A., Stephen, D. T., & Fernandez-Pello, A. C. (2006). On the trajectories of embers initially elevated or lofted by small scale ground fire plumes in high winds. *Fire Safety Journal*, 41(5), 349-363.
- Aseeva, R., Serkov, B., & Sivenkov, A. (2014). *Fire behavior and fire protection in timber buildings*. Springer.
- Babrauskas, V. (2002). Ignition of wood: a review of the state of the art. *Journal of Fire Protection Engineering*, 12(3), 163-189.
- Bakar, A. (2015). *Characterization of fire properties for coupled pyrolysis and combustion simulation and their optimised use*. Victoria University, Melbourne.
- Barrow, G. (1944). *A survey of houses affected in the Beaumaris fire, January 14, 1944*. Council for Scientific and Industrial Research.
- Batayneh, A. (2012). Toxic (aluminum, beryllium, boron, chromium and zinc) in groundwater: health risk assessment. *International Journal of Environmental Science and Technology*, 9(1), 153-162.
- Benfield, A. (2020, January) Australian bushfire season. *Risk frontiers*. Retrieved from <https://www.riskfrontiers.com>
- Bhattacharya, A. K., & Thyagarajan, G. (1981). Michaelis-arbuzov rearrangement. *Chemical Reviews*, 81(4), 415-430.
- Bigger, S. W., Cran, M. J., & Bohn, M. A. (2015). Novel theoretical and computer-assisted modeling of isothermal and non-isothermal depolymerization kinetics. *Polymer Testing*, 44, 1-7.

- Bigger, S. W., Cran, M. J., & Tawakkal, I. S. (2015). Two novel algorithms for the thermogravimetric assessment of polymer degradation under non-isothermal conditions. *Polymer Testing*, *43*, 139-146.
- Blanchi, R., Leonard, J., Haynes, K., Opie, K., James, M., & de Oliveira, F. D. (2014). Environmental circumstances surrounding bushfire fatalities in Australia 1901–2011. *Environmental Science & Policy*, *37*, 192-203.
- Blanchi, R., Leonard, J., & Leicester, R. H. (2006). *Bushfire risk at the rural/urban interface*. Paper presented at the In Australasian Bushfire Conference, 6-9.
- Blennow, A., Engelsen, S. B., Munck, L., & Møller, B. L. (2000). Starch molecular structure and phosphorylation investigated by a combined chromatographic and chemometric approach. *Carbohydrate Polymers*, 163-174.
- Blennow, A., Nielsen, T. H., Baunsgaard, L., Mikkelsen, R., & Engelsen, S. B. (2002). Starch phosphorylation: a new front line in starch research. *Trends in Plant Science*, *7*(10), 445-450.
- Boyd, C. W., Koch, P., McKean, H. B., Morschauser, C. R., Preston, S. B., & Wangaard, F. F. (2007). Wood for structural and architectural purposes. *Wood and Fiber Science*, *8*(1), 3-72.
- Bridgwater, A., Meier, D., & Radlein, D. (1999). An overview of fast pyrolysis of biomass. *Organic Geochemistry*, *30*(12), 1479-1493.
- Buchanan, A. H., & Levine, S. B. (1999). Wood-based building materials and atmospheric carbon emissions. *Environmental Science & Policy*, *2*(6), 427-437.
- Budrugaec, P. (2000). The evaluation of the non-isothermal kinetic parameters of the thermal and thermo-oxidative degradation of polymers and polymeric materials: its use and abuse. *Polymer Degradation and Stability*, *71*(1), 185-187.
- Candan, Z., Ayrilmis, N., & Akbulut, T. (2011). Dimensional stability performance of fire retardant treated veneer-oriented strandboard composites. *BioResources*, *6*(1), 308-316.
- Cogen, J. M., Lin, T. S., & Lyon, R. E. (2009). Correlations between pyrolysis combustion flow calorimetry and conventional flammability tests with halogen-free flame retardant polyolefin compounds. *Fire and Materials: An International Journal*, *33*(1), 33-50.
- Correia, J. R., Branco, F. A., & Ferreira, J. G. (2010). The effect of different passive fire protection systems on the fire reaction properties of GFRP pultruded profiles for civil construction. *Composites Part A: Applied Science and Manufacturing*, *41*(3), 441-452.

- Costes, L., Laoutid, F., Brohez, S., & Dubois, P. (2017). Bio-based flame retardants: When nature meets fire protection. *Materials Science and Engineering: R: Reports*, 117, 1-25.
- Cozzani, V., Tugnoli, A., & Salzano, E. (2007). Prevention of domino effect: From active and passive strategies to inherently safer design. *Journal of Hazardous Materials*, 139(2), 209-219.
- Daniel, Y. G., & Howell, B. A. (2017a). Flame retardant properties of isosorbide bis-phosphorus esters. *Polymer Degradation and Stability*, 140, 25-31.
- Daniel, Y. G., & Howell, B. A. (2017b). Synthesis and characterization of isosorbide bis-phosphorus esters. *Heteroatom Chemistry*, 28(3), e21369.
- Deans, T., Li, Y., Jefferson, L., & Schiraldi, D. A. (2018). Rapid screening test for flame retardation of wood, and its applicability to thermoplastic polymer systems. *Journal of Applied Polymer Science*, 135(32), 46602.
- Demirgöz, D., Elvira, C., Mano, J. F., Cunha, A. M., Piskin, E., & Reis, R. L. (2000). Chemical modification of starch based biodegradable polymeric blends: effects on water uptake, degradation behaviour and mechanical properties. *Polymer Degradation and Stability*, 70(2), 161-170.
- Di Blasi, C., Signorelli, G., Di Russo, C., & Rea, G. (1999). Product distribution from pyrolysis of wood and agricultural residues. *Industrial & Engineering Chemistry Research*, 38(6), 2216-2224.
- Dietenberger, M. (2002). Update for combustion properties of wood components. *Fire and Materials*, 26(6), 255-267.
- Dietenberger, M., & Hasburgh, L. (2016). Wood products thermal degradation and fire. *Reference module in materials science and materials engineering*, 1-8.
- Dollimore, D., Lerdkanchanaporn, S., & Alexander, K. S. (1997). The use of the Harcourt and Esson relationship in interpreting the kinetics of rising temperature solid state decompositions and its application to pharmaceutical formulations. *Thermochimica Acta*, 290(1), 73-83.
- Drysdale, D. (2011). *An introduction to fire dynamics*: John Wiley & Sons.
- Ebdon, J. R., Hunt, B. J., Joseph, P., Konkel, C. S., Price, D., Pyrah, K., Lindsay, C. I. (2000). Thermal degradation and flame retardance in copolymers of methyl methacrylate with diethyl (methacryloyloxymethyl) phosphonate. *Polymer Degradation and Stability*, 70(3), 425-436.

- Fang, F., Zhang, X., Meng, Y., Gu, Z., Bao, C., Ding, X., Tian, X. (2015). Intumescent flame retardant coatings on cotton fabric of chitosan and ammonium polyphosphate via layer-by-layer assembly. *Surface and Coatings Technology*, 262, 9-14.
- Feng, J. X., Su, S. P., & Zhu, J. (2011). An intumescent flame retardant system using β -cyclodextrin as a carbon source in polylactic acid (PLA). *Polymers for Advanced Technologies*, 22(7), 1115-1122.
- Flynn, J. H., & Wall, L. A. (1966). General treatment of the thermogravimetry of polymers. *Journal of Research of the National Bureau of Standards. Section A, Physics and Chemistry*, 70(6), 487.
- Freedman, B., Stinson, G., & Lacoul, P. (2009). Carbon credits and the conservation of natural areas. *Environmental Reviews*, 17, 1-19.
- Friedman, H. L. (1964). *Kinetics of thermal degradation of char-forming plastics from thermogravimetry. Application to a phenolic plastic*. In *Journal of polymer science part C: polymer symposia*.
- Gaan, S., & Sun, G. (2007). Effect of phosphorus and nitrogen on flame retardant cellulose: a study of phosphorus compounds. *Journal of Analytical and Applied Pyrolysis*, 78(2), 371-377.
- Gallina, G., Bravin, E., Badalucco, C., Audisio, G., Armanini, M., De Chirico, A., & Provasoli, F. (1998). Application of cone calorimeter for the assessment of class of flame retardants for polypropylene. *Fire and Materials*, 22(1), 15-18.
- Gebke, S., Thümmeler, K., Sonnier, R., Tech, S., Wagenführ, A., & Fischer, S. (2020). Flame Retardancy of Wood Fiber Materials Using Phosphorus-Modified Wheat Starch. *Molecules*, 25(2), 335.
- Greenwood, C. (1967). The thermal degradation of starch. *Advances in Carbohydrate Chemistry*, 22, 483-515.
- Gustavsson, L., & Sathre, R. (2006). Variability in energy and carbon dioxide balances of wood and concrete building materials. *Building and Environment*, 41(7), 940-951.
- Hagen, M., Hereid, J., Delichatsios, M., Zhang, J., & Bakirtzis, D. (2009). Flammability assessment of fire-retarded Nordic Spruce wood using thermogravimetric analyses and cone calorimetry. *Fire Safety Journal*, 44(8), 1053-1066.
- Harwood, L. M., Moody, C. J., & Percy, J. M. (1999). *Experimental organic chemistry: standard and microscale*.

- Haynes, K., Handmer, J., McAneney, J., Tibbits, A., & Coates, L. (2010). Australian bushfire fatalities 1900–2008: exploring trends in relation to the ‘Prepare, stay and defend or leave early’ policy. *Environmental Science & Policy*, 13(3), 185-194.
- Hou, X., Xue, Z., & Xia, Y. (2018). Preparation of a novel agar/sodium alginate fire-retardancy film. *Materials Letters*, 233, 274-277.
- Howell, B. (2007). The utilization of TG/GC/MS in the establishment of the mechanism of poly (styrene) degradation. *Journal of Thermal Analysis and Calorimetry*, 89(2), 393-398.
- Howell, B. A., Alomari, M. R., Dumitrescu, A., & Opperman, R. S. (2012, August). Properties of the Phosphoramidate Derived from Chitosan and 9, 10-Dihydro-9-oxa-10-phosphaphenanthrene-10-oxide. In *Proceedings of 40th annual technical meeting of the North American Thermal Analysis Society, Florida*, 12-15.
- Howell, B. A. (2002). The utility of variable temperature techniques in the determination of kinetic parameters. *Thermochimica Acta*, 388(1-2), 275-281.
- Howell, B. A., & Daniel, Y. G. (2015). Phosphorus flame retardants from esters of isosorbide and 10-undecenoic acid. In *Green polymer chemistry: biobased materials and biocatalysis* (pp. 339-367). ACS publications.
- Howell, B. A., Oberdorfer, K. L., & Ostrander, E. A. (2018). Phosphorus flame retardants for polymeric materials from gallic acid and other naturally occurring multihydroxybenzoic acids. *International Journal of Polymer Science*, 2018.
- Hu, S., Song, L., Pan, H., Hu, Y., & Gong, X. (2012). Thermal properties and combustion behaviors of flame retarded epoxy acrylate with a chitosan based flame retardant containing phosphorus and acrylate structure. *Journal of Analytical and Applied Pyrolysis*, 97, 109-115.
- Huggett, C. (1980). Estimation of rate of heat release by means of oxygen consumption measurements. *Fire and Materials*, 4(2), 61-65.
- Illy, N., Fache, M., Menard, R., Negrell, C., Caillol, S., & David, G. (2015). Phosphorylation of bio-based compounds: the state of the art. *Polymer Chemistry*, 6(35), 6257-6291.
- Janssens, M., & Parker, W. J. (1992). Oxygen consumption calorimetry. *Heat Release in Fires*, 3, 31-59.
- Jianli, Y., Hao, Q., Bingbing, L., Lijie, S., Lei, N., & Ruilan, F. (2016). Preparation of intumescent flame retardant by hydrolyzed starch as the carbon source and its application. *New Chemical Materials*(5), 50.

- Jones, M., Bhat, T., Kandare, E., Thomas, A., Joseph, P., Dekiwadia, C., Wang, C.-H. (2018). Thermal degradation and fire properties of fungal mycelium and mycelium-biomass composite materials. *Scientific Reports*, 8(1), 1-10.
- Joseph, P., Bakirtzis, D., Richard, Q., & Brulfert, R. (2017). Passive fire protection of lignocellulosic substrates using environmentally-friendly formulations. *Materials Today: Proceedings*, 4(4), 5282-5289.
- Joseph, P., & Tretsiakova-McNally, S. (2012). Combustion behaviours of chemically modified polyacrylonitrile polymers containing phosphorylamino groups. *Polymer Degradation and Stability*, 97(12), 2531-2535.
- Joseph, P., Tretsiakova-McNally, S., & McKenna, S. (2012). Characterization of cellulosic wastes and gasification products from chicken farms. *Waste Management*, 32(4), 701-709.
- Joseph, P., & Tretsiakova-McNally, S. (2011). Reactive modifications of some chain-and step-growth polymers with phosphorus-containing compounds: effects on flame retardance—a review. *Polymers for Advanced Technologies*, 22(4), 395-406.
- Keglevich, G., Bagi, P., Rapi, Z., Bakó, P., Drahos, L., Szolnoki, B., & Marosi, G. (2015, June). The Synthesis of Bio-Based Flame-Retarded Epoxy-Precursors. In *Macromolecular Symposia*, 352(1), 46-50.
- Kishore, K., & Mohandas, K. (1982). Action of phosphorus compounds on fire-retardancy of cellulosic materials: A review. *Fire and Materials*, 6(2), 54-58.
- Kozłowski, R., & Władyska-Przybylak, M. (2001). Natural polymers, wood and lignocellulosic materials. *Fire Retardant Materials*, 293-317.
- Kozłowski, R., & Władyska-Przybylak, M. (2008). Flammability and fire resistance of composites reinforced by natural fibers. *Polymers for Advanced Technologies*, 19(6), 446-453.
- Lau, D., Qiu, Q., Zhou, A., & Chow, C. L. (2016). Long term performance and fire safety aspect of FRP composites used in building structures. *Construction and Building Materials*, 126, 573-585.
- Leonard, J., Blanchi, R., & Bowditch, P. (2004). Bushfire impact from a house's perspective. In *Earth Wind and Fire—Bushfire 2004 Conference*, Adelaide.
- Leonard, J., & Bowditch, P. (2003). Findings of studies of houses damaged by bushfire in Australia. In *3rd International Wildland Fire Conference*, 3-6.
- Leonard, J., & McArthur, N. A. (1999). A history of research into building performance in Australian bushfires. In *Australian Bushfire Conference*, 219-225

- LeVan, S. L. (1984). *Chemistry of Fire Retardancy*. ACS Publications.
- Levchik, S. V., & Weil, E. D. (2006). A review of recent progress in phosphorus-based flame retardants. *Journal of Fire Sciences*, 24(5), 345-364.
- Lin, T. S., Cogen, J. M., & Lyon, R. E. (2007). Correlations between microscale combustion calorimetry and conventional flammability tests for flame retardant wire and cable compounds. In *Proceedings of the 56th IWCS*.
- Liodakis, S., Fetsis, I., & Agiovlasis, I. (2009). The fire-retarding effect of inorganic phosphorus compounds on the combustion of cellulosic materials. *Journal of Thermal Analysis and Calorimetry*, 98(1), 285-291.
- Liu, T., Jing, J., Zhang, Y., & Fang, Z. (2018). Synthesis of a novel polyphosphate and its application with APP in flame retardant PLA. *RSC Advances*, 8(8), 4483-4493.
- Liu, X., Wang, Y., Yu, L., Tong, Z., Chen, L., Liu, H., & Li, X. (2013). Thermal degradation and stability of starch under different processing conditions. *Starch-Stärke*, 65(1-2), 48-60.
- Lowden, L. A., & Hull, T. R. (2013). Flammability behaviour of wood and a review of the methods for its reduction. *Fire Science Reviews*, 2(1), 4.
- Luda, M. P., & Zanetti, M. (2019). Cyclodextrins and Cyclodextrin Derivatives as Green Char Promoters in Flame Retardants Formulations for Polymeric Materials. A Review. *Polymers*, 11(4), 664.
- Lyon, R. E., & Walters, R. N. (2004). Pyrolysis combustion flow calorimetry. *Journal of Analytical and Applied Pyrolysis*, 71(1), 27-46.
- Mahmud, H. (2016). *Simulation of the suppression of fires using water mists*. Victoria University.
- Manzello, S. L., Cleary, T. G., Shields, J. R., & Yang, J. C. (2006). Ignition of mulch and grasses by firebrands in wildland-urban interface fires. *International Journal of Wildland Fire*, 15(3), 427-431.
- Manzello, S. L., & Suzuki, S. (2013). Experimentally simulating wind driven firebrand showers in Wildland-Urban Interface (WUI) fires: overview of the NIST firebrand generator (NIST dragon) technology. *Procedia Engineering*, 62, 91-102.
- Maranghides, A., & Mell, W. E. (2009). *A case study of a community affected by the Witch and Guejito Fires*. Citeseer.
- McArthur, N. A., & Lutton, P. (1991). Ignition of exterior building details in bushfires: an experimental study. *Fire and Materials*, 15(2), 59-64.

- McInnes, J. A., Cleland, H. J., Cameron, P. A., Darton, A., Tracy, L. M., Wood, F. M., Gabbe, B. J. (2019). Epidemiology of burn-related fatalities in Australia and New Zealand, 2009–2015. *Burns*, 45(7), 1553-1561.
- Mohan, D., Pittman Jr, C. U., & Steele, P. H. (2006). Pyrolysis of wood/biomass for bio-oil: a critical review. *Energy & Fuels*, 20(3), 848-889.
- Morgan, A. B., Wilkie, C. A., & Nelson, G. L. (2012). *Fire and polymers VI: new advances in flame retardant chemistry and science*. ACS Publications.
- Muhammad, K., Hussin, F., Man, Y., Ghazali, H., & Kennedy, J. (2000). Effect of pH on phosphorylation of sago starch. *Carbohydrate Polymers*, 42(1), 85-90.
- Östman, B., Voss, A., Hughes, A., Jostein Hovde, P., & Grexa, O. (2001). Durability of fire retardant treated wood products at humid and exterior conditions review of literature. *Fire and Materials*, 25(3), 95-104.
- Ozawa, T. (1965). A new method of analyzing thermogravimetric data. *Bulletin of the Chemical Society of Japan*, 38(11), 1881-1886.
- Ozawa, T. (1992). Estimation of activation energy by isoconversion methods. *Thermochimica Acta*, 203, 159-165.
- Passauer, L., Liebner, F., & Fischer, K. (2009). Starch phosphate hydrogels. Part I: Synthesis by mono-phosphorylation and cross-linking of starch. *Starch-Stärke*, 61(11), 621-627.
- Poletto, M., Zattera, A. J., & Santana, R. M. (2012). Thermal decomposition of wood: kinetics and degradation mechanisms. *Bioresource Technology*, 126, 7-12.
- Price, D., Cunliffe, L. K., Bullett, K., Hull, T. R., Milnes, G. J., Ebdon, J. R., Joseph, P. (2007). Thermal behaviour of covalently bonded phosphate and phosphonate flame retardant polystyrene systems. *Polymer Degradation and Stability*, 92(6), 1101-1114.
- Qu, H., Wu, W., Wu, H., Xie, J., & Xu, J. (2011). Study on the effects of flame retardants on the thermal decomposition of wood by TG–MS. *Journal of Thermal Analysis and Calorimetry*, 103(3), 935-942.
- Ramage, M. H., Burrige, H., Busse-Wicher, M., Fereday, G., Reynolds, T., Shah, D. U., Densley-Tingley, D. (2017). The wood from the trees: The use of timber in construction. *Renewable and Sustainable Energy Reviews*, 68, 333-359.
- Reid, C. E., Brauer, M., Johnston, F. H., Jerrett, M., Balmes, J. R., & Elliott, C. T. (2016). Critical review of health impacts of wildfire smoke exposure. *Environmental Health Perspectives*, 124(9), 1334-1343.
- Rowell, R. (1984). *The chemistry of solid wood*. American Chemical Society.

- Sag, J., Goedderz, D., Kukla, P., Greiner, L., Schönberger, F., & Döring, M. (2019). Phosphorus-Containing Flame Retardants from Biobased Chemicals and Their Application in Polyesters and Epoxy Resins. *Molecules*, *24*(20), 3746.
- Sakharov, A., Sakharov, P., Lomakin, S., & Zaikov, G. (2014). Novel class of eco-flame retardants based on the renewable raw materials *Polymer Green Flame Retardants* (255-266). Elsevier.
- Salmeia, K. A., & Gaan, S. (2015). An overview of some recent advances in DOPO-derivatives: Chemistry and flame retardant applications. *Polymer Degradation and Stability*, *113*, 119-134.
- Schartel, B., Pawlowski, K. H., & Lyon, R. E. (2007). Pyrolysis combustion flow calorimeter: a tool to assess flame retarded PC/ABS materials? *Thermochimica Acta*, *462*(1-2), 1-14.
- Solorzano, J. A. P., Moinuddin, K. A. M., Tretsiakova-McNally, S., & Joseph, P. (2019). A Study of the Thermal Degradation and Combustion Characteristics of Some Materials Commonly Used in the Construction Sector. *Polymers*, *11*(11), 1833.
- Sonnier, R., Otazaghine, B., Ferry, L., & Lopez-Cuesta, J.-M. (2013). Study of the combustion efficiency of polymers using a pyrolysis–combustion flow calorimeter. *Combustion and Flame*, *160*(10), 2182-2193.
- Sorathia, U., Beck, C., & Dapp, T. (1993). Residual strength of composites during and after fire exposure. *Journal of Fire Sciences*, *11*(3), 255-270.
- Spearpoint, M. J., & Quintiere, J. G. (2001). Predicting the piloted ignition of wood in the cone calorimeter using an integral model—effect of species, grain orientation and heat flux. *Fire Safety Journal*, *36*(4), 391-415.
- Tarifa, C. S., Del Notario, P. P., & Moreno, F. G. (1965). *On the flight paths and lifetimes of burning particles of wood*. Paper presented at the Symposium (international) on combustion.
- Tawiah, B., Yu, B., Yuen, A. C., Yuen, R. K., Xin, J. H., & Fei, B. (2019). Thermal, crystalline and mechanical properties of flame retarded Poly (lactic acid) with a PBO-like small molecule-Phenylphosphonic Bis (2-aminobenzothiazole). *Polymer Degradation and Stability*, *163*, 76-86.
- Terzi, E., Kartal, S. N., White, R. H., Shinoda, K., & Imamura, Y. (2011). Fire performance and decay resistance of solid wood and plywood treated with quaternary ammonia compounds and common fire retardants. *European Journal of Wood and Wood Products*, *69*(1), 41-51.

- Thomas, A., Joseph, P., Moinuddin, K., Zhu, H., & Tretsiakova-McNally, S. (2020). Thermal and Calorimetric Evaluations of Some Chemically Modified Carbohydrate-Based Substrates with Phosphorus-Containing Groups. *Polymers*, 12(3), 588.
- Thomas, A., Moinuddin, K., Zhu, H., & Joseph, P. (2020). Passive fire protection of wood using bio-derived fire retardants. *Fire Safety Journal*: <https://doi.org/10.1016/j.firesaf.2020.103074>.
- Thornton, W. M. (1917). XV. The relation of oxygen to the heat of combustion of organic compounds. *The London, Edinburgh, and Dublin Philosophical Magazine and Journal of Science*, 33(194), 196-203.
- Tretniakova-McNally, S., & Joseph, P. (2015). Pyrolysis combustion flow calorimetry studies on some reactively modified polymers. *Polymers*, 7(3), 453-467.
- Trucchia, A., Egorova, V., Butenko, A., Kaur, I., & Pagnini, G. (2019). RandomFront 2.3: a physical parameterisation of fire spotting for operational fire spread models—implementation in WRF-SFIRE and response analysis with LSFIRE. *Geoscientific Model Development*, 12(1), 69-87.
- Tse, S. D., & Fernandez-Pello, A. C. (1998). On the flight paths of metal particles and embers generated by power lines in high winds—a potential source of wildland fires. *Fire Safety Journal*, 30(4), 333-356.
- Vyazovkin, S., Burnham, A. K., Criado, J. M., Pérez-Maqueda, L. A., Popescu, C., & Sbirrazzuoli, N. (2011). ICTAC Kinetics Committee recommendations for performing kinetic computations on thermal analysis data. *Thermochimica Acta*, 520(1-2), 1-19.
- Vyazovkin, S., & Wight, C. A. (1998). Isothermal and non-isothermal kinetics of thermally stimulated reactions of solids. *International Reviews in Physical Chemistry*, 17(3), 407-433.
- Wadhvani, R. (2019). *Physics-based simulation of short-range spotting in wildfires*. Victoria University, Melbourne
- Wadhvani, R., Sutherland, D., & Moinuddin, K. (2019). *Simulated transport of short-range embers in an idealised bushfire*. Paper presented at the Proceedings for the 6th International Fire Behavior and Fuels Conference.
- Wadhvani, R., Sutherland, D., Ooi, A., Moinuddin, K., & Thorpe, G. (2017). Verification of a Lagrangian particle model for short-range firebrand transport. *Fire Safety Journal*, 91, 776-783.
- Wang, L., Sánchez-Soto, M., Abt, T., MasPOCH, M. L., & Santana, O. O. (2016). Microwave-crosslinked bio-based starch/clay aerogels. *Polymer International*, 65(8), 899-904.

- Wang, L., Schiraldi, D. A., & Sánchez-Soto, M. (2014). Foamlike xanthan gum/clay aerogel composites and tailoring properties by blending with agar. *Industrial & Engineering Chemistry Research*, 53(18), 7680-7687.
- Wang, X., Hu, Y., Song, L., Xuan, S., Xing, W., Bai, Z., & Lu, H. (2010). Flame retardancy and thermal degradation of intumescent flame retardant poly (lactic acid)/starch biocomposites. *Industrial & Engineering Chemistry Research*, 50(2), 713-720.
- Wang, Y.-T., Zhao, H.-B., Degracia, K., Han, L.-X., Sun, H., Sun, M., Schiraldi, D. A. (2017). Green approach to improving the strength and flame retardancy of poly (vinyl alcohol)/clay aerogels: incorporating biobased gelatin. *ACS Applied Materials & Interfaces*, 9(48), 42258-42265.
- White, R. H., & Dietsberger, M. (2001). Wood products: thermal degradation and fire. *Encyclopedia of materials: science and technology*. [SI]. Elsevier Science Ltd, c2001. 9712-9716.
- Wu, K., Hu, Y., Song, L., Lu, H., & Wang, Z. (2009). Flame retardancy and thermal degradation of intumescent flame retardant starch-based biodegradable composites. *Industrial & Engineering Chemistry Research*, 48(6), 3150-3157.
- Xu, L., Lei, C., Xu, R., Zhang, X., & Zhang, F. (2017). Synergistic effect on flame retardancy and thermal behavior of polycarbonate filled with α -zirconium phosphate gel-silica. *Journal of Applied Polymer Science*, 134(19).
- Yang, H., Yan, R., Chen, H., Zheng, C., Lee, D. H., & Liang, D. T. (2006). In-depth investigation of biomass pyrolysis based on three major components: hemicellulose, cellulose and lignin. *Energy & Fuels*, 20(1), 388-393.
- Yates, C. P., Edwards, A. C., & Russell-Smith, J. (2009). Big fires and their ecological impacts in Australian savannas: size and frequency matters. *International Journal of Wildland Fire*, 17(6), 768-781.
- Yongjiang, X., Huaqing, X., Hongyan, W., Zhiping, L., & Chaohe, F. (2011). Kinetics of isothermal and non-isothermal pyrolysis of oil shale. *Oil Shale*, 28(3).
- Zhao, X., Xiao, D., Alonso, J. P., & Wang, D.-Y. (2017). Inclusion complex between beta-cyclodextrin and phenylphosphonicdiamide as novel bio-based flame retardant to epoxy: Inclusion behavior, characterization and flammability. *Materials & Design*, 114, 623-632.